SINGLE LIGHT EMITTERS IN THE CONFINEMENT OF POLYMERS

Nikodem Tomczak

Single Light Emitters in the Confinement of Polymers
Nikodem Tomczak

Thesis University of Twente, MESA$^+$ Institute for Nanotechnology,
Enschede, The Netherlands
ISBN 90-365-2205-6

This research was financially supported by the Council for Chemical Sciences of the Netherlands Organization for Scientific Research (NWO-CW), grant number 700.99.035.

Printed by PrintPartners Ipskamp, Enschede, the Netherlands,
http://www.ppi.nl

SINGLE LIGHT EMITTERS IN THE CONFINEMENT OF POLYMERS

PROEFSCHRIFT

ter verkrijging van
de graad van doctor aan de Universiteit Twente,
op gezag van de rector magnificus,
prof. dr. W.H.M. Zijm,
volgens besluit van het College voor Promoties
in het openbaar te verdedigen
op woensdag 18 mei 2005 om 15.00 uur

door

Nikodem Tomczak

Geboren op 11 April 1976

te Gdynia, Polen

Dit proefschrift is goedgekeurd door:

Promotor:	prof. dr. G.J. Vancso
Promotor:	prof. dr. N.F. van Hulst

TABLE OF CONTENTS

Chapter 1

General introduction and scope

1.1 General introduction

Swift development in chemistry and chemical technology during the XX^{th} century has resulted in the discovery of many new and advanced materials with novel properties, use and function. Among the materials of the last century plastics have had the most significant impact on our everyday life. In fact, the second half of the XX^{th} century has often been referred to as the "plastics age". Still, after almost a century of research, our knowledge about the basic relationships between the macromolecular chain chemical structure, processing and final thermal or mechanical properties of polymers remains relatively poor. It is recognized that the understanding of microscopic or nanoscopic processes at the polymer segmental scale is essential to predict macroscopic materials behavior. Additionally, heterogeneity present in the material (both structural and dynamic) can greatly impact the materials final, macroscopic properties.

Development of experimental techniques able to combine non-ensemble averaging with intrinsic nanoscale probing is therefore on the forefront of the scientific research. Within the last 15 years technological barriers for observing and manipulating single molecules have been overcome. Scanning Tunneling Microscopy (STM) and Atomic Force Microscopy (AFM) represent a major breakthrough in surface science and analytical techniques. Individual atoms, molecules or larger molecular assemblies like macromolecules or dendrimers can be visualized and addressed while present on surfaces. These techniques have grown beyond imaging and become enabling platform in nanotechnology for studies of properties as well as for use in nanofabrication.

New optical techniques, not confined to investigate only surface properties, were developed and optical properties of condensed matter can now be probed with unprecedented resolution. In the optical domain, Near-Field Scanning Optical Microscopy (NSOM) has beaten the diffraction limit. Observation of emission of light by single light emitters embedded in a solid or liquid host has become possible. Rapid progress in the field of photon detection devices and other optical instrumentation made single molecule fluorescence detection to grow into a

significant research tool and soon additional single molecule techniques like Scanning Confocal Microscopy (SCM) or Wide-Field Microscopy (WFM) have been developed.

The ability to probe optical properties of condensed matter with nanometer resolution triggered new exciting developments in the field of optics. More generally, photonics as the field of all-encompassing optical science and technology, has impacted scientific - technological progress and our everyday life from information technology, via advanced materials, to medical care. Recent breakthrough discoveries in optical instrumentation, materials chemistry and nanotechnology have brought the length scale in photonics down to the nanometer range: NanoPhotonics was born. Single molecules can be watched to emit light, and quantum mechanical processes can be observed in real time thanks to the enabling tools and approaches in NanoPhotonics.

This relatively young field of science has already resulted in significant progress. By employing related, advanced optical tools and techniques to observe and manipulate individual fluorescent molecules embedded within a solid, or immersed in a liquid, breakthrough advances have been reported regarding interactions between light and matter on the nanoscale, and on the matter nanoscale structure and dynamics. New physical phenomena, on the level of individual molecules, otherwise hidden, were revealed and separated from ensemble-averaged behavior, which is usually probed using other techniques. The use of single molecule optical labeling methods improved our knowledge of basic biological processes like molecular transport through cell membranes or structure and dynamics of single functional biological entities (e.g. proteins or DNA). The ability to follow single proteins on a cell surface or to monitor the path of single particles within a cell is the requirement for future developments of site-specific drug delivery or targeted repair of single cells within a living organism.

Engineering of photonic properties of single light-emitters has been achieved by tailoring the environment of the emitters on the nanoscale. Careful shaping of matter present near-by the emitter, at different length scales (ranging from micro- to nanometers) would ultimately serve as a means to gain control of the optical properties of the chromophores (e.g. to optimize quantum efficiency, photostability or radiative decay rates), without the necessity to change their chemical structure or spatial conformation. Molding the flow of light using nanostructured matter together with preprogrammed properties of single light-emitting species is pushing us towards new, emerging technologies for information processing. Development of devices with ultra-fast operational speed at a low cost, fabricated using polymers, in combination with basic knowledge acquired from NanoPhotonic research will be aggressively pursued in the XXIst century.

1.2 Scope of this thesis

The research described in this thesis is concerned with three main objectives. The first objective is to develop and apply new experimental techniques based on single molecule fluorescence detection and spectroscopy to probe polymers on the nanoscale without ensemble averaging. Different single molecule fluorescence detection methods are applied to look at single molecules diffusing in a polymeric host or to look at the segmental scale relaxation processes below the polymer glass transition temperature. The second objective of this thesis is to establish a relation between polymer properties and degree of polymer chain confinement. To this end probing polymeric materials in the bulk, in thin films, and in cylindrical geometry of a polymer fiber is performed. The third goal of this thesis is to evaluate how the presence of a polymer matrix influences the optical properties of the single light emitters. The investigation of radiative decay rates in polymer thin films and polymer fibers is carried out.

Chapter 2 and Chapter 3 serve as introductory chapters. Introduction to topics in polymer physics is presented in Chapter 2. A special accent is put on the reviewing of the current status in the investigations of the dynamic properties of polymers at interfaces and in different degree of confinement. In Chapter 3 single molecule fluorescence methods are introduced and their application in polymer studies is reviewed. The need for the development of new experimental techniques to investigate polymers on the nanoscale is underlined. Techniques based on optical single molecule detection are shown to be the most promising candidates to resolve the controversies present in the polymer field concerning segmental scale dynamics or heterogeneous dynamics near the glass transition.

Single molecule detection, localization, and tracking are used to obtain information on the dynamics present in the polymeric system and are presented in Chapter 4. Wide-field single-molecule methods are employed to study the heterogeneous dynamics in polymers present at different experimental conditions. It is also shown how the photodynamics of the single molecule probes embedded in the polymer can be used to obtain information on the static heterogeneities present in the polymer below the glass transition temperature.

In Chapter 5 we demonstrate how the monitoring of the fluorescence lifetime of individual probes embedded in different polymer is used to obtain the information on the local, segmental scale, density fluctuations in the polymer matrix. Applying the Simha-Somcynsky equation of state theory we obtain the number of polymer segments taking part in the rearranging volume around the probe (N_S). N_S is found to be dependent on temperature and to decrease for higher temperatures.

In Chapter 6 we investigate the fluorescence lifetime of single molecules in thin polymer films. The electromagnetic boundary conditions influences the radiative decay rate through feeding back to the molecule the emitted electromagnetic field and changing the density of state in the molecule surroundings. Data shows that the excited state lifetime depends on the distance and orientation of the molecule with respect to the interfaces. We demonstrate that single molecule investigations based on monitoring of the radiative properties of fluorescence probes should carefully estimate and take into account the effect of the structured surroundings. It is also shown that the effects related to the electromagnetic boundary conditions are not to play a major role in the investigation of polymer dynamics in thin films below the glass transition temperature.

In Chapter 7 we make use of method described in Chapter 5 to probe the polymer segmental scale dynamics in thin polymer films. Fluorescent molecules were embedded into a polymer confined into thin films with thickness values ranging from 10 to 200 nm. We investigate how the dynamics of the polymer segments changes when decreasing the polymer film thickness. Changes in the polymer dynamics observed are attributed to the effect of the interfaces with increased dynamics, which propagates deep into the thin film sample even far below the glass transition temperature. We estimate that the width of the surface region with enhanced dynamics is around 10 nm. Additionally, we show that the dynamics in films with thickness lower than 100 nm is more heterogeneous than in thicker polymer films. To discriminate between local effects connected with density fluctuations and global effects connected with thin film geometry we make use of the knowledge acquired in Chapter 6.

Luminescent nanofibers prepared by electrospinning are the subject of Chapter 8. We show that one can prepare hybrid luminescent structures by embedding fluorescent molecules or nanoparticles (quantum dots) into the fibers. Fluorescence lifetime is used to monitor the effects a cylindrical geometry can have on the spontaneous emission rates of the chromophore. Single molecule imaging techniques serve to evaluate the structure of the electrospun fibers, in particular to obtain information on the internal structure of polymer beads formed during electrospinning.

In Chapter 9 we present a brief outlook of the possible future research directions.

Chapter 2

Introduction - topics in polymer physics

2.1 Introduction

The wide range of properties one can achieve by manipulating chemical constitution, chain length, and molecular architecture makes polymers ideal for numerous applications [1-3]. These properties can be tailored by the primary chemical composition, which – in turn – together with the thermo-rheological history or processing determines the morphology and structural hierarchy. It is useful to divide polymers into two main classes: amorphous and semicrystalline. A low degree of symmetry in the chain structure will generally suppress polymer crystallization. Polymers with an irregular primary structure when cooled from the melt form glasses. Upon cooling, glass-forming polymers grow increasingly viscous, until the viscosity becomes so large that they fail to flow on experimental time-scales. While glasses remain microscopically disordered, like liquids, with no long-range molecular order present, they retain the mechanical properties more common to solids. The microscopic disorder remains essentially unchanged as the polymer transforms from the glassy state to the liquid state. In contrast to semicrystalline polymers, the glassy polymers will show no sharp Bragg reflections in the X-ray diffractograms. From organic and inorganic liquids, through proteins to synthetic polymers, almost any material can in fact form a glassy state. Amorphous materials have been subject of intense investigations not only in the polymer field. New classes of materials having amorphous structures, like metallic glasses [4] or amorphous semiconductors, have emerged. The amorphous structure of these materials resulted in unique thermal, mechanical or electronic properties.

Despite the great technological relevance of polymeric glasses, our knowledge of the amorphous state remains very incomplete. The relationship between the primary chemical structure of the polymer chain to the structural, thermal and mechanical properties of the resulting amorphous material is still under investigation. Although a wealth of experimental data exists, it is fair to say that our knowledge about the microscopic mechanisms underlying the glass transition, the transition from the liquid to the glassy state, is still relatively poor [5-8]. It may come as a surprise after decades of intensive scientific research, that there is still no theory, which offers a description of all aspects of the dynamics of glass forming materials. Several theories were developed throughout the years, successfully describing parts

of the phenomena, however they have been proven to fail in certain specific aspects of the glass formers dynamics. For example, the mode coupling theory of Sjorgen and Gotze [9] successfully describe the dynamics of glass formers at high temperatures, however it failed to describe the dynamics at temperatures close to the glass transition.

In this Chapter we present the main, still unresolved, issues regarding the structure and dynamics of glassy polymers. In particular, the topics of the microscopic structure and dynamics of polymer glasses are addressed. Mobility of polymers at interfaces and in confinement is also presented and the related literature is reviewed. Most of the concepts reviewed in this part of the thesis will be used in the subsequent chapter.

2.2 Structure of glassy polymers

Knowledge of the static structure at different length scales is essential for the understanding of the physical and chemical properties of liquids and amorphous solids [10]. However, since the long range correlation between structural units in these materials is totally absent, therefore, the accurate determination of the structure by means of known diffraction methods is difficult because the interference function obtained is only a one-dimensional representation of a three dimensional structure. Nevertheless there were widespread attempts to obtain some information on the structure of polymeric glasses by using wide-angle X-ray scattering (WAXS) [11], small angle X-Ray scattering (SAXS) [12], and small angle neutron scattering (SANS) [13]. Also relaxation techniques like nuclear magnetic resonance (NMR) were used to study the amorphous state [14].

Although the structure of glasses is believed to be statistical in nature [15] there is still a discussion in the literature about the possibility that there is a certain degree of order on the nanoscale [16]. Figure 1 shows different models of the amorphous state each including a certain degree of short-range order. It should be noted that the experimental evidence makes it difficult to distinguish between macromolecules that have either a random coil (Figure 1a) or locally folded chain conformations. The issue of the microstructure of macromolecules in the amorphous state is far from being resolved and new experimental evidence is needed.

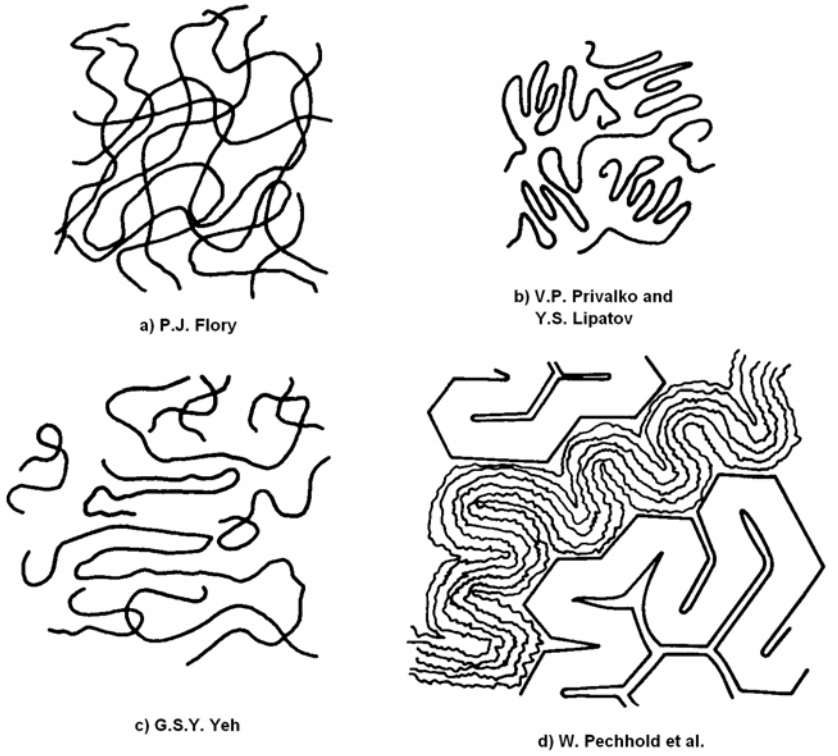

Figure 1. Various models of the amorphous state. a) Flory's random coil model [17]. b) Privalko and Lipatov's randomly folded chain conformation [18]. c) Yeh's folded chain fringed-micellar model [19]. d) Pechhold's meander model [20]. Figure adopted from ref [2].

2.3 Polymer mobility and the glass transition

In Figure 2 we present the main transitions of amorphous polymers. The dependence of the Young's modulus (E) as a function of temperature shows several characteristic regions, where the polymer exhibits different physical and mechanical behavior. At low temperatures, amorphous polymers are hard, glassy and brittle (region 1). In this region the value of the modulus is in the order of 10^9 Pa for most common glassy polymers. As the temperature increases, the polymer softens, the modulus drops by several orders of magnitude in a narrow temperature range and the polymer undergoes a glass-rubber transition – the glass transition (region 2). This transition happens at temperatures at which the polymer softens because of the onset of long-range molecular motion. Whereas the molecular motion in the rubbery (region 3) and liquid states (region 5) involves many polymer units, molecular motion in glasses is restricted to vibrations, rotations and motions of relatively short parts of polymer chains. The temperatures for which the glass transition occurs varies depending on many parameters like the polymer chemical structure, molar mass, tacticity or pressure among others. It is important to emphasize that the glass transition temperature is by far the most

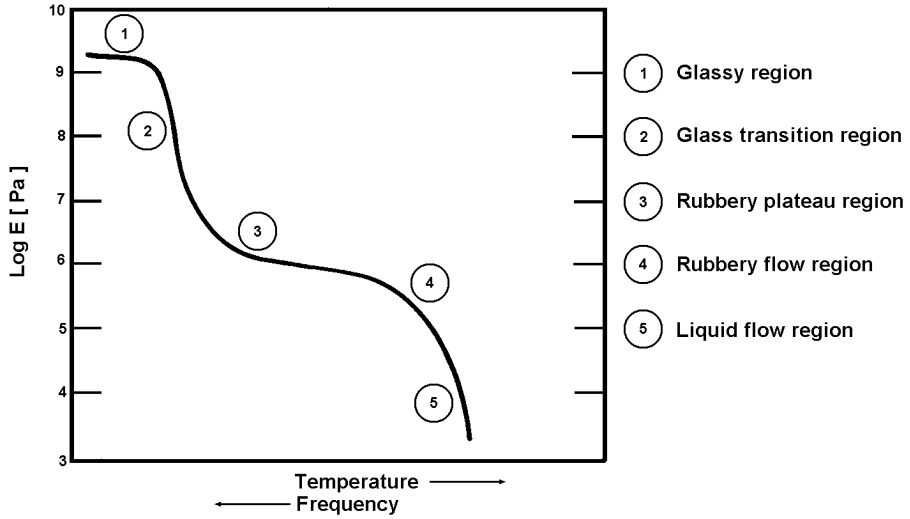

Figure 2. Idealized Young modulus dependence on temperature (and frequency) for amorphous polymers. Main regions and transitions are indicated by numbers and explained in the legend and in the text.

important property used to characterize amorphous polymers and most applications of glassy polymers depend on this parameter. Due to time-temperature superposition, the effects of increasing temperature or decreasing frequency result in similar changes of the mechanical properties.

In the rubbery plateau region (region 3), for linear polymers, the modulus will drop slowly. The molecular motion in this region is governed by the principles of self-diffusion and reptation. The reptation model for polymer chain diffusion was developed originally by Edwards [21] and deGennes [22]. In this model the individual polymer chains can move by local Brownian motion, however they are restricted in their movement by topological constraints of the neighboring chains. This model of polymer chain motion within a hypothetical "tube" defined by the entanglements of the chain with other chains was confirmed experimentally for the bulk [23,24] and at the single macromolecule level [25].

At higher temperatures the rubbery flow region is reached (region 4). In this region the material displays elastic or flow properties depending on temperature or time-scale (frequency) of the experiment. Finally, after increasing the temperature even further, the polymer start to flow displaying liquid-like mechanical properties.

The temperature (or frequency) behavior of the type presented in Figure 2 is one of the main factors, which determine the final application of an amorphous polymer. It is therefore of great interest to understand and more importantly predict this behavior and establish structure-property relationships for glassy polymers. Despite the great technological

significance of such knowledge, one can still find many scientific challenges in the physics of the glassy state or in the glass transition phenomena.

Despite the fact that the glass transition has been studied for many years, it is still a challenging subject of interest from a scientific and technological point of view. Common methods used to observe the glass transition are dilatometry, various types of thermal (like differential thermal analysis - DTA), mechanical (e.g. dynamic mechanical spectroscopy – DMS) or dielectric methods. The main question concerning the glass transition is how molecular motion is arrested in the glassy state to result in slow dynamics. At high temperatures the viscosity (η) of polymers follows the well-known exponential Arrhenius behavior:

$$\eta \propto \exp\left(\frac{\Delta E}{k_B T}\right), \tag{1}$$

where ΔE is the energy barrier associated with polymer flow. If crystallization of the polymer cannot take place, upon cooling a supercooled liquid is obtained. When decreasing the temperature further, measurements of the temperature dependence of viscosity (η) and related time-scales involved in long-range polymer motion show non-Arrhenius behavior known as the Vogel-Fulcher law:

$$\eta = \eta_0 \exp\left(\frac{B}{T - T_0}\right), \tag{2}$$

where η_0 is the viscosity at the T_0 temperature (the Vogel-Fulcher temperature) and B is an empirical parameter. At the glass transition temperature (T_g) the viscosity increases by orders of magnitude and the polymer chain motion become slow compared with the experimental time-scales i.e. the liquid forms a glass. Additionally, the glass transition is marked by discontinuities in the thermodynamic quantities which are the second derivatives of free energy i.e. entropy, heat capacity and volume. Therefore, the glass transition is reminiscent of a second-order thermodynamic phase transition. Entropy is not an experimentally measurable quantity, however determination of the heat capacity and volume changes during thermal treatment is a common way to evaluate the glass transition temperature by calorimetry or dilatometry.

Unlike ordinary phase transitions, occurring at a well-defined temperature, the glass transition temperature depends on the time-scale of the experiment. It is usually defined in terms of the viscosity, which at T_g reaches a value of 10^{12} Pa s. The size of polymer chains implies a large number of degrees of freedom, which can give rise to molecular motion

encompassing many decades of time units and happening on a broad range of length scales. Relaxation of polymers is often interchangeably used with molecular motion. The relaxation phenomena involve environmental friction resistance and polymer bond rotational motions. The relaxation time is in this respect referred to the time it takes for the polymer chains to respond to temperature, pressure changes or external mechanical perturbations. At T_g, defined above by viscosity, the relaxation times associated with the main-chain long-range motions, connected to viscous flow (the so called α–relaxation processes), are in the range of 10 seconds. When cooling a glass forming liquid to below T_g, the system no longer reaches thermodynamic equilibrium on the experimental time-scale. Although main-chain long-range molecular mobility (α-relaxation) is relatively suppressed in polymers below T_g, still, small-scale backbone fluctuations are possible through main chain rotations, vibrations or flips (like the Schatzki crankshaft rotation). Such secondary relaxation processes, commonly referred to as the Johari-Goldstein β relaxation, are usually associated with the motion of polymer side groups rotating around the bond linking them to the main chain and to the localized motions of subunits within the side groups [26]. The frequency dependence of the α and β processes in polystyrene is presented in Figure 3. For the α process responsible for the glass transition one can obtain the usually reported glass transition temperature of 100 °C by taking the defined 10 s relaxation time at T_g. The secondary relaxations are believed to involve a non-cooperative molecular motion and the assignment of a particular secondary relaxation process (like β, γ, etc.) to a specific type of motion will depend on the polymer used. Such short-scale, localized motions can have profound influence on the macroscopic properties of polymers below the glass transition temperature like toughness, impact strength and influence polymer aging.

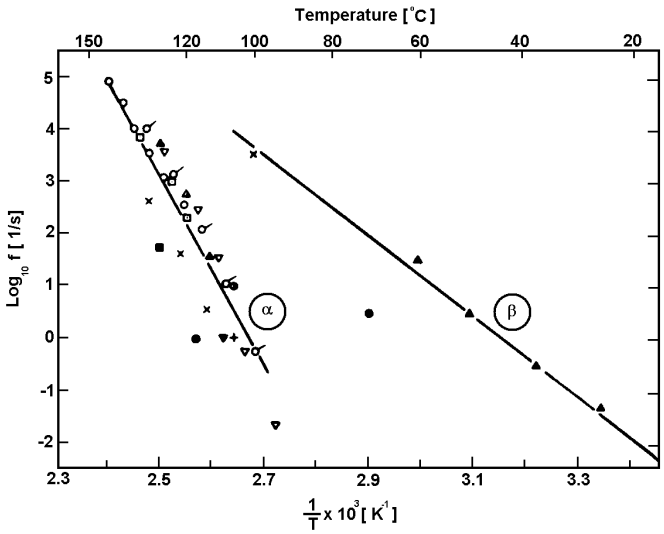

Figure 3. Frequency dependence of the α and β transitions as a function of temperature for polystyrene. Different symbols indicate work of different researchers. Figure adopted from Sperling [2].

Above the glass transition temperature the secondary β-relaxation process splits from the α-relaxation process and follows an Arrhenius behavior below T_g, at which the α-relaxation processes are frozen. Until now there is no satisfactory explanation of the splitting of one high temperature relaxation process into two processes: the α or cooperativity process and the local β or Johari-Goldstein process [27]. Some interpretations based on the potential energy surface concepts have been put forward [5], however no experimentally proven mechanisms are known to date.

As mentioned, at present there is still no generally accepted theory of the glass transition. Several attempts to describe the glass transition include the free volume concept, kinetic and thermodynamic treatments. The mode-coupling theory and models that consider segmental cooperativity are widely discussed [9]. However, as mentioned in the introduction the mode-coupling theory appears to be useful only at temperatures tens of Kelvins above T_g and breaks down at molecular time-scales of orders of 10^{-9} s.

The idea behind cooperativity models, introduced by Adam and Gibbs [28], oscillates around the assumption of the existence of a certain characteristic length scale for which the relaxation may take place only when a number of particles rearrange collectively. Close to T_g this length scale is estimated to be in the range of 1-2 nm for polymers [29]. The increase of relaxation time observed as the glass transition temperature is approached from above comes from the increase in size of the cooperatively rearranging regions (CRR). To ensure a Vogel-Fulcher dependence of the relaxation time and viscosity of the system, η and τ should depend on the number of particles, or chain segments, which have to move within the cooperatively rearranging regions. Specifically Adam and Gibbs proposed that at the molecular level the dependence of the viscosity or relaxation time is given by:

$$\eta(T), \tau(T) = C \exp\left(\frac{Z^* \Delta\mu}{k_B T}\right), \tag{3}$$

where C is a constant – a frequency factor, Z^* is the number of molecules in CRR and $\Delta\mu$ is the energy barrier for the single molecule to move. The non-Arrhenius behavior is a direct consequence of the increasing size of the CRR at low temperatures. In the absence of cooperativity (Z^*=1) equation 3 reduces to the Arrhenius equation (equation 1).

In close connection to CRR are the so-called dynamical heterogeneities in supercooled liquids [30,31]. For times shorter than the structural relaxation time (α-relaxation) the polymer systems are found to be composed of dynamically distinct regions of highly correlated motion. In other words, the dynamics in one region in space can be different than in another located a few nanometers away. In fact, the upper limit for the size of the CRRs is

considered to be the length scale of the dynamic heterogeneity. As the temperature decreases, the size of dynamic heterogeneities as well as CRR increases. One of the consequences of such a picture of polymer dynamics near T_g is the nonexponential character of the ensemble averaged relaxation processes resulting in a KWW (Kohlrausch-Williams-Watts) response function $\Phi(t)$:

$$\Phi(t) = \exp\left[-(t/\tau)^{\beta}\right], \tag{4}$$

where β is the nonexponentiality parameter related to the distribution of relaxation times. Spatially heterogeneous dynamics was witnessed experimentally by NMR [30] or by dielectric hole burning [32]. However, the time and length scales associated with the spatially heterogeneous dynamics and its relation with the CRRs still remain a main topic of investigations.

The concept of free volume was widely used in interpreting phenomena associated with the glass transition and polymer dynamics [33-35]. Free volume theories are based on the assumption that liquids contain a certain amount of excess space unoccupied by the polymer, which is available to permit thermal motion of polymer chains. Free volume (V_f) is usually defined as the difference between the total volume (V_t) and the occupied volume (V_0) by the polymer molecules:

$$V_f = V_t - V_0 . \tag{5}$$

It should be noted here that there is a lack of a precise definition of the occupied volume. This makes a quantitative application of free volume difficult. One of the definitions of V_o is that it is the fluctuation volume swept by the center of gravity of the molecules as a result of thermal motion [36]. The important aspect of the free volume concept is that it can confer upon the amorphous polymer a large mobility even after the polymer is turned into a glass upon cooling. It is argued that the fractional free volume V_f / V_t can be written as a simple linear function of temperature

$$\frac{V_f}{V_t} = f_g + \alpha_f (T - T_g), \tag{6}$$

where f_g is the fractional free volume at the glass transition T_g and α_f is the expansion coefficient of the free volume. If there is a simple relationship between the free volume and viscosity η of the form (the Doolittle equation):

$$\eta = a \exp\left(\frac{bV_t}{V_f}\right), \tag{7}$$

where *a* and *b* are constants, then the Vogel-Fulcher relationship can be recovered.

Early work by Simha and Boyer led to the suggestion that the glass transition point is an iso-free volume state. For infinite molecular weight the free volume could be expressed above T_g as:

$$V_f = K + (\alpha_R - \alpha_G)T\,, \tag{8}$$

where K is the free volume at 0 K, and α_R and α_G are the volume expansion coefficients in the rubbery and glassy states, respectively. According to Simha and Boyer, at T_g the free volume can be defined as:

$$V_f = V_t - (V_{0,R} + \alpha_G T)\,. \tag{9}$$

By substituting the quantity:

$$V_t = V_{0,R} + \alpha_R T\,, \tag{10}$$

into equation 9, Simha and Boyer concluded that the free volume at the glass transition temperature is a constant.

$$(\alpha_R - \alpha_G)T_g = K_1 = 0.113\,. \tag{11}$$

From a number of experiments K_1 was evaluated to be equal to 11.3 %. However, this value is relatively large and in fact the largest proposed in the literature. Other numbers for the free volume fraction at the glass transition include 0.025 (from the Williams-Landel-Ferry equation) or 0.08 (from the work of Hirai and Eyring). The large discrepancies between the reported values indicate the need for further studies of amorphous polymer microstructure. At the moment free-volume theories of the glass transition, although appealing, need to be refined and new theoretical concepts should be developed.

A natural extension of the concept of free-volume is to consider the distribution of free volume size resulting in nonuniform local density and subsequently to local density fluctuation, which can be detected for example by X-ray scattering techniques [37]. Such treatment allowed explaining for example the experimentally observed isothermal volume relaxation in polymers.

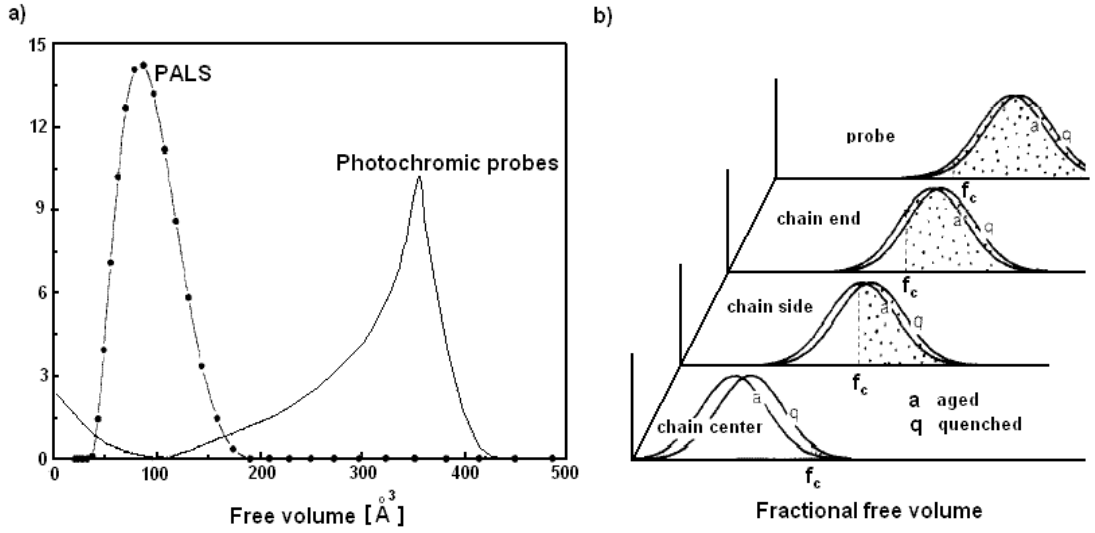

Figure 4. a) Free volume distributions as determined by PALS and photochromic probes studies. Figure adopted from Liu et al. [38]. b) Free volume distribution determined by fluorescent probes at different locations along the polymer chain. Figure adopted from Yu et al. [39].

To estimate the amount of free volume in glassy polymers, different techniques like small angle X-ray scattering [37,40], light scattering (both through thermal density fluctuations [41,42]), photochromic probes and labels [39,43], fluorescence spectroscopy [44], dilatometry [34], positron annihilation lifetime spectroscopy (PALS) [45-48], specific volume experiments [49] or theoretical model calculations [50] were employed. The size of free volume in polystyrene was found to be of the range of 4 to 4000 Å^3, depending on the technique used in the investigations. The free volume size distributions in polystyrene were investigated by using photochromic and fluorescent probes [51,52] and positron annihilation lifetime studies [38]. In Figure 4a we show the comparison of the free volume distributions obtained with two different techniques (PALS and fluorescence probe). There is a quite obvious discrepancy in the measured values. The free volume measured by PALS was found to be much smaller than that measured by fluorescent probes. Yu et al. [39] have additionally found that the free volume associated with different sites along a polymer chain can be different (Figure 4b), therefore adding an additional level of complexity involved in the free volume distributions and pointing towards the necessity to locally probe the free volume properties of amorphous polymers without being obscured by ensemble averaging.

In summary, the results of the reported free volume studies have contributed to a qualitatively self-consistent free volume concept, yet quantitative aspects of the free volume, its distribution and local dynamics still remain to be solved. Also a more direct knowledge of the microstructure of amorphous polymers is needed to verify the main assumptions made in the derivations of the free volume theories. To resolve the questions related to the free-volume concepts new experimental techniques are needed.

2.4 Polymers at interfaces

2.4.1 Interfaces

Surfaces and interfaces are unavoidable attributes of materials. To design a highly functionalized surface it is usually necessary to control surface structure, and to reveal the degree of molecular motions near the surface regions, which in turn can be very different than in the bulk [53-55]. The physical properties at the solid substrate interface, or at the free surfaces of glassy polymers, are important for many materials engineering applications like coatings, adhesives, biomaterials or microelectronics among many others [56-60]. One of the well-known examples is the buffing process of polyimides widely used as components in flat panel displays [61]. X-ray scattering experiments demonstrated that the polyimide chains near the surface are very well aligned after the buffing. However, the glass transition temperature for this polymer is equal to 350 ºC and the buffing is usually done at room temperature. The fact that any orientation of the polymer chains was found and that this orientation propagates at most 100 Å into the film suggest that for polyimides the properties, especially the mobility, at the surface are different form the bulk. Enhancement of the mobility is an indication that the relaxation times for the system are changed and that the surface exhibits different thermal properties than the bulk.

2.4.2 Polymer dynamics near free interfaces

In 1992 Meyers et al. [62] in their report entitled: "Is the molecular-surface of polystyrene really glassy?" investigated pattern formation on a polystyrene surface when scanned with an AFM tip. They concluded that the polystyrene near the surface behaves more like a material exhibiting rubber elasticity than like one in the glassy state and postulated that the polymer chains possess an extra degree of freedom at the surface. A fundamental question however remains: How does the lack of mirror symmetry at a polymer interface influence the conformation and/or dynamics of the polymer chains?

A series of experiments employing various techniques based on Atomic Force Microscopy aiming at evaluating the dynamics at polymer surfaces were reported [63-65], however no conclusive results were found [66]. Kajiyama et al. used scanning viscoelasticity microscopy (SVM) and lateral force microscopy (LFM) [69] techniques where the dynamic properties at the sample surface can be evaluated by measuring the amplitude of the modulated deformation of the sample and the phase lag between the modulation-signal. These authors found that T_g at the surface decreases with a decrease of the polymer chain length and that this dependence is stronger than that found for T_g in the bulk. Similar results were obtained

by lap shear and friction force measurements [70]. These reported results have clearly shown that the polymer properties at their interfaces are different than in the bulk.

It is not clear, however, how far into the sample the surface effects could propagate, mainly because there are only few techniques that could be used to perform depth-dependent studies. Molecular dynamics simulations of free surfaces of glassy polymers showed [71] surface enhancement in bond and atomic mobilities compared to the bulk, and sigmoid density profiles decaying over a 0.7 nm thick region were observed. X-ray photoelectron spectroscopy studies (XPS) showed that the T_g at the surface of PS was lower than the bulk value and decreased as the analytical depths came closer to the outermost surface [72]. Contradictory results were found in the investigations of polymer surfaces by positronium annihilation lifetime spectroscopy (PALS). The measurements of Xie et al. [73] showed no indication of surface-enhanced mobility. However, subsequent reports by DeMaggio et al. showed [74] a reduction in the void expansion during thermal treatment, which was correlated to a reduction in the apparent T_g as film thickness decreased. Similar work was performed by Jean et al. [75], who calculated the depression of the glass transition at the surface from the WLF equation. Relating the free volume fraction obtained by PALS, to the T_g by a semi-empirical equation, they found a depression of several tens of degrees for the 2-20 Å top surface layer. The same research group used another method of positron annihilation, Doppler broadening of energy spectra (DBES) of annihilation radiation coupled with a slow positron beam, to investigate T_g near the surface of PS [76]. The DBES study showed significant T_g depressions from 50 Å to about 500 Å from the surface.

The amount of experimental evidence for modified surface dynamics is still sparse. Careful depth profiling on the segmental scale was not performed due to the lack of appropriate experimental techniques, as mentioned. Due to the high impact of the properties of polymer surfaces in technological applications, especially in the microelectronic industry using thin polymer photoresist films, in-depth examination of the possible gradients in polymer properties from the surface to the bulk should be performed. Results obtained from such investigations will help to understand the behavior of glassy polymers when confined into nanometer-scale structures.

2.5 Polymers in confinement

The number of applications of polymers with structures possessing dimensions in the nanometer range is steadily growing. Although the trend is generally towards the preparation of geometrically complex structures, our understanding of the influence of the dimensions of the particular system on the polymer structure or dynamics remains relatively poor. For many

applications it is important to perform a check whether the nanoscale material will differ substantially in properties from the bulk values. For example, the stability of polymer films will limit the thickness of polymer resist films for photolithography in the semiconductor industry. Polymer nanospheres are attractive materials for medical or advanced photonic applications. Nanoscale polymer fibers are used in separation technologies, in sensing, electronics and tissue engineering. Also for these materials it is important to assess dimension-dependent properties. Finally, the glass transition behavior for single, isolated macromolecular chains is of great interest in the physics of protein folding (for a review see [77]). Du et al. [78] showed on a cubic lattice model that the way proteins approach their native state can depend on the underlying geometry in the semicompact globular state after passing the freezing transition. Therefore, confining proteins into specific geometries might strongly influence the folding mechanism and/or kinetics.

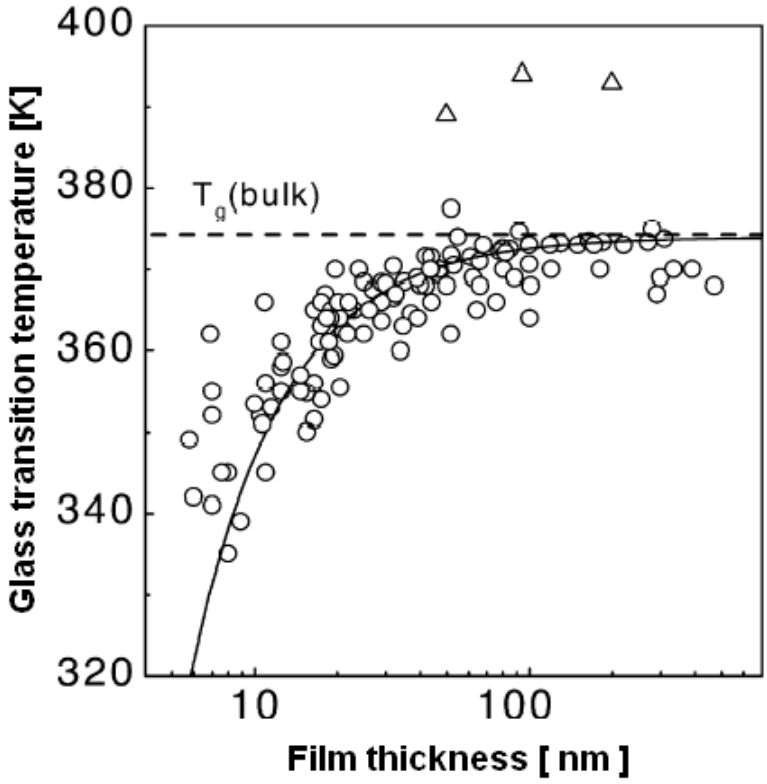

Figure 5. Glass transition temperatures of thin supported PS films compiled from many different studies. The results obtained by Wallace et al. [79] are also presented as open triangles. The dashed line indicates the bulk glass transition temperature. The solid line is the fit to the empirical equation obtained by Keddie et al. [80] (equation 12).

From all properties investigated, the glass transition in thin polymer films received the most attention. The large number of experimental studies of polymer behavior in thin film geometries was dictated mainly by the technological relevance of thin polymer films. Thin films can be prepared with a broad range of thicknesses ranging from several nanometers to micrometers using, for example, spin-coating techniques. The thickness of the resulting films can be easily adjusted to cross the radius of gyration of the polymer chains, therefore thin film geometry allows one to study the chain confinement effects. In a pioneering work Keddie et al. measured the glass transition temperature of thin polystyrene films as a function of film thickness [80]. When the films were thinner than about 100 nm, substantial reductions in T_g were apparent (Figure 5). Films made of PS with molar masses from 120 kg/mol to 2900 kg/mol were investigated, however no dependence of the T_g reductions on the molar mass was found. Thus, the reduction of the T_g for supported Ps films could not be associated directly with the polymer chain dimensions e.g. to the radius of gyration of the polymer chains. The results obtained by Keddie et al. could be described by a single empirical relation of the form:

$$T_g(h) = T_g(bulk)\left[1 - \left(\frac{\delta}{h}\right)^{\xi}\right], \tag{12}$$

where $T_g(h)$ is the measured glass transition temperature for a film with thickness h, and δ, ξ are fitting parameters. Because the reduction of T_g was found for films with thickness values much larger than the size of CRR, the changes in T_g could not be related to finite size effects. Such effects are believed to play a substantial role when the investigated system is confined into dimension close to the CRR size e.g. in porous glasses [81] or layered silicates [82]. It was suggested that the observed reduction in T_g is rather the result of the existence of a polymer surface layer with a characteristic size, where the chain dynamics is enhanced compared to the bulk. The size of the liquid-like layer was estimated to be 80-130 Å.

A similar decrease of T_g for thin supported films was also found for many different systems like poly(methyl methacrylate) (PMMA) on hydrophobic glass substrates [83], polycarbonate [84] or polysulfone [85] and by using a number of different techniques like ellipsometry [86], positron annihilation [74] or dielectric techniques [87]. A compilation of the results for thin PS films is presented in Figure 5. It should be noted that not all experiments showed a decrease of the glass transition for PS in thin films. Wallace et al. used X-ray reflectivity [79] to measure the thermal expansion of thin polystyrene films, and reported observations of elevation of the T_g when decreasing the film thickness. The results of their study are plotted also in Figure 5 for comparison. Soon it became clear that the chemistry of the substrate surface and therefore the strength of interactions between the substrate and the polymer might substantially influence the glass transition [88]. Strong adsorption of the chains can lead to a

highly distorted chain conformation, which would influence the chain mobility and expansion. Monte-Carlo simulations [89] of the influence of hard walls on the structure of some polymer glasses have shown that for strongly supercooled melts the perturbation introduced by the presence of the walls penetrates into the bulk and decays on a length scale which can be larger than the radius of gyration. To explore the effect of attraction/repulsion of the surface Keddie and Jones examined films composed of chains covalently attached to the substrate at one end [90]. They obtained and compared T_g in ultrathin (10 nm) films of PS on SiO_2, PS-COOH grafted to the substrate and PS-COOH just spin coated onto the substrate. In case of PS-COOH they observed an increase in T_g with decreasing thickness, regardless of the substrate. Also for PMMA films deposited onto a native oxide coating of Si wafers the measured T_g values increased with decreasing film thickness. Strong interaction between PMMA and the substrate due to hydrogen bonding was assumed to be responsible for the observed elevation of T_g. Poly(2-vinylpyridine) (P(2)VP) on an acid-cleaned Si substrate is considered as a system exhibiting much more favorable interactions with Si than those for PMMA on the same substrate. It was found that the magnitude of the shifts to higher glass transition temperatures for P(2)VP is indeed much larger (>50 ºC for a 7.7 nm film) than those found for PMMA, or any other system [91]. The details of the interaction between the polymer and the substrate are important. Both a decrease [92] and increase [93,94] of the glass transition for liquids and polymers confined in nanoscale pores were reported. For pores with diameters smaller than 2 nm there was no detectable glass transition at all. In many cases there is evidence that the confined polymer adopts a layered structure normal to the pore walls. Neutron scattering experiments on the dynamics of poly(dimethylsiloxane) (PDMS) in nanoscale pores showed two counteracting effects: acceleration of dynamics at the pore centers and a reduction of the mobility near the walls [95].

If no strong interactions between the polymer and the substrate are present, for supported polymer films there is a widespread agreement that reduced dimensions of the films will cause a decrease of the glass transition temperature. Among different explanations of such a behavior, like changes in polymer density, degree of entanglement or chain confinement effects, considerable attention was paid to the influence that a free polymer surface would have on the measured T_g of thin films. For a reliable evaluation of the glass transition in thin polymer films it is necessary to take into account the effects of individual interfaces, each influencing the chain dynamics in its own way. We have discussed earlier that there is experimental evidence that the polymer dynamics at the free polymer surface is different than the dynamics found in the bulk. The inherent asymmetry of supported thin films is the main source of concern when one wants to understand the effect of individual interfaces on the dynamics of polymer films. To investigate finite size effects, without being hampered by the presence of substrates, the influence of surfaces should be separated from the internal structural characteristic of the film. One is able to eliminate the substrate entirely and

measure the T_g of symmetric freestanding films. Such films provide an ideal sample geometry because they are symmetric with respect to the mid-plane of the film and no substrate-polymer interactions are present.

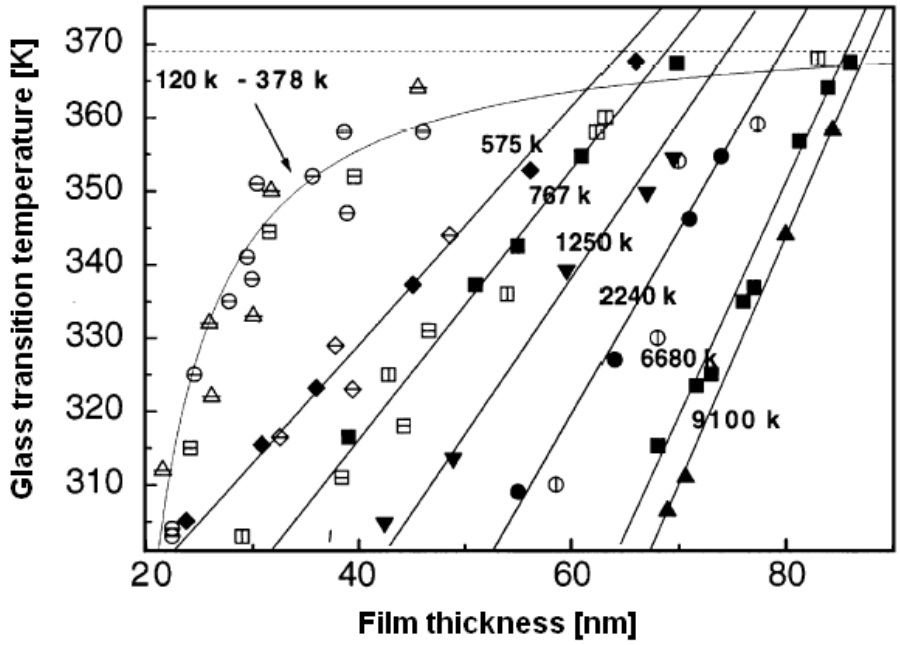

Figure 6. Glass transition temperature for freestanding polymer films [86,96,97]. Note the molar mass dependence of T_g as a function of film thickness. The dashed line indicates bulk T_g. Straight black lines are linear fits to the data obtained for different polymer molar masses (Equation 13). The gray line is the fit to the empirical equation obtained by Jones et al. (Equation 12). Solid symbols represent data obtained by ellipsometry [96] and hollow symbols represent data obtained by BLS [86,97].

Forrest et al performed first measurements of T_g for thin freestanding PS films with thickness values between 20 an 200 nm [98]. They used the Brillouin Light Scattering (BLS) technique, which probes the elastic properties through observation of film-guided acoustic phonons [99]. The results obtained for freestanding PS films for different polymer molar masses are shown in Figure 6. In contrast to supported thin films, the T_g of thin freestanding films below a certain critical thickness value was a linear function of the film thickness for higher molar masses and could be described with an empirical relation:

$$T_g(h) = \begin{cases} T_g(h)\left(1 - \dfrac{(h_0 - h)}{\rho}\right), & h < h_0 \\ T_g(bulk), & h \geq h_0 \end{cases} \qquad (13)$$

where h_0 is the critical film thickness and ρ is a fitting parameter. The strong molar mass dependence observed in these studies revealed also the importance of chain confinement effects. Additionally, a much larger critical film thickness effect was observed for freestanding films and the value of h_0 was found to be twice as large as in supported thin films. This effect was attributed to the influence of the free interfaces, now confining the structure from both sides of the sample. Recently, Sharp and Forrest [100] compared the T_g of films capped from one and from both sides (Figure 7) and showed that the free surface is indeed responsible for the decreased glass transition for the case studied. It should be kept in mind that the use of freestanding polymer structures is rather limited and that supported polymer films are much more widely used in many different technologically relevant applications. Nevertheless, freestanding polymer films will remain an attractive choice for fundamental thin film studies.

Although the amount of experimental data reported for polymer thin films is large, studies of thermal or dynamic properties of nanoscale polymer fibers or spheres are sparse. Large surface areas and chain confinement effects thought to be responsible for larger glass transition depression for freestanding films are also to be excepted for polymer spheres. Polymer microspheres are usually prepared by microemulsion polymerization (chemical route) or by atomizer spraying [101] or freeze-drying [102] (physical route).

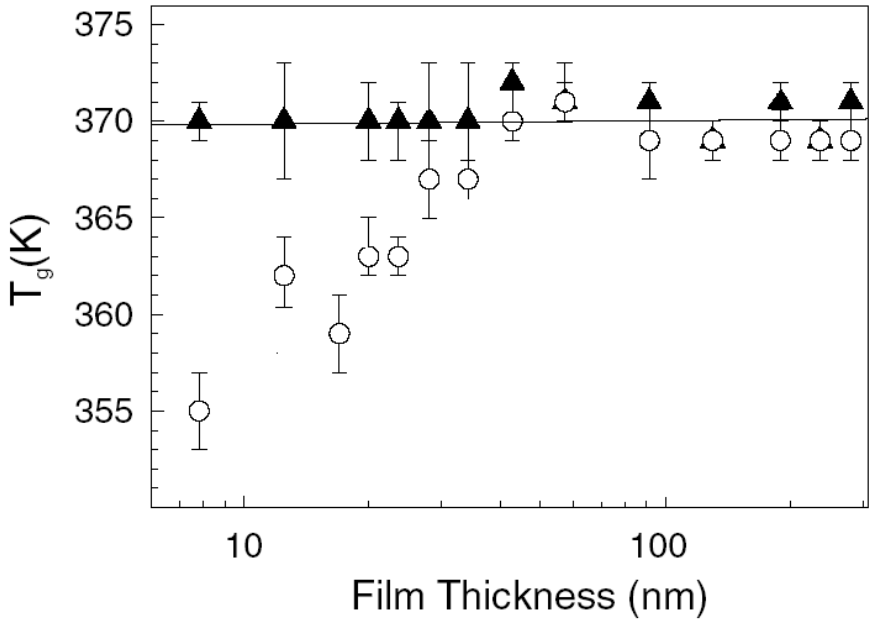

Figure 7. T_g values for supported (○) and capped (▲) PS films. The presence of free surface causes the depressions in the glass transition temperature [100].

Large T_g reductions of up to 64 K were found for small (20-60 nm) polystyrene particles prepared by freeze-drying [101,102]. It has been suggested that these result are due to the highly nonequilibrium chain conformation present directly after preparation, which causes the chains to collapse first and then aggregate [102,103]. Early reports on the glass transition temperature in polystyrene nano- and microspheres showed no significant changes of the T_g. In these studies the T_g was determined by calorimetric methods. Additional exotherms during the first heating scans were observed, probably due to the loss of surface area due to coalescence [104-107]. To avoid coalescence, Sasaki et al. [103] presented calorimetric studies of the glass transition of polystyrene spheres in aqueous suspensions. Although they found a value of the glass transition temperature close to the bulk T_g, the heat capacity jumps observed at the transition decreased with smaller sphere diameters. The changes in the heat capacity were attributed to the presence of a liquidlike surface with significantly faster dynamics. The thickness of this layer was estimated to be 4 nm and was very similar to the one found for supported [84] or free-standing [108] polystyrene films.

The main problem in investigations of polymer nanofibers is that the fibers after preparation are usually far away from equilibrium and there is a significant amount of stresses present in the fibers induced by the preparation technique. Annealing of such structures present a challenge hard to overcome. Increasing the temperature to above the glass transition, or melting temperatures causes shape deformation and the system cannot be defined as fibrous anymore. Kim and Lee [109] reported a lower T_g for a variety of electrospun polyesters, however they attributed this observation to the decrease of the molar mass of the polymer chains due to the electrospinning process, or thermal degradation during T_g determination. It remains a challenge form the experimental point of view to probe such structure and new experimental techniques are needed.

2.6 Segmental mobility in polymer films

Many investigations of the glass transition temperature in thin films using a number of different techniques were reported to date. Most of the results obtained showed a similar trend for a variety of polymers: a decrease of the glass transition temperature with decreasing film thickness. The changes in T_g were associated usually with the effects of the interfaces. However, several problems remained unresolved. It is for example unknown how deep the interfaces can affect the polymer dynamics or whether the transition from the surface to the bulk is smooth or abrupt. Also the question whether the size of the surface region is a function of temperature and film thickness is still open [84]. Although for smaller and smaller structures one can expect that the free surface will have a greater impact on the whole structure dynamics, the results reported for polymer spheres and single polymer chains do not give a direct answer to this problem. In particular it is of interest to know how the free

surfaces affect the segmental scale dynamics in polymers. Measurements of the glass transition are an indirect probe of the dynamics in polymer films. To study directly the segmental scale relaxation processes, different approaches have been taken, which will be briefly reviewed below.

Diffusion of polymer chains is directly related to the segmental relaxation processes. However, it is important to mention that chain mobility requires much larger motion, e.g. reptation, than the segmental motion required for the glass transition to occur. Studies of lateral diffusion of PS chains in thin films performed by Frank et al. [110] using fluorescence recovery after patterned photobleaching (FRAP) showed a decrease in the lateral diffusion constant and hence lower mobility for films with a thickness below 1500 Å, representing a distance equal to 25 R_g for the polymer studied. The diffusion coefficient fell into two regimes. For films with thickness values approaching 1500 Å from above the diffusion coefficient was independent from the film thickness with an average value the same as in the bulk. As the film thickness decreased below 1500 Å the diffusion coefficient decreased. For the smallest thickness investigated (500 Å) the diffusion coefficient differed by a factor of two from the one obtained for the film of 1500 Å thickness. These results suggest that the polymer chain dynamics is suppressed in the films investigated and therefore the glass transition is increased, in sharp contrast to the previous reports on T_g of thin supported PS films. However it was stressed that in order to use chain diffusion studies to compare T_g values, it is the temperature dependence of the diffusion coefficient, which should be measured because the long-range diffusion of polymer chains might be decoupled from local segmental mobility for thin films where the chains can be effectively pinned to the substrate. Such studies have not been performed to date.

Another approach to study the segmental scale dynamics of polymers is to introduce molecular probes into the polymer matrix. The mobility of the probes is related to the amount of free volume present in the polymer and to the mobility of the matrix itself, therefore to the viscosity. The diffusion behavior of the tracers is then translated into polymer dynamics. However, as simple as it seems, the results obtained by monitoring probe diffusion in thin films reported in the literature are quite contradictory. Hall and Torkelson [112] used small molecule probe translational diffusion to study the mobility in thin supported films and found that the substrate does not affect segmental mobility at distances greater than 400 Å. Small-molecule translational diffusion in thin polymer films studied by fluorescence nonradiative energy transfer (NRET) [113] also suggested that there is little or no change in diffusion behavior of the probes as film thickness decreases from 1500 Å down to 30 Å.

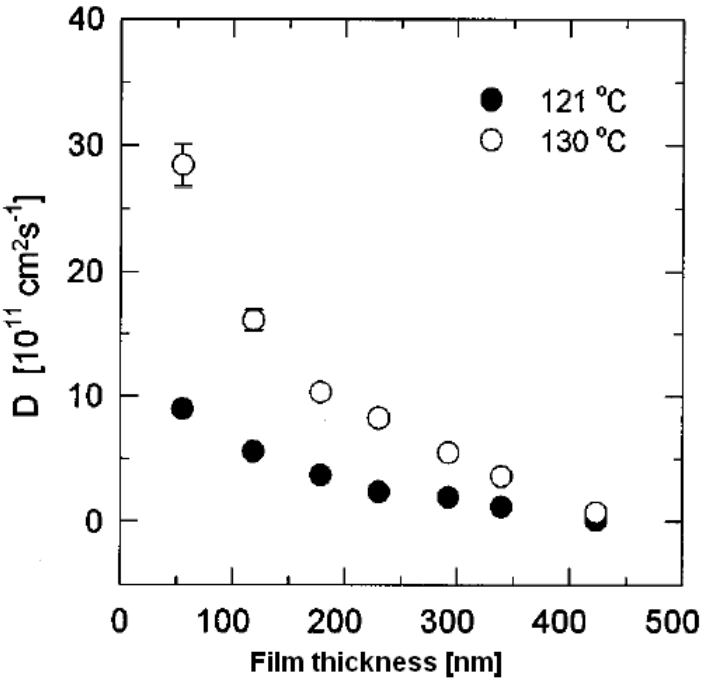

Figure 8. Diffusion coefficient D of a molecular tracer in PS films as a function of film thickness [111].

However, the results reported by Tseng, Turro and Durning [111] showed that the tracer in-plane diffusion coefficient, at temperatures above T_g, increases above the bulk values as the polymer film thickness decreases towards R_g. Surprisingly, the changes in the diffusion coefficients were first appearing in films with thickness of 20 R_g (Figure 8), i.e. at a length scale much larger than the thickness for which any changes in T_g were previously reported (usually in the range of 3-5 R_g). The increase of the diffusion coefficients reported by Tseng et al. was explained by the segregation of the dyes in the supposed liquid layer at the free surface. The thickness of the surface layer with dye mobility 10 – 100 times greater than that in the bulk was estimated to be 1-3 nm. To study the segmental scale relaxation in polymers, Hall, Hooker and Torkelson [114] employed second harmonic generation (SHG) using non-linear Disperse Red 1 optical dyes and subsequently monitored the chromophores reorientation in time. These authors did not observe any trend in the average relaxation time with the film thickness. Since segmental relaxation is a strong function of T-T_g, they concluded that there is no change in T_g from the bulk value as thickness decreases from 10000 Å to 70 Å. However, in the same study a large broadening of the relaxation distribution functions for thin films (230 Å) was observed. This could be caused by changes in the segmental-scale heterogeneity in the polymer matrix.

Clearly, methods used to estimate the segmental scale polymer dynamics based on tracer diffusion need more in-depth and systematic investigations. A better insight into molecular level diffusion processes in polymers is also needed as the probe size, shape and chemical

structure can play an important role. Additionally, the presence of dynamic heterogeneities, their characteristic length- and time-scales should also be taken into account.

Fukao and Miyamoto [87] performed an investigation of the relationship between the thickness dependence of T_g and of the dynamics of the α-process near the glass transition through dielectric measurements on thin PS films. The thickness dependence of the width of the dielectric loss peak of the α-process was closely related to T_g and this width was monotonically increasing with thickness for films below 100 nm. The peak position of the dielectric loss remained almost constant and started to decrease only after a critical thickness was reached. This critical film thickness was strongly dependent on the molar mass of the polymer and was related to the radius of gyration of the bulk polymer coil. These intriguing observations should be studied further with complementary techniques which are able to probe the distribution of relaxation functions in thin polymer films.

In studies of the segmental scale relaxation processes in thin polymer films large discrepancies have been reported. Additionally, no agreement on the critical thickness values has been reached. Modified dynamics was found for a broad range of film thickness values ranging from R_g to 25 R_g depending on the experimental technique used. Clearly, additional experiments are needed to obtain an adequate insight into the effects a confinement has on segmental scale dynamics in polymers. Additionally a deeper understanding of molecular level diffusion in polymer matrices and in thin films is technologically relevant for example in lithographic applications.

2.7 Conclusions

Despite the large amount of experimental information available, our understanding of the structure of polymer glasses at the scale of segments remains relatively poor. Additionally, properties of polymers confined into nanoscale dimensions can be substantially different than in the bulk. If progress is to be made in our understanding of the structure and dynamics of amorphous polymers, and of the effects of the confinements, new experimental techniques to probe polymers on the nanoscale must be developed. Such techniques should not only be sensitive to the segmental scale polymer mobility but because of the complexity of the investigated systems it is also required that they must provide results not obscured by the average properties of the investigated systems. For example, the new experimental approaches must be capable to depth-profile thin polymer films to investigate the anticipated free surface effects. It is our intention to show in the next and subsequent Chapters of this Thesis that single molecule detection is just such a technique.

2.8 References

[1] Gedde, U. W. *Polymer Physics*; Chapman & Hall: London, 1995.

[2] Sperling, L. H. *Introduction to Physical Polymer Science*; Wiley-Interscience: New York, 1986.

[3] Jones, R. A. L. *Soft Condensed Matter*; Oxford University Press: Oxford, UK, 2002.

[4] Greer, A. L. *Science* **1995**, *267*, 1947.

[5] Stillinger, F. H. *Science* **1995**, *267*, 1935.

[6] Frick, B.; Richter, D. *Science* **1995**, *267*, 1939.

[7] Stein, D. L.; Palmer, R. G. *Phys. Rev. B* **1988**, *38*, 12035.

[8] Angell, C. A. *J. Res. Natl. Inst. Stand. Technol.* **1997**, *102*, 171.

[9] Gotze, W.; Sjogren, L. *Rep. Prog. Phys.* **1992**, *55*, 241.

[10] Haward, R. N.; Young, R.J. *The Physics of Glassy Polymers*, 2nd ed.; Chapman & Hall: London, UK, 1997.

[11] Mitchell, G. R. In *Order in the Amorphous State of Glassy Polymers*; Keinath, S. E., Miller, R. L., Rieke, J. K., Eds.; Plenum Press: New York,1987.

[12] Fitzpatrick, J. R.; Ellis, B. In *The Physics of Glassy Polymers*; Haward, R. N., Ed.; Applied Science Publishers: London, 1973; Chapter 2.

[13] Wignall, G.; Ballard, D. G. H.; Schelten, J. *J. Macromol. Sci., Phys.* **1976**, *B12*, 75.

[14] Schmidt-Rohr, K,; Spiess, H. W. *Multidimensional Solid-State NMR and Polymers*. Academic Press: London, 1994.

[15] Flory, P. J. *J. Chem. Phys.* **1949**, *17*, 303.

[16] Boyer, R. F. In *Order in the Amorphous State of Glassy Polymers*; Keinath, S. E., Miller, R. L., Rieke, J. K., Eds.; Plenum Press: New York, 1987, pp 135.

[17] Flory, P. J. *Principles of Polymer Chemistry*; Cornell University Press: Ithaca, NY, 1953.

[18] Privalko, V. P.; Lipatov, Y. S. *Makromol. Chem.* **1972**, *175*, 641.

[19] Yeh, S. H. *J. Makromol. Sci. Phys.* **1972**, *6*, 451.

[20] Pechhold, W.; Hauber, M. E. T.; Liska, E. *Kolloid Z. Z. Polym.* **1973**, *251*, 818.

[21] Edwards, S. F. *Proc. Phys. Soc. London* **1967**, *92*, 9.

[22] deGennes, P. G. *Scalling Concepts in Polymer Physics*; Cornell Univ. Press: Ithaca, NY, 1979.

[23] Green, P. F.; Kramer, E. J. *J. Mater. Res.* **1986**, *1*, 2002.

[24] Klein, J.; Briscoe, B. J. *Proc. R. Soc. London, Ser. A* **1979**, *365*, 53.

[25] Perkins, T. T.; Smith, D. E.; Chu, S. *Science* **1994**, *264*, 822.

[26] Heijboer, J. *Intl. J. Polym. Mater.* **1977**, *6*, 11.

[27] Garwe, F.; Schonhals, A.; Lockwenz, H.; Beiner, M.; Schroter, K.; Donth, E. *Macromolecules* **1996**, *29*, 247.

[28] Adam, G.; Gibbs, J. H. *J. Chem. Phys.* **1965**, *43*, 139.

[29] Donth, E. *Relaxation and thermodynamics in Polymers: Glass Transition*; Akademie: Berlin, 1992.

[30] Schmidt-Rohr, K.; Spiess, H. W. *Phys. Rev. Lett.* **1991**, *66*, 3020.

[31] Sillescu, H. *J. Non-Cryst. Solids* **1999**, *243*, 81.

[32] Schiener, B.; Bohmer, A.; Loidl, A.; Chamberlin, R. V. *Science*, **1996**, *274*, 752.

[33] Fox, T. G.; Flory, P. J. *J. Appl. Phys.* **1950**, *21*, 581.

[34] Simha, R.; Boyer, R. F. *J. Chem. Phys.* **1962**, *37*, 1003.

[35] Cohen, M. H.; Grest, G. S. *Phys. Rev. B* **1979**, *20*, 1077.

[36] Simha, R.; Somcynsky, T. *Marcromolecules* **1969**, *2*, 342.

[37] Wendorff, J. H.; Fischer, E. W. *Kolloid Z. Z. Polym.* **1973**, *251*, 876.

[38] Liu, J.; Deng, Q.; Jean Y. C. *Macromolecules* **1993**, *26*, 7149.

[39] Yu, W.-C.; Sung, C. S. P.; Robertson, R. E. *Macromolecules* **1988**, *21*, 355.

[40] Song, H. H.; Roe, R.-J. *Macromolecules* **1987**, *20*, 2723.

[41] Curro, J. J.; Roe, R.-J. *Polymer* **1984**, *25*, 1424.

[42] Roe, R.-J.; Curro J. J. *Macromolecules* **1983**, *16*, 428.

[43] Lamarre, L.; Sung, C. S. P. *Macromolecules* **1983**, *16*, 1729.

[44] Loutfy, R. O. *Macromolecules* **1981**, *14*, 270.

[45] Wang, Y. Y.; Nakanishi, N.; Jean, Y. C.; Sandreczki, T. C. *J. Polym. Sci., Part B: Polym. Phys.* **1990**, *28*, 1431.

[46] Deng, Q.; Jean Y. C. *Macromolecules*, **1993**, *26*, 30.

[47] Jean, Y. C. *Microchem. J.* **1990**, *42*, 72.

[48] Dlubek, G.; Pionteck, J.; Bondarenko, V.; Pompe, G.; Taesler, C.; Petters, K.; Krause-Rehberg, *Macromolecules* **2002**, *35*, 6313.

[49] Plazek, D. J. *J. Chem. Phys.* **1965**, *69*, 3480.

[50] Bondi, A. A. *Physical properties of Molecular Crystals, Liquids, and Crystals*; Wiley & Sons: New York, 1960.

[51] Victor, J. G.; Torkelson, J. M. *Macromolecules* **1987**, *20*, 2241.

[52] Victor, J. G.; Torkelson, J. M. *Macromolecules* **1988**, *21*, 3490.

[53] Jones, R. A. L. *Interfaces*. In *The Physics of Glassy Polymers,* 2nd ed.; Haward, R. N., Young, R. J., Eds.; Chapman & Hall: London, UK, 1997.

[54] Jones, R. A. L.; Richards, R. W. *Polymers at Surfaces and Interfaces*; Cambridge University Press: Cambridge, UK, 1999.

[55] Allara, D. C.; Atre, S.; Parikh A. N. In *Polymer Surfaces and Interfaces*; Feast, W. J., Munrom, H. S., Richards, R. W., Eds.; Wiley & Sons: New York, 1993.

[56] *Polymer Surfaces*; Clark, D. T., Feast, W. J., Eds.; John Wiley & Sons, Ltd.: Chichester, UK, 1978.

[57] *Polymer Surfaces and Interfaces*; Feast, W. J., Munro, H. S., Eds.; John Wiley & Sons, Ltd.: Chichester, UK, 1987.

[58] Wu S. *Polymer Interfaces and Adhesion*; Marcel Dekker: New York, 1982.

[59] *Physics of Polymer Surfaces and Interfaces*; Sanchez, I. C., Ed.; Butterworth-Heinemann: Boston, 1992.

[60] Garbassi, F.; Morra, E.; Occhiello, E. *Polymer Surfaces, from Physics to Technology*; Wiley: Chichester, 1994.

[61] Toney, M. F.; Russell, T. P.; Logan, J. A.; Kikuchi, H.; Sands, J. M.; Kumar, S. K. *Nature* **1995**, *374*, 709.

[62] Meyers, G. F.; Dekoven, B. M.; Seitz, J. T. *Langmuir* **1992**, *8*, 2330.

[63] Kajiyama, T.; Tanaka, K.; Ge, S.-R.; Takahara, A. *Prog. Surf. Sci.* **1996**, *52*, 1.

[64] Kawaguchi, D.; Tanaka, K.; Takahara, A.; Kajiyama, T. *Macromolecules* **2001**, *34*, 6164.

[65] Tsui, O. K. C.; Russell, T. P.; Hawker, C. J. *Macrmolecules* **2001**, *34*, 5535

[66] Ge, S.; Pu, Y.; Zhang, W.; Rafailovich, M.; Sokolov, J.; Buenviaje, C.; Buckmaster, R.; Overney, R. M. *Phys. Rev. Lett.* **2000**, *85*, 2340.

[67] Kajiyama, T.; Tanaka, K.; Ohki, I.; Ge, S. R.; Yoon, J. S.; Yakahara, A. *Macromolecules* **1994**, *27*, 7932.

[68] Kajiyama, T.; Tanaka, K.; Takahara, A. *Polymer* **1998**, *39*, 4665.

[69] Kajiyama, T.; Tanaka, K.; Takahara, A. *Macromolecules* **1997**, *30*, 280.

[70] Zhang, X.; Tasaka, S.; Ingaki, N. *J. Polym. Sci., Part B: Polym. Phys.* **2000**, *38*, 654.

[71] Mansfield, K. F.; Theodorou, D. N. *Macromolecules* **1991**, *24*, 6283.

[72] Kajiyama, T.; Tanaka, K.; Takahara, A. *Macromolecules* **1995**, *28*, 3482.

[73] Xie, L.; DeMaggio, G. B.; Frieze, W. E.; DeVries, J.; Gidley, D. W. *Phys. Rev. Lett*. **1995**, *74*, 4947.

[74] DeMaggio, G. B.; Frieze, W. E.; Gidley, D. W.; Zhu, M.; Hristov, H. A.; Yee, A. F. *Phys. Rev. Lett.* **1997**, *78*, 1524.

[75] Jean, Y. C.; Cao, H.; Dai, G. H.; Suzuki, R.; Ohdaira, T.; Kobayashi, Y.; Hirata, K. *Appl. Surf. Sci.* **1997**, *116*, 251.

[76] Jean, Y. C.; Zhang, R.; Cao, H.; Yuan, J.; Huang, C.; Nielsen, B.; Asoka-Kumar, P. *Phys. Rev. B* **1997**, *56*, R8459.

[77] Pande, V. S.; Grosberg, A. Y.; Tanaka, T. *Rev. Mod. Phys.* **2000**, *72*, 259.

[78] Du, R.; Grosberg, A. Y.; Tanaka, T.; Rubinsten, M. *Phys. Rev. Lett.* **2000**, *84*, 2417.

[79] Wallace, W. E.; van Zanten, J. H.; Wu, W. L. *Phys. Rev. E* **1995**, *52*, R3329

[80] Keddie, J. L.; Jones, R. A. L.; Cory, R. A. *Europhys. Lett.* **1994**, *27*, 57.

[81] Jackson, C. L.; McKenna, G. B. *Chem. Mater.* **1996**, *8*, 2128.

[82] Anastasiadis, S. H.; Karatasos, K.; Vlachos, G.; Manias, E.; Giannelis, E. P. *Phys. Rev. Lett.* **2000**, *84*, 915.

[83] Prucker, O.; Christian, S.; Bock, H.; Ruhe, J.; Frank, C. W.; Knoll, W. *Macromol. Chem. Phys.* **1998**, *199*, 1435.

[84] Kawana, S.; Jones, R. A. L. *Phys. Rev. E* **2001**, *63*, 021501.

[85] Kim, J. S.; Lee, D. S. *Polym. J.* **2000**, *32*, 616.

[86] Forrest, J. A.; Dalnoki-Veress, K.; Dutcher, J. R. *Phys. Rev. E* **1997**, *56*, 5705

[87] Fukao, K.; Miyamoto, Y. *Europhys. Lett.* **1999**, *46*, 649.

[88] Torres, J. A.; Nealey, P. F.; de Pablo, J. J. *Phys. Rev. Lett.* **2000**, *85*, 3221.

[89] Baschnagel, J.; Binder, K. *Macromolecules* **1995**, *28*, 6808.

[90] Keddie, J. L.; Jones, R. A. L. *Isr. J. Chem.* **1995**, *35*, 21.

[91] van Zanten, J. H.; Wallace, W. E.; Wu, W. *Phys. Rev. E* **1996**, *53*, R2053.

[92] Arndt, M.; Stannarius, R.; Groothues, H.; Hempel, E.; Kremer, F. *Phys. Rev. Lett.* **1997**, *79*, 2077.

[93] Schuller, J.; Mel'nichenko, Y. B.; Richter, R.; Fischer, E. W. *Phys. Rev. Lett.* **1994**, *73*, 2224.

[94] Park, J.-Y.; McKenna, G. B. *Phys. Rev. B* **2000**, *61*, 6667.

[95] Zorn, R.; Frick, B.; Hartmann, L.; Kremer, F.; Schonhals, A.; Richter, D. *Physica B* **2004**, *350*, e1115.

[96] Dalnoki-Veress, K.; Forrest, J. A.; Murray, C.; Gigault, C.; Dutcher, J.R. *Phys. Rev. E.* **2001**, *63*, 031801.

[97] Mattsson, J.; Forrest, J. A.; Borgesson, L. *Phys. Rev. E* **2000**, *62*, 5187.

[98] Forrest, J. A.; Dalnoki-Veress, K.; Stevens, J. R.; Dutcher, J. R. *Phys. Rev. Lett.* **1996**, *77*, 2002.

[99] Forrest, J. A.; Dalnoki-Veress, K.; Dutcher, J. R.; Stevens, J. R. *Mater. Res. Soc. Symp. Proc.* **1996**, *407*, 131.

[100] Sharp, J. S.; Forrest, J. A. *Phys. Rev. Lett.* **2003**, *91*, 235701.

[101] Ding, J; Xue, G.; Dai, Q.; Cheng, R. *Polymer* **1993**, *34*, 3325.

[102] Xue, G.; Lu, Y.; Shi, G.; Dai, Q. *Polymer* **1994**, *35*, 892.

[103] Sasaki, T.; Shimizu, A.; Mourey, T.; Thurau, C. T.; Ediger, M. D. *J. Chem. Phys.* **2003**, *119*, 8730.

[104] Mahr, T. G. *J. Phys. Chem.* **1970**, *74*, 2160.

[105] Guar, U.; Wunderlich, B. *Marcomolecules* **1980**, *13*, 1618.

[106] Qian, R.; Wu, L.; Shen, D.; Napper, D. H.; Mann, R. A.; Sangster, D. F. *Macromolecules* **1993**, *26*, 2950.

[107] Ming, W. H.; Zhao, J.; Lu, X. L.; Wang, C. C.; Fu, S. K. *Macromolecules* **1996**, *29*, 7678.

[108] Forrest, J. A.; Dalnoki-Veress, K. *Adv. Colloid Interface Sci.* **2001**, *94*, 167.

[109] Kim, J. S.; Lee, D. S. Polym. J. **2000**, *32*, 616.

[110] Frank, B.; Gast, A. P.; Russell, T. P.; Brown, H. R.; Hawker, C. *Macromolecules* **1996**, *29*, 6531.

[111] Tseng, K. C.; Turro, N. J.;, Durning, C. *J. Phys. Rev. E* **2000**, *61*, 1800.

[112] Hall, D. B.; Torkelson, J. M. *Macromolecules* **1998**, *31*, 8817.

[113] Hall, D. B.; Miller, R. D.; Torkelson, J. M. *J. Polym. Sci., Part B: Polym. Phys.* **1997**, *35*, 2795.

[114] Hall, D. B.; Hooker, J. C.; Torkelson, J. M. *Macromolecules* **1997**, *30*, 667.

Chapter 3

Single molecule fluorescence detection and spectroscopy: application to polymer research

3.1 Introduction

As we proceed toward a more detailed understanding of polymer structure and dynamics, an increasing need is felt to develop a microscopic picture of processes underlying polymer mobility in the melt and in the glassy state. When approaching the glass transition temperature, the complexity of the relaxation processes increases and local, segmental scale investigations are needed to understand how glasses are being formed. Needless to say such knowledge is of primary importance in various technologically relevant applications (such as in lithography for the microelectronics industry) and can pave the way for better or new polymeric materials with enhanced properties. However, if substantial progress is to be made in the field of polymer physics, new experimental techniques with the ability to probe structure and dynamics of materials on the nanoscale are required.

The high sensitivity of the fluorescence to the changes in the chromophore surroundings has turned fluorescence spectroscopy into a successful tool for the investigation of various properties of matter [1]. In particular, fluorescence based techniques have a long tradition in polymer research [2]. Within the past decade significant breakthroughs have been made in the field of optical detection, characterization, and manipulation of individual molecules. Single molecule detection offers the possibility to select, track, sort and manipulate individual light emitters [20]. The main advantage of single molecule approaches lies in the elimination of the ensemble average. Both static and dynamic heterogeneities, if present, can be studied by obtaining, for a given physicochemical quantity, data at the single molecule level, as well as full distributions, at a given time and by time-dependent studies, respectively. Another advantage of single molecule experiments is that in the time-domain the need for synchronization (as in molecule ensembles) is removed. Additionally there is no necessity to remove the molecules from their original environment. This approach gives the opportunity to test theories of bulk ensemble behavior by looking at individual members of the population. Finally, ensemble measurements can obscure processes, hidden, when large populations are being measured, thus new phenomena and properties might not be revealed.

Single molecule detection (SMD) is emerging as an indisputably valuable tool across all the different fields of science such as biology [3-6], chemistry [7-9] and physics [10]. Fluorescence emission has been reported for single chromophores deposited on surfaces [11], located at interfaces [12], embedded in gels [13], silicate thin films [14], polymers [15,16] in organic crystals [17,18] and liquid crystals [19]. For detailed information on the single molecule optical detection the reader is referred to excellent books [20], book chapters [21,22] and finally to recent review articles [23-27].

It was underlined many times across Chapter 2 of this thesis, that a substantial number of important issues in the field of polymer physics in general and in the physics of polymeric glasses in particular have remained unresolved. Among others the issues regarding the free-volume, molecular level mobility and diffusion processes, polymer relaxation behavior above the glass transition and the glass transition itself are still under intensive investigation. To deepen our understanding of polymer dynamics it is necessary to obtain information on the molecular level processes, simultaneously on both the microscopic and macroscopic levels.

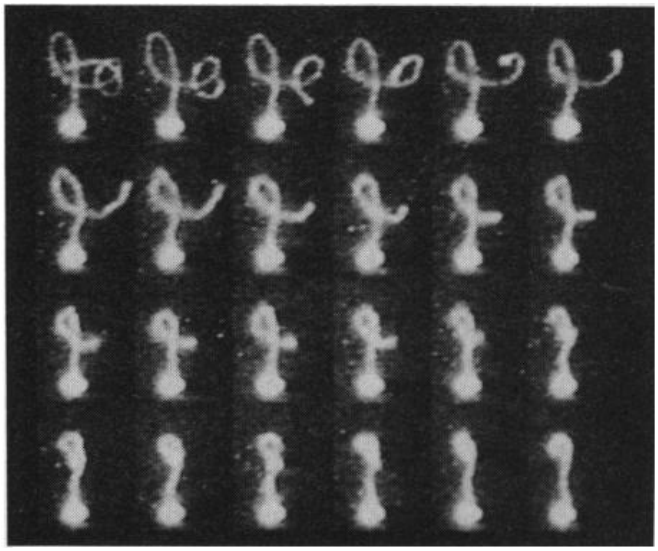

Figure 1. A series of images showing a single macromolecule labeled with fluorescent dyes moving in a polymer solution. The result of these experiments constituted a direct proof that polymer entanglements do exist and confirmed the theoretical predictions of the reptation model for polymer diffusion [28].

As an example of the great potential laying in experimental approaches, where one is able to observe individual members of an ensemble, we recall the experiments reported by Perkins et al. By labeling a single polymer chain with fluorophores, Perkins et al. [28] showed directly the tube-like motion of a single macromolecule in an entangled solution of unlabeled molecules (Figure 1). This allowed one to verify the main assumptions of the reptation model

introduced by deGennes, Edwards and Doi [29-31]. In this model, the motion of a polymer chain is governed by one-dimensional diffusion within a tube created by topological constraints, entanglements, created by the neighboring chains. Although the polymer chains in the study were stained with a large number of fluorescent molecules, these experiments were among the first to demonstrate the strength of single (macro)molecule experimental approaches in polymer science.

3.2 Introduction to fluorescence

3.2.1 Fluorescence and related processes

Various molecular processes involved in absorption and emission of light can be illustrated by the so-called Jablonski diagram (Figure 2). An electronic transition consists of the promotion of an electron from an orbital of a molecule in the ground state (S_0) to an higher energy unoccupied orbital by absorption of a photon (with energy $h\nu_A$). The absorption of photons is a fast process occurring on the femtosecond timescale. The Frank-Condon principle says that during the time it takes to absorb a photon, the positions of the nuclei are not changed. Following photon absorption the molecule is said to be in the excited state (S_1). Since the chromophore will be usually excited to one of the higher vibrational levels it will rapidly relax to the lowest vibrational level of the excited state, in about 10^{-12} sec.

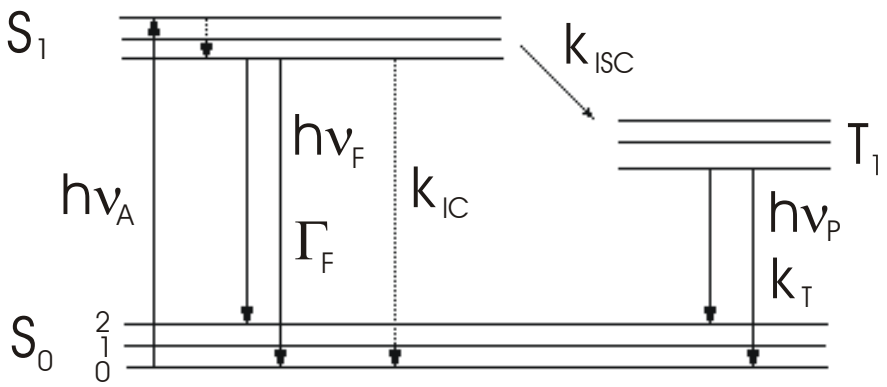

Figure 2. The Jablonski diagram for a three-level system [2]. The symbols and transitions are explained throughout the text.

Once being in the excited state, the molecule can relax by emission of a photon (radiative transition) or through a series of transitions where no light emission occurs (non-radiative transitions e.g. internal conversion). Spontaneous emission of light from electronically excited species is generally called luminescence. Fluorescence is a particular case of luminescence, where the deactivation occurs through a singlet-singlet (S_1-S_0) transition (spin-allowed), occurring typically on the nanoseconds time-scale after excitation. Due to the vibrational relaxation in the excited state and possible interaction of the chromophore with its surrounding, the fluorescence spectrum is usually shifted towards higher wavelengths with respect the absorption spectrum (Stokes shift).

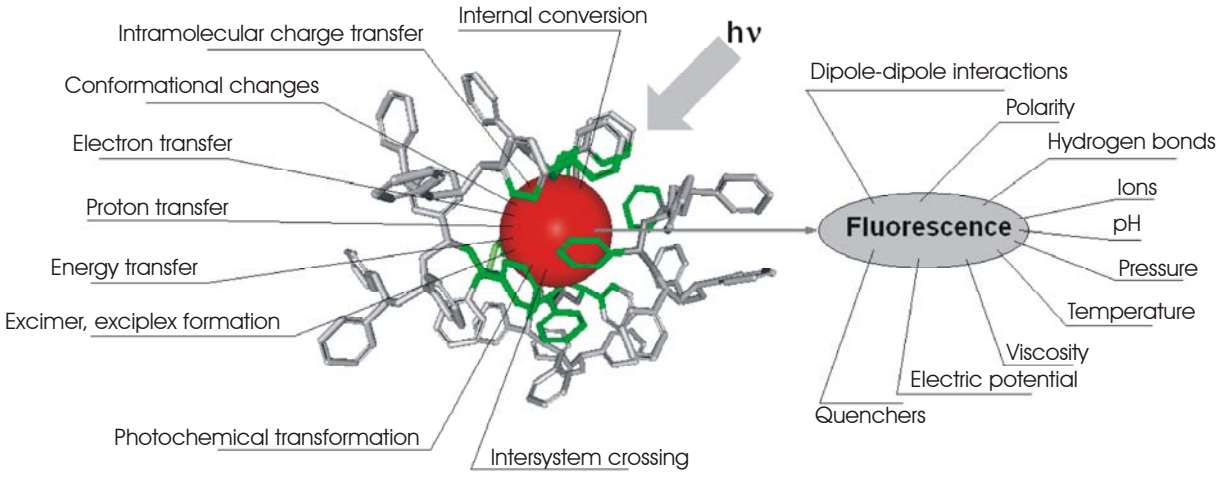

Figure 3. Schematic picture showing a probe embedded in a polymer matrix (center). After absorption of light and promotion to the excited state the molecule can undergo a large number of de-excitation processes (left) competing with fluorescence emission (right). Fluorescence in turn is sensitive to many physical and chemical parameters characterizing a microenvironment of the probes (right).

Several processes are possible, through which the molecule can decay from the excited state, other than by emitting a photon (Figure 3). The most significant ones are internal conversion, energy transfer, intersystem crossing, and photochemical processes. Internal conversion is a non-radiative transition between two electronic states with the same spin multiplicity. The excess energy can be transferred by collisions from the excited molecule to the molecules in the surrounding medium. Intersystem crossing is also a nonradiative transition, however between states with different spin-multiplicity. Such transitions are spin forbidden, therefore the intersystem crossing rates (k_{ISC}) are usually very low and the transition from the singlet S_1 state to triplet T_1 state is relatively rare compared to S_1-S_0 transition. From the triplet state the molecule can be deactivated by emitting a photon (of energy $h\nu_P$) resulting in phosphorescence. Since the T_1-S_0 transition is again spin forbidden, the rate k_T associated with the transition is low and subsequently the time molecules spend in the T_1 state is long,

ranging typically from 10^{-6} to 10^{-3} seconds for most organic chromophores. The last route of deactivation is sometimes called photobleaching and means, that the molecule structure was altered in some way making the molecule not optically active anymore. Photobleaching can occur from both the singlet S_1 and the triplet T_1 state (after intersystem crossing) through a variety of mechanisms usually involving reaction with molecular oxygen.

3.2.2 Quantum yield and fluorescence lifetime

Fluorescence quantum yield (QY) is defined as the ratio of the number of emitted photons (through fluorescence) to the total number of absorbed photons. Quantum yield can be conveniently expressed in terms of rates of the radiative (k_r) and nonradiative (k_{nr}) processes:

$$QY = \frac{k_r}{k_r + k_{nr}} \tag{1}$$

The nonradiative decay rate k_{nr} in the above equation is the sum of all possible rates of deactivation processes, which do not result in fluorescence emission:

$$k_{nr} = \sum_i k_i \,, \tag{2}$$

where k_i is the rate of a given deactivation process e.g. k_{ISC} or k_{IC}, as it can be seen in Figure 2.

Fluorescence lifetime (τ_F) corresponds to the effective time the molecule spends in the excited state and can be expressed as:

$$\tau_F = \frac{1}{k_r + k_{nr}} \tag{3}$$

The rich spectrum of processes and phenomena associated with absorption and emission of light makes fluorescence studies an attractive choice as analytical tool. For example fluorescent lifetime is known to be very sensitive to the properties of the surroundings of the molecule, such as viscosity and polarity. Fluorescent lifetime can also be used to distinguish between two different chromophores present simultaneously in the investigated system. Therefore fluorescent probes are a natural choice for use as molecular level reporters of their surroundings.

3.3 Single fluorescent molecules as probes

3.3.1 Introduction

Recently, single molecules have become the center of attention as probes of their surroundings [27]. Such molecular probes report on the static or dynamic properties of their nanoenvironment by emission of light. All required information needed is therefore contained in the detected fluorescence photon streams, e.g. one can extract polarization, wavelength or arrival time of the photons after pulsed excitation. There are many parameters one can extract from the fluorescence emission. We list them here: molecule position, fluorescence intensity, fluorescence lifetime, emission dipole moment, absorption dipole orientation, anisotropy decay and amplitude, intersystem crossing yield, triplet lifetime, photostability, emission spectrum, and quantum yield (we limit ourselves here to fluorescence, however parameters connected to phosphorescence emission can be used as well). Cross-correlations may exist among these parameters in certain cases, i.e. variations in one property may be accompanied by changes in another (coupled) characteristic, e.g. in the quenching process the total emission intensity is correlated with fluorescence lifetime. Therefore, cross-correlation analysis involving a large number of parameters generally adds substantial valuable information to the range of data [32].

Most of the parameters listed above can be followed in time, therefore allowing one to access the information in the time-domain. Such measurements are performed wherever system "dynamics" will have to be probed. Of course, the quality of the extracted information will depend on the number of detected photons and on the signal to background ratio. The latter has to be considerably large (at least higher than 1 for the photon collection time considered) for reliable, single molecule experiments. It is important to remember that a molecule can emit a limited number of photons during a given time interval, therefore one will have to trade between accuracy and multiparameter experiments. Usually, most single molecule experiments are limited to the extraction of few (3-5) observables simultaneously. For example, simultaneous detection of fluorescence lifetime and emission spectrum requires splitting the emitted light into two different channels, therefore decreasing the number of photons in each of the detection channels. In the time-domain, moving toward higher time resolution and keeping the data fidelity constant requires an increased amount of photons per time bin. A careful choice of the observable is therefore very important in studies where molecules serve as probes of their surroundings.

3.3.2 Single-molecule reporter in a solid host

Fluorescent probes can be incorporated into polymer matrices (Figure 4) as dispersed dopants by prior mixing in solution or by covalent attachment directly to the polymer chain. Many spontaneous or photoinduced processes are sensitive to the immediate environment around the probe. Mechanisms such as spectral diffusion or fluorescence lifetime are linked directly to fluctuations in the environment [66]. In Figure 3 we show that many environmental parameters can in principle influence fluorescence emission of the probes: presence of quenchers, temperature, viscosity, pressure, pH, hydrogen bonds formation, polarity, ions, electric potential or dipole-dipole interactions. Depending on the chemical structure of the probes and the surrounding polymer matrix, formation of exciplexes and excimers is also possible [2].

A number of different techniques has been developed to visualize and probe the dynamics of single molecules in both room and low temperature studies. Each of the techniques has it own advantages and disadvantages and the main selection criteria are the temporal and spatial resolutions one wishes to obtain of the parameter one wants to look at. The prerequisite for detecting a single light emitter is the reduction of background signals arising from the surrounding matrix and from impurities. The background signals arise from scattered light and detector dark counts. Fluorescence and Raman scattering from the surrounding polymer matrix can be reduced by decreasing the probed sample volume and by operating at wavelengths close to the red part of the electromagnetic spectrum. The first can be realized by employing confocal imaging, total internal reflection, or techniques based on near-field illumination schemes.

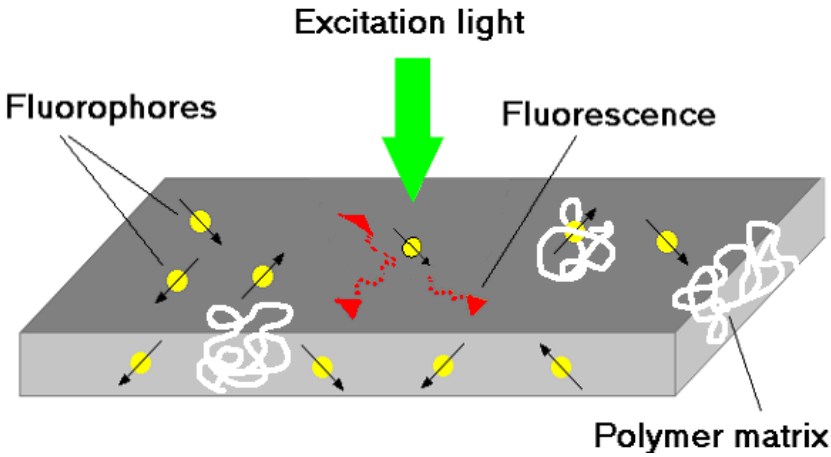

Figure 4. A scheme depicting chromophores dispersed in a polymer matrix. Individual dyes can be selected and optically addressed. Single molecule diffusion processes can be followed and probe photophysical properties can be studied in the time-domain.

3.4 Single molecule probing of polymers

3.4.1 Introduction

The number of experimental studies published with the intention to evaluate the physical properties of polymers using SMD approaches is relatively low compared to the wide spread of SMD in the biomolecular domain. So far the investigated polymeric systems and the techniques used are rather diverse. Clearly, the field of single molecule optical probing is still in its infancy. It is important to mention that the already existing reports provide valuable insights into polymer dynamics and structure on the nanoscale. Since in single molecule experiments one is able to avoid the ensemble averaging, studies aiming at the evaluation of heterogeneities present in the polymer matrix are usually the main target of investigations. The spatial and temporal variations of the polymer dynamics (and even structure) are of course important from the technological as well as scientific points of view. The results discussed in this section will demonstrate the strength of the single molecule approaches in polymer science.

3.4.2 Polymer dynamics at low temperatures (<10 K)

From a historical point of view we should first mention low temperature (<10K) investigations on the influence of the polymer matrix on single molecule photophysical properties. When Orrit and Bernard [33,34] detected single molecule impurities by fluorescence excitation for the first time, time-resolved experiments revealed fluctuations in the position of spectral lines of the single molecules. Such spectral diffusion behavior was believed to be the consequence of relaxation processes of the matrix surrounding the chromophores. However this study was clearly motivated by physical optics rather than by materials related issues.

To explain the experimental observations of spectral diffusion, the model of a two-level system was often invoked. The main ingredient in such approach is the notion that the potential energy surface of glasses consists of a large amount of energy minima (Figure 5a). Locally, the transition between two minima in a two-level system (TLS) can describe the lattice dynamic properties. When the molecule is coupled to an individual TLS by strain or electric fields the transition frequency of the molecule changes when the TLS jumps from one metastable well to another (Figure 5b).

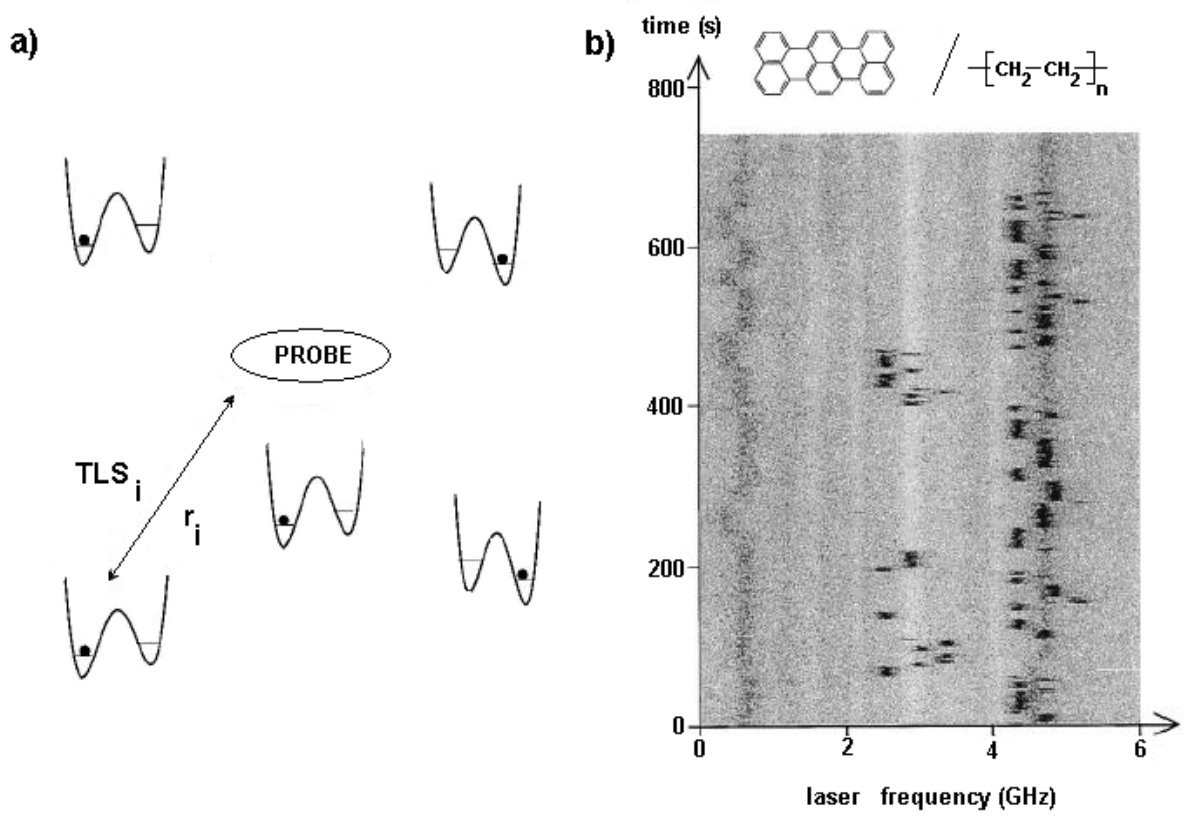

Figure 5. a) Schematic representation of a probe molecule in a glass interacting with a number of two-level-systems. The probe molecule is at a distance r_i from the i^{th} TLS system. b) Spectral diffusion of a single molecule coupled two three independent two-level-systems. For given integration time a fluorescence excitation spectrum is recorded (emission intensity is represented by the gray scale) (adopted from [35]).

Donley and Plakhotnik [36] observed a broad distribution of lifetime-limited linewidths of chromophores in a polymer host at 30 mK. They concluded that this is caused by the inherent disorder present in the investigated system. The authors introduced a microscopic model where the linewidth distributions where analyzed taking into account an effective interaction between voids present in the matrix and the impurity molecules. At such low temperatures the changes in the configuration of the matrix can be considered to be nonexistent and the changes in the density can be negligible. This, however, will not be true at higher temperatures and the fluorescence lifetimes of chromophoric probes can change in time depending on the timescale of the local density fluctuations. Such single molecule fluorescence lifetime fluctuations are indeed observed at room temperature for specific probes and are the subject of Chapter 5 of this thesis.

Although experiments performed at low temperatures gave a valuable insight into the structure and dynamics of glasses most of the applications of polymeric materials are at room

temperature (or higher) where most of the phenomena observed at low temperatures can not be visualized anymore. Nevertheless, low temperature studies were the first to demonstrate the potential of single molecules to report on the structure and dynamics of matter, and of glasses in particular.

3.4.3 Probing polymers with single fluorescent molecules

Spatially heterogeneous dynamics close to the glass transition temperature of polymers is currently a matter of great scientific interest [37,38]. In particular, it is suggested that the nonexponential nature of the α-relaxation processes at temperatures close to the glass transition temperature is a direct consequence of the existence of long-lived spatial heterogeneities [39]. The ensemble techniques can at best provide results averaged over many different sub-ensembles, or can give an indication of the spread of values through non-exponential shapes of the relaxation functions of the parameters investigated. Although the existence of the segmental scale heterogeneous dynamics was confirmed experimentally [37-39], still many questions regarding the length and time scales associated with heterogeneities in polymer systems remain unresolved. The need for locally resolved studies without ensemble averaging is therefore as obvious as challenging.

One of the main attributes of the single molecule detection is the ability to avoid ensemble averages and obtain the full distributions of the relevant parameters. In contrast to single molecule methods, ensemble average methods provide instead of distributions only discrete, average values. Single molecule methods are therefore suitable to study systems with structural and dynamical heterogeneities. Both spatial (property depending on position) and temporal heterogeneities (property changing for a given position in time) can be probed and distributions of static or dynamic properties can be therefore subsequently obtained. Obviously such distributions contain much more information than the average alone. In many cases, developing models for the description of a given physical property requires a detailed knowledge of the full distribution and, in some cases, even the contribution of each member of the population to the ensemble averaged behavior must be known. In the context of spatially heterogeneous dynamics in polymer glasses both above and below the glass transition temperature it is of great interest to follow individual heterogeneous sites for many individual single molecule probes. This will allow one to discriminate between spatial and temporal variations in the matrix dynamics. To study the heterogeneous dynamics in polymeric system using SMD two main approaches have been used. The first was based on single molecule tracking and observations of probe rotational and translational diffusion. The second approach relied on the monitoring of the photophysical properties of the probes. Both the spatial and temporal heterogeneities in the polymer matrix were addressed and we describe some representative result of these studies below.

Significant advances in our understanding of polymer dynamics above the glass transition temperature were made by studies based on single molecule localization and positional and orientational tracking. In contrast to bulk techniques, single molecule investigations allow one to follow the motion of an individual Brownian particle and obtain the probability distribution of the particle displacement as a function of time. Full distributions of the diffusion coefficients are therefore obtained. On the other hand, even if the ensemble average behavior could appear as Brownian in nature, single molecule techniques are also able to resolve anomalous sub-ensembles. Since a single molecule is a dipolar light source, its orientation can be determined by polarization resolved fluorescence. Thus one can follow reorientational dynamics of single probes in time and at different locations in the sample and obtain the full distributions of rotational correlation times. Therefore, SMD approaches are ideal to obtain the time and length scales associated with the heterogeneities present in the polymeric systems.

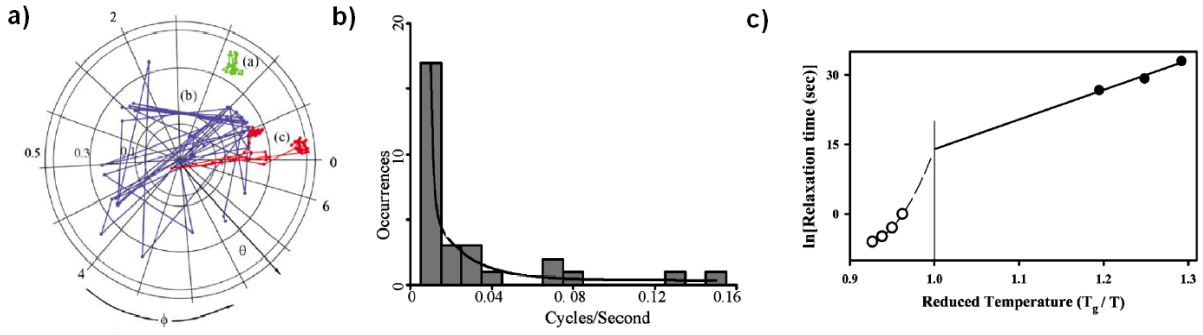

Figure 6. a) Three different orientational trajectories of single molecules in PMMA at room temperature. Θ and Φ are radial and angular axis respectively. b) Histogram of reorientation rates of many different single molecules. c) Single molecule reorientation times (filled circles) and time scales associated with bulk α-relaxation processes (open circles) as a function of temperature. The full and dashed lines correspond to the Williams-Landel-Ferry (WLF) and Arrhenius scalings respectively (pictures adopted from [40]).

Below the glass transition temperature Bartko et al. measured [40] the three-dimensional orientational motion [41] of single fluorescent molecules in poly(methyl methacrylate). The experiments were performed at room temperature, i.e. tens of degrees below the glass transition temperature of PMMA, which is at around 105 ºC. The authors found a broad distribution of orientational motion behavior (Figure 6a) and related this to the heterogeneity present in the polymer matrix below T_g. Additionally they found a signature of hopping-mediated diffusion processes (such processes are believed to be partially responsible for the translational-rotational paradox for diffusion in glass-forming liquids [42,43], where the

rotational dynamics display stronger temperature dependence than the translational diffusion when approaching the glass transition temperature). Broad distributions of the reorientational rates were subsequently obtained (Figure 6b) and the average reorientation times were investigated in function of temperature (indirectly, by changing the molar mass of PMMA) (Figure 6c). Extrapolation of both the Williams-Landel-Ferry scaling for temperatures above T_g (obtained from bulk experiments) and of the Arrhenius scaling for temperatures below T_g intersects at $T = T_g$ indicating that the probe molecules probe the nanoscale dynamics resulting from α-relaxation processes.

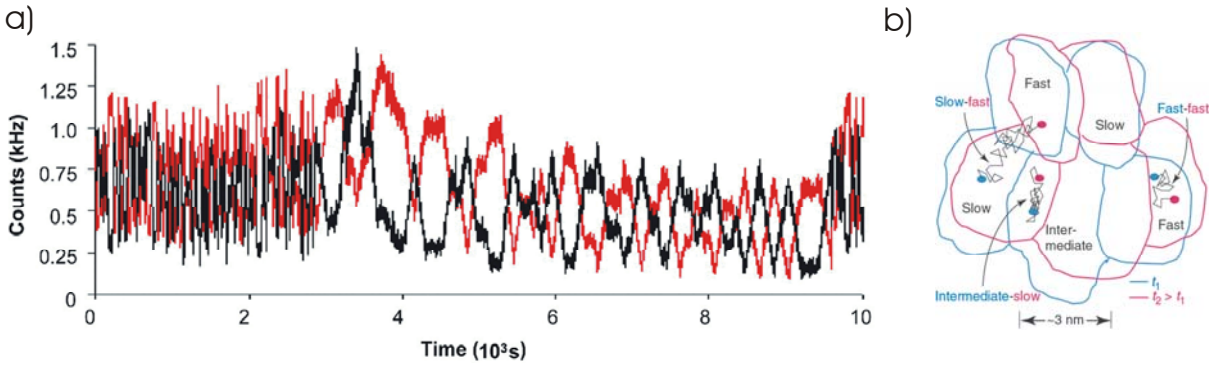

Figure 7. a) Fluorescence intensity detected for two orthogonal polarization channels for a long-lived single rhodamine 6G molecule embedded in PMA. Switching between different dynamics characterized with different time-scales is clearly visible on the time trace [44]. b) Schematic drawing with possible scenarios of the dynamics of individual molecules near T_g in relation to the regions of different dynamics at two different times. Possible trajectories of different single molecules in such heterogeneous environment are shown [46].

In a seminal work Deschenes and Vanden Bout [44,45] using a confocal microscope followed the orientational diffusion of individual rhodamine molecules embedded in poly(methyl acrylate) above and close to the glass transition temperature (Figure 7a). The authors showed directly that individual molecules embedded in a polymer matrix can abruptly change their orientational dynamics in time and that spatial heterogeneities are responsible for the characteristically nonexponential relaxation dynamics in polymers close to T_g (Figure 7b). For example, on the two-polarization channel intensity trace shown in Figure 7a one can clearly see that the molecule starts to rotate much slower after the initial period of 3000 s. The consequence of such changes is that the orientational relaxation function for the whole time-trace is nonexponential, indicating a broad distribution of time-scales associated with the system close to T_g. One is able, however, to identify parts of the trace were the correlation function displays an exponential decay shape. Such observations demonstrate that spatially varying environmental heterogeneities are responsible for the non-exponential relaxation dynamics close to T_g. The lifetime of the heterogeneities could be measured directly from the traces. As the temperature is lowered (from T_g + 15 K to T_g + 5 K) the time needed to observe

a change in the probe reorientational dynamics increases and the distribution of the heterogeneity lifetimes becomes broader. The ensemble average correlation time obtained from single molecule experiments was the same as obtained from bulk fluorescence anisotropy decay studies [45].

Bopp et al. [47] monitored the room temperature diffusion of single molecules dispersed in a poly(vinylbutyral) (PVB) matrix using near-field scanning optical microscopy (NSOM). The spatial resolution of SNOM is not diffraction limited as it is if far-field techniques are used. At present the challenges in the fabrication of near-field probes limits the spatial resolution, however, theoretically sub-molecular resolution can be obtained with the near-field methods. Bopp et al. found the diffusion of single rhodamine-6G dyes in PVB on the sub-micrometer scale to be non-random and explained this behavior by the presence of local heterogeneities in the structure of the polymer matrix. The statistical average over large numbers of diffusion traces displayed random walk behavior with a diffusion constant in good agreement with the bulk value.

By using far-field microscopy, Dickson et al. [13] performed room temperature tracking of single Nile Red molecules solvated in the pores of a poly(acrylamide) gel. The fluorophores were excited by an evanescent wave generated by total internal reflection (TIR) at the cover slip/sample boundary. The TIR method with its intrinsic fall-off of the excitation intensity allowed the authors to estimate the molecule position in the z direction. Their results showed that, on the time-scale from 0.1 to 1 s, the structure of the gel matrix hindered the Brownian motion by two orders of magnitude in each direction.

Studies based on monitoring photophysical processes are usually performed in rigid or semi-rigid macromolecular environments [14], usually below the melting point or the glass transition of the polymers. One important requirement for such investigations to be reliable is that the chromophore should be immobile in the polymer matrix during the experiment. Due to the large degree of mobility above the glass transition temperature, the interpretation of the data remains difficult and the results cannot be related in a straightforward manner to the host dynamics [48-50].

The analysis of single molecule fluorescence spectra was used to obtain detailed information on the polarity and rigidity of molecular scale environments in poly(vinyl alcohol) (PVA) and poly(methyl methacrylate) (PMMA) by Higgins and coworkers [51]. It was shown that single molecule spectroscopy using a Nile Red dye as a probe molecule is able to provide detailed information on both the structure and on the matrix dynamics, simultaneously. For PMMA it was found that distinct environments exist, for which the polarity is the same but where the environments can differ in rigidity. In case of PVA the water content in the environment

influenced matrix rigidity. Experimental methods where the chemical structure and dynamics can be probed on the nanoscale and can be effectively separated are candidates to study heterogeneous systems like block copolymers, or biologically relevant macromolecules.

Ye et al. [50,52] and Ishikawa et al. [48] performed a series of experiments, which aimed at probing the dynamics and structural heterogeneities of a polymer matrix. The experiments were based on monitoring the fluorescence properties of a dye molecule (in this case crystal violet – CV) with a flexible molecular structure. Such probes have an effective nonradiative decay channel, which is very sensitive to the rigidity of the local environment. When embedded in a poly(methyl methacrylate) matrix, the histograms of fluorescence photocounts and fluorescence lifetimes of individual crystal violet dyes displayed bimodal distributions (Figure 8a). The authors attributed this behavior to the existence of two distinct classes of sites present in the matrix with different relative viscosities. The distributions were found to be directly responsible for the nonexponential fluorescence decay observed in comparative bulk measurements. Biju et al. [49] probed the spatially heterogeneous dynamics through single molecule fluorescence lifetime and obtained information about the ratio between fast and slow relaxation sites in a poly(vinyl acetate) film near T_g. Upon raising the temperature from T_g - 8 K to T_g + 7 K the slow relaxation component of the distributions decreased and finally disappeared at T_g + 30 K (Figure 8 b).

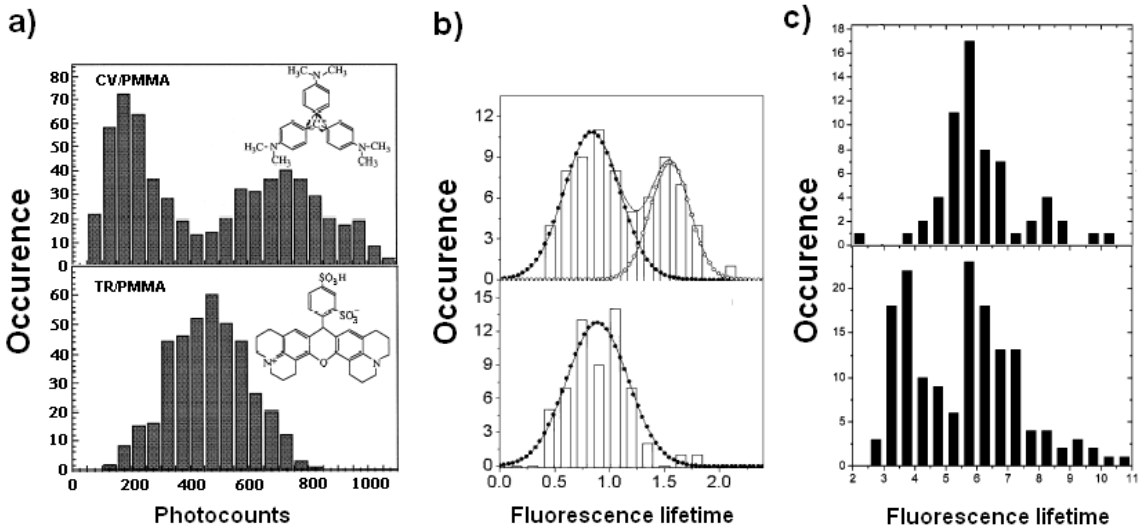

Figure 8. a) Bimodal distribution of CV dye photocounts when embedded in a PMMA matrix (upper histogram). Single peak distribution of a nonflexible dye for comparison (lower histogram) [50]. b) Histogram of fluorescence lifetime of single Cy3 molecules in a PVAc film at T_g - 8 K (upper histogram) and at T_g + 30 K (lower histogram). At high temperatures the higher lifetime component vanishes [49]. c) Distributions of single molecule fluorescence lifetime of TPDI molecules embedded in PMMA (upper histogram) and in P*n*BMA (lower histogram) matrices [54].

In another study, dyes, which could adopt different conformations depending on the interaction with the polymer matrix, were used [53]. The changes of the dye conformations were monitored by fluorescence lifetime. For more mobile, or heterogeneous, regions in the polymer matrix the fluorescence lifetime decay was shown to adopt a stretched exponential shape. This was explained by time dependent variations in the fluorescence lifetime due to a varying environment of the probe molecules. For some of the molecules a double-exponential decay was found which was attributed to an interconversion process between two stable dye conformations on a time scale of 2 ms and 5 ms for poly(norbornene) (PN) and poly(methyl methacrylate), respectively. Although the different time scales found for two different polymers might suggest that the probes are sensitive to the matrix dynamics, the glass transition temperature for PN is higher than for PMMA. Therefore the matrix influences the dye also in other way not related to polymer dynamics.

Recently, studies aiming at evaluation of the free volume present in polymers below the glass transition temperature were performed. Vallée et al. have shown [54] that single molecule conformational changes can probe directly the local free volume in a polymer matrix. When the conformation of the used chromophore changed, the fluorescence lifetime of the chromophores also changed. The volume difference between two different conformations was equal to 0.201 nm^3. Therefore these experiments were able to distinguish between free volume sizes larger or smaller than 0.201 nm^3. By embedding the probes in different polymers (Figure 8c) the authors found that the free volume available locally for the chromophores was higher in poly(*n*-butyl methacrylate) (P*n*BMA) than in PMMA, in agreement with literature values. Usually the information about the local free volume and its distributions is hidden in the ensemble average. Using different probes able to probe different free volume sizes would allow one to look in more details at free volume distributions and monitor free volume size and distributions as a function of temperature. Such an experimental check is of major importance to confirm the main predictions of the free volume theories of the glass transition.

3.4.4 Covalent attachment of probes to macromolecules

Dye molecules dispersed in the polymer matrix usually report on the dynamics of the surroundings as a whole without discriminating between particular polymer chains. Additionally, coupling of the chromophores' mobility to the matrix dynamics can be very complex and can depend on probe size or chemistry. In general, single molecule detection techniques allow one to investigate single polymer chain in solution or in the melt. Observation of chain conformation and its fluctuations can contribute to a better understanding of the relaxation processes occurring in the polymer matrix when crossing the

glass transition. Additionally, by positioning the chromophores at specific locations along the polymer chain, the degree of the dynamics associated with given chain segments can be probed. Although such an approach is rather straightforward and very appealing, there are only few reports on single molecule studies of dyes attached to polymer chains. Although one can easily ensure that there will be no more than one dye attached to one polymer chain it is quite difficult to ensure that all unreacted dyes will be removed from the reaction vessel since this would require single molecule separation sensitivity. This is not easy to achieve and still remains a challenge.

Bowden et al. [55] reported on the dynamics of various single polymer chains by following the orientational changes of perylene diimides attached to the chain end and in the middle of the chain, respectively. The polymers were prepared by free radical polymerization using perylene labeled initiators. Styrene, butyl acrylate, butadiene and isoprene monomers were polymerized into various homopolymers and block copolymers. Polybutadiene chains labeled in the center of the polymer and incorporated into a PMMA matrix were investigated at the single molecule level. It was found that most of the polymers are frozen in the glassy PMMA matrix, however 5 % of the investigated molecules exhibited reorientational dynamics on the time-scale of the experiment (100 ms). The report does not mention how the distinction between labeled and unlabeled probes could be made to rule out the possibility that unlabeled probes were visualized or to ensure that only covalently attached dyes were probed. Nevertheless, approaches based on polymer chain labeling are very promising.

3.4.5 Phosphorescence, triplet lifetime and intersystem crossing yield

Although usually fluorescence is used for monitoring the probe response to the environment, in some cases also intersystem crossing to the triplet state, triplet state lifetime [56] and single molecule phosphorescence [57] were employed in polymer studies. English et al. [58] obtained information on the degree of the static and dynamic disorder in a PMMA film by monitoring changes in the optical transitions of single DiI molecules depending on the oxygen content in the environment [59-61]. They estimated the static disorder to be smaller in a six day old sample compared to a freshly prepared one, indicating that dynamic processes are taking place in the polymer matrix in time. The dynamic disorder in the polymer matrix was evaluated by looking at temporal fluctuations of the triplet lifetime and was found to be relatively small. In contrast, Veerman et al. [62] have shown the dynamic disorder (on the same timescales) to be much larger. The respective studies were performed at different oxygen concentrations. It is likely that there was a large contribution of the temporal fluctuation of the accessibility of the probe to the oxygen controlled by local polymer motion. Additionally, Veerman et al. have shown that the photophysics of the triplet state of single

molecules is strongly dependent on the type of the polymer matrix used [62,63]. This was related to the solubility and diffusion coefficients of oxygen in the respective polymers. Under argon atmosphere a weak dependence of the single molecule triplet state lifetime on the polymer matrix type was found [64]. Torsional motion or cis/trans izomerization can be an additional pathway involved in intersystem crossing between the singlet and the triplet states [65]. Such changes in molecular conformations, often visible in solutions, are however relatively rare in a rigid polymer matrix.

Methods based on monitoring single molecule photophysical processes, other than fluorescence, are relatively unexplored in the context of probing polymer structure or dynamics. However, the reported studies so far are very promising especially when one considers the importance of knowing if impurities such as solvent or oxygen are present in the polymer system. One can think of studies, where on one hand the fluorescence is used to e.g. study molecule diffusion through single molecule tracking, while processes related to phosphorescence and the triplet state are used to determine the chemical nature of the surroundings, e.g. oxygen content. Therefore one can follow two independent parameters simultaneously without the necessity to change the probes or experimental conditions.

3.5 Conclusions

In this chapter we presented an introduction to fluorescence, single molecule detection and its application in polymer research. New information on polymer structure and dynamics, otherwise not attainable by ensemble averaging techniques, can be obtained through single molecule localization, tracking, or monitoring the photophysical parameters of the molecular probes. Although the research reported to date gave valuable information on various polymer systems, the use of SMD in polymer science is still in its infancy.

3.6 References

[1] Tucker, K.-T.; Brennan, J. D. *Chem. Mater.* **2001**, *13*, 3331.

[2] Guillet, J. E. *Polymer Photophysics and Photochemistry: An Introduction to the Study of Photoprocesses in Macromolecules*; Cambridge University Pres: Cambridge, 1985.

[3] Tokunaga, M.; Kitamura, K.; Saito, K.; Iwane, A. H.; Yanagida, T. *Biochem. Biophys. Res. Commun.* **1997**, *235*, 47.

[4] Pierce, D. W.; Hom-Booher, N.; Vale, R. D. *Nature* **1997**, *388*, 338.

[5] Wiess, S. *Science* **1999**, *283*, 1676.

[6] García-Parajó, M. F.; Koopman, M.; van Dijk, E. M. H. P.; Subramaniam, V.; van Hulst, N. F. *Proc. Natl. Acad. Sci. U.S.A.* **2001**, *98*, 14392.

[7] Trabesinger, W.; Schutz, G. J.; Gruber, H. J.; Schindler, H.; Schmidt, T. *Anal. Chem*. **1999**, *71*, 279.

[8] Zhang, P.; Tan, W. H. *Chem.-Eur. J.* **2000**, *6*, 1087.

[9] Ha, T.; Xu, J. *Phys. Rev. Lett.* **2003**, *90*, 223002.

[10] Hettich, C.; Schmitt, C.; Zitzmann, J.; Kuhn, S.; Gerhardt, I.; Sandoghdar, V. *Science* **2002**, *298*, 385.

[11] Betzig, E.; Chichester, R. J. *Science* **1993**, *262*, 1422.

[12] Hashimoto, F.; Tsukahara, S.; Watarai, H. *Langmuir* **2003**, *19*, 4197.

[13] Dickson, R. M.; Norris, D. J.; Tzeng, Y.-L.; Moerner, W. E. *Science* **1996**, *274*, 966.

[14] Higgins, D. A.; Collinson, M. M.; Saroja, G.; Bardo, A. M. *Chem. Mater.* **2002**, *14*, 3734.

[15] Trautman, J. K.; Macklin, J. *J. Chem. Phys.* **1996**, *205*, 221.

[16] Bopp, M. A.; Tarrach, G.; Lieb, M. A.; Meixner, A. J. *J. Vac. Sci. Technol., A* **1997**, *15*, 1423.

[17] Orrit, M.; Bernard, J. *Mod. Phys. Lett. B* **1991**, *210-211*, 417.

[18] Moerner, W. E.; Ambrose, W. P. *Phys. Rev. Lett.* **1991**, *66*, 1376.

[19] Kawai, T.; Yoshihara, S.; Iwata, Y.; Fukaminato, T.; Irie, M. *ChemPhysChem* **2004**, *5*, 1606.

[20] *Single Molecule Optical Detection, Imaging, and Spectroscopy*; Basché, T., Moerner, W. E., Orrit, M., Wild, U. P., Eds.; Verlag-Chemie, Weinheim, Germany, 1997

[21] Xie, X. S.; Bian, R. X.; Dunn, R. C. In *Focus on Multidimensional Microscopy*; Chen, P. C., Hwang, P.P., Wu, J. L., Wang, G., Kim, H., Eds.; World Scientific: River Edge, NJ, 1997; Vol. 1.

[22] Higgins, D. A.; Hou, Y. In *Encyclopedia of Nanoscience and Nanotechnology*; James, A., Schwartz, C. C., Putyera, K., Eds.; Marcel Dekker: New York, 2003.

[23] Tamarat, P.; Maali, A.; Lounis, B.; Orrit, M. *J. Phys. Chem. A* **2000**, *104*, 1.

[24] Moerner, W. E. *J. Phys. Chem. B* **2001**, *106*, 910.

[25] Jung, Y.; Barkai, E.; Silbey, R. J. *J. Chem. Phys.* **2002**, *117*, 10980.

[26] Hecht, B. *Phil. Trans. R. Soc. London, Ser. A* **2004**, *362*, 881.

[27] Kulzer, F.; Orrit, M. *Ann. Rev. Phys. Chem.* **2004**, *55*, 585.

[28] Perkins, T. T.; Smith, D. E.; Chu, S. *Science* **1994**, *264*, 819.

[29] deGennes, P. G. *Scaling Concepts in Polymer Physics*; Cornell Univ. Press: Ithaca, NY, 1979.

[30] Edwards, S. F. *Proc. Phys. Soc., London* **1967**, *92*, 9.

[31] Doi, M.; Edwards, S. F. *The Theory of Polymer Dynamics*; Clarendon: Oxford, 1986.

[32] Stracke, F.; Blum, C.; Becker, S.; Müllen, K.; Meixner, A. J. *Chem. Phys.* **2004**, *300*, 153.

[33] Orrit, M.; Bernard, J. *Phys. Rev. Lett.* **1990**, *65*, 2716.

[34] Bernard, J.; Orrit, M. *C. R. Acad. Sci.* **1990**, *311*, 923.

[35] Tamarat, Ph.; Maali, A.; Lounis, B.; Orrit, M. *J. Chem. Phys. A* **2000**, *104*, 1.

[36] Donley, E. A.; Plakhotnik, T. *J. Chem. Phys.* **2001**, *114*, 9993.

[37] Schmidt-Rohr, K.; Spiess, H. W. *Phys. Rev. Lett.* **1991**, *66*, 3020.

[38] Russell E. V.; Israeloff N. E. *Nature* **2000**, *408*, 695

[39] Wang, C. Y.; Ediger M. D. *J. Phys. Chem. B* **1999**, *103*, 4177.

[40] Bartko, A. P.; Xu, K.; Dickson, R. M. *Phys. Rev. Lett.* **2002**, *89*, 026101.

[41] Bartko, A. P.; Dickson, R. M. *J. Phys. Chem. B* **1999**, *103*, 3053.

[42] Stillinger, F. H.; Hogdon, J. A. *Phys. Rev. E* **1994**, *50*, 2064.

[43] Cicerone, M. T.; Ediger, M. D. *J. Phys. Chem.* **1993**, *97*, 10489.

[44] Deschenes, L. A.; Vanden Bout, D. A. *Science* **2001**, *292*, 255.

[45] Deschenes, L. A.; Vanden Bout, D. A. *J. Chem. Phys.* **2002**, *116*, 5850.

[46] Ediger, M. D. *Science* **2001**, *292*, 233.

[47] Bopp, M. A.; Meixner, A. J.; Tarrach, G.; Zschokke-Granacher, I.; Novotny, L. *Chem. Phys. Lett.* **1996**, *263*, 721.

[48] Ishikawa, M.; Ye, J. Y.; Maruyama, Y.; Nakatsuka, H. *J. Phys. Chem. A* **1999**, *103*, 4319

[49] Biju, V. P.; Ye, J. Y.; Ishikawa, M. *J. Phys. Chem. B* **2003**, *107*, 10729.

[50] Ye, J. Y.; Ishikawa, M.; Yogi, O.; Okada, T.; Maruyama, Y. *Chem. Phys. Lett.* **1998**, *288*, 885.

[51] Hou, Y.; Bardo, A. M.; Martinez, C.; Higgins, D. A. *J. Phys. Chem. B* **2000**, *104*, 212.

[52] Ye, J. Y.; Hattori, T.; Nakatsuka, H.; Maruyama, Y.; Ishikawa, M. *Phys. Rev. B* **1997**, *56*, 5286.

[53] Vallée, R. A. L.; Cotlet, M.; Hofkens, J.; De Schryver, F. C.; Müllen, K. *Macromolecules* **2003,** *36*, 7752**.**

[54] Vallée, R. A. L.; Cotlet, M.; Van der Auweraer, M; Hofkens, J.; Müllen, K; De Schryver, F. C. *J. Am. Chem. Soc.* **2003**, 126, 2296.

[55] Bowden, N. B.; Willets, K. A.; Moerner, W. E.; Waymouth, R. M. *Macromolecules* **2002**, *35*, 8122.

[56] Basché, T.; Kummer, S.; Brauchle, C. *Nature* **1995**, *373*, 132.

[57] Mei, E.; Vinogradov, S.; Hochstrasser, R. M. *J. Am. Chem. Soc.* **2003**, *125*, 13198.

[58] English, D. S.; Furube, A.; Barbara, P. F. *Chem. Phys. Lett.* **2000**, *324*, 15.

[59] Turro, N. J. *Modern Molecular Photochemistry*; Benjamin/Cummings: Menlo Park, CA, 1978.

[60] Hubner, C. G.; Renn, A.; Renge, I.; Wild, U. P. *J. Chem. Phys.* **2001**, *115*, 9619.

[61] Stracke, F.; Heupel, M.; Thiel, E. *J. Photochem. Photobiol., A* **1999**, *126*, 51.

[62] Veerman, J. A.; Garcia-Parajo, M. F.; Kuipers, L.; van Hulst, N. F. *Phys. Rev. Lett.* **1999**, *83*, 2155.

[63] García-Parajó, N. F.; Veerman, J. A.; Bouwhuis, R.; Vallée, R.; van Hulst, N. F. *ChemPhysChem* **2001**, *2*, 347.

[64] Haase, M.; Hubner, C. G.; Reuther, E.; Herrmann, A.; Mullen, K.; Basché, T. *J. Phys. Chem. B* **2004**, 108, 10445.

[65] Weston, K. D.; Carson, P. J.; Metiu, H.; Buratto, S. K. *J. Chem. Phys*. **1998**, *109*, 7474.

[66] Vallée, R. A. L.; Tomczak, N.; Kuipers, L.; Vancso, G. J.; van Hulst, N. F. *Phys. Rev. Lett.* **2003**, *91*, 038301.

Chapter 4

Direct monitoring of single molecule rotational and translational diffusion in a polymer host*

The diffusion of guest molecules within a polymeric matrix provides a wealth of information about the molecular scale dynamics of the host. Using wide-field fluorescence microscopy we monitored molecular motion at a single-molecule level in different polymers at room temperature. Application of single molecule based techniques offered us the possibility to observe heterogeneous dynamics and revealed diffusion processes otherwise hidden in the ensemble average. Far above the glass transition temperature of the polymeric host (poly(dimethylsiloxane)), the translational diffusion of single $DiIC_1(5)$ molecules occurred over micrometer length scales and displayed a "Brownian" behavior. Close to the glass transition, the translational diffusion was arrested and reorientational processes dominated the diffusion behavior. Simultaneous observation of different single 5-TRITC dye probe molecules in poly(methyl acrylate) gave a direct evidence for the presence of broad heterogeneous dynamics in the investigated system. The rotating molecules displayed a nonexponential relaxation behavior indicating that multiple timescales were involved in the rotational process. Below the glass transition no apparent translational or rotational diffusion processes for single probe molecules in poly(styrene) were present on the experimental time-scale. The presence of static heterogeneity in the sample was assessed in an indirect way by observing changes in the photophysical properties of the same set of single molecules upon oxygen removal.

* Part of this Chapter has been published in: Tomczak, N.; Vallée, R. A. L.; van Dijk, E. M. H. P.; García-Parajó, M. F.; Kuipers, L.; van Hulst, N. F.; Vancso, G. J. Probing polymers with single fluorescent molecules. *Europ. Polym. J.* **2004**, *40*, 1001.

4.1 Introduction

Changes in the nanoscale polymer dynamics across the glass transition are a topic of great current interest in polymer physics [1-3]. The presence of nonexponential relaxation processes close to the glass transition temperature (T_g) and their possible origin from the spatially heterogeneous dynamics are still under investigation [4-6]. Remarkably, no microscopic theories able to explain in detail the glass relaxation phenomena at temperatures $T_g<T<1.2T_g$ are available. Although diffusion in polymeric and low molecular glasses has been studied for many years on the ensemble level [7], no conclusive theory has been established on the nature of diffusion on the microscopic level [8].

Single molecule fluorescence detection with its inherent ability to capture details beyond the ensemble averages is a perfect candidate to study molecular level processes in liquids or in solids (for a recent review see for example [9]). Since the advent of optical single molecule research it has been recognized that single molecule *localization*, *orientation* determination, and *tracking* have enormous potential as tools for various studies across different fields of science [10]. In the polymer field it is still under debate whether molecular relaxation processes close to the glass transition should be described by intrinsically non-exponential relaxation functions in a homogeneous system or rather by a distribution of exponentials, each with a characteristic time-scale. Single molecule detection offers the possibility to observe the heterogeneous processes directly [11-13].

Although there are methods which allow one to obtain information about polymer dynamics by monitoring the *photophysical* properties of the probes [11-15], due to the large degree of mobility above the glass transition temperature the interpretation of the corresponding data remains difficult and the results cannot be related in a straightforward manner to the host dynamics [13]. The application of scanning-based methods to study large-scale molecular motion is rather limited, and only few studies were performed by scanning confocal microscopy [16] or near-field optical microscopy [17-19]. Fluorescence correlation spectroscopy [20-22] or fluorescence burst analysis [23,24] was extensively used to study diffusion in liquids, however both techniques average over a large population of different single molecules.

A more convenient approach from the experimental point of view is to use wide-field methods [25-29]. In these methods, a large area of the sample is being illuminated. This allows one to localize and track many different single molecules simultaneously. Therefore, the requirements for locality and spatially resolved investigations necessary to obtain information about the heterogeneous dynamics are met. For example by using far-field microscopy, Dickson et al. [30] performed room temperature tracking of single Nile Red

molecules solvated in pores of poly(acrylamide) gel. Their results revealed that, on the time-scale from 0.1 to 1 s, the structure of the gel matrix hindered the Brownian motion. Investigations on the influence of the specific structure of the surroundings on the Brownian motion of single molecules or nanoparticles [31] were also performed for nanoporous networks made of sol-gel glasses [32], in fluid lipid membranes [33-35] or in cytoplasmic membranes of living cells [36].

Upon approaching the glass transition temperature, the translational diffusion processes slow down. Reorientation of the chromophore mixed into the polymer provides a means to characterize the range of the segmental scale dynamics [37-39]. At the single molecule level Deschenes and Vanden Bout [40,41] used scanning confocal microscopy to follow the orientational diffusion of single rhodamine molecules embedded in poly(methyl acrylate) above the glass transition temperature of the polymer. Non-exponential correlation functions of the molecular reorientation processes were found and broad distributions of characteristic time-scales for diffusion were obtained. It was shown that the nonexponential behavior resulted from a superposition of many different exponential processes at shorter time-scales. Additionally, their study gave substantial evidence for the spatially heterogeneous dynamics near the glass transition.

Below the glass transition temperature, Bartko et al. measured [42] the three-dimensional orientational motion of single molecules in poly(methyl methacrylate). They found a signature of hopping-mediated diffusion processes. Such processes are believed to be partially responsible for the different temperature dependencies of the translational and rotational diffusion in glass-forming liquids close to the glass transition [43,44]. To obtain full three-dimensional information about the molecular orientation, the use of more sophisticated, dedicated, optical setups combined with advanced pattern analysis are required. The orientation of the emission dipole moment for all three coordinates was estimated by introducing specific aberrations into the optical path [45-47] or by slightly defocusing the optics [48,49]. The absorption dipole moment orientation was obtained by recording the excitation rate of the chromophore as it was raster scanned through an inhomogeneous field generated by near-field optical probes [50,51] or by employing the so-called anullar illumination scheme [52,53]. However, most of the methods described required fitting of the single molecule fluorescence images captured to physical models. To obtain reliable patterns, long integration times are needed, which limits these methods to study processes with rather slow dynamics. Additionally, for such methods post-acquisition analysis is usually time-consuming. For systems with high mobility present it is therefore more convenient to use circularly polarized light for excitation and resolve the orientation of the emission dipole moment in two-polarization channels.

In this Chapter we describe single molecule investigations of polymer dynamics by using wide-field microscopy. Far above the glass transition temperature we follow translational diffusion of single molecules and for each single molecule we extract translational diffusion constants. We obtain a distribution of the diffusion coefficients resulting from the presence of polymer heterogeneities, very likely associated with the presence of interfaces. Close to the glass transition temperature, by employing a polarization sensitive detection scheme we follow the reorientational diffusion of single chromophores. Simultaneous investigations of many different single molecules give a direct evidence of spatially heterogeneous dynamics. Additionally, the single molecule method used here allowed us to visualize processes otherwise hidden in the ensemble average. Below the glass transition temperature, we show, through indirect studies, that there is a static heterogeneity in the polymer structure. The methods described in this Chapter open a new platform for polymer investigations on the nanoscale using wide-field microscopy.

4.2 Experimental part

4.2.1 Materials and sample preparation

To investigate the heterogeneous dynamics in polymers, various different dye/polymer samples were prepared. As host matrices we chose polystyrene (PS, Polymer Standard Service, molar mass M_n=89.3 kg/mol, polydispersity M_w/M_n=1.06, glass transition temperature T_g = 100 ºC), poly(methyl acrylate) (PMA, Aldrich, M_n=120 kg/mol, T_g = 8 ºC) and poly(dimethylsiloxane) (PDMS, Sylgard 184, Dow Corning, T_g = -150 ºC). All experiments were performed at room temperature. Therefore, for different polymers we were able to perform experiments at a different distance from their respective glass transition. The probes used in this study were DiD (1,1'dioctadecyl-3,3,-3',3'-tetramethylindodicarbocyanine perchlorate, Molecular Probes D-307), $DiIC_1(5)$ (1,1',3,3,3',3'-haxamethylindodicarbocyanine, Molecular Probes, D-307) and 5-TRITC (tetramethylrhodamine-5-isothiocyanate, G isomer, Molecular Probes T-1480). The chemical structures of the chromophores and polymers are presented in Figure 1. Solutions of dyes in toluene (for DiD and DiIC1(5)) or tetrahydrofuran (THF, for 5-TRITC) containing various amounts of polymers were spin-coated at 3000 rpm for 60 s onto a cleaned glass cover slides (with a diameter of 10 mm or 20 mm, Fisher Scientific) to produce uniform thin coatings with thickness values ranging from 300 to 500 nm. Prior to spin coating, the glass cover slides were cleaned using a Piranha solution (mixture of 1:4 of 30% H_2O_2 and concentrated H_2SO_4), rinsed with Milli-Q water and ethanol, and finally dried in a stream of nitrogen gas. *Caution! Piranha solution is a very strong oxidant, reacts violently with organic materials, and should be handled with utmost care!* The concentration of the dyes in the resulting films

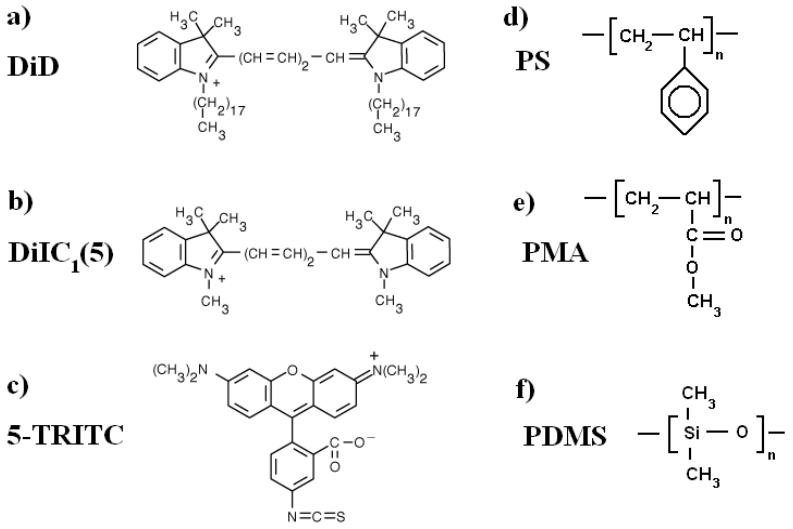

Figure 1. Chemical structures of fluorescent probes and polymers used in this study. Probes: DiD (a), $DiIC_1(5)$ (b), 5-TRITC (c) and polymers: polystyrene (d), poly(methyl acrylate) (e), poly(dimethylsiloxane) (f).

was kept low (10^{-9}-10^{-10} M) to ensure adequate spatial separation for optical single molecule observations. The PS samples were subsequently annealed in vacuum, first for 12h at 60 °C and subsequently for 3h at 105 °C. PMA and PDMS samples were annealed at room temperature in vacuum for 12h.

4.2.2 Wide Field Microscopy (WFM)

Light from a CW Ar^+-Kr^+ ion laser at wavelengths of 531 nm and 647 nm or from a HeNe laser at a wavelength of 632 nm was used for excitation. A circularly polarized laser beam passed through a beam expander and was focused onto the back aperture of a high NA objective (Zeiss, NA=1.4, oil immersion) (Figure 2b). The fluorescence photons emitted from the illuminated area were collected by the same objective and after passing through emission filters were split into two orthogonal polarization channels using a Wollaston prism (Linos 037808) and subsequently imaged with a lens (Linos 063827) onto an intensified charged coupled device (CCD camera, Pentamax GEN IV) (schematic picture of the setup is shown in Figure 2a). The rate of the camera data acquisition was set to 50 or 100 ms/frame. An example of a fluorescence frame obtained with WFM is shown in Figure 2c. The images from the camera were processed by custom LabView software. Information regarding intensity and polarization for each pixel on the frame was obtained simultaneously. Fluorescence images were collected for at least 60s. The position of the molecules was determined by the brightest pixel method, or by fitting a two-dimensional Gaussian function to the molecule intensity pattern. No difference between the two methods in the calculated diffusion coefficient was found.

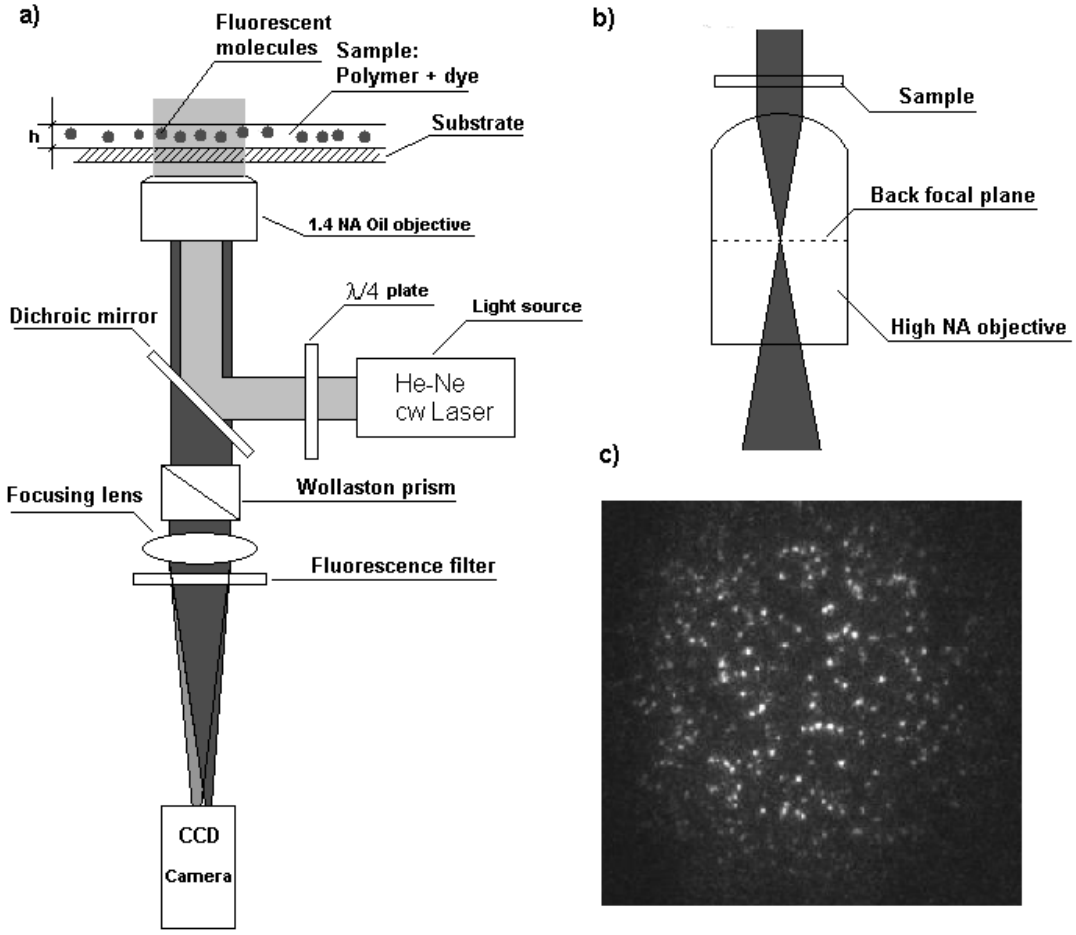

Figure 2. a) Schematics of the wide field setup. b) By focusing the excitation light on the back focal plane of the objective a large area is excited. A 22x22 μm^2 fluorescence intensity frame of single $DiIC_1(5)$ molecules embedded in polystyrene is shown in (c).

4.3 Results and discussion

4.3.1 Single molecule translational diffusion far above the glass transition

It is expected that the polymer relaxation processes far above the glass transition temperature are homogeneous and the resulting distributions of the polymer diffusion coefficients are narrow. To estimate the amount of mobility present in the polymer matrix one can follow the diffusion of molecular tracers. The probe will be coupled with the polymer relaxation processes and report on the polymer matrix dynamics. We mixed $DiIC_1(5)$ molecules into PDMS and investigated them by means of wide-field microscopy. Figure 3 shows fifteen 10x10 μm^2 fluorescence intensity frames (out of the total 400 subsequent frames) obtained by wide-field microscopy. The time delay between every subsequent frame is 5 seconds.

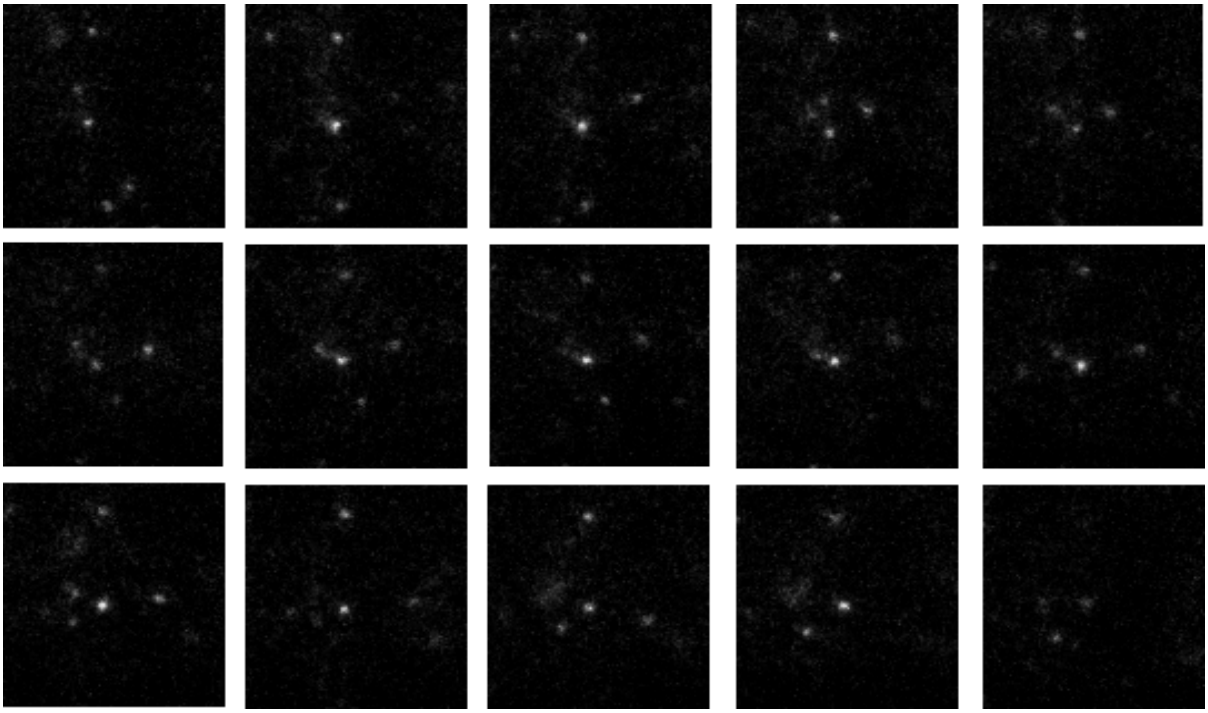

Figure 3. Sequence of fifteen 10x10 μm^2 fluorescence intensity frames obtained with a wide-field microscope (reading from left to right in subsequent rows, from top to bottom). The frames integration time is 100 ms and the time difference between the frames is 5s. Translational diffusion of individual $DiIC_1(5)$ molecules in PDMS is clearly visible.

It is apparent form the frame sequence that many molecules undergo translational diffusion. Some of the molecules appear and disappear from the field of view. The main reasons for this are photobleaching, diffusion of the molecules away from the focal plane, and possibly strong fluorescence quenching due to interaction of the dye with the glass substrate.

Once the molecules have been localized and tracked, one can estimate the molecular diffusion coefficients. To obtain qualitative and quantitative information about the diffusion process for each molecule, first we extract a set of space-time coordinates $\{x(t_i), y(t_i), t_i\}$, where x, y is the position of the molecule, *t* is time and the index *i* is the discrete observation time point. This allows us to obtain 2D projections of the single-molecule trajectories. Several examples of such trajectories are shown in Figure 4a. Although in general the traces appear to display a random walk behavior, there is always a question whether the diffusion of the single molecules monitored is indeed isotropic. To check whether directional bias due to flow, mechanical drifts or anisotropy of the prepared samples occurred, all position shifts were plotted to produce a scatter plot of step sizes and directions (Figure 4b).

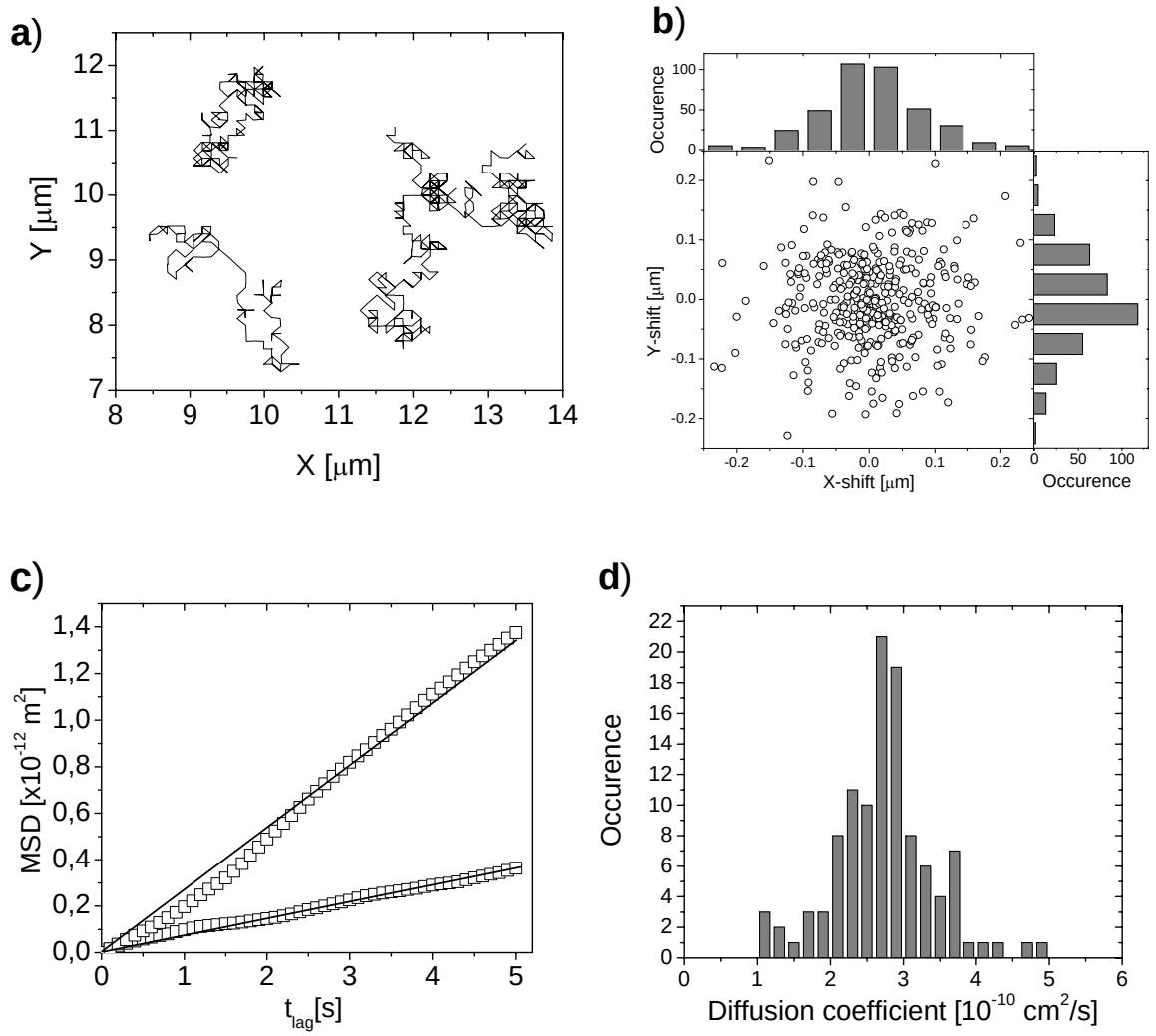

Figure 4. a) Diffusion trajectories for different single $DiIC_1(5)$ molecules embedded in a PDMS matrix. b) Scatter plot of the position shifts for the time-traces shown in (a). c) Plots of the calculated mean square displacement as a function of time-lag. Linear relationship between the mean square displacement and time shows that the molecules display a Brownian-like diffusion. The solid lines are fits to equation 2. d) Histogram of single molecule diffusion coefficients obtained for 111 single $DiIC_1(5)$ molecules.

The distribution of the displacement direction (Figure 4b) shows that the diffusion is isotropic in two x, y dimensions on the length scale of 20 μm x 20 μm and that there is no constant instrumental drift present. From the obtained single molecule trajectories we calculated the mean square displacement (*MSD*) for every time lag ($t_{lag}=n\delta t$, δt is the frame integration time, n is the number of frames) in the form of:

$$MSD = < (x_{i+n} - x_i)^2 + (y_{i+n} - y_i)^2 >, \quad (1)$$

where *i* ranges from 1 to *N-n*, *N* is the total number of molecule positions recorded, *n* takes on values 1,2,3…*N*/2. The linear behavior of *MSD* as a function of the time lag shows that the translational diffusion of single $DiIC_1(5)$ molecules in PDMS far above its glass transition temperature is Brownian in nature [57].

Because we observe only the projections of the emission dipole moments into the focal plane of the objective, an evaluation of the diffusion traces is performed using the theory for two-dimensional diffusion (derived from the Einstein diffusion equations) leading to the relationship:

$$MSD = 4Dt_{lag} \tag{2}$$

Using equation 2 and obtaining the slopes of the *MSD* plots (Figure 4c) we calculated the single molecule diffusion coefficient *D*. Figure 4d shows the histogram of the diffusion coefficients for 111 individual $DiIC_1(5)$ molecules. The mean diffusion coefficient was found to be equal to $(2.6 \pm 0.1)\ x10^{-10}\ cm^2/s$. However, the diffusion coefficients of single $DiIC_1(5)$ translating inside the PDMS matrix can be different from each other by a factor of 4. The broadening of the distribution is not caused by the experimental accuracy but rather by the presence of heterogeneities in the sample. Broadening towards both higher and lower values can be due to diffusion of the molecules near the polymer/substrate or polymer/air interfaces. The thickness of the polymer films was estimated to range from 300 to 500 nm and the trajectories presented in Figure 4a show that the molecules translated many micrometers during the observation time. That means that the molecules could spend significant amount of time close to the interfaces. Also, when focusing very close to the glass substrate we observed large populations of molecules with diffusion coefficients low enough to categorize them as immobile (within the experimental time scale). Such molecules are not present in the deeper parts of the samples (further away from the substrate). Additionally, certain portion of molecules showed deviations from the linear dependency of mean square displacement with time. Such behavior is an indication of anomalous diffusion [54, 55]. We attribute this observation to the adsorption of the chromophore to the glass substrate and to time dependent interactions of the probes with the glass substrate causing the nonlinear behavior.

We have shown in this section that wide-field microscopy is a suitable technique to follow long-range molecular diffusion processes occurring in a polymer melt. Our setup has also the capability to resolve the polarization of the fluorescence emission. In the case of $DiIC_1(5)$ molecules in PDMS we observed that the rotational diffusion of the chromophores occurs on time-scales much shorter than the integration time and therefore the molecules could rotate many times between two consecutive frames. This did not allow us in this study to determine

the characteristic time-scales associated with the rotational diffusion for the investigated system ($DiIC_1(5)$ in PDMS at room temperature).

4.3.2. Single molecule rotational diffusion near the glass transition

For most polymers, different theories predict an arrest of the homogeneous viscous flow at a temperature T_c, well above the glass transition temperature. Also the spatially heterogeneous dynamics is believed to set on at T_c [56-59]. For single 5-TRITC molecules embedded in poly(methyl acrylate) at room temperature, the translational diffusion slowed down the point where it was not possible to observe probe diffusion on the time scale of minutes and over distances larger than the spatial resolution of the setup (~100 nm) [60]. Even though the long-range molecular diffusion processes were suppressed at these temperatures, still the molecules were free to rotate. If the rotation is on the time-scale of the observation time, it can be visualized directly and single molecule rotational behavior can be extracted. The single molecule rotational behavior can serve as a basis to characterize the environment of the probe molecule.

As it was already mentioned in the experimental section, WFM allows one to obtain 2-D fluorescence images ("frames") of many single molecules simultaneously (Figure 2c). By placing a Wollaston prism in the detection path we were able to resolve the emission into two orthogonal polarization channels [61]. Polarization resolved detection allowed us to obtain fluorescence intensity traces for the two independent polarization channels for each pixel, or group of pixels. Figure 5a shows a time-trace for a single 5-TRITC molecule embedded in a thin (~100 nm) PMA film at room temperature. The total fluorescence intensity fluctuates in time, reflecting the changes in the time-dependent emission properties (e.g. fluorescence lifetime [62], triplet excursions [63,64], dark state statistics [65], or absorption and emission spectra [66]) of the molecule and/or the out-of-plane rotational motion of the molecule. Because the excitation rate is proportional to the out-of-plane orientation of the absorption dipole moment of the chromophore, in case of purely out-of-plane reorientation of the probe the signals in the two polarization channels will be correlated. In some parts of the trace (one of them indicated by the arrows), anticorrelated intensity levels in the two polarization channels are also observed. Since the total intensity level for the part indicated by arrows in Figure 5a remained constant, the molecule undergoes in-plane rotational motion. Excitation with circularly polarized light ensures an excitation independent of the in-plane orientation and ensures the best signal to noise ratios throughout the trace.

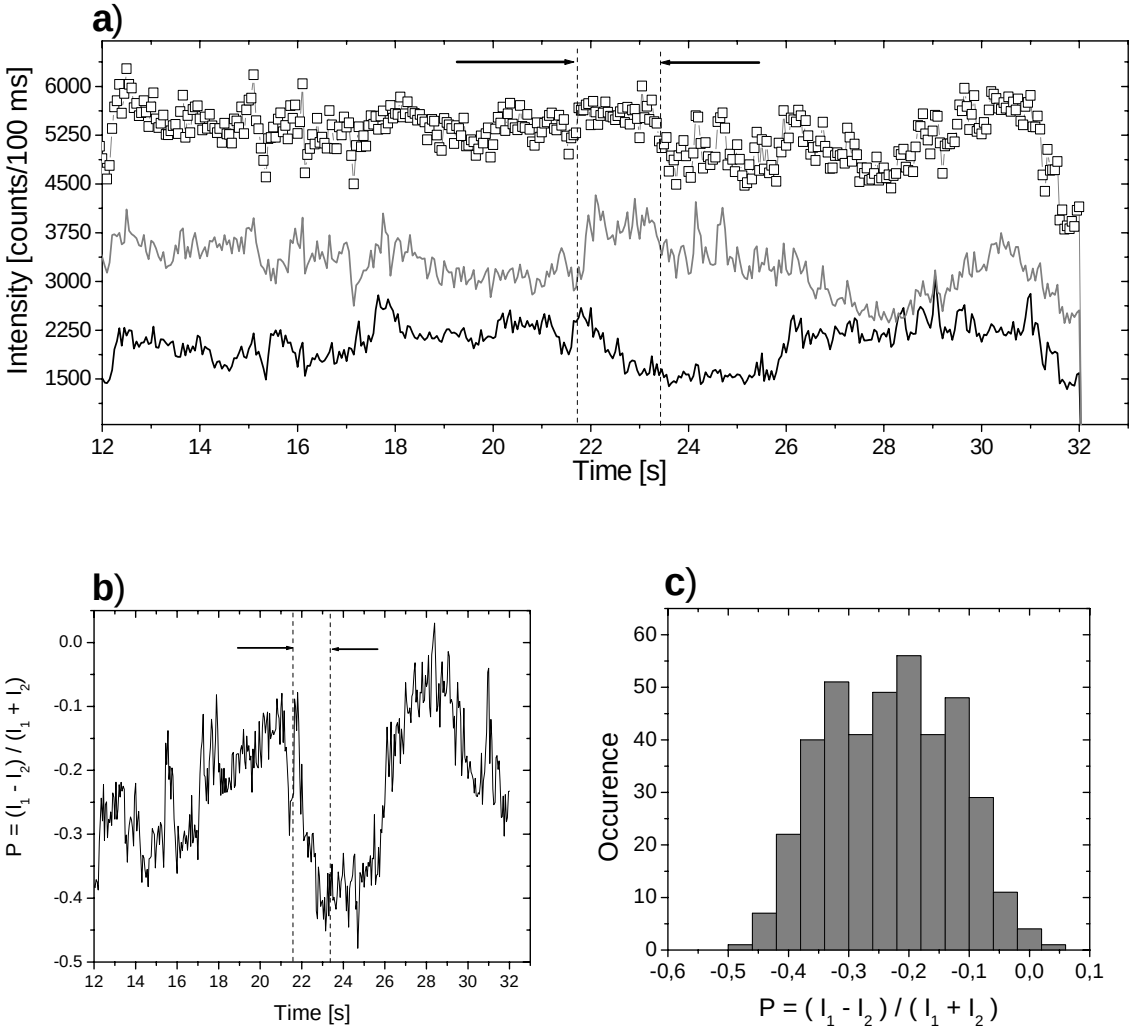

Figure 5. (a) Total fluorescence intensity (gray connected rectangles) and the intensities in the two orthogonal polarization directions (gray and black) for a single 5-TRITC molecule embedded in PMA. (b) The degree of polarization (P) was calculated using equation 3. The arrows in (a) and (b) indicate where in-plane rotational motion occurred for this molecule. (c) Static distribution of P values taken from the time trace displayed in (b).

To estimate the orientation and orientational motion of the probes from single molecule fluorescence intensity time-traces, values of the degree of polarization (P) are calculated (Figure 5b):

$$P(t) = \frac{I_1(t) - I_2(t)}{I_1(t) + I_2(t)}, \tag{3}$$

where I_1 and I_2 are the intensities in the two orthogonal polarization channels, respectively, and t is time.

Such a treatment of data ensures that the orientational diffusion probed is not affected by laser intensity fluctuations, or triplet excursions. Additionally, the knowledge of the full three-dimensional orientation is not required because it is contained already in the fluctuations of the polarization. The values of P can range from –1 to +1 with extreme values attainable through a in-plane rotation of 90º. The time-trace of P presented on Figure 5b shows directly that the probe reorients in different directions while being embedded within the polymer matrix. For molecules diffusing out-of-plane, there will be a substantial coupling to both of the channels due to the use of a high NA objective. Therefore the values of P will attain the extreme (–1 and 1) values only when the diffusion is isotropic and occurring on time-scales longer than the integration time.

Not all investigated probes showed clear molecular reorientations. To quantify the extent of molecular mobility of the probes first we classified the molecules as "fixed" or "rotating", during the collection time, by looking at the widths of their static distributions of P (Figure 5c) [67]. As a reference for the "fixed" species we chose the width of the distribution found for DiD molecules in a PS matrix at room temperature (80 degrees below the T_g of PS in the bulk). Scanning confocal experiments described in Chapter 5 of this thesis showed that for such conditions the molecules do not show any orientational diffusion in the polymer matrix on the timescale of our measurements (minutes).

For 5-TRITC embedded in PMA at 22 ºC we found that 30 % of the investigated molecules could be termed as "fixed" and 50% of molecules were termed as "rotating". For the remaining 20% of the molecules, extensive hopping was observed and the corresponding time traces exhibited a more complex behavior. We will discuss these time traces later in this Chapter.

To extract the typical time-scales of the rotational diffusion for the molecules which did not show extensive "hopping", the autocorrelation function $C(t)$ of P was calculated

$$C(t) = \frac{\sum_{t'=0}^{T} P(t')P(t'+t)}{\sum_{t'=0}^{T} P(t')P(t')} \qquad (4)$$

A typical plot of $C(t)$ is presented in Figure 6. The first point representing the noise was removed from the plot. For all molecules investigated the autocorrelation function deviated significantly from a single exponential decay function. In the framework of spatially heterogeneous dynamics there can be two reasons for the observed nonexponential behavior. Firstly, the dynamics of the probes is nonexponential in nature.

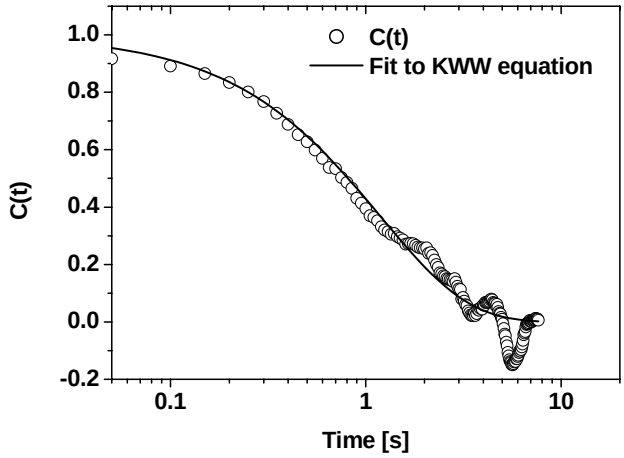

Figure 6. Autocorrelation function of the degree of polarization and the fit to the KWW equation for one single 5-TRITC molecule in PMA.

The second reason for the nonexponential shape of the correlation function might be that the probe dynamics is changing in time along the trace, a feature often called rate exchange or "heterogeneity lifetime" [68]. To address these issues we looked at the rate of the molecular reorientation. The emission intensities in the two channels for isotropic excitation are:

$$\begin{aligned} I_1 &= I_0 \cos^2 \varphi \\ I_2 &= I_0 \sin^2 \varphi \end{aligned}, \tag{5}$$

where I_0 is the total emission intensity and φ is the in-plane dipole angle. For the diffusing molecule, for each time-interval, the in plane angle can be calculated:

$$\varphi(t) = \tan^{-1} \sqrt{\frac{I_1(t)}{I_2(t)}} \tag{6}$$

In Figure 7a we plot the degree of polarization and in Figure 7b the absolute value of the first derivative of the orientation angle ($d\varphi/dt$) with respect to time. Parts of the trace clearly show that the orientational behavior of the molecule is changing in time and subsets of the trace where the reorientational behavior is substantially different from the average (faster or slower) can be identified. Unfortunately, the time scale of such subsets is too short to perform more detailed analysis and check whether the processes within the subsets are purely exponential. Nevertheless, it is obvious that the presence of exchange times shorter than the total observation time will be the cause of the nonexponentiality present in the autocorrelation function. Many processes found in Nature (e.g. relaxation behavior of glass

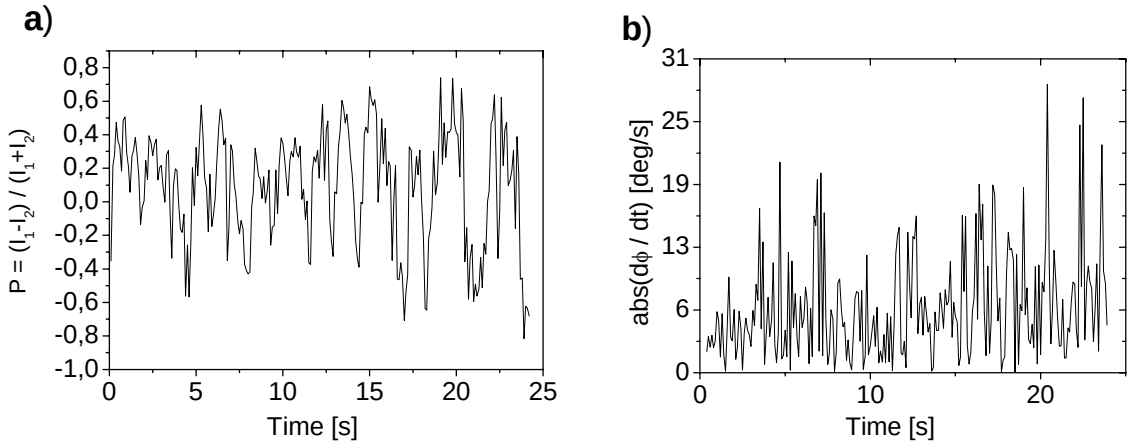

Figure 7. a) The degree of polarization and b) the absolute value of the first derivative of the in-plane emission dipole moment orientation angle (dφ/dt) for a single $DiC_1(5)$ as a function of time.

forming materials near the critical temperature) cannot be expressed in terms of an exponential relaxation process with one relaxation time [69,70]. As a consequence, empirical fitting functions are being applied, one of the functions being the Kohlrausch-Williams-Watts (KWW) distribution function [71]:

$$C(t) = \exp\left[-\left(t / \tau_{KWW}\right)^{\beta}\right], \tag{7}$$

where $C(t)$ is the autocorrelation function and τ_{KWW} is the characteristic time describing the process. The fitting parameter β determines the shape of the autocorrelation function. This parameter is often called the stretching parameter and its value reflects the breath of the relaxation spectrum ($0<\beta<1$; $\beta=1$ for a single exponential process). The advantage of using such a fitting is that one does not need to make assumptions about the nature of the relaxation process (incorporating single or multiple time-scales). As shown in Figure 6 the KWW equation describes our experimental data well. The average rotational correlation time (τ_R) can be calculated by directly integrating $C(t)$ but it can be also obtained by making use of the fitting parameters τ_{KWW} and β [71]:

$$\tau_R = \int_0^{\infty} C(t)dt = \int_0^{\infty} \exp\left[-\left(\frac{t}{\tau_{KWW}}\right)^{\beta}\right]dt = \frac{\tau_{KWW}\Gamma(1/\beta)}{\beta}, \tag{8}$$

where Γ stands for the Gamma function. In Figures 8a and 8b we show the histograms of τ_R and β values obtained from many different single molecule observations. The subset of 5-TRITC molecules, which were called "rotating", exhibit a broad range of rotational time-scales when embedded in the same polymer matrix. The mean relaxation time of the distributions $<\tau_R>$= 3.81 s is in excellent agreement with the reported literature values

obtained by other authors (3.3 s for Rhodamine 6G in PMA at 18 ˚C) [75]. The β parameter distribution shows that for almost all molecules investigated, the exchange times are much shorter than the total observation time (from seconds to minutes). It seems to be quite clear that bulk ensemble experiments performed on the same system will result in β parameters which are substantially lower than 1, i.e. the relaxation process will show nonexponential behavior. The main advantage of our wide-field approach is the ability of spatially mapping the heterogeneous molecular dynamics inside the polymer, above the glass transition directly. Although we are able to follow the differences form molecule to molecule, due to the far-field characteristic of the detection method, our experiments do not allow us to determine accurately the size of the "domains" [5] that could be characterized with one relaxation behavior.

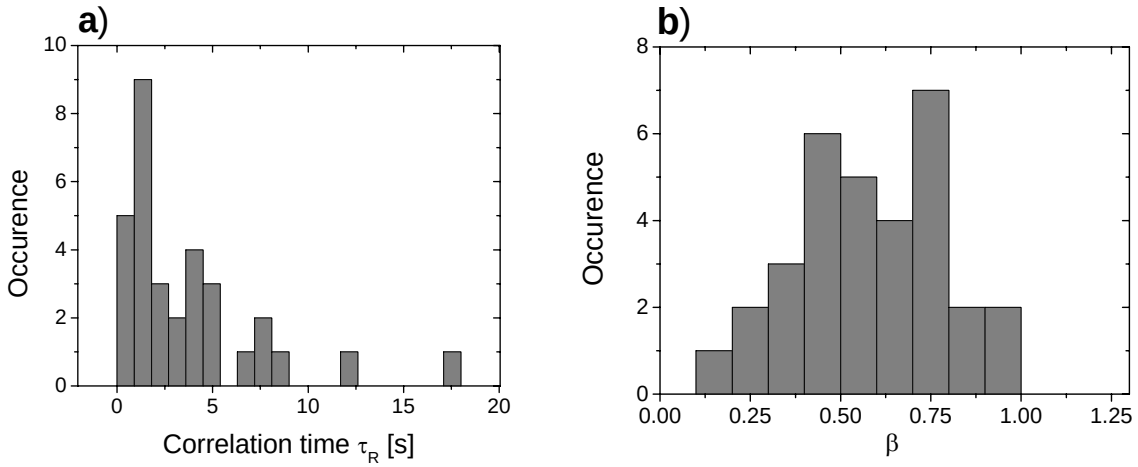

Figure 8. Histograms of τ_R (a) and β (b) parameters obtained for different single 5-TRITC molecules embedded in the same PMA matrix at room temperature (12 degrees above T_g).

As mentioned earlier, not all molecules could be termed as rotating and 20 % of all molecules investigated exhibited more complex behavior. As an example of a *P* time-trace one such molecule is presented in Figure 9a. Regions of slow and fast rotational motions can be distinguished and a significant frequency of orientational "jumps" is observed. The static distribution of *P* (Figure 9b) is also broad in this case meaning that the molecule probes many different orientations during the investigation time. However, the distribution does not show one broad peak but rather can be described as a multi-modal distribution. The lines in Figure 9a indicate the values, which correspond to the peak positions in the histogram (Figure 9b). A time-trace of *P* presented in Figure 9a might suggest that not only the rotational diffusion of $DiIC_1(5)$ molecules in poly(methyl acrylate) is mediated by consecutive hopping from one spatial position to another but that the rotational diffusion is also the result of hopping

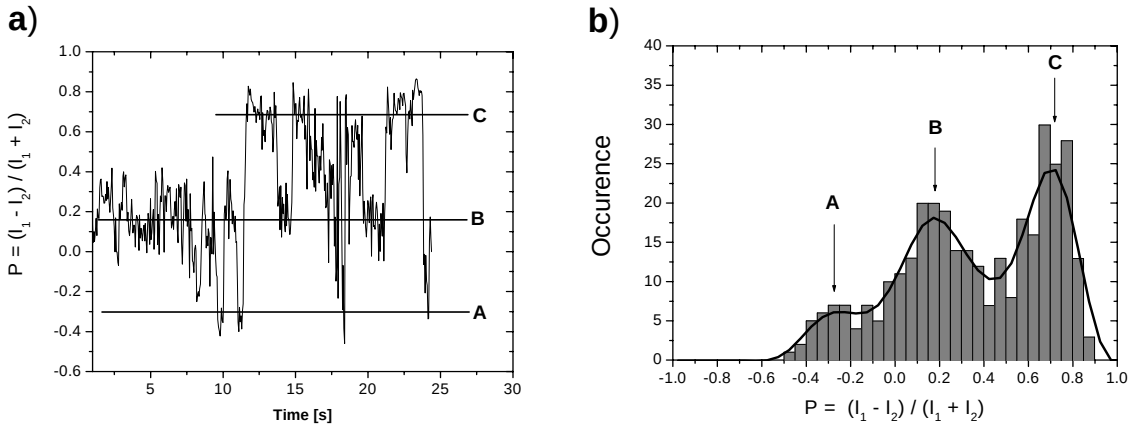

Figure 9. a) Time trace of the degree of polarization for a single 5-TRITC molecule in PMA exhibiting a complex rotational behavior. The black solid lines are guides to the eye. b) Static distribution of *P* presented in (a). The peak values of *P* at positions A, B and C are the same as indicated in (a). The black line is obtained after FFT smoothing of the data.

between a few different orientations (or "sites") within the polymer matrix in which the probe can reside for different amount of times before switching to another "site" or to start to rotate with different rates.

As suggested by Bartko et al. [42], such small uncorrelated motion including jump-like behavior at the single molecule level is likely to contribute significantly to the translational-rotational paradox near T_g observed in the bulk, where the ensemble-measured translation appears to be orders of magnitude faster than the rotational motion [5,43,44]. Similar hopping mechanisms [72] were also witnessed for single dye probes incorporated within the gel phase of supported lipid bilayers [35]. The reason for such a diffusion mechanism was explained by the presence of a microscopic heterogeneity determined by local arrangements of lipids in the crystalline packing, which undergo constant dynamics changes. Our single molecule study shows directly that such pocket-like microscopic regions in the polymer develop already 12 degrees above the glass transition temperature for the system investigated. Additionally, switching of the dye between similar orientations in space means that the probe environment displays a rather high degree of rigidity. The molecular motion is therefore a result of the polymer-defined nanoenvironment combined with the thermal agitation and the flexibility of the probe. If the polymer freezes further, upon approaching the glass transition, it is likely that the jump frequency goes down. Below the glass transition the jumps are not frequent and are governed by the structure of the probe combined with the amount of free volume accessible to the probe in the matrix [73]. It would be of interest to investigate the size of the rigid environments above the glass transition by changing the size of the probes up to a few nanometers.

It is our intention throughout this Thesis to probe the dynamics of the polymer rather than that of the probes. It was certainly showed in this Chapter that the degree of mobility in the surrounding matrix influences the molecular tracers. However, the question about the coupling between the probe and the polymer dynamics was left unanswered. In bulk [74] and single molecule experiments [41], it was found that the motion of the probes is coupled to a certain degree to the α-relaxation of the polymer chains i.e. the probe motion follows the same temperature dependence. For small probes, however, a substantial decoupling from the α-relaxation was found starting at temperatures 30 to 50 degrees above the glass transition [75]. The origins of this behavior are largely unknown but it has been suggested that smaller probes better couple to the higher order relaxations like the β or γ processes.

The relationship between the relaxation times of the probe (τ_R) and the time scale for the relaxation of the polymer chains (τ_{pol}) was described with the relation [76]:

$$\left\langle \tau_{pol} \right\rangle = C_i \left\langle \tau_R \right\rangle_i^{\xi}, \quad 0<\xi< 1 \tag{9}$$

where $i = \alpha, \beta, \gamma$ denotes a given relaxation process and for ξ=1 there is a full coupling to given relaxation process. The constant C is related to the characteristic length scale of the given relaxation process and to the size of the probe. In our study the rotational behavior varied greatly from molecule to molecule within the same sample and even between molecules, which were collected simultaneously on the same frame. Introduction of heterogeneous dynamics found in our single molecule experiments (broad β and τ_R distributions) and especially the presence of the hopping mechanism for diffusion, into equation 9 makes the problem of obtaining one coupling parameter subtler. Describing the system with only average relaxation time without a proper knowledge of the exact shape of the distribution of the relaxation times will not allow us to obtain the full picture of the microscopic diffusion processes of the polymer chains. To be able to describe the polymer dynamics and reveal the coupling mechanism directly, additional single molecule experiments should be performed using probes with different dimensions, chemistry and under different experimental conditions. An approach to overcome the problems of the host-guest coupling strengths would include covalent attachment and labeling of the polymer chain by the probe [77]. Molecules with well-defined transition dipole moments could be incorporated within the polymer chain giving valuable information on the macromolecular motion. Here, we have opened a new experimental platform for such investigations by using a single molecule wide-field setup.

4.3.3 Static heterogeneity below the glass transition

Below the glass transition, $DiIC_1(5)$ molecules embedded in polystyrene were effectively trapped in the polymer matrix and did not display any visible rotational or translational diffusion on the experimental time-scale (minutes). Although our wide-field setup was successfully applied to observe large-scale molecular dynamics, its application to study slow molecular motion is limited due to the lack of high spatial resolution and the presence of setup drift. To determine whether the static heterogeneity in the polymer in the glassy state can be investigated by single molecule probes, we performed indirect studies based on oxygen removal. First, the single molecule fluorescence time-traces were recorded when the sample was in atmospheric environment. We then removed the oxygen from the samples by placing an environmental chamber above the sample stage and flushing nitrogen through the chamber for several hours. Subsequently we decreased the nitrogen flux to obtain a laminar flow through the chamber. After such a procedure the fluorescent intensity was recorded again for *the same* set of single molecules. Observations made on the same set of probes exclude therefore the possibility to sample different regions in the polymer with different structure and/or dynamics.

It is known that molecular oxygen plays an important role in photochemical processes common for most of the fluorophores like triplet excursions or photobleaching [78,79]. Reduction of the triplet state lifetime [80] in the presence of oxygen supports the idea that the formation of the singlet oxygen species occurs through a triplet-triplet annihilation mechanism between the dye and the oxygen [81-83]. The production of singlet oxygen can lead to a subsequent photochemical oxidation [78]. Upon removing the oxygen from the dye surroundings, the triplet lifetimes were found to increase considerably by many orders of magnitude from tens of microseconds [84,85] to tens of milliseconds for special conditions [80,81]. Temporal fluctuations of single molecule triplet lifetime were attributed to temporal fluctuations in the oxygen concentration in the environment of the probe [86]. To obtain information on the static disorder in a polymer film, English et al. [80] monitored changes in the photophysical behavior of many *different* single molecules depending on the oxygen content. Probing the same molecules after changing external conditions will ensure that the heterogeneity obtained by English et al. is not due to the dynamic properties of the polymer. Such experiments were not performed until now.

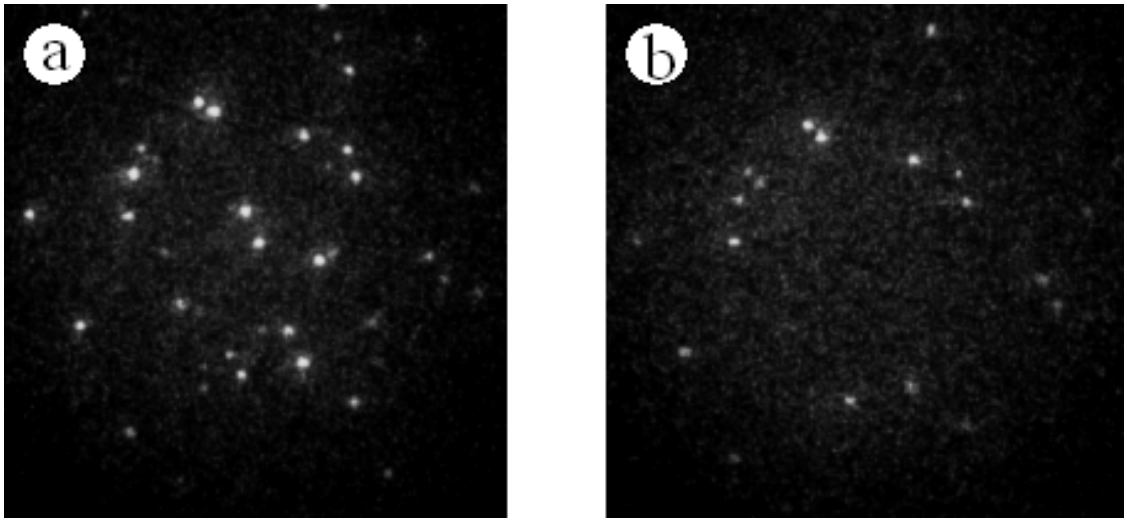

Figure 10. Fluorescence intensity frames obtained by wide-field microscopy. The spots are single fluorescent $DiIC_1(5)$ molecules imaged in air (a) and in nitrogen atmospheres (b). The same set of molecules present in both images can be clearly identified. Several molecules bleached during the data acquisition in air and are not visible in (b).

Figure 10 shows fluorescent intensity frames of single $DiIC_1(5)$ molecules in polystyrene obtained with a wide-field microscope. The same set of single $DiIC_1(5)$ molecules on both frames can be clearly identified. Several molecules are missing in part (b) because of the irreversible photobleaching process. For each molecule that persisted and could be imaged in both conditions we obtained intensity time-traces as presented in Figure 11. On the right side of the time-traces in Figure 11, intensity histograms for each of the conditions are plotted. The fluorescence emission of single molecules in part (a) and part (b) of Figure 11 shows a drastic change upon changing the environment. While being exposed to air, most of the time-traces had a constant intensity level and the resulting intensity histograms were narrow and symmetrical. When exposed to nitrogen, the time-traces displayed higher amplitude fluctuations in the intensity with several excursions to the background level. Since the reported triplet lifetime is usually much shorter than the integration time of our setup [85,87], we are not able to obtain *quantitative* information on the intersystem crossing yield and the triplet lifetime. However, the changes observed in the time-traces can be *qualitatively* explained by longer average triplet lifetimes after the removal of the molecular oxygen. This is also supported by the fivefold increase of the average time before photobleaching (from 20s in air to 90s in nitrogen) for the different conditions. Therefore, we attribute the changes in the time-traces to the changes in oxygen concentration in the polymer films. For a lower oxygen content the probability of probe-oxygen collision is lower, therefore the probability for triplet quenching is also lower. We performed a check whether the observed behavior could be caused by the level of humidity, however changes in the relative humidity from 3%

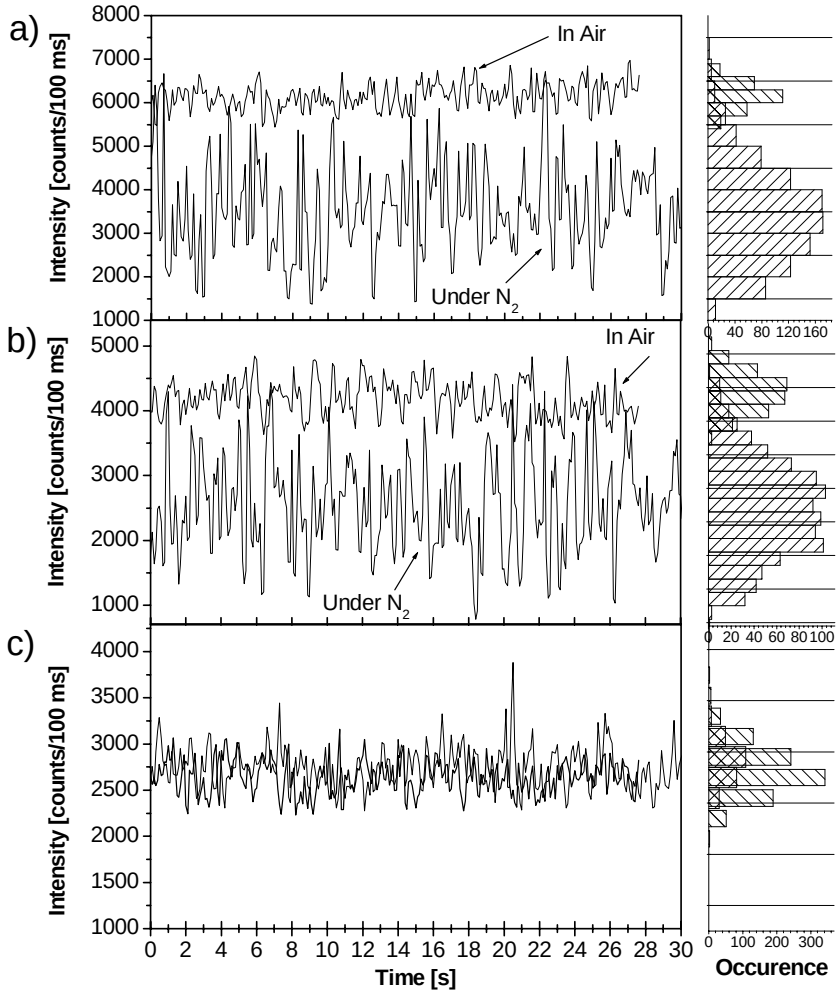

Figure 11. Fluorescence intensity time traces of individual $DiIC_1(5)$ molecules embedded in polystyrene at different imaging conditions i.e. in air and in nitrogen atmospheres, respectively. On the right hand side of the time traces the histograms of the fluorescence intensity are plotted. Nitrogen flushing had a dramatic effect on molecules in (a) and (b), while the molecule in (c) was not affected. The time traces in (c) overlap almost perfectly.

to 80% at room temperature did not cause any significant changes in the single molecule time traces. Not all of the investigated molecules (10-15%) had a visible change in the intensity time traces (Figure 11c). This can be explained by different rigidity of the polymer matrix or by different amount of the free volume [88-90] available for the oxygen to diffuse in the matrix [91,92]. The spatial distribution of molecules not influenced by the experimental procedure exemplifies the heterogeneous structure and/or dynamics present below the glass transition. It should be noted that this method probes only the threshold for oxygen diffusion in the polymeric host. For polystyrene, the oxygen molecules are relatively free to diffuse (diffusion constant of oxygen in PS at room temperature is equal to ~ $2x10^{-7}$ cm^2/s) [93,94],

therefore only the most rigid polymer surroundings could slow down the diffusion process [92].

Lower absolute intensity values, large intensity fluctuations and the appearance of long dark states when imaging under nitrogen were also the reason why the diffusion experiments described in this chapter where performed in air. For example, blinking processes during translational diffusion causes shortening of the diffusion traces. Longer triplet lifetimes lower the total intensity per integration time, therefore worsen the localization accuracy [95].

4.4 Conclusions

The translational and rotational diffusion of single molecules in polymer matrices were followed in time and the characteristic time scales of related processes were extracted. Above the glass transition temperature of the polymeric host the translational diffusion displayed Brownian like behavior. The distribution of the diffusion coefficient obtained from two-dimensional molecular traces was broad and was influenced by the presence of heterogeneities in the sample. When approaching the glass transition, the rotational motion dominated over translational diffusion over lengths scales smaller than the resolution of the experimental setup. Different populations of diffusion behavior were identified. Rotational diffusion mediated by hopping was witnessed. Evidence for heterogeneous dynamics was obtained directly from the single molecule experiments. While in some parts of the sample the molecules where free to rotate, in others the rigidity of the polymer matrix did not allow for movement of the probe on the time-scale of the experiments. No rotational and translational diffusion could be observed below T_g. Information about the presence of a static heterogeneity was obtained with an indirect method based on monitoring the photophysics of the same individual molecules under different experimental conditions. The results described in this chapter show that single-molecule detection and tracking are a powerful tool to study polymer dynamics above and close to the glass transition of polymers.

4.5 References

[1] Frick, B.; Richter, D. *Nature* **2001**, *267*, 1939.

[2] Stillinger, F. H. *Science* **1995**, *267*, 1935.

[3] Angel, C. A.; Ngai, K. L.; Mckenna, G. B.; McMillan, P. F.; Martin, S. W. *J. Appl. Phys.* **2000**, *88*, 3113.

[4] Schmidt-Rohr, K.; Spiess, H. W. *Phys. Rev. Lett.* **1991**, *66*, 3020.

[5] Ediger, M. D. *Annu. Rev. Phys. Chem.* **2000**, *51*, 99.

[6] Russell, E.; Israeloff, N. E. *Nature* **2000**, *408*, 695.

[7] Vieth, W. R. *Diffusion in and Through Polymers. Principles and Applications*; Hanser Publishers: Munich, 1991.

[8] Sillescu, H. *J. Non-Cryst. Solids* **1999**, *243*, 81.

[9] Kulzer, F.; Orrit, M. *Annu. Rev. Phys. Chem.* **2004**, *55*, 585.

[10] Xu, X.-H.; Yeung, E. S. *Science* **1997**, *275*, 1106.

[11] Vallée, R. A. L.; Cotlet, M.; Hofkens, J.; De Schryver, F. C.; Mullen, K. *Macromolecules* **2003**, *36*, 7752.

[12] Ye, J. Y.; Ishikawa, M.; Yogi, O.; Okada, T.; Maruyama, Y. *Chem. Phys. Lett.* **1998**, *288*, 885.

[13] Ishikawa, M.; Ye, J. Y.; Maruyama, Y.; Nakatsuka, H. *J. Phys. Chem. A* **1999**, *103*, 4319.

[14] Hou, Y.; Higgins, D. A. *J. Phys. Chem. B* **2002**, *106*, 10306.

[15] Biju, V. P.; Ye, J. Y.; Ishikawa, M. *J. Phys. Chem. B* **2003**, *107*, 10729.

[16] Seebacher, C.; Hellriegel, C.; Deeg, F.-W.; Brauchle, C.; Altmaier, S.; Behrens, P.; Mullen, K. *J. Phys. Chem. B* **2002**, *106*, 5591.

[17] Bopp, M. A.; Meixner, A. J.; Tarrach, G.; Zschokke-Granacher, I.; Novotny, L. *Chem. Phys. Lett.* **1996**, *263*, 721.

[18] Ruiter, A. G. T.; Veerman, M. F.; García-Parajó, M. F.; van Hulst, N. F. *J. Phys. Chem. A* **1997**, *101*, 7318.

[19] Bopp, M. A.; Tarrach, G.; Lieb, M. A.; Meixner, A. J. *J. Vac. Sci. Technol. A* **1997**, *15*, 1423.

[20] Rigler, R.; Mets, U.; Widengren, J.; Kask, B. *Eur. Biophys. J.* **1993**, *22*, 169.

[21] Widengren, J.; Mets, U.; Rigler, R. *J. Phys. Chem.* **1995**, *99*, 13369.

[22] Eigen, M.; Rigler, R. *Proc. Natl. Acad. Sci. U.S.A.* **1994**, *91*, 5740.

[23] Schuster, J.; Cichos, F.; Wrachtrup, J.; von Borczyskowski, Ch. *Single Mol.* **2000**, *1*, 299.

[24] Chiu, D. T.; Zare, R. N. *J. Am. Chem. Soc.* **1996**, *118*, 6512.

[25] Moerner, W. E. *Rev. Sci. Insttum.* **2003**, *74*, 3597.

[26] Bohmer, M.; Enderlein, J. *ChemPhysChem* **2003**, *4*, 793.

[27] Tokunaga, M.; Kitamura, K.; Saito, K.; Iwane, A. H.; Yanagida, T. *Biochem. Biophys. Res. Comm.* **1997**, *235*, 47.

[28] Yokota, H.; Saito, K.; Yanagida, T. *Phys. Rev. Lett.* **1998**, *80*, 4606.

[29] Schuster, J.; Cichos, F.; von Borczyskowski, C. *J. Phys. Chem. A* **2002**, *106*, 5403.

[30] Dickson, R. M.; Norris, D. J.; Tzeng, Y.-L.; Moerner, W. E. *Science* **1996**, *274*, 966.

[31] Lee, G. M.; Ishihara, A.; Jacobson, K. A. *Proc. Natl. Acad. Sci. U.S.A.* **1991**, *88*, 6274.

[32] Hellriegel, C.; Kirstein, J.; Brauchle, C.; Latour, V.; Pigot, T.; Olivier, R.; Lacombe, S.; Brown, R.; Guieu, V.; Payrastre, C.; Izquierdo, A.; Mocho, P. *J. Phys. Chem. B* **2004**, *108*, 14699.

[33] Schmidt, T.; Schutz, G. J.; Baumgartner, W.; Gruber, H. J.; Schindler, H. *J. Phys. Chem.* **1995**, *99*, 17662.

[34] Ke, P. C.; Naumann, C. A. *Langmuir* **2001**, *17*, 5076.

[35] Stevens, B. C.; Ha, T. *J. Chem. Phys.* **2004**, *120*, 3030.

[36] Lommerse, P. H. M.; Blab, G. A.; Cognet, L.; Harms, G. S.; Snaar-Jagalska, B. E.; Spaink, H.; Schmidt, T. *Biophys. J.* **2004**, *86*, 609.

[37] Thurau, C. T.; Ediger, M. D. *J. Chem. Phys.* **2002**, *116*, 9089.

[38] Inoue, T.; Cicerone, M. T.; Ediger, M. D. *Macromolecules* **1995**, *28*, 3425.

[39] Dhinojwala, A.; Wong, G. K.; Torkelson, J. M. *Macromolecules* **1992**, *25*, 7395.

[40] Deschenes, L. A.; Vanden Bout, D. A. *Science* **2001**, *292*, 255.

[41] Deschenes, L. A.; Vanden Bout, D. A. *J. Chem. Phys.* **2002**, *116*, 5850.

[42] Bartko, A. P.; Xu, K.; Dickson, R. M. *Phys. Rev. Lett.* **2002**, *89*, 026101.

[43] Stillinger, F. H.; Hogdon, J. A. *Phys. Rev. E* **1994**, *50*, 2064.

[44] Cicerone, M. T.; Ediger, M. D. *J. Phys. Chem.* **1993**, *97*, 10489.

[45] Dickson, R. M.; Norris, D. J.; Moerner, W. E. *Phys. Rev. Lett*. **1998**, *8*, 5322.

[46] Bartko, A. P.; Dickson, R. M. *J. Phys. Chem. B* **1999**, *103*, 3053.

[47] Bartko, A. P.; Dickson, R. M. *J. Phys. Chem. B* **1999**, *103*, 11237.

[48] Sepiol, J.; Jasny, J.; Keller, J.; Wild, U. *Chem. Phys. Lett.* **1997**, *273*, 444.

[49] Patra, D.; Gregor, I.; Enderlein, J. *J. Phys. Chem. A* **2004**, *108*, 6836.

[50] Betzig, E.; Chichester, R. J. *Scienc*e **1993**, *262*, 1422.

[51] Van Hulst, N. F.; Veerman J. A.; García-Parajó, M. F.; Kuipers, L. *J. Chem. Phys.* **2000**, *112*, 7799.

[52] Sick, B.; Hecht, B.; Novotny, L. *Phys. Rev. Lett.* **2000**, *85*, 4482.

[53] Hubner, C. G.; Ksenofontov, V.; Nolde, F.; Mullen, K.; Basche, Th. *J. Chem. Phys.* **2004**, *120*, 10867.

[54] Saxton, M. J.; Jacobson, K. *Annu. Rev. Biophys. Biomol. Struct.* **1997**, *26*, 373.

[55] Seisenbeger, G.; Ried, M. U.; Endress, T.; Buning, H.; Hallek, M.; Brauchle, C. *Science* **2001**, *294*, 1929.

[56] Douglas, J. F.; Hubbard, J. B. *Macromolecules* **1999**, *24*, 3163.

[57] Douglas, J. F. *Comp. Mater. Sci.* **1995**, *2*, 292.

[58] Kob, W.; Donati, C.; Plimpton, S. J.; Poole, P. H.; Glotzer, S. C. *Phys. Rev. Lett.* **1997**, *79*, 2827.

[59] Donati, C.; Douglas, J. F.; Kob, W.; Plimpton, S. J.; Poole, P. H. *Phys. Rev. Lett.* **1998**, *80*, 2338.

[60] Deschenes et al. reported a translational diffusion constant for Rhodamine molecules in PMA equal to $4x10^{-18}$ m^2/s

[61] Harms, G. S.; Sonnleitner, M.; Schutz, G. J.; Gruber, H. J.; Schmidt, T. *Biophys. J.* **1999**, *77*, 2864.

[62] Donley, E. A.; Plakhotnik, T. *J. Chem. Phys.* **2001**, *114,* 9993.

[63] Basché, T.; Kummer, S.; Brauchle, C. *Nature* **1995**, *373,* 132.

[64] Veerman, J. A.; García-Parajó, M. F.; Kuipers, L.; Van Hulst, N. F. *J. Microscopy* **1999**, *194*, 477.

[65] Zondervan, R.; Kulzer, F.; Orlinskii, S. B.; Orrit, M. *J. Phys. Chem. A* **2003**, *107,* 6770.

[66] Xie, X. S. *Acc. Chem. Res.* **1996**, *29*, 598.

[67] Viteri, C. R.; Gilliland, J. W.; Yip, W. T. *J. Am. Chem. Soc.* **2003**, *12,* 1980.

[68] Wang, L.-M.; Richter, R. *J. Chem. Phys.* **2004**, *120*, 11082.

[69] Laherrere, J.; Sornette, D. *Europ. Phys. J. B* **1998**, *2*, 525.

[70] Lee, K. C. B.; Siegel, J.; Webb, S. E. D.; Leveque-Fort, S.; Cole, M. J.; Jones, R.; Dowling, K.; Lever, M. J.; French, P. M. W. *Biophys. J.* **2001**, *81*, 1265.

[71] Lindsey, C. P.; Patterson, G. D. *J. Chem. Phys.* **1980**, *73*, 3348.

[72] Schober, H. R. *Phys. Rev. Lett.* **2002**, *88*, 145901.

[73] Vallée, R. A. L.; Cotlet, M.; Van der Auweraer, M.; Hofkens, J.; Müllen, K.; De Schryver, F. C. *J. Am. Chem. Soc.* **2004**, *126*, 2296.

[74] Blackburn, F. R.; Cicerone, M. T.; Hietpas, G.; Wagner, P. A.; Ediger, M. D. *J. Non-Cryst. Solids* **1994**, *172,* 256.

[75] Hooker, J. C.; Torkelson, J. M. *Macromolecules* **1995**, *28,* 7683.

[76] Andreozzi, L.; Faetti, M.; Giordano, M.; Leporini, D. *J. Phys.: Condens. Matter* **1999**, *11,* A131.

[77] Bowden, N. D.; Willets, K. A.; Moerner, W. E.; Waymouth, R. M. *Macromolecules* **2002**, *35*, 8122.

[78] Turro, N. J. *Modern Molecular Photochemistry*; Benjamin/Cummings: Menlo park, CA, 1978.

[79] Christ, T.; Kulzer, F.; Bordat, P.; Basché, T. *Angew. Chem., Int. Ed. Engl.* **2001**, *40*, 4192.

[80] English, D. S.; Furube, A.; Barbara, P. F. *Chem. Phys. Lett.* **2000**, *324*, 15.

[81] Hubner, C. G.; Renn, A.; Renge, I.; Wild, U. P. *J. Chem. Phys.* **2001**, *115*, 9619.

[82] Stracke, F.; Heupel, M.; Thiel, E. *J. Photochem. Photobiol., A* **1999**, *126*, 51.

[83] Lill, Y.; Hecht, B. *Appl. Phys. Lett.* **2004**, *84*, 1665.

[84] Ha, T.; Enderle, T.; Chemla, D. S.; Selvin, P. R.; Weiss, S. *Chem. Phys. Lett*. **1997**, *271*, 1.

[85] García-Parajó, M. F.; Veerman, J.-A.; Bouwhuis, R.; Vallée, R.; van Hulst, N. F. *ChemPhysChem* **2001**, *2*, 347.

[86] Veerman, J.A.; García-Parajó, M. F.; Kuipers, L.; van Hulst, N. F. *Phys. Rev. Lett.* **1999,** *83,* 2155.

[87] Yip, W.-T.; Hu, D.; Yu, J.; Vanden Bout, D. A.; Barbara, P. F. *J. Phys. Chem. A* **1998**, *102,* 7564.

[88] Cohen, M. H.; Turnbull, D. *J. Chem. Phys.* **1959**, *31*, 1164.

[89] Vrentas, J. S.; Vrentas, C. M. *J. Polym. Sci., Part B: Polym. Phys*. **1992**, *30*, 1005.

[90] Vrentas, J. S.; Duda, J. L. *J. Polym. Sci., Part B: Polym. Phys.* **1977**, *15*, 403.

[91] Barbari, T.A. *J. Polym. Sci., Part B: Polym. Phys.* **1997**, *35*, 1737.

[92] Thran, A.; Kroll, G.; Faupel, F. *J. Polym. Sci., Part B: Polym. Phys.* **1999**, *37*, 3344.

[93] Poulsen, L.; Ogilby, P. R. *J. Phys. Chem. A* **2000**, *104*, 2573.

[94] Kneas, K. A.; Demas, J. N.; Nguyen, B.; Lockhart, A.; Xu, W.; DeGraff, B. A. *Anal. Chem.* **2002**, *74*, 1111.

[95] Ober, R. J.; Ram, S.; Ward, E. S. *Biophys. J.* **2004**, *86*, 1185.

Chapter 5

Polymer segmental scale dynamics probed by single molecule fluorescence lifetime fluctuations[*]

Photophysical properties of single fluorophores embedded within a polymer matrix depend on the structure and dynamics of the chromophore surroundings. In particular, the fluorescence lifetime of single DiD molecules embedded in polystyrene or poly(isobutyl methacrylate) matrices is shown to fluctuate in time. This time-dependent behavior reflects the local density fluctuations in the polymer matrix. The number of polymer segments taking part in the rearrangement volume (N_S) around the probes is extracted from the lifetime data by applying an effective medium approximation together with the Simha-Somcynsky thermodynamic equation of state. N_S is found to be dependent on temperature, decreasing for higher temperatures. This trend is described by a master curve as a function of reduced temperature $(T-T_g)/T_g$ for different polymers. Our method is shown to report on the heterogeneous segmental scale dynamics present in polymer systems below the glass transition temperature.

[*] Part of this Chapter has been published in: Vallée, R. A. L.; Tomczak, N.; Kuipers, L.; Vancso, G. J.; van Hulst, N. F. Single molecule lifetime fluctuations reveal segmental dynamics in polymers. *Phys. Rev. Lett.* **2003**, *91*, 038301.

5.1 Introduction

Photophysics and photochemistry in polymer science has been one of the central areas of interest for a long time [1]. Recently developed single molecule fluorescence methods [2-6] offer two main advantages as compared to bulk techniques, which have been used to probe polymer structure and dynamics. First, single molecule probes allow one to probe polymers on the truly microscopic level. Second, single molecule methods offer the possibility to resolve ensemble averaging, therefore providing a check on how the particular member of a population contributes to the whole distribution. Such a unique combination of locality and nonensemble measurements has proven powerful in the investigations of various polymer systems both at cryogenic and room temperature as reviewed in Chapter 2.

Here, we exploit the fluorescence lifetime to investigate the dynamics of polymeric glasses. Fluorescence lifetime is a photophysical parameter known to be extremely sensitive to the dielectric and chemical changes in the surroundings. For a given static situation, the fluorescence lifetime of the chromophoric probes will have a fixed value. When the properties of the probe environment fluctuate in time, the changes in the fluorescence lifetime will reflect the dynamics in the probe surroundings. At low temperatures, the variations in the configuration of the matrix shell around a chromophore can be neglected and the fluctuations in the density are negligible. At cryogenic conditions the optical linewidths of chromophores are lifetime limited. Therefore the observed distributions of linewidths reflect the inherent disorder present in the investigated system [7]. At room temperature, however, due to the high mobility present in the polymer matrix, this is not true anymore. Inhomogeneously broadened spectra are observed, and the fluorescence lifetime of chromophoric probes fluctuates in time. Monitoring the lifetime of individual probes will give information on the local, nanoscale, polymer dynamics. Knowledge of such molecular level processes helps to improve our understanding of structure – property relationships for polymer glasses.

In this chapter we describe our work aiming at monitoring single molecule fluorescence lifetime fluctuations. We show that the fluctuations are related to the local density fluctuations present in the polymer matrix. To relate the density fluctuation to polymer dynamics we combine an effective medium approximation with the Simha-Somcynsky thermodynamic equation of state [8]. We determine the number of polymer segments (N_S) taking part in the relaxation processes around the chromophore. We find that N_S depends on temperature and its value decreases with increasing temperature for two different polymers investigated. Clearly our method can be used to probe the spatially heterogeneous dynamics present in polymeric glasses at the segmental scale. Although the exact microscopic mechanism for the observed density fluctuations is not yet fully elucidated, we compare the

behavior of N_S for the two different polymers and conclude that the secondary relaxation processes around the probe are not the main contributors to the density fluctuations observed.

5.2 Experimental section

5.2.1 Materials and sample preparation

As host matrices we chose polystyrene (PS, number average molar mass M_n=89300 g/mol, polydispersity M_w/M_n=1.06, Polymer Standard Service, T_g=100 ºC) and poly(isobutyl methacrylate) (P*i*BMA, molar mass M_n=67200 g/mol, polydispersity M_w/M_n=2.8, custom made by UV polymerization, T_g=56 ºC). The probe used in this study was DiD (1,1'dioctadecyl-3,3,-3',3'-tetramethylindodicarbocyanine perchlorate, Molecular Probes D-307). The choice of the dye was dictated by the fact that it should have a high fluorescence quantum yield when embedded in polymer matrices, and a large absorption cross-section, which for DiD is 7.4×10^{-16} cm^2. Additionally, DiD molecules in polymer matrices are relatively more stable compared to other chromophores. Solutions of the dyes in toluene, and tetrahydrofuran, containing different amounts of polymer were spin-coated at 3000 rpm for 60 s onto a cleaned glass cover slides (with a diameter of 10 mm or 20 mm, Fisher Scientific) to produce uniform, thin coatings with thickness values ranging from 70 to 200 nm. Prior to spin-coating, the glass cover slides were cleaned using a Piranha solution (mixture of 1:4 of 30% H_2O_2 and concentrated H_2SO_4), rinsed with Milli-Q water and ethanol, and finally dried in a stream of nitrogen gas. The concentration of the dyes in the resulting films was kept low enough (10^{-9}-10^{-10} M) to ensure adequate spatial separation of the dye molecules for optical single molecule observations. The PS and P*i*BMA samples were subsequently annealed in vacuum. For PS this annealing included a treatment of 12h at 60 °C followed by 3h at 105 °C. For P*i*BMA the treatment was 12h at room temperature (22 °C) and 3h at 80 °C. The annealing was performed to remove the residual solvent, relax the remaining stresses introduced by the spin-coating technique and the two-stage process used helped to avoid polymer dewetting.

5.2.2 Thin film morphology examined with Atomic Force Microscopy

A NanoScope IIIa (Veeco, Digital Instruments, Santa Barbara, USA) Atomic Force Microscope (AFM) was used to examine the sample surface. The AFM was operating in the tapping mode using a cantilever with a nominal spring constant of 40-60 N/m. The tip-scratch method was used to determine the film thickness. AFM was also used to determine the planarity and roughness (<1nm) of the samples.

5.2.3 Scanning Confocal Microscopy and time resolved experiments

The scheme of the Scanning Confocal Microscope setup employed in our studies is depicted in Figure 1a. Picosecond pulses from a pulsed diode laser (635nm, PicoQuant, 800-B, 100 mW, 80 MHz repetition rate) were used for excitation and time-resolved experiments. The excitation light was made circularly polarized using a ¼λ plate and focused onto the sample to a diffraction-limited spot using a high NA oil objective (Olympus, NA=1.4, 100x). To separate the fluorescence emission from the excitation, suitable dichroic mirrors, emission, and excitation filters were used. Fluorescence photons were collected by the same objective and sent to two avalanche photodetectors (SPCM-AQ-14, EG&G Electro Optics) placed after a polarization beam splitter (splitting into two perpendicular components). For time-resolved experiments an SPC 500 time-correlated single-photon counting card was used to build photon arrival histograms. The fluorescence lifetime was obtained by a single exponential decay fit to the histogram. A custom-built piezo-scan table with an active x-y feedback loop mounted on a commercial optical microscope (Zeiss Axiovert inverted microscope) was used. The sample was scanned through the focus of the excitation spot at a pixel frequency of 1 kHz, producing two-dimensional fluorescence intensity images (for two independent polarization channels when required) (Figure 1b). Custom written LabView software was used to control the scanning process and data acquisition. A custom-made heating stage was placed between the objective and the sample and the temperature was controlled with an accuracy of 2 ºC during the experiment.

5.3 Methodology

In Figure 1b we show a 10x10 μm^2 fluorescence intensity scan of DiD molecules embedded in a PS matrix. The fluorescence photons were collected in two orthogonal polarization channels and a false color scale was applied to the normalized intensity difference between the two detectors at each pixel. The polarization sensitive detection optics provides information on the in-plane orientation of the emission dipole moment of the embedded molecules. It should be noted that such a method of determination of the orientation of the molecule has its limits. Especially in the case when high NA objectives are being used there is a coupling of the signal to both detectors for molecules which have significant out-of-plane orientations. However, here, it will be of more importance to monitor the changes in the molecular orientation and to ensure that there is no rotational diffusion present for the molecules under investigation, within the experimental time-scale. Each intensity spot visible on the scan in Figure 1b is attributed to single DiD molecules embedded in the PS film.

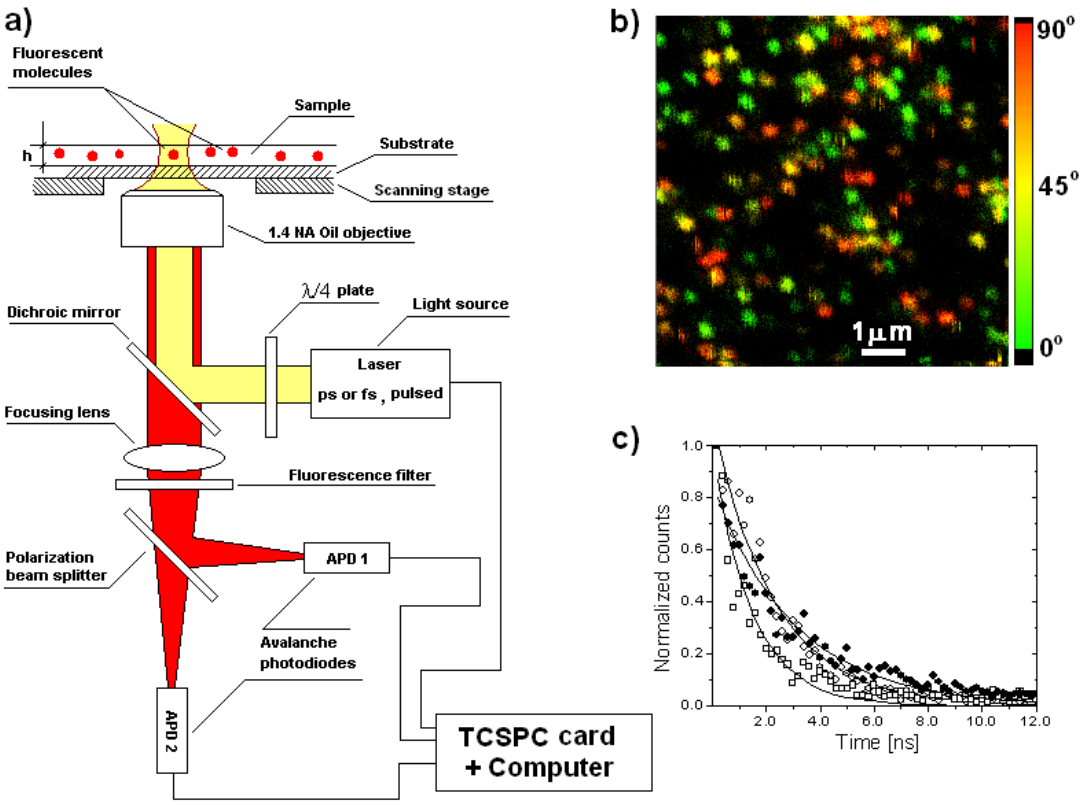

Figure 1. a) Scanning Confocal Fluorescence Microscope setup. For a detailed explanation see text. b) 10x10 μm^2 fluorescence intensity scan of single DiD molecules embedded in a 200 nm thick PS film. The false color scale is related to the in-plane orientation of the emission dipole moments of the chromophores. c) Examples of three arrival time histograms integrated over 100 ms generated for three different molecules (scatter plots). The histograms were fitted with single exponential decays (solid lines) to obtain the fluorescence lifetime in a 100ms time interval.

There are several ways, which allow one to determine whether the spots are single emitters. On the scan the spots have a discrete value of the polarization and the size of the spots corresponds to a diffraction-limited image of a point-like light source. Later, on the time-traces the molecules also display step-like intensity excursions to the background level (blinking) and one-step photobleaching. Such behavior is sufficient to discriminate with confidence between multiple and single molecule behaviors.

To perform single-molecule time-resolved experiments, each of the molecules was moved to the excitation focus. At the moment when the fluorophore reached the focus, the recording of photon arrival times with respect to pulsed laser excitation was started. The arrival times were integrated over each 100 ms and histograms were built to produce fluorescence decays (Figure 1c). The decays were fitted to single exponential decay functions using a Levenberg-Marquadt algorithm. The background fluorescence was taken into account in the fitting procedure as a constant offset of the fluorescence signal. From the fits the fluorescence

lifetime was obtained. By repeating such procedures many times for each integration time interval, fluorescence intensity, orientation and lifetime time-traces were obtained from the integration over all detected photons, the two polarization channels and the arrival time histograms, respectively.

5.4 Results and discussion

5.4.1 Fluorescence lifetime fluctuations and distributions

The fluorescence lifetime and intensity time-traces were obtained for many different single DiD molecules embedded in PS and P*i*BMA films with thickness values ranging from 70 to 200 nm. Remarkably, the appearance of the time-traces obtained varied from molecule to molecule. More specifically, large differences appeared in the behavior of the fluorescence lifetime in time. In Figure 2 we compare the data collected for two different single DiD molecules embedded in a 70 nm thick PS film at room temperature. For the molecule on the left (Figure 2a) the values of both the fluorescence lifetime and the emission intensity are constant in time. The second molecule (Figure 2d) also exhibits constant emission intensity but there are large variations in the fluorescence lifetime. Peculiar excursions towards longer values of the lifetime are visible along the time trace and changes as much as 400 % in the lifetime can be observed. The magnitude and frequency of such fluorescence lifetime jumps depended on the molecule investigated. The difference between the lifetime traces can be exemplified by plotting the corresponding histograms of the lifetime values for each of the molecules (Figure 2c and 2f). For a stable fluorescence lifetime the resulting histograms are symmetric and centered around one mean value of the lifetime (Figure 2c). Traces, where frequent lifetime jumps are observed result in a skewed distribution elongated towards higher lifetime values (Figure 2f).

To evaluate the asymmetries present in the single molecule fluorescence lifetime destitutions, we obtained fluorescence lifetime time-traces for each of the molecules investigated. From the lifetime trajectory we built lifetime distributions, which we fit with a gamma distribution function $g(x) = \beta(\beta x)^{\alpha-1}e^{-\beta x}/\Gamma(\alpha)$ [9-11] (solid line in Figure 2c and 2f). The first two moments of the distribution are given by $x_{av} = \alpha/\beta$ and $<\delta x^2>_{av} = \alpha/\beta^2$, where α and β are the shape and the scale parameters characterizing the distribution, Γ stands for the gamma function. The gamma distribution function $g(x)$ is symmetric for large α and develops to an asymmetric distribution for α approaching down to α =1.

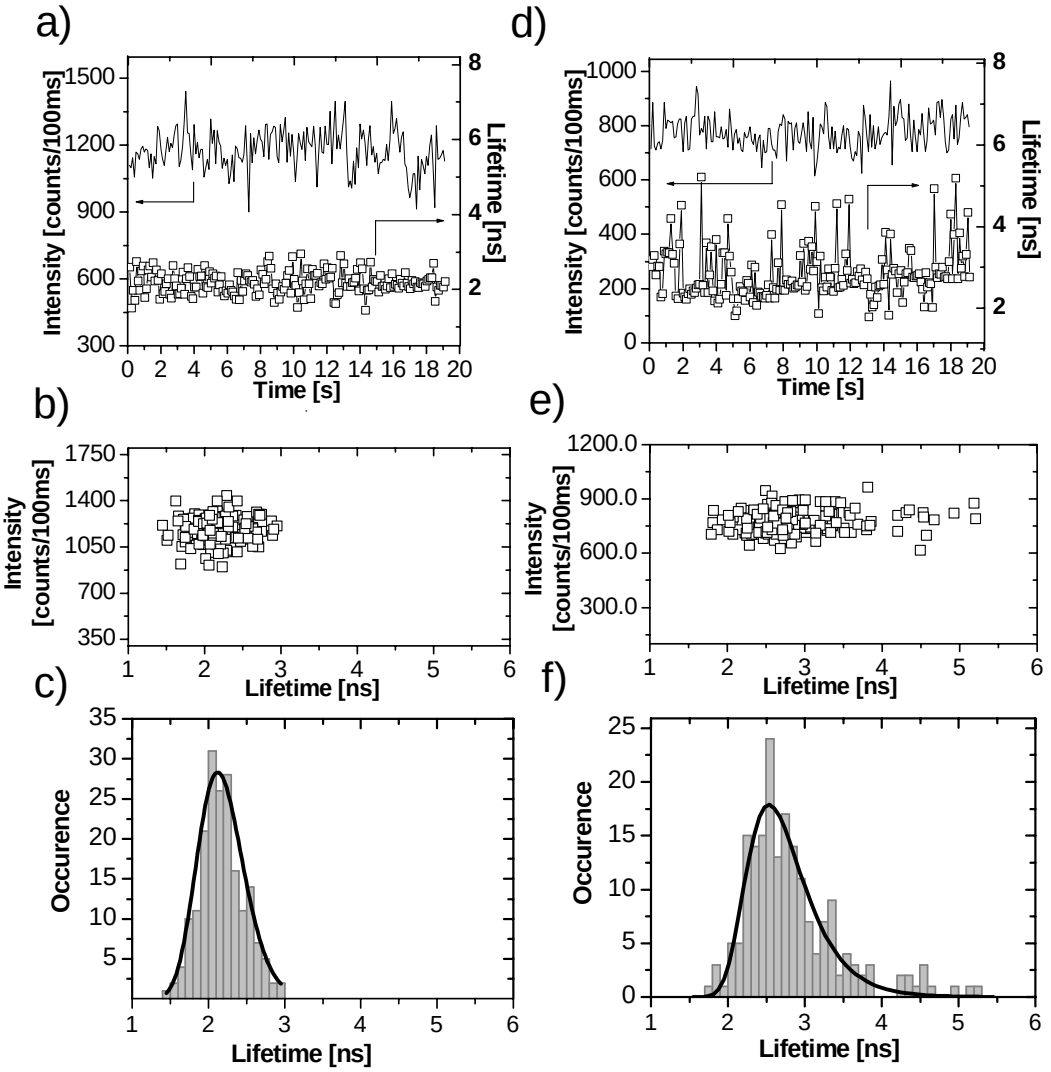

Figure 2. (a)(d) Fluorescence intensity and lifetime time-traces for single DiD molecules embedded in a PS matrix. The binning time was 100 ms. (b)(e) Correlation plots between fluorescence intensity and lifetime of single DiD molecules. (c)(f) Histograms of fluorescence lifetimes from the time-traces presented in (a) and (d). Solid lines are fits to the histograms with a gamma distribution function.

In the presence of lifetime fluctuations the distributions are asymmetrically broadened towards higher values (see Figure 2f) and the extent of the asymmetry is described by the characteristic shape parameter α obtained from the fit. A histogram of α is built from many different single molecules at a given temperature. Such a distribution is presented in Figure 3a. We observed [12,13] that the distributions of α shift toward lower values when increasing the temperature (Figure 3b). There are several mechanisms, which could influence the experimentally determined fluorescence lifetime. Since the investigated chromophores are embedded in a polymer matrix we will also address the question whether the fluctuations may arise from the changes in the polymer dynamics.

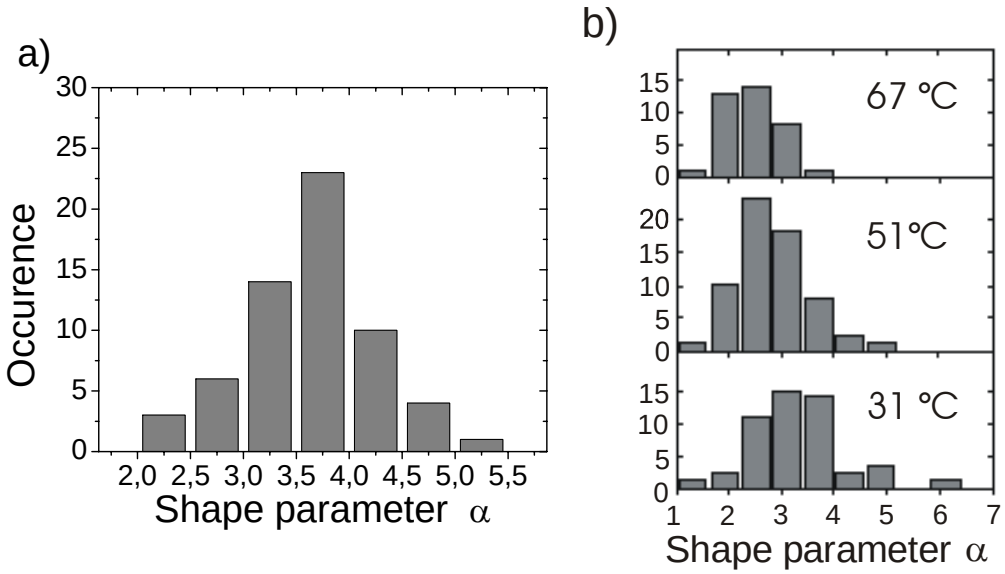

Figure 3. a) Distribution of the shape parameter α obtained for DiD molecules embedded in a PS film at room temperature. b) Distributions of the shape parameter of DiD molecules in P*i*BMA as a function of temperature. The distributions shift towards lower values with increasing temperature.

5.4.2 Origin of lifetime fluctuations

For a chromophore embedded in a polymer several processes can influence the excited state lifetime of the probes including quenching, changes of the photophysical properties of the dyes due to changes in the dye molecular conformation, effects imposed by the thin film geometry of the sample and finally changes in the probe environment.

In Chapter 4 of this thesis we demonstrated that the changes in the molecular environment (changes not necessarily associated with the polymer) have a significant impact on the single molecule photophysical behavior. The molecules can decay from the excited state both in a radiative and nonradiative way, where particular decay rates k_r and k_{nr} are associated with each of these two processes, respectively. In this study, the experimentally obtained fluorescence lifetime (τ_F) corresponds to the effective lifetime of the excited state and can be expressed as:

$$\tau_F = \frac{1}{k_r + k_{nr}} \qquad (1)$$

Opening of new nonradiative decay channels, quenching, reduces the experimentally determined lifetime. In such cases a positive correlation between τ_F and the measured intensity should be visible. In Figure 2b and 2e we show that this trend is not observed: no

correlation between intensity and lifetime is observed regardless of the magnitude of the lifetime variations. Therefore, the fluorescence lifetime fluctuations are not related to a quenching process. Additionally, the observed variations in lifetime and deviations from the average are predominantly towards higher values. DiD dyes were reported to exhibit high quantum yields, close to unity, when embedded in a polymer matrix. Since the fluorescence quantum yield (QY) is defined as:

$$QY = \frac{k_r}{k_r + k_{nr}}, \tag{2}$$

the decay from the excited state for DiD is almost purely radiative in nature. Any lifetime change can only occur with a substantial reduction of fluorescence. It should be noted that in fact a few molecules showed a correlation between lifetime and intensity. This was attributed to the presence of a quencher nearby the chromophores. These few molecules were discarded from further analysis.

Modification of the transition frequency, or the transition dipole moments can also result in fluorescence lifetime fluctuations. However, Vallée et al. [14] have investigated a chromophore with chemical structure similar to the chromophore used in this study (the conjugated part was the same) and found that in case of dicarbocyanines, the ground and the excited states have the same configurational structure. Furthermore, changes of the conformation of DiD molecules caused by thermal agitation at room temperature are relatively small and are not expected to contribute more than 10 % to any lifetime changes. Careful observation of Figure 2d reveals lifetime changes of up to a factor of 4. It should also be kept in mind that the glassy polymeric environment can obscure conformational changes for which large activation volumes are required. Vallée et al. [14] have shown that already in the case of small side group twisting (volumes smaller than in case of DiD) such events are extremely rare. We conclude that conformational changes of the chromophores cannot be responsible for the observed lifetime fluctuations.

The time averaged fluorescence lifetime level from which the lifetime excursions were occurring was slightly different from molecule to molecule. This is due to cavity effects [15,16] introduced by the thin film structure. The effect structures with dimensions smaller than the wavelength have on the radiative decay rates will be discussed in more detail in Chapter 6. Here we will only state that such effects are static in nature and unless the molecule does not translate or reorient itself with respect to the interfaces, these effects do not play any role in the observed lifetime fluctuations [17-20]. The collection of the emitted fluorescence was performed in two orthogonal channels to obtain the information on the molecular orientation. The observation of the degree of polarization during the fluorescence

lifetime collection clearly showed that for all investigated molecules any orientational or translational diffusion of the probes in the polymers on the time scale from seconds to minutes was absent. Therefore "global" cavity effects are not responsible for the lifetime fluctuations.

5.4.3 Spontaneous emission in dielectrics

It is well known that the characteristics of the spontaneous emission of electromagnetic radiation of an excited molecule are not only inherent to the molecule but are also strongly dependent on the molecular environment. The photonic mode density (into which a photon can be released) in the surroundings mediates this dependency. When the molecule is moved from vacuum and placed within a homogeneous dielectric, the spontaneous emission rate of the chromophore changes and becomes dependent on the dielectric constant of the medium (ε) through the following relation [21,22]:

$$\Gamma = \sqrt{\varepsilon}\Gamma_0 , \tag{3}$$

where Γ and Γ_0 are the spontaneous emission rates in free space and in the dielectric medium, respectively. The local, microscopic electromagnetic field at the location of the chromophores is often different from the averaged field for the whole sample volume. This introduces a local field correction factor L and equation (3) transforms into:

$$\Gamma = \sqrt{\varepsilon}\Gamma_0 L^2 \tag{4}$$

The effect of the local fields [23-25] on the spontaneous emission rates was investigated both theoretically and experimentally [15,26-31]. Experimental results on the variation of the radiative decay rate of rare earth ions (Eu^{3+}) with the refractive index [32] in supercritical gas [33], alcohols [34] or glasses [35] are in agreement with the so-called real cavity model. For the real cavity model equation 4 transforms into the following form:

$$\Gamma = \sqrt{\varepsilon}\Gamma_0 \left(\frac{3\varepsilon}{2\varepsilon + 1} \right)^2 \tag{5}$$

Equation (5) clearly shows the relation between the spontaneous emission rates and a material specific constant, and will serve as a basis in our subsequent considerations.

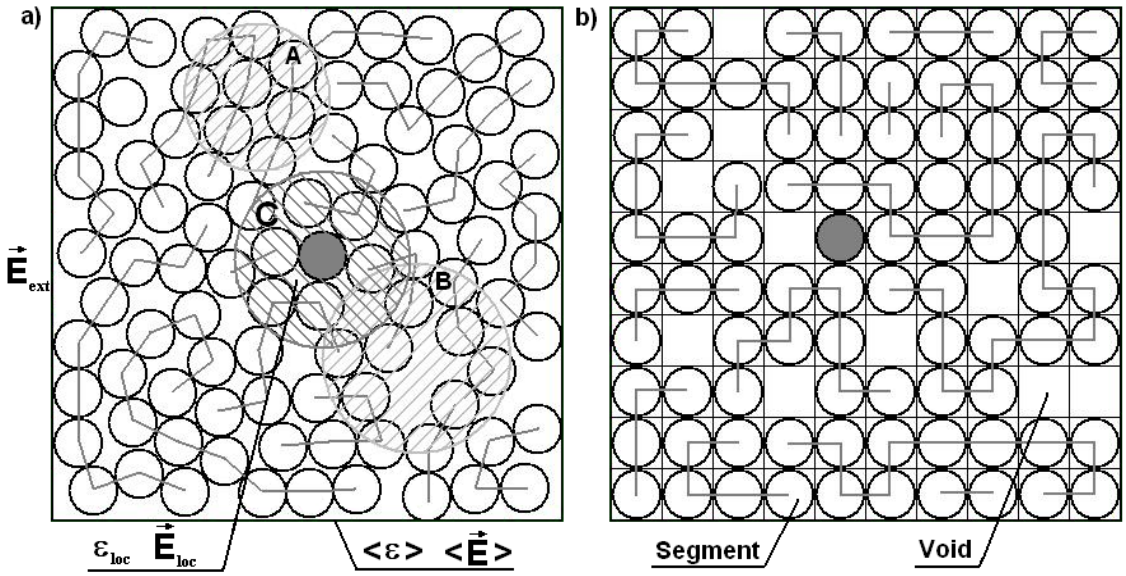

Figure 4. a) Schematic representation of the disorder present in a glassy polymer matrix. Regions A and B show that the packing efficiency can be very much different from place to place. In region C, where the probe is present, the local dielectric constant and therefore the local electric field is different from the average. b) In the cell model the lattice consists of voids and segments competing for available space. The gray shaded circle in both figures corresponds to the chromophore. The black circles are polymer segments and the gray lines correspond to bonds determining the polymer chains.

In Figure 4a we show a schematic drawing of a chromophoric probe embedded in a disordered, glassy, polymer matrix. A gray shaded circle represents the chromophore and the other circles represent polymer segments, which are connected to each other (by gray lines). These connected circles represent covalently bound segments of polymer chains. The number of polymer segments in a polymer chain is equal for all polymer chains. The visible "length" of the polymer chains in Figure 4a is different from one chain to another because the polymer chain can be continued in the out of plane direction. Because of the imperfect spatial packing of polymers in the glassy state one can identify regions e.g. A, B or C where the segmental density is substantially different. Such regions will display different dielectric and dynamic properties. In this schematic picture the probe introduced into the matrix will be affected by the polymer structure and dynamics in the space around the probe, indicated as region C. It was shown theoretically [36,37] and confirmed experimentally [38,39] that the spontaneous emission is able to sense the local refractive index within a sphere with radius in the order of the wavelength of light [40]. However, this ability decays very fast with distance and the molecules are primarily influenced by the changes in their near-field regions. Given such a schematic picture of a polymer as in Figure 4a. one can ask, how particular environments will affect the chromophore excited state lifetime to produce the observed lifetime fluctuations. The local conditions for spontaneous decay will vary depending in which region in the polymer matrix the chromophore is located. Therefore the probes can have different values of

lifetimes reflecting the static picture of the polymer structure and, as mentioned earlier, the possible influence of the interfaces. Due to thermal energy the polymer chain segments will change their position in time and will compete with the voids for available space. If the polymer environment fluctuates, the local dielectric properties become time-dependent and the probe will exhibit lifetime fluctuations, which reflect the density fluctuations in the dielectric surroundings. Figure 4a also shows that the local dielectric constant ε_{loc} can be different from the average over many different polymer environments ($<\varepsilon>$) because on the molecular scale the dielectric cannot be treated as continuum and macroscopic concepts like the dielectric constant are not applicable in their common forms. Since the chromophores will be predominantly influenced by changes occurring in their near-field one would ask whether the fluorescence lifetime will reflect the local density fluctuations. The observed shifts of the α distribution with temperature towards lower values suggest that this is indeed the case. Lower values of α mean larger fluorescence lifetime fluctuations, which according to the discussion above are related to the surrounding matrix through the material constant ε.

5.4.4 Effective medium approximation

To relate the fluctuations in the fluorescence lifetime directly to changes in the local structure of the matrix, first, we make use of the effective medium approximation, where the system is described as a medium consisting of polymer and voids competing to occupy space. The local effective dielectric constant in the region nearby the probe can therefore be defined as:

$$\varepsilon_{eff} = h\varepsilon_{vac} + (1-h)\varepsilon_{pol}, \tag{6}$$

where ε_{vac}=1 and ε_{pol}=2.5 are the dielectric constant of vacuum and of the polymer respectively, and h is the fraction of voids present in the medium. Therefore, different local effective dielectric constants are associated with regions A, B and C in Figure 4a. Changes in the number of voids present in the chromophores polymer surrounding will change its local dielectric properties, which in turn will influence the radiative decay rates from the excited state through the magnitude of the local field at the molecule location. The dynamics of void formation and annihilation through localized motion of polymer segments will cause local density fluctuations and affect the measured fluorescence lifetime. The reaction field at the chromophore position will change each time a void is being occupied by a polymer segment with given polarizability. The effective dielectric constant will therefore also depend on the number and type of the surrounding dipoles. The effective medium approximation shown here represents a rather coarse approach. However in the low hole fraction regime (<10%) we show that the gamma distributed fluorescence lifetimes can be translated into the corresponding gamma distribution of the fraction of holes where both distributions can be

described with the same shape parameters (with a maximum estimated error of 4%). In particular, the expression, which relates the two probability densities of h and τ_F, is a smooth linear relationship in the form of:

$$\frac{d\tau_F}{dh} = ah + b \tag{7}$$

5.4.5 Simha-Somcynsky equation of state

In the preceeding section we have established a connection between the fluorescence lifetime and the local dielectric properties of the surroundings. We have also shown that the fluorescence lifetime distributions can be translated into the corresponding distributions of fraction of holes present in the system. In polymer physics there is a widespread attempt to relate directly the density fluctuations present in the polymer matrix to the polymer chain molecular packing and relaxation behavior. To achieve this, the pressure-volume-temperature (PVT) behavior of polymer glasses was accurately measured for various polymers. To explain the PVT behavior of polymers, lattice-hole theories were developed. Here we will make use of the Simha-Somcynsky cell model developed for the equation of state of polymer liquids [8,41]. In Figure 4b we showed a cubic lattice of sites, each of which can accommodate one polymer segment. To account for molecular disorder, a temperature and volume dependent fraction h of vacancies or holes is introduced. Similarly as in Figure 4a the probe resides in one of the sites. The configurational partition function for a system of N s-mer polymers, occupying a fraction y of the total number of available sites is given by:

$$Z = g(N,y)\left[v_f(V,y)\right]^{cN} \exp\left[\frac{-E_0(V,y)}{kT}\right], \tag{8}$$

where g represents the combinatory factor arising from mixing between the molecules and unoccupied sites (given by the Flory-Huggins theory), v_f is the free volume per each of three of the total number $3c$ of external degrees of freedom attributed to a chain, and E_0 is the potential energy of the system at rest. Assuming Lennard-Jones interaction between nonbonded segments, E_0 is given by:

$$2E_0 = yNqx\varepsilon^* \left[1.011\tilde{\omega}^{-4} - 2.409\tilde{\omega}^{-2}\right] \tag{9}$$

where qx is the number of the nearest-neighbor segments per chain and ε^* is the characteristic attraction energy per segment, $\tilde{\omega} = yV / v^* Ns$ is the reduced segmental cell volume, V is the

measured volume of N molecules, and v^* is the characteristic volume per segment. The Helmholz free energy (F) is related to the partition function Z by:

$$F = -kT \ln Z = -kT \ln\left(g(N, y)\right) - cNkT \ln\left(v_f(V, y)\right) + E_0 \tag{10}$$

From $p=-(\partial F/\partial V)_T$, and using $(\partial F/\partial y)_{V,T} = 0$ to determine the occupancy fraction $y(V,T)$, an equation of state can be written as:

$$\frac{\tilde{p}\tilde{V}}{\tilde{T}} = \left[1 - y(2^{\frac{1}{2}} y\tilde{V})^{-\frac{1}{3}}\right]^{-1} + \left(\frac{y}{\tilde{T}}\right)\left[2.022(y\tilde{V})^{-4} - 2.409(y\tilde{V})^{-2}\right] \tag{11}$$

where $\tilde{p} = p/p^* = psv^*/(qx\varepsilon s)$, $\tilde{V} = V/V^* = V/(Nsv^*)$, and $\tilde{T} = T/T^* = ckT/(qxe^*)$, are the reduced variables of state, with p^*, V^*, and T^* being the characteristic scaling parameters for each polymer material. Corresponding values for specific polymers can be found in the literature [42,43]. If not known, they can be determined by fitting the p, V, T data obtained experimentally to equation (11) [44].

The motion of polymer segments and the relaxation of polymers in the glassy state will depend on the local hole fraction as well as on the local fluctuations in the hole fraction. At equilibrium, the free volume around the probe in Figure 4b is not constant in time and its mean-square thermal fluctuations from the mean free volume can be calculated from:

$$\left\langle \delta h^2 \right\rangle = kT\left(\frac{\partial^2 F}{\partial y^2}\right) \tag{12}$$

where $\delta h = h - h_{av}$, h_{av} being the average hole fraction.

From equation (10), for specific PVT conditions one obtains:

$$\left\langle \delta h^2 \right\rangle = \frac{1}{Ns}\left\{\frac{\left[1 + (2/y)\ln(1-y) + 1/(1-y)\right]}{y^2} + \right.$$
$$\frac{1}{3}\frac{(2^{1/2} y\tilde{V})^{2/3} - (8/3)y(2^{1/2} y\tilde{V})^{1/3} + 3y^2}{y^2\left[\left(2^{1/2} y\tilde{V}\right)^{1/3} - y\right]^2} +$$
$$\left.(1/3y\tilde{T})[6.066(y\tilde{V})^{-4} - 2.409(y\tilde{V})^{-2}]\right\}^{-1}, \tag{13}$$

where *Ns* is the total number of segments. By assuming a number of segments s per chain sufficiently large, and setting the flexibility ratio $s/3c = 1$, *Ns* can be replaced by N_S, the number of polymer segments in any size volume in which the fluctuations are desired [45]. Indeed, to build a distribution of free volume one should set a priori the value of N_S. This, in many cases, is done totally arbitrarily [46].

The single molecule fluorescent lifetime method presented in this chapter reverses the situation. By assuming a gamma distribution as a distribution of free volume [10,45,47], we propose to directly relate the number of segments involved in a local rearrangement cell to the shape parameter. In the case of a gamma distribution N_S has a direct linear relation with the shape parameter α:

$$N_S = \alpha f(y, \tilde{V}, \tilde{T}) \tag{14}$$

We can therefore convert our shape parameter distributions into the corresponding distributions of N_S. We have monitored the changes of N_S as a function of temperature for PS and P*i*BMA. In Figure 5 the peak values of N_S distributions are plotted against a reduced temperature. T_g of 100 ºC and 56 ºC was taken for PS and P*i*BMA respectively and the dashed line in Figure 5 indicates the reduced glass transition temperature for both polymers.

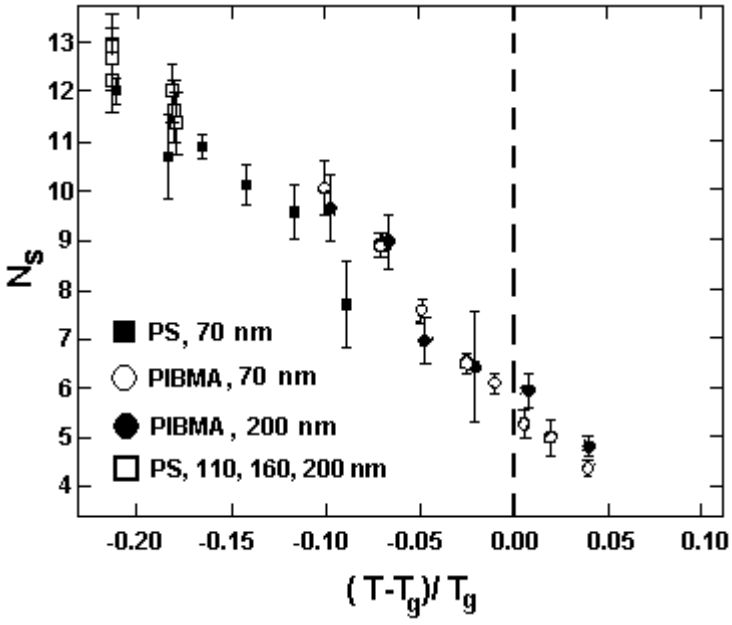

Figure 5. Mean values of the effective number of polymer segments in the rearrangement volume around the single molecule probes as a function of reduced temperature. A T_g of 56 ºC for P*i*BMA and 100 ºC for PS was taken for calculations. For PS and P*i*BMA, data for different film thickness are shown.

The number of segments taking part in the rearrangement volume around the chromophoric probes decreases with temperature for both polymers studied. Surprisingly, N_S shows a similar behavior for both polymers. Additionally, at the glass transition temperature the number of polymer segments taking part in the rearrangement volume seems to be almost the same for both polymers within the error of our measurement. We will discuss briefly the origins of the density fluctuations later in this chapter. Here we can say that probably our molecular probes are able to sense changes in the polymer conformations in a volume extending further than the nearest polymer chains.

5.4.6 Heterogeneous dynamics below the glass transition

The major strength of single molecule methods is that they offer the possibility to obtain directly the distribution of parameters rather than their average values and allow one to verify how the individual members of a large population contribute to the ensemble behavior. Recently it was experimentally verified that the nonexponential behavior of relaxation processes near the glass transition has its origins in the spatially heterogeneous dynamics [48,49]. The dynamics of the polymer chains in one place can be very much different from the dynamics of the polymer in regions located only several nanometers away. Although above the glass transition temperature such heterogeneities can be accessed in a relatively easy way, below the glass transition temperature such attempts are not trivial due to the long time-scales involved in the polymer dynamics. In Chapter 4 we showed that the static picture of the structure of the polymer matrix (in this case PS) obtained through changes of the photophysical behavior of the probes after a change in the environment is far from being homogenous. Such inhomogeneities were found in many other single molecule polymer studies [50-53].

In a similar way, the broad distributions of the α parameter and associated N_S presented here show that the dynamics in the polymer matrix is heterogeneous on the segmental scale. In Figure 6 a fluorescence intensity scan of single DiD molecules embedded in a PS matrix is shown. The numbers are the values of N_S assigned to each molecule investigated. Not all molecules present on the scan could have their N_S assigned due to photobleaching. Figure 6 nicely illustrates the capability of single molecule methods in probing the spatial variations in polymer dynamical properties. Two important points should be noted. The far-field optical technique used here limits the spatial resolution to around $\lambda/2$, λ being the wavelength of the exciting light. There are methods based on near-field detection or specific image analysis schemes, which allow one to overcome this limit, however their combination with reliable fluorescence lifetime detection was not shown until now.

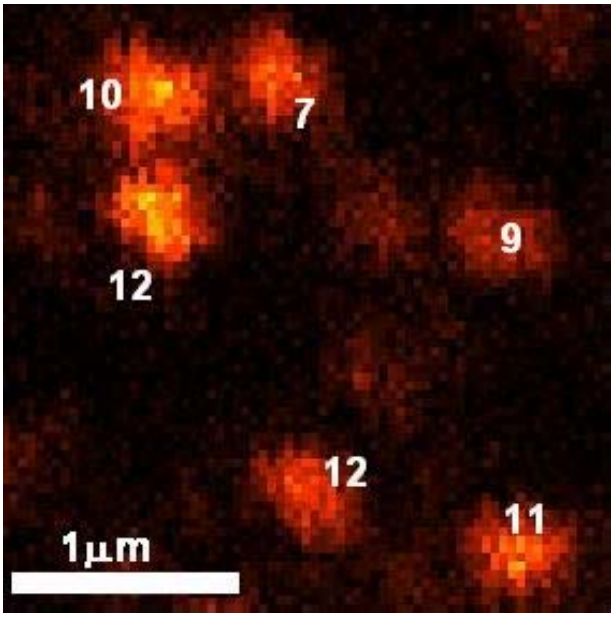

Figure 6. Fluorescence intensity scan of single DiD molecules embedded in a PS matrix. The numbers close to each of the molecules correspond to the value of the N_S parameter.

The length-scales associated with the spatially heterogeneous dynamics were reported to range from nanometers to tens of nanometers, therefore our results represent a rather coarse picture of this phenomenon. Still, we show that the dynamical and spatial heterogeneities in the local, segmental scale dynamics can be accessed with single molecule fluorescence methods in a relatively easy way.

5.4.7 Microscopic origins of the detected density fluctuations

Polymer systems exhibit relaxation processes which span a broad range in time and which are associated with different mechanisms [54]. It is not clear at present which mechanism of polymer motion is responsible for the density fluctuations sensed by the chromophores in the present study. For both P*i*BMA and PS, the main chain relaxation processes (α-relaxation) occur on time-scales, which are orders of magnitude larger than our experimental time-scale. It was briefly described in the introductory chapter of this thesis that localized motions, so-called higher order relaxation processes also exist in the polymer matrix. These "slower" processes are usually separated from the main α-relaxation process somewhat above T_g and persist below the glass transition. Additionally, neutron or Raman scattering experiments identified picosecond range processes, however they showed only weak temperature dependence.

It is speculated here, that the density fluctuations detected with our method originates from simultaneous motion of a number of polymer segments within a large volume around the probe rather than being the result of the motion of groups located closest to the probe. The secondary relaxation processes for both polymers studied have different molecular origins and happen at different time-scales. In case of poly(methacrylates) a β relaxation process is identified at 10 ºC at 1Hz and attributed to the rearrangement of the -COO- portion of the side groups by rotation [55,56]. At our experimental conditions we expect therefore large side group rotations in case of P*i*BMA. In case of PS Yano and Wada [57,58] found a β-relaxation peak at 77 ºC at 10 Hz, which was generally associated with the phenyl ring motion. The highest experimental temperature in our experiments was 60 ºC, therefore no significant effect of the phenyl rings should be observed. (There are also higher order relaxation processes present in both polymers, however they occur at temperatures and frequencies, which are in the range far outside of the range used in this study). Similar slopes of α and N_S with temperature for P*i*BMA and PS found in this study mean therefore, that the probe is sensitive to density fluctuations coming from larger volumes around the probe rather than being sensitive to localized motions that occur near the probe. To assess which mechanism is responsible for the fluorescence lifetime fluctuations a microscopic model is needed. However, one should proceed with caution; in the usually used coupled-dipole models of polymer chains, which are used in the microscopic description, one should also include all different time-scale characteristics for a given relaxation processes. In addition, this will likely be structure dependent. Models used to explain single molecule linewidth broadening might not be applicable.

5.4.8 Remarks

In this chapter a number of assumptions have been made to obtain the information on the polymer segmental scale dynamics. We will not discuss all in detail here, but we rather want to list them for future referencing. We are confident that the general temperature behavior of N_S for two different polymers indicates that most of the assumptions hold. Nevertheless, we realize the need to perform additional experiments to sustain our claims.

1. Introduction of the probe into the polymer does not significantly affect the density fluctuations in the chromophore surroundings.

2. The chromophore QY is constant and close to 1.

3. The fluorescence decay is single exponential for all fluorescence lifetimes for a given integration time.

4. The first order effective medium approximation sufficiently well describes the local dielectric constant.

5. There is no exchange of dynamics around the probe during the time-trace collection.

6. The number of segments s per chain is large enough that the flexibility ratio $s/3c$ =1.

7. The distribution of free volume in the polymer matrix can be accurately described with a gamma distribution function.

8. $(\partial F/\partial y)_{V,T} = 0$ holds. For glasses that assumption might not be entirely true.

9. The polymer was equilibrated long enough after each jump in temperature.

5.5 Conclusions

Density fluctuations in a glassy polymer matrix were observed by monitoring single molecule fluorescence lifetime fluctuations. This method allowed obtaining the information on the local, nanoscale polymer dynamics without being obscured by ensemble averaging. To relate the density fluctuation with polymer physics we introduced an effective medium composed of segments and voids competing for the available space. We used the Simha-Somcynsky equation of state theory and determined the number of polymer segments (N_S) taking part in the elementary segment rearrangement processes around the probe. We have followed N_S in function of temperature and found that N_S decreased with increasing temperature for the two different polymers under study. Similar values of dN_S/dT for two distinctively different polymers showed that the probes were not affected primarily by secondary relaxation but rather sensed fluctuation in density from larger volumes around the probes. A unique combination of small probed volumes and nonensemble measurements resulted in full distributions of segmental scale dynamics. The distributions were found to be broad reflecting the extent of the dynamic heterogeneities present within a glassy polymer matrix. We will show in Chapter 7 that our method can be successfully applied to studies of the segmental scale dynamics of thin polymer films.

5.6 References

[1] Guillet, J. E. *Polymer Photophysics and Photochemistry: an Introduction to the Study of Photoprocesses in Macromolecules*; Cambridge University Press: Cambridge, 1985.

[2] Nie, S. M.; Chiu, D. T.; Zare, R. N. *Science*, **1994**, *266*, 1018.

[3] Xie, S. X. *Acc. Chem. Res.* **1996**, *29*, 598.

[4] Moerner, W. E.; Orrit, M. *Science* **1999**, *283*, 1670.

[5] Moerner, W. E. *J. Phys. Chem. B* **2002**, *106*, 910.

[6] Moerner, W. E. *Science* **1994**, *265*, 46.

[8] Simha, R.; Somcynsky, T. *Macromolecules* **1969**, *2*, 342.

[9] Patel, J. K.; Kapadia, C. H.; Owen, D. B. *Statistics: Textbooks and Monographs*; Marcel Dekker: New York, 1976, Vol. 29.

[10] Liu, J.; Deng, Q.; Jean, Y. C. *Macromolecules* **1993**, *26*, 7149.

[11] Yu, W.-C.; Sook, C.; Sung, P.; Robertson, R. E. *Macromolecules* **1988**, *21*, 355.

[12] Tomczak, N.; Vallée, R. A. L.; van Dijk, E. M. H. P.; Kuipers, L.; van Hulst N. F.; Vancso, G. J. *J. Am. Chem. Soc.* **2004**, 126, 4748.

[13] Vallée, R. A. L.; Tomczak, N.; Kuipers, L.; Vancso, G. J.; van Hulst N. F. *Phys. Rev. Lett.* **2003**, *91*, 038301.

[14] Vallée, R. A. L.; Vancso, G. J.; van Hulst N. F.; Calbert, J.-P.; Cornil, J.; Bredas, J. L. *Chem. Phys. Lett.* **2003**, *372*, 282.

[15] Purcell, E. M. *Am. Phys. Soc.* **1946**, *69*, 681.

[16] Kleppner, D. *Phys. Rev. Lett.* **1981**, *47*, 233.

[17] Vallée, R. A. L.; Tomczak, N.; Gersen, H.; van Dijk, E. M. H. P.; Garcíia-Parajó, M. F.; Vancso, G. J.; van Hulst, N. F. *Chem. Phys. Lett.* **2001**, *348*, 161.

[18] Macklin, J. J.; Trautman, J. K.; Harris, T. D.; Brus, L. E. *Science* **1996**, *272*, 255.

[19] Kreiter, M.; Prummer, M.; Hecht, B.; Wild, U. P. *J. Chem. Phys.* **2002**, *117*, 9430.

[20] Astilean, S.; Barnes, W. L. *Appl. Phys. B* **2002**, *75*, 591.

[21] Nienhuis, G.; Alkemade, C. Th. J. *Physica A* **1976**, *81C*, 181.

[22] Glauber, R. J.; Lewenstein, M. *Phys. Rev. A* **1991**, *43*, 467.

[23] Jackson, J. D. *Classical Electrodynamics*; Wiley: New York, 1975.

[24] Bottcher, C. J. F. *Theory of Electric Polarization*; Elsevier: Amsterdam, 1973.

[25] Agranovich, V. M.; Galanin, M. D. *Electronic Excitation Energy Transfer in Condensed Matter*; North Holland: Amsterdam, 1982.

[26] Dexter, D. L. *Phys. Rev.* **1956**, *101*, 48.

[27] Milloni, P. W. *J. Mod. Opt*. **1995**, *42*, 1991.

[28] Wijers, C. M. *J. Phys. Stat. Sol. A* **2001**, *188*, 1251.

[29] Cao, C.; Long, W.; Cao, H. *Phys. Lett. A* **1997**, *232*, 15.

[30] Berman, P. R.; Milonni, P. W. *Phys. Rev. Lett.* **2004**, *92*, 053601.

[31] Toptygin, D. *J. Fluoresc.* **2003**, *13*, 201.

[32] Rikken, G. L. J. A.; Kessener Y. A. R. R. *Phys. Rev. Lett.* **1995**, *74*, 880

[33] Schuurmans, F. J. P.; de Lang, D. T. N.; Wegdam, G. H.; Sprik, R.; Lagendijk, A. *Phys. Rev. Lett.* **1998**, *80*, 5077.

[34] Schuurmans, F. J. P.; Lagendijk, A. *J. Chem. Phys.* **2000**, *113*, 3310.

[35] Kumar, G. M.; Rao, D. N. *Phys. Rev. Lett.* **2003**, *91*, 203903.

[36] Drexhage, K. H. *J. Lumin.* **1970**, *1*, 693.

[37] Lukosz, W. *Phys. Rev. B* **1980**, *22*, 3030.

[38] Drexhage, K. H. In *Progress in Optics*; Wolf, E., Ed.; North-Holland: Amsterdam, 1974; Vol. 12; Chapter 4.

[39] Lukosz, W.; Kunz, R. E. *Opt. Commun.* **1979**, *31*, 42.

[40] Toptygin, D.; Savtchenko, R. S.; Meadow, N. D.; Roseman, S.; Brand, L. *J. Phys. Chem. B* **2002**, *106*, 3724.

[41] Simha, R. *Macromolecules* **1977**, *10*, 1025.

[42] Quach, A.; Simha, R. *J. Appl. Phys.* **1971**, *42*, 4592.

[43] Oels, H.; Rehage, G. *Macromolecules* **1977**, *10*, 1036.

[44] Zoller, P.; Walsh, D. J. *Standard Pressure-Volume-Temperature Data for Polymers*; Technomic Publishing: Lancaster, 1995.

[45] Robertson, R. E.; Simha, R.; Curro, J. G. *Macromolecules* **1984**, *17*, 911.

[46] Robertson, R. E. *Computational Modeling of Polymers, Free-volume Theory and Its Application to Polymer Relaxation in the Glassy State*; Bicerano, J., Ed.; Marcel Deker: New York, 1992.

[47] Robertson, R. E. *J. Polym. Sci. Polym. Symp*. **1978**, *63*, 173.

[48] Schmidt-Rohr, K.; Spiess, H. W. *Phys. Rev. Lett.* **1991**, *66*, 3020.

[49] Richter, R. *J. Phys. Chem. B* **1997**, *101*, 6323.

[50] Wang, H.; Bardo, A. M.; Collinson, M. M.; Higgins, D. A. *J. Phys. Chem.* **1998**, *102*, 7231.

[51] Vallee, R. A. L.; Cotlet, M.; Hofkens, J.; de Schryver, F. C. *Macromolecules* **2003**, *36*, 7752.

[52] Biju, V. P.; Ye, J. Y.; Ishikawa, M. *J. Phys. Chem. B* **2003**, *107*, 10729.

[53] Ye, J. Y.; Ishikawa, M.; Yogi, O.; Okada, T.; Maruyama, Y. *Chem. Phys. Lett.* **1998**, *288*, 885.

[54] Frick, B.; Richter, D. *Science* **1995**, *267*, 1939.

[55] Hoff, E. A. W.; Robinson, D. W.; Willburn, A. H. *J. Polym. Sci.* **1955**, *18*, 161.

[56] Heijboer, J. *Br. Polym. J.* **1969**, *1*, 3.

[57] Yano, O.; Wada, Y. *J. Polym. Sci., Polym. Phys. Ed.* **1971**, *9*, 669.

[58] Yano, O.; Wada, Y. *J. Polym. Sci., Polym. Phys. Ed.* **1974**, *12*, 665.

Chapter 6

Fluorescence lifetime of single-molecules embedded in thin polymer layers[*]

The fluorescence lifetime of chromophores is a parameter that is very sensitive to the chromophore surroundings. We showed (Chapter 5) that the fluctuations in the radiative decay rates reflect the dynamics in the surrounding bulk polymer matrix. Before moving towards investigations of the dynamics in thin polymer films it is important to investigate to what extent the specific geometry of the system can affect the determined lifetimes. As shown here, the rate with which the molecule decays from the excited state can be influenced by the presence of dielectric interfaces. In particular, when the chromophore is embedded in thin dielectric layers, the orientation of the chromophore with respect to the interfaces plays a substantial role. Also the distance to the interfaces can influence the emitter. We show that the distributions of single molecule fluorescence lifetimes shift towards higher values of the latter when decreasing the film thickness. We attribute this shift to the electromagnetic boundary conditions imposed on the molecule by the thin film structure. We simulate the excited state lifetime of light sources embedded in thin dielectric films and find a similar trend as in our experimentally determined lifetimes. We also find that the molecules entering into the experimentally obtained distributions are mainly oriented in-plane and lower absolute values of the lifetime are obtained.

[*] Part of this work has been published in: Vallée R. A. L.; Tomczak, N.; Gersen, H.; van Dijk, E. M. H. P.; García-Parajó, M. F.; Vancso, G. J.; van Hulst, N. F. On the role of electromagnetic boundary conditions in single molecule fluorescence lifetime studies of dyes embedded in thin films. *Chem. Phys. Lett.* **2001**, *348*, 161.

6.1 Introduction

The radiative properties of fluorophores are not only inherent to the emitters but also depend on the emitter's environment [1]. The spontaneous emission of a chromophore from its excited state depends on the local photonic mode density into which the photon may be released. In most of the experimental procedures involving fluorophores, the presence of dielectric or metallic interfaces is inevitable. Therefore it is of great importance to know how the presence of such electromagnetic boundaries affects the experimental fluorescence observable.

Modifications of the excited state lifetime, angle-dependent intensity, polarization and energy transfer efficiencies as a function of distance and orientation of fluorophores to the interfaces were all reported [1,2-9]. Modification of the spontaneous emission rates of ensembles of europium ions (Eu^{3+}) [10,11] or organic chromophore ensembles [12,13] placed close to a thin *metal* mirror were investigated. The theoretical description of these experiments was performed later by Chance et al. [14]. Enderlein [15,16] investigated theoretically the influence a metal layer has on single molecule fluorescence and Yokota [17] reported the first successful detection of single molecules attached to proteins on metal surfaces. Also the effect of *dielectric* interfaces on the spontaneous emission rates of chromophores was investigated both theoretically [18-22] and experimentally [10,23-27] for an ensemble of emitters. At the single molecule level, Macklin et al. [28] showed that the electromagnetic boundary conditions imposed on the radiated field of a single molecule deposited on glass substantially modifies the fluorescence lifetime of the molecule. Furthermore, by monitoring the fluorescence emission rates they also showed that molecules with out-of-plane dipole moments indeed have longer lifetimes as was shown earlier by Lukosz and Kunz [25,29] for ensembles of dyes. Kreiter et al. [30] used annular illumination to obtain simultaneous information on the out-of-plane orientation of the absorption dipole moment and the fluorescence lifetime. The fluorescence lifetimes of molecules oriented parallel and perpendicular to the interfaces were different by a factor of two. The distributions of the decay rates were broader than statistically expected, which was attributed to the inhomogeneities present in the surrounding polymer matrix.

In this Thesis we focus primarily on probing the structure and dynamics of polymers. However, before reaching a conclusion about polymer properties it is important to discriminate between other possible influences on the experimental parameter than the polymer specific property in question. In this chapter we present a study on the effect of the electromagnetic boundaries on the excited state lifetime of single fluorescence molecules. The extent of the modification of the radiative properties of single DiD molecules embedded in thin PS films was found to depend on the position and orientation of the molecules with

respect to the interfaces. We prepared a series of thin polymer films with thickness values ranging from 10 to 200 nm and obtained a distribution of single molecule fluorescence lifetimes for each film thickness. We found that the mean values of the fluorescence lifetime distributions depend on the thickness of the polymer films. For very thin films a steep increase of the fluorescence lifetime was found, consistent with the increased influence of the polymer/air interface. The variation of the lifetime between different molecules was much larger than expected from the film thickness dependence. Consequently we attribute the broad distributions observed to the orientation of the transition dipole moments with respect to the interfaces or to the inhomogeneities in the polymer matrix

A deeper understanding of the influence of nanostructured surroundings on the radiative properties of fluorescent molecules [31-33] will help to design devices with tailored optical properties for nanophotonics e.g. new generations of lasers [34], organic light emitting diodes [35], directional antennas [36] etc. Detailed knowledge of the effect of the interfaces is also relevant whenever identification or investigation of single molecules is performed through time-resolved fluorescence detection [37-39]. Thus, this chapter is devoted to a description of the electromagnetic boundary conditions effects on single molecule fluorescence lifetimes in thin film geometries.

6.2 Experimental part

6.2.1 Materials and sample preparation

To study the influence the film thickness has on the radiative properties of single light emitters we embedded chromophores in a number of thin film samples with thickness values ranging from 10 to 200 nm. The probe used in this study was DiD (1,1'dioctadecyl-3,3,3',3'-tetramethylindodicarbocyanine perchlorate, Molecular Probes D-307). The choice of the dye was dictated by the fact that it has a high fluorescence quantum yield when embedded in polymer matrices and a large absorption cross-section of 7.4×10^{-16} cm^2. Additionally DiD molecules in polymer matrices are relatively stable compared to other chromophores. As host matricx we chose polystyrene (PS, molar mass M_n = 89300 g/mol, polydispersity M_w/M_n = 1.06, Polymer Standard Service, glass transition temperature T_g = 100 ºC). Solutions of the dyes in toluene containing different amounts of polymer were spin-coated at 3000 rpm for 60 s onto microscope glass cover slides (diameter Φ = 20 mm, Fisher Scientific) to produce uniform thin coatings with thickness values ranging from 10 to 200 nm. Changing the concentration of the polymers in the solution varied the thickness as anticipated [40]. Prior to spin coating the glass cover slides were cleaned using a Piranha solution (mixture of 1:4 of 30% H_2O_2 and concentrated H_2SO_4), rinsed with Milli-Q water and ethanol, and finally dried

in a stream of nitrogen gas. The concentration of the dyes in the resulting films was kept low enough (10^{-9}-10^{-10} M) to ensure adequate spatial separation for optical single molecule observations. The PS samples were subsequently annealed in vacuum, first for 12 h at 60 °C and later for 3 h at 105 °C. Such thermal treatment was performed to remove the residual solvent, relax the stressed introduced by the spin-coating technique while the two-stage process used helped to avoid dewetting.

6.2.2 Atomic Force Microscopy

A NanoScope IIIa (Veeco, Digital Instruments, Santa Barbara, USA) Atomic Force Microscope (AFM) was used to examine the sample surface and the tip-scratch method [41,42] was used to determine the film thickness. To determine the planarity and surface roughness, the AFM was operating in the tapping mode (when used for imaging) using a cantilever with a nominal spring constant of 40-60 N/m.

6.2.3 Single molecule fluorescence lifetime detection

A picosecond-pulsed dye laser (635nm, PicoQuant, 800-B, 100mW, 80 MHz repetition rate) was used for excitation and time-resolved experiments. The excitation light was made circularly polarized using a ¼ λ plate and focused onto the sample to a diffraction-limited spot using a high NA oil objective (Olympus, NA=1.4, 100x). To separate the fluorescence emission from the excitation, suitable dichroic mirrors, emission, and excitation filters, were used. Fluorescence photons were collected by the same objective and subsequently focused onto two avalanche photodetectors (SPCM-AQ-14, EG&G Electro Optics) placed after a polarization beam splitter. A custom-built piezo-scan table with an active x-y feedback loop mounted on a commercial optical microscope (Zeiss Axiovert inverted microscope) was used. The sample was scanned over the focus of the excitation spot at a pixel frequency of 1 kHz, producing a two-dimensional fluorescence intensity images (for two independent polarization channels when required) (Figure 1a). For time resolved experiments the detected fluorescence signal was fed into a time-correlated single photon counting card (TCSPC). Custom LabView software was used to control the scanning process and data acquisition. For higher temperature measurements a custom-built hot-stage was placed below the sample and the temperature was monitored with an accuracy of 2 °C. For each film thickness investigated, 400 molecules were analyzed at two different temperatures (22 °C and 35 °C).

6.3 Fluorescence emission near interfaces

Since the early experiments of Drexhage et al. [10] it is known that the lifetime of an excited molecule fluorescing near an interface between two media can be altered substantially owing to reflection and absorption at the interface. Chance et al. [14] and Lukosz and Kunz [29] have described this interaction, showing that the field of the dipole is perturbed in the presence of a second medium. In a simple approximation a dye molecule can be considered as an oscillating point dipole with a transition dipole moment $\vec{p}$, when driven by the alternating electric field of the incoming light wave. The dipole acts as a source of a secondary wave. When surrounded by an isotropic medium, this secondary wave does not influence the oscillator. The well-known butterfly pattern for the total emitted power W radiated by the molecule in an isotropic medium can be described by the Larmor fomula:

$$W = \frac{\mu\omega^4 \left|\vec{p}\right|^2}{12\pi c} \tag{1}$$

with $\vec{p}$ the dipole moment, μ the permeability of the considered medium, ω the dipole emission frequency and c the speed of light. In geometries where interfaces are present, the interface can produce a reflected field which acts to drive the dipole moment associated with the emission. Additionally, interference between the directed and reflected parts of the emitted light wave will occur. If the reflected field is in phase with the source then emission is enhanced; if it is out of phase then the emission is inhibited [31]. Therefore, the result depends on the optical properties of the interfaces and on the size of the system.

The reflection of electromagnetic waves at a plane interface can be treated using the classical Fresnel formulas. This dependence on the reflection coefficients illustrates that the total radiated power is strongly dependent on the distance d separating the dipole from the air interface, as well as on the orientation α of the dipole with respect to the air interface. In the underlying problem the dipole is so close to the interface between the different media that the exponentially decaying part of the fields play an important role and should be taken into account. This is performed by taking the complex Fresnel coefficients as a function of the dielectric constant rather than depending on the angles employed in a more familiar geometrical optical picture. Lukosz and Kunz [29] calculated the following expression for the total power radiated by an arbitrarily oriented dipole in the presence of a second medium:

$$\frac{W(d)}{W} = \cos^2\alpha\left[\frac{W(d)}{W}\right]_{\perp} + \sin^2\alpha\left[\frac{W(d)}{W}\right]_{\parallel}, \tag{2}$$

where the radiated power emitted by the dipole in a homogeneous medium (W) is used to normalize the result. The determination of the fluorescence lifetime is thus equivalent to measuring the power radiated in the whole space surrounding the dipole. The ratio of observed fluorescence lifetimes in two different optical environments is then given by the inverse ratio of the total power radiated by the fluorescent molecule.

$$\frac{\tau(d)}{\tau} = \left[\frac{W(d)}{W}\right]^{-1}, \tag{3}$$

Where τ is the fluorescence lifetime in vacuum. In equation 3, $\tau(d)$ consists of the nonradiative and radiative components

$$\frac{1}{\tau(d)} = \frac{1}{\tau_{nr}} + \frac{1}{\tau_r}, \tag{4}$$

where τ_{nr} and τ_r are the nonradiative and radiative lifetimes, respectively. Therefore, the quantum yield (QY) of the fluorescence emission is an important parameter, which has to be taken into account. Lower quantum yields will generally lower the magnitude of the effects of the reflecting interfaces [31,32].

6.4 Determination of the fluorescence lifetime

To localize single DiD molecules within the polystyrene matrix, first, fluorescence intensity images were acquired. Figure 1a shows a 10x 10 μm^2 fluorescence intensity scan obtained with a scanning confocal microscope. The color scale in Figure 1a indicates the in-plane orientation of the emission dipole moment of the chromophores. Frequent blinking and one-step photobleaching are visible on the scan for different molecules, indicating that the fluorescence spots correspond to single molecules. Each of the single molecules identified was centered at the laser focus and time-resolved experiments were performed. The fluorescence lifetime was determined by fitting a single exponential decay function to experimentally obtained histograms of the arrival times taken after pulsed laser excitation [6]. The fits were repeated for each 100 ms integration time and the lifetime traces of 10 to 30 s total observation time were obtained (Figure 2b). The total observation time was limited by photobleaching of the probes. For each single molecule lifetime transient we built lifetime distributions (Figure 2c). In Chapter 5 we have shown that many single molecules exhibit fluorescence lifetime excursions towards higher values, rendering the fluorescence lifetime distributions to have an asymmetric shape. A question arises about the most appropriate way to determine the chromophores lifetime for such molecules? Since we would like to

discriminate between the matrix dynamics and the electromagnetic boundary conditions one should avoid including data which result from the changes in the molecule's surroundings. Therefore, the static and the dynamic nature of the fluorescence lifetime distribution should be separated as much as possible. Integrating over the whole time-trace duration will result in non-exponential fluorescence decays influenced primarily by the frequency of the lifetime jumps, therefore the result will depend on the matrix. Taking into account all lifetime points from all time-traces into one histogram for a given sample will bias the fluorescence lifetime towards longer values. To decouple these effects we make use of the same fitting procedure as in Chapter 5 and determine the average fluorescence lifetime. We fit the obtained lifetime histograms with a gamma distribution function $g(x) = \beta(\beta x)^{\alpha-1}e^{-\beta x}/\Gamma(\alpha)$ [43] (solid line in Figure 2c). The first moment of the distribution, the average, is given by $x_{av} = \alpha/\beta$, where α and β are the shape and the scale parameters characterizing the distribution; Γ stands for the gamma function.

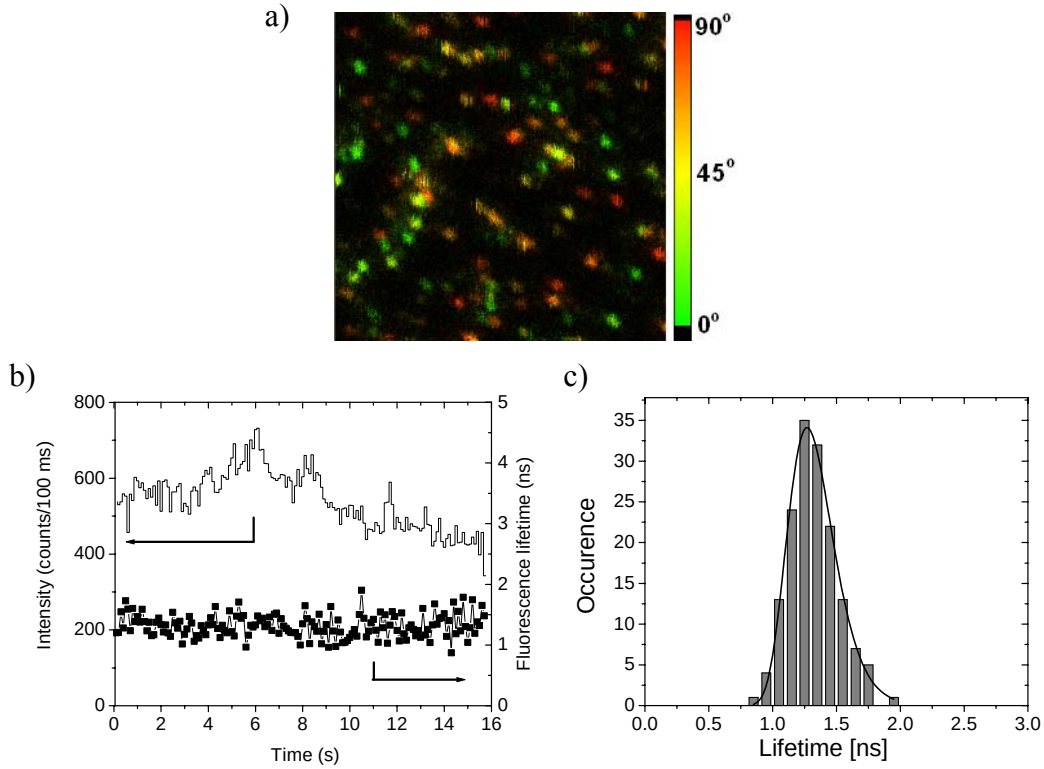

Figure 1. a) 10x10 μm^2 fluorescence intensity scan of DiD molecules embedded in a PS film obtained with a scanning confocal microscope. The color scale indicates the in-plane orientation of the emission dipole moment b) Fluorescence intensity and lifetime time-traces for a single DiD molecule. c) Distribution of the fluorescence lifetimes. The distribution was fitted with a gamma function (solid line) and the average lifetime (τ_{av}) was extracted.

6.5 Results and discussion

To establish whether the electromagnetic boundary condition have an effect on the experimentally determined fluorescence lifetime we collected the time-traces for about 100 single DiD molecules embedded in polymer films with given thickness values ranging from 10 nm to 200 nm. For each molecule investigated we built the lifetime distributions, fitted with the gamma distribution function and finally obtained the average fluorescence lifetimes. By repeating the procedure for all single molecules we obtained distributions of the average fluorescence lifetime of single DiD chromophores embedded in PS films. We also repeated the whole procedure for a higher temperature. The variation of temperature was needed as we will investigate polymer segmental dynamics in thin films in the subsequent Chapter 7 at these two temperatures. In Figure 2 we show the full fluorescence lifetime distributions obtained for each sample with different thickness values at two different temperatures. Most of the distributions peak at a specific fluorescence lifetime value. In some cases, however, broad distributions with no distinct peak (e.g. the 70 nm thick sample at 22 ºC) or asymmetric distributions (e.g. the 10 nm thick sample at 22 ºC) were also found. A possible reason for this is the presence of heterogeneity in the polymer matrix and the limited number of investigated molecules. To compare the result for different samples we calculated the mean fluorescence lifetime, as shown in Table 1. The lifetime data follow a similar trend for the two temperatures. The values for the 160 nm and 70 nm samples (at 22 ºC) are slightly off, however they are still similar within the error of the measurement.

Film thickness [nm]	T = 22 ºC Mean lifetime [ns]	T = 35 ºC Mean lifetime [ns]
200	1.84 ± 0.08	1.76 ± 0.08
160	2.06 ± 0.10	1.88 ± 0.08
110	1.88 ± 0.08	1.86 ± 0.10
70	1.57 ± 0.16	1.82 ± 0.08
55	1.81 ± 0.08	1.91 ± 0.12
35	1.96 ± 0.10	1.95 ± 0.10
25	2.01 ± 0.10	2.10 ± 0.10
10	2.75 ± 0.20	2.16 ± 0.10

Table 1. The mean fluorescence lifetime obtained for the distributions shown in Figure 2.

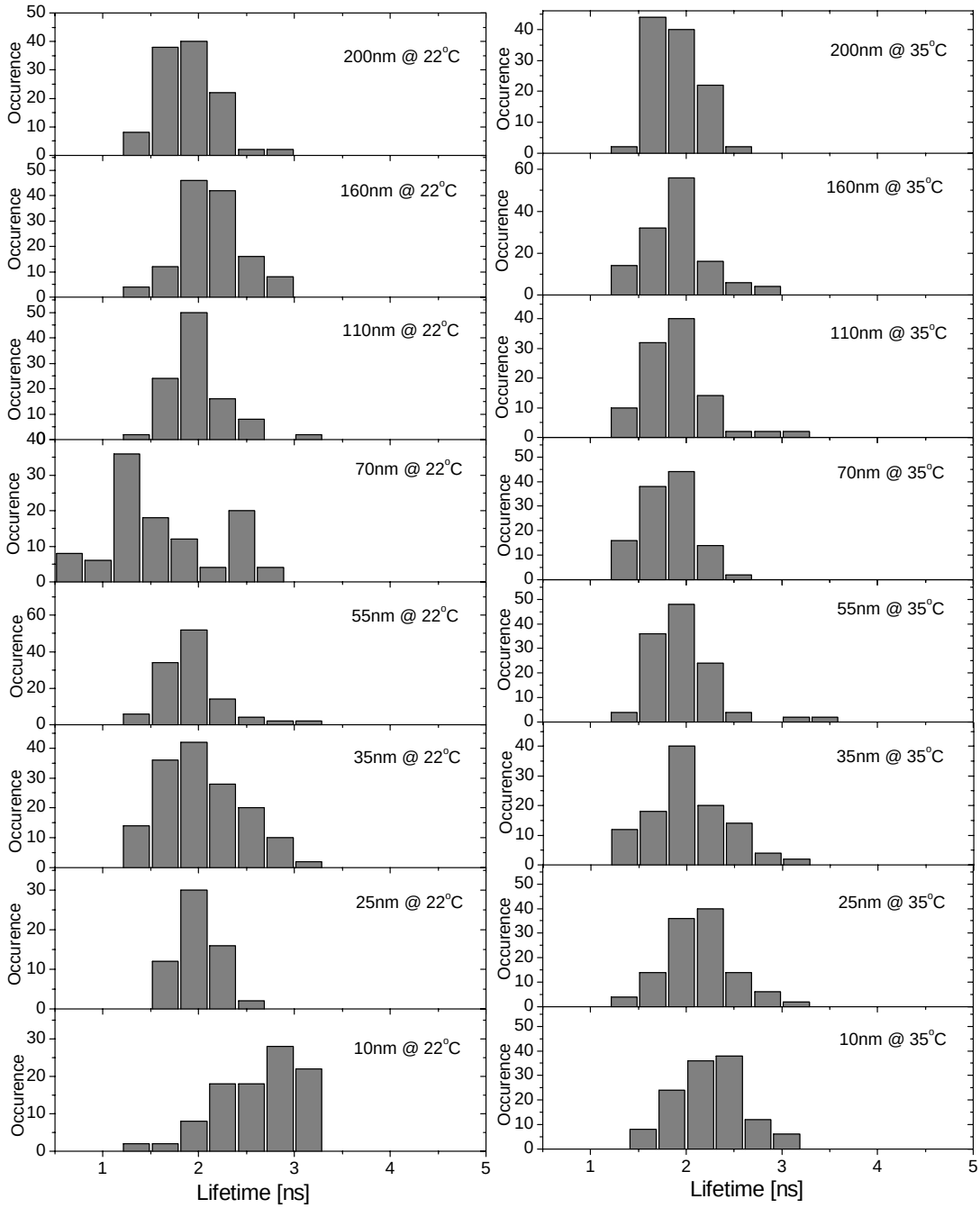

Figure 2. Histograms of the average fluorescence lifetime as a function of film thickness measured at two temperatures: 22 ºC (left column) and 35 ºC (right column). The mean values of the distributions were extracted and are presented in Table 1. For the thinnest films a shift towards higher lifetime values is observed for both temperatures.

The possible effect of the electromagnetic boundary conditions for higher film thicknesses is rather difficult to observe in the data presented in Figure 2. However, the key observation is that for the lowest film thickness the distribution of the fluorescence lifetime as well as the mean fluorescence lifetime shift towards longer lifetime values. To check whether the observed shifts are due to the electromagnetic boundary effects we calculated the fluorescence lifetime of dipoles embedded in thin dielectric layers. The model and the relevant data taken for the calculations are shown in Figure 3.

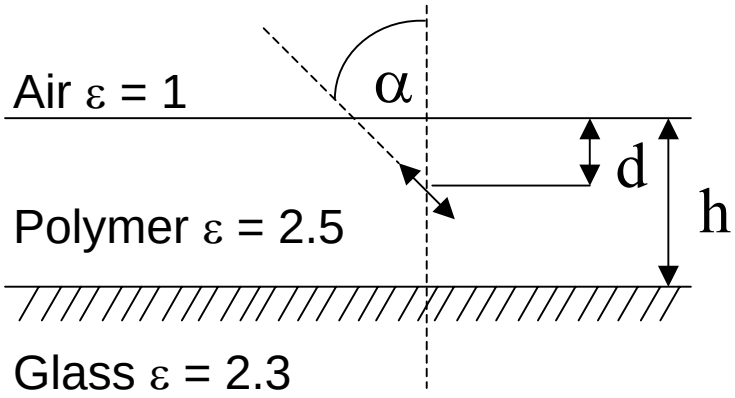

Figure 3. Schematic of the three-layer model used in this study. The polymer film is placed between glass and air. The molecule is represented as a dipolar light source and is placed inside the film at a distance *d* from the air interface and is oriented with an angle α relative to the normal of the polymer –air interface. The film thickness is equal to *h*.

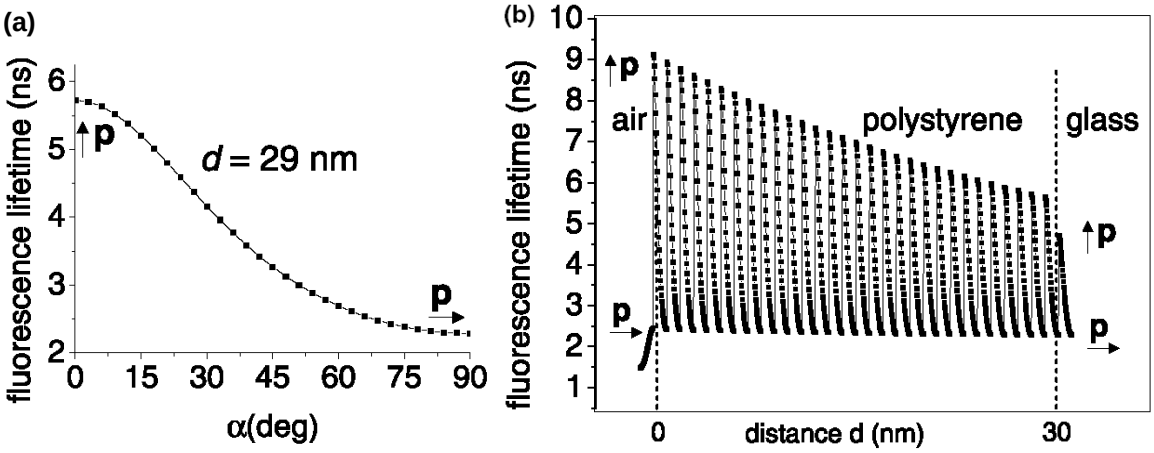

Figure 4. a) Calculated dependence of the fluorescence lifetime as a function of the orientation of the molecule with respect to the polymer/air interface. The molecule was embedded in a 30 nm thick sample and located 29 nm away from the polymer/air interface. b) The calculated values of the fluorescence lifetimes for all depths and orientations for a 30 nm thick film. The distance step is 1 nm and the angle step is 3º.

In Figure 4a we show the calculated values of the fluorescence lifetime as a function of the orientation of the molecule. When the molecule is orientated perpendicular to the polymer/air interface, substantially higher values of the fluorescence lifetime are observed. It should be noted that in this study we preferentially excite in-plane molecules. Due to signal-to-background reasons only the molecules with significant in-plane orientation could therefore be investigated. As can be seen in Figure 4a, the lifetime of the in-plane molecules is not so sensitive to the chromophore orientation for angles ranging from 60 to 90 degrees. Therefore, we would not expect that the electromagnetic boundary effects will be only associated with the orientation of the chromophores. As it was mentioned earlier, the fluorescence lifetime of the molecules is also dependent on the distance to the interfaces. In Figure 4b we plot the fluorescence lifetime in function of the position of the molecule within the dielectric film for all orientations. When the molecule is placed closer to the polymer/air interface, the sensitivity of the fluorescence lifetime to the orientation increases. Also, in general, higher values of the fluorescence lifetime are observed closer to the polymer/air interface. It is expected therefore that for the same set of molecules the average fluorescence lifetime will depend on the total film thickness. By assuming a random arrangement of the molecules placed in all depths within the polymer films, each with an isotropic distribution of orientations, we calculate the fluorescence values for each film thickness investigated. In Figure 5 we plot our results together with the experimentally determined mean fluorescence lifetimes.

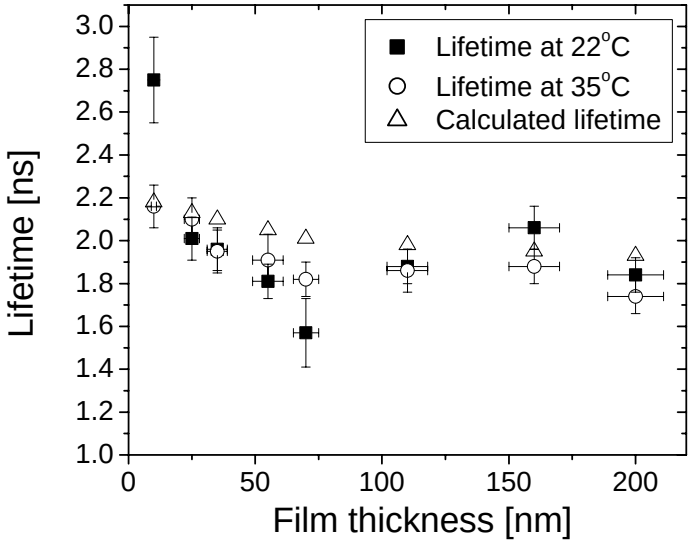

Figure 5. Mean values of the fluorescence lifetime of single DiD molecules embedded in PS as a function of polystyrene film thickness. The open triangles represent the calculated values of the fluorescence lifetime.

For higher film thicknesses the calculated values are, within the error, similar to the experimentally obtained values. For intermediate film thickness, however, a small offset towards higher lifetime values is observed. For the thinnest films the calculated lifetime is again in good agreement with the experiment. The key observation in Figure 4 is that for both the theoretical and experimental data the fluorescence lifetime follows the same trend i.e. the lifetime increases with decreasing film thickness. The small discrepancies between the experiments and calculations can be due to the fact that we probed a larger subset of molecules with in-plane orientation. In such a case the overall fluorescence lifetime, as seen from Figure 4a, will be lower.

The electromagnetic boundary conditions effect can indeed reproduce the observed dependence of the fluorescence lifetime with film thickness. Comparing to the lifetime fluctuations observed in Chapter 5, these effects for an ensemble of dyes are rather small. It is expected that the thin film geometry, although shifting slightly the lifetimes towards higher values, will not change substantially the sensitivity of the molecule to the dielectric surroundings in cases were the molecule is not rotating or translating with respect to the interfaces.

6.6 Conclusions

In this Chapter we have shown that the electromagnetic boundary conditions can play an important role when the fluorescence lifetime is the investigated parameter. We found that the distributions of the fluorescence lifetime of single molecules embedded in polystyrene films shift towards higher values, most profoundly for the thinnest films investigated. We have modeled our samples as a three-level system consisting of a dielectric sandwiched in between glass and air and we showed that these shifts of the distributions can be explained by taking account the effects associated with the presence of the optical interfaces. The results presented in this Chapter should be taken into account when interpreting the fluorescence lifetime of single molecules in nanoscale surroundings. For the fluorescence lifetime fluctuation method presented in Chapter 5 we conclude that these effects are not so significant and will not affect the sensitivity of the method.

6.7 Acknowledgements

The theoretical calculations of the fluorescence lifetime were performed with Dip_Rad software written and kindly provided by Henkjan Gersen.

6.8 References

[1] Purcell, E. M. *Am. Phys. Soc.* **1946**, *69*, 681.

[2] Novotny, L. *Appl. Phys. Lett.* **1996**, *69*, 3806.

[3] Novotny, L. *J. Opt. Soc. Am. A* **1997**, *14*, 91.

[4] Sullivan, K. G.; Hall, D. G. *J. Opt. Soc. Am. B* **1997**, *14*, 1160.

[5] Xiao, M.; Chen, X. *Opt. Commun.* **1998**, *158*, 11.

[6] Vallée, R. A. L.; Tomczak, N.; Gersen, H.; van Dijk, E. M. H. P.; García-Parajó, M. F.; Vancso, G. J.; van Hulst, N. F. *Chem. Phys. Lett.* **2001**, *348*, 161.

[7] Trabesinger, W.; Kramer, A.; Kreiter, M.; Hecht, B.; Wild, U. P. *Appl. Phys. Lett.* **2002**, *81*, 2118.

[8] Klimov, V. V.; Ducloy, M. *Phys. Rev. A* **2004**, *69*, 013812.

[9] Arnoldus, H. F.; Foley, J. T. *J. Opt. Soc. Am. A* **2004**, *21*, 1109.

[10] Drexage, K. H. in Wolf E (Ed), Progress in Optics XII, North-Holland, Amsterdam, 1974, 165.

[11] Amos, R. M.; Barnes, W. L. *Phys. Rev. B* **1997**, *55*, 7249.

[12] Danz, N.; Heber, J.; Brauer, A.; Kowarschik, R. *Phys. Rev. E* **2002**, *66*, 063809.

[13] Vasilev, K.; Knoll, W.; Kreiter, M. *J. Chem. Phys.* **2004**, *120*, 3439.

[14] Chance, R. R.; Prock, A.; Silbey, R. *Adv. Chem. Phys.* **1978**, *37*, 1.

[15] Enderlein, J. *Chem. Phys.* **1999**, *247*, 1.

[16] Enderlein, J. *Biophys. J.* **2000**, *78*, 2151.

[17] Yokota, H.; Saito, K.; Yanagida, T. *Phys. Rev. Lett.* **1998**, *80*, 4606.

[18] Carniglia, C. K.; Mandel, L. *Phys. Rev. D* **1971**, *3*, 280.

[19] Hellen, E. H.; Axelrod, D. *J. Opt. Soc. Am. B* **1987**, *4*, 337.

[20] Khosravi, H.; Loudon, R. *Proc. R. Soc. London, Ser. A* **1991**, *433*, 337.

[21] Lukosz, W. *Phys. Rev. B* **1980**, *22*, 3030.

[22] Urbach, H. P.; Rikken, G. L. J. A.; Rikken, *Phys. Rev. A* **1998**, *57*, 4913.

[23] Drexage, K. H. *J. Lumin.* **1970**, *12*, 693.

[24] Carniglia, C. K.; Mandel, L.; Drexhage, K. H. *J. Opt. Soc. Am.* **1972**, *62*, 479.

[25] Lukosz, W.; Kunz, R. E. *Opt. Commun.* **1977**, *20*, 195.

[26] Lukosz, W.; Kunz, R. E. *Opt. Commun.* **1979**, *31*, 42.

[27] Kunz, R. E.; Lukosz, W. *Phys. Rev. B* **1980**, *21*, 4814.

[28] Macklin, J. J.; Trautman, J. K.; Harris, T. D.; Brus, L. E. *Science* **1996**, *272*, 255.

[29] Lukosz, W.; Kunz, R. E. *J. Opt. Soc. Am.* **1977**, *67*, 1607.

[30] Kreiter, M.; Prummer, M.; Hecht, B.; Wild, U. P. *J. Phys. Chem. 117*, 9430.

[31] Astilean, S.; Barnes, W. L. *Appl. Phys. B* **2002**, *75*, 591.

[32] Astilean, S.; Garrett, S.; Andrew, P.; Barnes, W. L. *J. Mol. Structure* **2003**, *651-653*, 277.

[33] Blanco, L. A.; Garcia de Abajo, F. J. *Phys. Rev. B* **2004**, *69*, 205414.

[34] Yokoyama, H. *Science* **1992**, *256*, 66.

[35] Lidzey, D.; Pate, M. A.; Whittaker, D. M.; Bradley, D. D. C.; Weaver, M. S.; Fisher, T. A.; Skolnik, M. S. *Chem. Phys. Lett.* **1996**, *263*, 655.

[36] Blanco, L. A.; Garcia de Abajo, F. J. *Optics Express* **2004**, *29*, 1494.

[37] Prummer, M.; Hubner, C. G.; Sick, B.; Hecht, B.; Renn, A.; Wild, U. P. *Anal. Chem.* **2000**, *72*, 443.

[38] Zander, C.; Sauer, M.; Drexhage, K. H.; Ko, D.-S.; Schulz, A.; Wolfrum, J.; Brand, L.; Eggeling, C.; Seidel, C. A. M. *Appl. Phys. B* **1996**, *63*, 517.

[39] Li, Q.; Ruckstuhl, T.; Seeger, S. *J. Phys. Chem. B* **2004**, *108*, 8324.

[40] Hall, D. B.; Underhill, P.; Torkelson, J. M. *Pol. Eng. Sci.* **1998**, *38*, 2039.

[41] Lobo, R. F. M.; Perira-da-Silva, M. A.; Raposo, M.; Faria, R. M.; Oliveira, Jr O. N. *Nanotechnology* **1999**, *10*, 389.

[42] Ton-That, C; Shard, A. G.; Bradley, R. H. Langmuir **2000**, *16*, 2281.

[43] Patel, J. K.; Kapadia, C. H.; Owen, D. B. *Statistics: Textbooks and Monographs*; Marcel Dekker: New York, 1976, Vol. 20.

Chapter 7

Segmental scale dynamics in thin polymer films[*]

Changes in segmental scale dynamics in polystyrene thin films far below the glass transition have been investigated using the single-molecule fluorescence lifetime method introduced in Chapter 4. For film thickness values ranging from 200 nm down to 10 nm the mean number of polymer segments taking part in the rearrangement volume was determined. Modified segment dynamics was found when the polymer was confined into films with thickness values below 60 nm. This film thickness is larger than the radius of gyration (R_g) of the polymer chains used (9 nm). Our results point towards the existence of interfacial regions with enhanced dynamics. The surface effects were found to propagate into the sample over distances comparable with, but larger than the R_g of the polymer, even at temperatures far below T_g. Monitoring the distributions of segment dynamics showed additionally that below a critical film thickness the surface dynamics starts to dominate the overall thin film behavior. Simultaneously, the dynamics became more heterogeneous than in thick films, indicating that such a transition behavior is critical for the whole thin film system.

[*] Part of this Chapter has been published in: Tomczak, N.; Vallée, R. A. L.; van Dijk, E. M. H. P.; Kuipers, L.; van Hulst, N. F.; Vancso, G. J. Segment dynamics in thin polystyrene films probed by single molecule optics *J. Am. Chem. Soc.* **2004**, *126*, 4748.

7.1 Introduction

Recently, increasing attention is paid to the dynamics of polymers films in the glassy and viscoelastic states due to their relevance in microelectronics, lithography, membrane technology, or nanocomposites. Sub-100 nm layers of polymers, as required by the microelectronic industry, introduce the problem of the integrity or stability of the resist films. The stability of polymer layers is an essential condition for the coatings industry. In multilayered systems, where the behavior of the systems depends on the stability of particular layers and on the interactions between them, the ability to predict the system behavior is of great importance. Compared to the large amount of available information concerning the glass transition and polymer chain mobility in bulk polymers [1-4] and in thin films made of simple liquids [5] relatively little is known about related phenomena at polymer interfaces [6-8] and in polymeric thin films [9,10]. Polymers have recently been demonstrated to exhibit different chain dynamic behavior when confined into the geometry of ultrathin films, as compared to the bulk [11,12]. It was found that the thin film geometry significantly alters many physical properties of polymers, like crystallization [13,14], microphase separation [15-18], melting temperature [19], heat capacity [20], tribology [21], aging [22,23] or electronic properties [24,25]. Investigations of the glass transition temperature (T_g) of thin, supported, polystyrene films by ellipsometry [26], Brillouin light scattering [27], dielectric spectroscopy [28] or positron annihilation lifetime spectroscopy (PALS) [29], among others, showed large T_g depressions. This behavior is thought to be due to the existence of a surface layer where the polymer chain dynamics is enhanced over that in the bulk. This layer becomes dominant for very thin films, thereby shifting the T_g of the films towards lower temperatures. The existence of such a surface layer is also supported by measurements of T_g for freestanding polymer films [27] and by a direct examination of the polymer surface by PALS [30].

Also non-polymeric materials which exhibit a glassy transition have been subject of investigations. One example is the study of the thermal properties of low-k dielectric (carbon doped silicon dioxide) thin films used in the integrated circuits industry [31-33] or the glass transition thermodynamics of small organic nanoparticles, like o-terphenyl, or benzyl alcohol [34-36]. Recently, Steponkus and Shalaev [37] reported a glass transition temperature depression for sucrose confined in a phospholipid mesophase. The ability of sugars to form a glassy state is considered to be one of the most important mechanisms of stabilization of liposomes and biological membranes. The depression of T_g is assumed to be the result of confinement of the sucrose in one of the phospholipids phase. The understanding of the behavior of thin films of glassy materials is also important in biopreservation. If a protein-based drug is mixed with a sugar-based solution and then freeze-dried, the sugars – which turn glassy as they dry – pull the proteins into a stable state. This can increase the shelf life of protein- based drugs [38].

Apart from its biological and technological significance, the study of thin films of glassy polymers can help to understand glass transition phenomena in the same way as the study of finite-size effects helped to better understand the critical regions of thermodynamic phase transition [35,39,40].

Unfortunately, most of the experimental techniques used to study thin polymer films provide ensemble-averaged information. Single molecule fluorescence detection (SMD) intrinsically avoids ensemble averaging. SMD is an ideal tool to investigate structure and dynamics of the probe environment on the nanoscale as it also provides high spatial and temporal resolution. Using different approaches, SMD has been already employed with success to study macromolecular systems (see also Chapter 3 of this thesis) [41,42] and inorganic/organic composite films [43].

In Chapter 5 we have introduced a new single molecule approach based on fluorescence lifetime fluctuations [44], which gives direct insight into local, nanoscale dynamics of the polymer matrix on the segmental level. In this Chapter we apply this method to investigate thin film effects in a glassy polymer system at temperatures far below bulk T_g. We find that the surroundings of the probe become more dynamic when the constituent macromolecules are confined into a thin film. The characteristic film thickness, at which this behavior becomes noticeable, is several times larger than the radius of gyration (R_g) of the polymer chain used. Our results point towards the existence of interfacial regions with enhanced dynamic behavior and represent the first step towards depth resolved studies of polymer films on the nanoscale using SMD.

7.2 Experimental methods and procedures

7.2.1 Materials and sample preparation

To investigate the effects reduced dimensions have on the polymer dynamics, a series of thin film samples deposited on glass were prepared. Glass cover slides (diameter Φ = 20 mm, Fisher Scientific) were cleaned using a Piranha solution (1:4 mixture of 30% H_2O_2 and concentrated H_2SO_4), rinsed with Milli-Q water and ethanol, and finally dried in a stream of nitrogen gas. Samples were prepared by spin-coating polymer solutions containing 1,1'–dioctadecyl-3,3,3',3'-tetramethylindodicarbocyanine (DiD) molecules (Molecular Probes, D-307) directly onto thin glass cover slides. The polymer used was a monodispersed (polydispersity M_w/M_n = 1.06) polystyrene (PS, Polymer Standard Service, molar mass M_n = $9x10^4$ g/mol, bulk glass transition temperature $T_{g,b}$ =100 ºC). The concentration of the dye in

the resulting PS films was 10^{-9} M. The amount of polymer in the spinning solution was used to control the sample thickness [45]. The resulting sample thickness was controlled from 10 to 200 nm.

7.2.2 Film thickness determination

A NanoScope IIIa (Digital Instruments, Santa Barbara) Atomic Force Microscope (AFM) was used to examine the sample surface and the tip-scratch [46,47] method was used to determine the film thickness. The AFM was operating in the tapping mode using a cantilever with a nominal spring constant of 40-60 N/m.

7.2.3 Single molecule fluorescence lifetime detection

A picosecond-pulsed dye laser (635 nm, PicoQuant, 800-B, 100 mW, 80 MHz repetition rate) was used for excitation and time-resolved experiments. The excitation light was made circularly polarized using a ¼ λ plate and focused onto the sample to a diffraction-limited spot using a high NA oil objective (Olympus, NA=1.4, 100x). To separate the fluorescence emission from the excitation, suitable dichroic mirrors, emission, and excitation filters were used. Fluorescence photons were collected by the same objective and subsequently focused onto two avalanche photodetectors (SPCM-AQ-14, EG&G Electro Optics) placed after a polarization beam splitter (splitting into s and p components). A custom-built piezo-scan table with an active x-y feedback loop mounted on a commercial optical microscope (Zeiss Axiovert inverted microscope) was used. The sample was scanned over the focus of the excitation spot at a pixel frequency of 1kHz, producing two-dimensional fluorescence intensity images (for two independent polarization channels, when required). For time resolved experiments the detected fluorescence signal was fed into a time-correlated single photon counting card (TCSPC). Custom LabView software was used to control the scanning process and data acquisition. For higher temperature measurements a custom-built hot-stage was placed below the sample and the temperature was monitored with an accuracy of +/- 2 °C. For each film thickness investigated, 400 molecules at two different temperatures (22 °C and 35 °C) were analyzed.

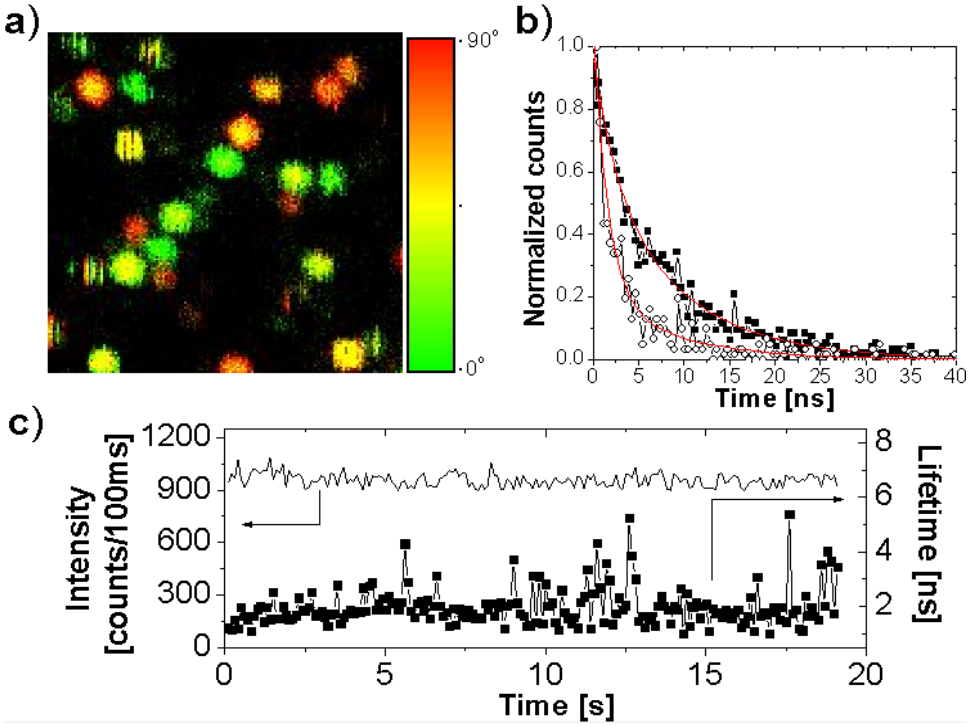

Figure 1. a) 5 x 5 μm^2 fluorescence intensity scan of single DiD molecules in a 110 nm thick PS film at 22 ºC. The color scale indicates the polarization of the fluorescence, which is a measure for the in-plane orientation of the molecules. Constant color confirms that the molecules are not rotating in the matrix. b) Fluorescence decays of one DiD molecule from which both short (2.5 ns - ○) and long (6 ns - ■) fluorescence lifetimes were extracted. The red lines correspond to single exponential fits to the data. c) Fluorescence intensity and lifetime traces for a single DiD in PS. Excursions to longer lifetimes (up to 5 ns) are clearly visible.

7.3 Results and discussion

7.3.1 Methodology

In Chapter 5 we demonstrated that single fluorescent molecules can be used as molecular probes to report on the local density fluctuations in the surrounding polymer matrix. By applying the Simha-Somcynsky equation of state theory one obtains the number of polymer segments (N_S) (see Chapter 5) taking part in the cooperatively rearranging volume around the single-molecule probe. Here we briefly indicate the main methodological steps to obtain information on the segmental scale dynamics. Using the scanning confocal microscope technique we located the fluorescent molecules embedded within a solid polymer matrix. Figure 1a depicts a 5x5 μm^2 fluorescence intensity scan of single DiD molecules in a polystyrene thin film. The color scale indicates the polarization of the emitted photons.

Characteristic discrete polarization, on-off behavior and single step photobleaching observed on the scan confirm that the spots on the image correspond to single emitters. Each of the molecules was parked in the laser focus and time-resolved experiments were performed. By using the TCSPC card we obtained the fluorescence decays from which we determined the fluorescence lifetime by fitting a single exponential function to the decays. Examples of decay curves (two snapshots at different time for the same molecule) are presented in Figure 1b. The decays were integrated over 100 ms. In this way we obtained the fluorescence intensity and lifetime time-traces presented in Figure 1c. The time traces usually lasted for 20 to 60 s, and were mainly limited by photobleaching. The accuracy of lifetime determination was on the order of 300 ps. Changes in the lifetime as a function of time for the same molecule are clearly visible. When looking at fluorescence dynamics of dyes placed in geometries that are smaller than the wavelength of the emitted light one should consider the effect of the electromagnetic boundaries (Chapter 6). However, for a single molecule that does not move or rotate with respect to the interfaces, these effects cannot be responsible for large lifetime fluctuations. For each molecule we followed its planar (two polarization channels in the detection path) and out of plane (mean lifetime) orientations, respectively. Based on the constant response in time of these parameters we exclude the possibility that the observed fluctuations are caused by an increased rotational or translational activity of the probe in thinner films at the experimental temperatures (65 and 80 degrees below the bulk glass transition temperature ($T_{g,b}$), respectively) [48].

From the lifetime trajectory of each molecule we built lifetime distributions, which were fitted with a gamma distribution function. From the fitting parameters we determined the effective number of polymer "segments" (N_S) taking part in the rearrangement volume around the single probe using the method described in detail in Chapter 5. N_S determined by this procedure provides direct information concerning local, segmental scale polymer dynamics and its spatial distribution. The value of N_S is very sensitive to small density fluctuations around the probe within the probed time interval. Higher values of N_S can be visualized as a larger collection of polymer segments, which must move cooperatively during segmental relaxation around the probe, therefore indicating slower system dynamics. In Figure 2 we show full N_S histograms as a function of film thickness measured at two temperatures: 22 ºC (left column) and 35 ºC (right column). The histograms were fitted with a Gaussian distribution function. The peak values and the widths of the fitted distributions are presented in Table 1.

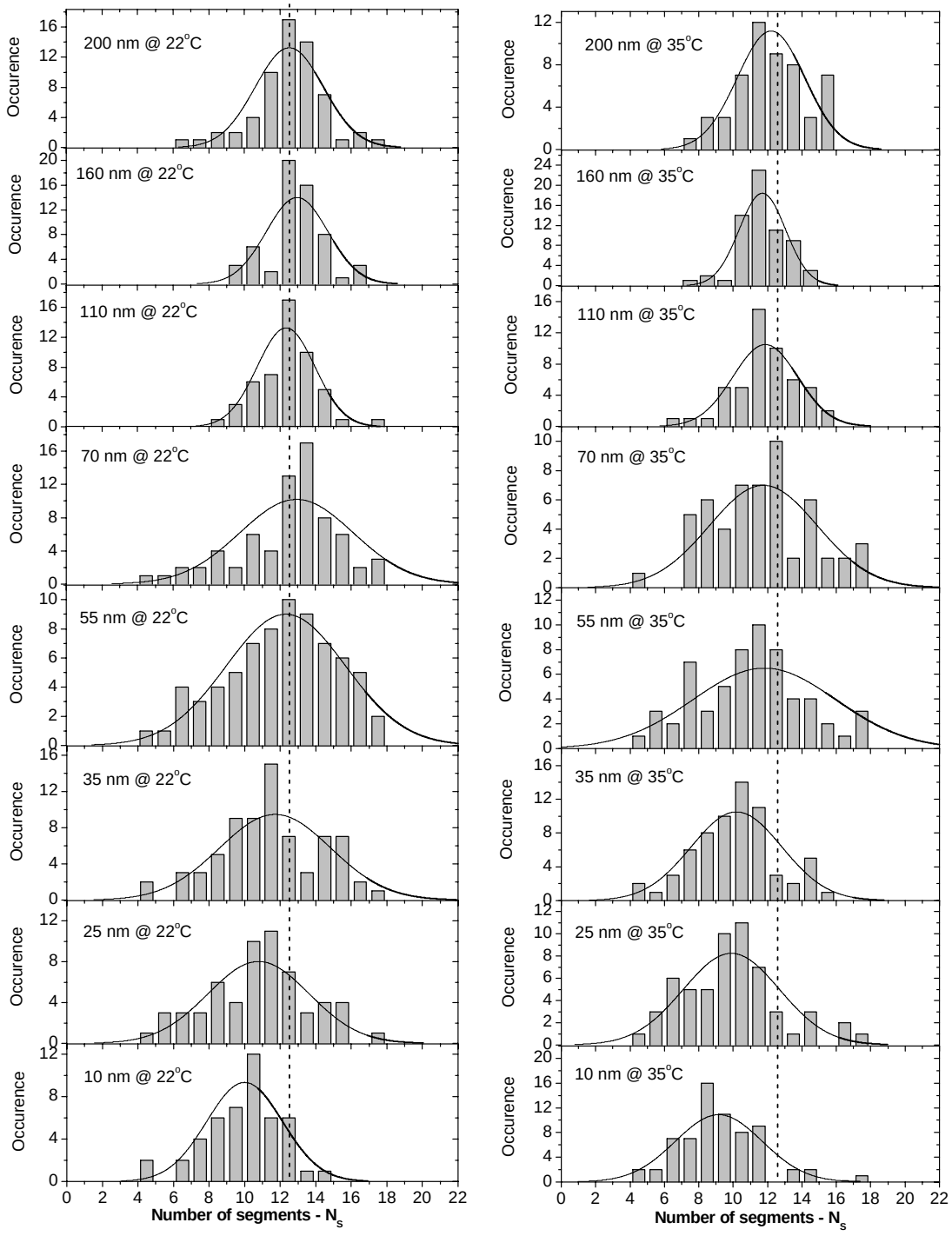

Figure 2. N_S histograms as a function of film thickness measured at two temperatures: 22 ºC (left column) and 35 ºC (right column). The histograms were fitted with a Gaussian distribution function. The peak values and the widths of the distributions were extracted and are presented in Table 1. The dashed line is drawn to guide the eye, centered at $N_S = 12.5$. A clear shift towards lower N_S values for films with a thickness of 55 nm, and below, is observed. Note also the broadening of the distributions for films with a thickness of 70 nm and lower.

Film thickness [nm]	T = 22 ºC		T = 35 ºC	
	N_S	fwhm [N_S]	N_S	fwhm [N_S]
200	12.7 ± 0.4	4.4 ± 0.6	12.0 ± 0.4	4.7 ± 0.6
160	12.9 ± 0.4	4.0 ± 0.4	11.4 ± 0.4	3.3 ± 0.3
110	12.6 ± 0.2	3.5 ± 0.3	11.7 ± 0.2	4.5 ± 0.3
70	13.2 ± 0.6	7.4 ± 1.0	11.9 ± 0.6	7.2 ± 0.7
55	12.6 ± 0.4	7.8 ± 0.7	11.6 ± 0.6	8.4 ± 1,1
35	11.6 ± 0.4	7.3 ± 0.9	10.1 ± 0.4	6.2 ± 0.7
25	11.0 ± 0.8	6.7 ± 0.7	10.0 ± 0.4	6.5 ± 0.7
10	10.1 ± 0.4	4.7 ± 0.6	9.2 ± 0.2	5.7 ± 0.3

Table1. The values of N_S and the full width at half maximum (fwhm) of N_S distributions shown in Figure 2.

7.3.2 The number of segments in the rearrangement cell as a function of film thickness

The peak N_S values as a function of film thickness obtained from the histograms are plotted in Figure 3. For each investigated thickness we observed a decrease of N_S with increasing temperature [44]. The influence of temperature on N_S is consistent with our earlier results, presented in Chapter 5. Such behavior was consistent with a picture of increased fluctuation in the chromophore surroundings, affecting directly the fluorescence lifetime through the modulation of the local dielectric properties. Interestingly, the behavior of N_S as a function of film thickness appears different in two thickness regions. One region can be assigned to film thickness values above a certain threshold value h_0, where N_S remains essentially constant. Below h_0, N_S becomes a function of thickness and decreases with decreasing film thickness. The transition (h_0) between the two regions is estimated to be located at around 60 nm. In Figure 4 we also show the values of the width of the N_S distributions as a function of film thickness. For thicker films, the N_S distributions are relatively narrow, then broaden significantly with decreasing thickness starting from the film with a thickness of 70 nm, and finally the width of the distributions decreases again for the thinnest films. The critical film thickness where a substantial change in the overall behavior of the polymer film is therefore found at around 50 - 70 nm. Our experimental results clearly show that the geometry of a polymer film affects the polymer dynamics on the segmental scale. Several scenarios could explain the observed influence of the film thickness on the segmental scale dynamics. Polymer dewetting processes, reduced degree of entanglement, chain confinement effects, interface effects and chain-end segregation are the ones, which received the most attention. We will discuss each of these possibilities in the paragraphs below.

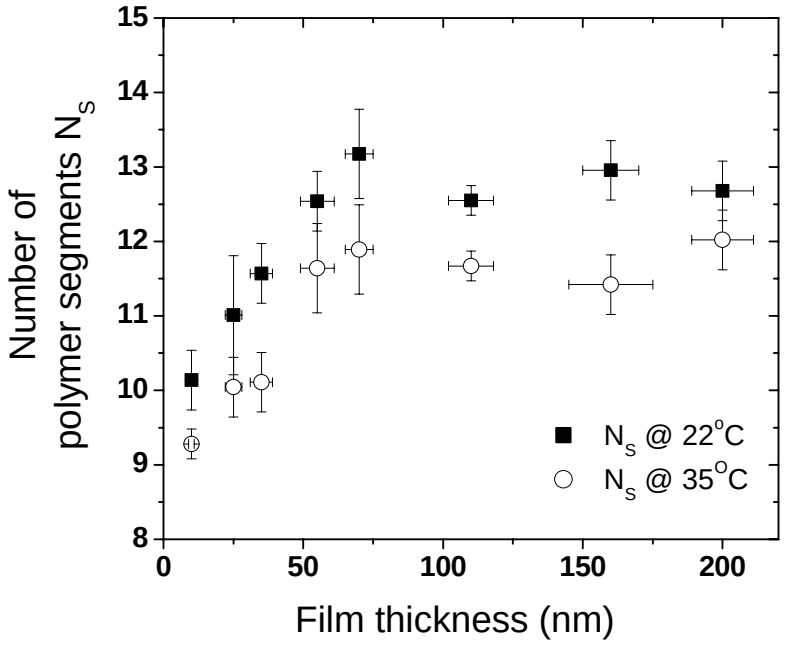

Figure 3. The mean value of the effective number of polymer segments in the rearrangement volume around the single molecule probes as a function of PS film thickness.

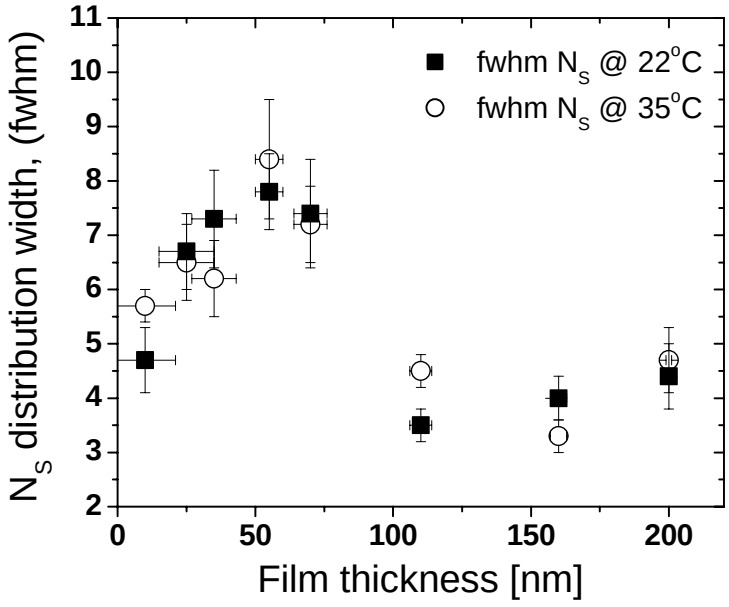

Figure 4. Widths of the N_S distributions as a function of PS film thickness. The N_S widths increase significantly for film thickness below 70 nm. Note the decreased width for the thinnest film indicating that the surface effects propagate into the sample for distances larger than 10 nm.

The dewetting process [49-55] and especially its thickness dependence observed for thin films [56] was the first, strong indication that the thin film geometry may change the polymer properties. Stange et al. [57] using STM and AFM concluded that for a given combination of polymer, solvent and substrate there is a lower limit on the thickness of a continuous film that can be obtained with spin coating. Reiter [58,59] studied dewetting of polystyrene (PS) spin coated on a silicon surface. PS films with thickness values lower than 100 nm, dewetted and broke up when annealed at temperatures even ~ 25 °C below the bulk T_g (~ 100 °C). Reiter has also observed that the dewetting temperature of PS increases with increasing film thickness and with increasing polymer molar mass. To this end we have systematically verified the potential effect of dewetting on N_S behavior observed in this study. We performed a series of AFM investigations of our thin films deposited on glass. Before annealing, we did not observe any visible changes in the thin film morphologies over a period of months, when stored at room temperature. When the films were annealed far above T_g (130 ºC) for more than 24 hours, we indeed observed pinhole formation for the lowest film thickness, characteristic for the dewetting process. However, when annealing at 105 ºC for only several hours, the pinhole formation could not be observed. Moreover, all our films remained stable during our single molecule experiments as was evidenced by additional surface examination after the single molecule experiments had been performed. Therefore we exclude dewetting as a possible cause of the N_S decrease for the thinnest films.

A reduced degree of entanglement can cause a drop of T_g, decreased viscosity and increased diffusion [60,61]. Only a few experiments were performed for thin films to check this effect and quantify its influence on T_g (see Chapter 2). It is believed that the process of spin coating used to prepare polymer films can produce samples with entanglement concentrations that are far below the equilibrium value [62]. The rate of reentanglement is related to the reptation time. In our study we annealed our samples above the glass transition temperature where reptation times are relatively short. Long annealing times ensure also that the chain conformations acquire a bulk statistical value for entanglement density.

For the molar mass of the polymer used here, the average radius of gyration (R_g) of the macromolecules is 9-10 nm assuming a chain conformation as in the theta state, i.e. 6 times smaller than the value of h_0 determined from the N_S plot. Thus, chain confinement found for higher molar mass polymer chains (M_n = 5x10^5 g/mol) [63] is not expected to play a major role in our case.

Polymer dynamics at the interfaces and its influence on the overall thin film dynamics were investigated in detail earlier [64-66]. The polymer substrate interface was found to have a minor effect on polymer mobility in thin polymer films and the substrate's influence on the thin film T_g was usually associated with the strength of interaction between the polymer segments and the substrate [67]. For a system similar to the one used in this study (consisting

of air/polystyrene/glass), it was reported that the polymer/glass interface does not perturb significantly the film dynamics [64]. Additionally, the substrate usually decreases the dynamics of the nearby polymer segments and changes the segmental dynamics only at the distance of a few segments into the bulk region of the film. Thus, we conclude that for our system the substrate effects can be neglected.

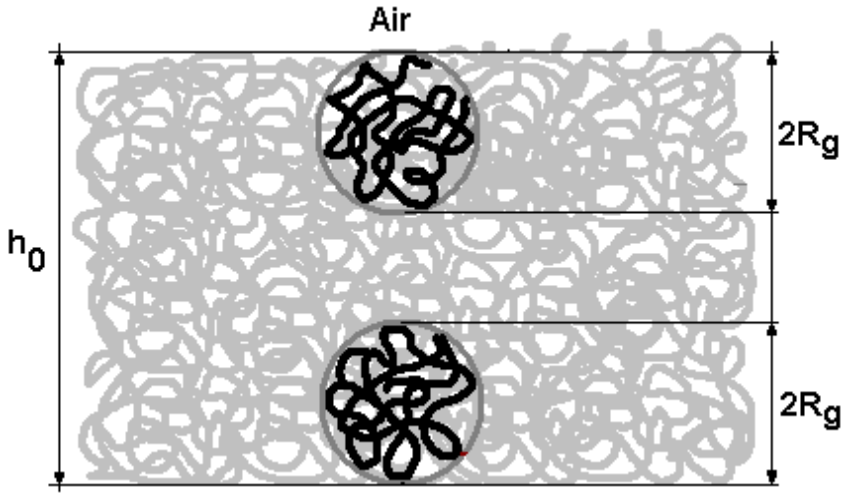

Figure 5. Polymer chains in the geometry of a thin film in relation to R_g=10 nm and h_0=60 nm.

We attribute the decrease of N_S for small film thicknesses to modified polymer dynamics induced by the presence of a free polymer surface [68]. In Figure 5 we show a schematic picture of the polymer chains in the thin film geometry for a thickness of 60 nm and assuming the R_g of the polymer to be 10 nm. Assuming, that the polymer coils are not significantly perturbed at the interfaces, the critical thickness estimated from the N_S drop or from the N_S width increase is the thickness, which is around $6R_g$. Therefore, each of the chains in the film has a neighbor, which is located at one of the interfaces. However, from one side of the sample there is an impenetrable substrate. The widths of the N_S distribution for the thinnest 10 nm films are as narrow as for thicker films (> 60 nm), indicating that segmental scale dynamics throughout the polymer film is more homogeneous. This means that the surface region with enhanced dynamics is larger than 10 nm i.e. is larger than R_g. It also suggests that the transition between surface and bulk dynamics is rather abrupt and not influenced significantly by the sample thickness.

Several reports suggested that the segregation of the chain ends to the polymer/air interface could be responsible for increased surface dynamics [69]. Mayes [70] demonstrated via a simple scaling analysis that chain end localization at the surface can have an enormous impact on the interfacial properties of amorphous polymers. Several authors reported experimental evidence for surface chain-end segregation using neutron reflectivity [71] or

static secondary ion mass spectroscopy (SIMS) [72]. Although the amount of polymer chain ends for a polymer with a molar mass on the order of 10^4 g/mol could not influence the surface dynamics with the magnitude observed in our study, the presence of chain ends at the surface could induce a sliding mechanism for diffusion as introduced by deGennes [73] and influence the dynamics deeper inside the samples. It is important to note that the PS dynamics is modified far below the bulk glass transition temperature ($T_{g,b}$=100 °C as measured by DSC) even though a large fraction of the macromolecules cannot "sense" the possible effect of the interfaces nor are they forced to adopt a different conformation due to the confinement represented by the thin film. Apparently due to the connectivity and interpenetration of polymer chains, surface induced enhancement of polymer dynamics propagates into the sample. The temperature dependence of N_S for PS films yields dN_S/dT= - 0.11 [*segments /deg*] [44] (see Chapter 5), thus the dynamics in the thinnest film is equivalent to the dynamics in thicker films (thickness > h_0) if it was observed at temperatures elevated by as much as 30 °C. Similar depressions of the glass transition temperature for PS on glass (or silicon oxide) were reported in the literature.

7.4 Conclusions

We used the single molecule lifetime fluctuation technique to study the influence of the film thickness on local polymer dynamics on the nanometer length scale at temperatures far below the glass transition temperature. We found modified segmental scale dynamics when the polymer was confined into films with a thickness below 60 nm, corresponding to 6 times the radius of gyration of the polymer used. This behavior was attributed to the influence of the polymer free surface. These effects propagated deep into the polymer sample over distances larger than the radius of gyration. The broadening of the distributions of the N_S parameter proves that the interfacial region with modified polymer dynamics broadens significantly below a critical film thickness pointing towards the existence of different mechanisms for polymer dynamics in thin films, which are not associated with the polymer chain dimensions.

7.5 References

[1] Proceedings of the 3rd International Discussion Meeting on Relaxation in Complex Systems *J. Non-Cryst. Solids* **1998**, *235-237*.

[2] Proceedings of the Second Workshop on Non-Equilibrium Phenomena in Supercooled Fluids, Glasses and Amorphous Materials *J. Phys.: Condens. Matter* **1999**, *11*, 10A.

[3] Donth, E.-J. *Relaxation and thermodynamics in polymers: Glass transition*; Akademie Verlag: Berlin, 1992.

[4] Nieuwenhuizen, Th. M. *J. Phys.: Condens. Matter* **2000**, *12*, 6543.

[5] Angell, C. A. *Science* **1995**, 267, 1924.

[6] de Gennes, P.-G. *Adv. Colloid Interface Sci.* **1987**, *27*, 189.

[7] Edwards, S. F. *Faraday Discuss.* **1994**, *98*, 1.

[8] Aubouy, M. *Phys. Rev. E* **1997**, *56*, 3370.

[9] *Physics of Polymer Surfaces and Interfaces;* Sanchez, I. C., Ed.; Butterworth-Heinemann: Boston, 1992.

[10] Allara, D. L.; Atre, S. V.; Parikh, A. N. In *Polymer Surfaces and Interfaces II*, Feast, W. J., Munrom, H. S., Richards, R. W. Eds.; John Wiley & Sons: Chichester, 1993.

[11] Jones, R. A. L. *Curr. Opin. Colloid. Interface Sci.* **1999**, *4*, 153.

[12] Forrest, J. A.; Dalnoki-Veress, K. *Adv. Colloid Interface Sci*. **2001**, *94*, 167.

[13] Frank, C. W.; Rao, V.; Despotopoulou, M. M.; Pease, R. F. W.; Hinsberg, W. D.; Miller, R. D.; Rabolt J. F. *Science* **1996**, *273*, 912.

[14] Aharoni, S. M. *Polym. Adv. Technol.* **1998**, *9*, 169.

[15] Tanaka, K.; Yoon, J. S.; Takahara, A.; Kajiyama, T. *Macromolecules*, **1995**, *28*, 934.

[16] Dalnoki-Veress, K.; Forrest, J. A.; Stevens, J. R.; Dutcher, J. R. *J. Polym. Sci., Part B: Polym. Phys.* **1996**, *34*, 3017.

[17] Muller-Buschbaum, P.; Stamm, M. *Colloid Polym. Sci.* **2001**, *279*, 376.

[18] Wang, H.; Composto, R. J.; Hobbie, E. K.; Han, C. C. *Langmuir*, **2001**, *17*, 2857.

[19] Kim, J. H.; Jang, J.; Zin, W.-C. *Macromol. Rapid Commun.* **2001**, *22*, 386.

[20] Chao, C. Y.; Lo, C. R.; Wu, P. J.; Pan, T. C.; Veum, M.; Huang, C. C.; Surendranath, V.; Ho, J. T. *Phys. Rev. Lett.* **2002**, *88*, 0855.

[21] Bushan, B. *Handbook of Micro/Nanotribology*; CRC Press: Boca Raton, FL, 1995.

[22] Dorkenoo, D. K.; Pfromm, P. H. *J. Polym. Sci., Part B: Polym. Phys.* **1999**, *37*, 2239.

[23] Dorkenoo, D. K.; Pfromm, P. H. *Macromolecules* **2000**, *33*, 3747.

[24] Dimitriev, O. P. *Synth. Met.* **2001**, *122*, 315.

[25] Liang, T.; Makita, Y.; Kimura, S. *Polymer*, **2001,** *42*, 4867.

[26] Keddie, J. L.; Jones, R. A. L.; Cory, R. A. *Europhys. Lett.* **1994**, *27*, 59.

[27] Forrest, J. A.; Dalnoki-Veress, K.; Dutcher, J. R. *Phys. Rev. E* **1997**, *56*, 5705.

[28] Fukao, K.; Miyamoto, Y. *Phys. Rev. E* **2001**, *64*, No. 011803.

[29] DeMaggio, G. B.; Frieze, W. E.; Gidley, D. W.; Zhu, M.; Hristov, H. A.; Yee, A. F. *Phys. Rev. Lett.* **1997**, *78*, 1524.

[30] Cao, H.; Zhang, R.; Yuang, J. P.; Huang, C. M.; Jean, Y. C.; Suzuki, R.; Ohdaira, T.; Nielsen, B. *J. Phys.: Condens. Matter* **1998**, *10*, 10429.

[31] Zhou, H.; Kim, H. K.; Shi, F. G.; Zhao, B.; Yota, J. *Microelectron. J.* **2002**, *33*, 221.

[32] Hsu, D. T.; Kim, H. K.; Shi, F. G.; Zhao, B.; Brongo, M.; Schilling, P.; Wang, S. Q. Proceedings of the SPIE Conference on Multilevel Interconnect Technology III 1999, 3883, 60.

[33] Kim, H. K.; Shi, F. G. *J. Mater. Sci.: Mater. El.* **2001**, *12*, 361.

[34] Zhang, Z.; Zhao, M.; Jiang, Q. *Physica B* **2001**, *293*, 232.

[35] Jackson, C. L.; McKenna, G. B. *Chem. Mater.* **1996**, *8*, 2128.

[36] Jiang, Q.; Shi, H. X.; Li, J. C. *Thin Solid Films* **1999**, *354*, 283.

[37] Shalaev, E. Y.; Steponkus, P. L. *Langmuir* **2001**, *17*, 5137.

[38] Fox, K. C. *Science* **1995**, *267*, 1923.

[39] Fisher, M. E.; Barber, M. N. *Phys. Rev. Lett.* **1972**, *28*, 1516.

[40] Despotopoulou, M. M.; Frank, C. W.; Miller, R. D.; Rabolt, J. F. *Macromolecules* **1996,** *29*, 5797.

[41] Dickson, R. M.; Norris, D. J.; Tzeng, Y. L.; Moerner, W. E. *Science* **1996**, *274*, 966.

[42] Deschenes, L. A.; Vanden Bout D. A. *Science* **2001**, *292*, 255.

[43] Bardo, A. M.; Collinson, M. M.; Higgins, D. A. *Chem. Mater.* **2001**, *13*, 2713.

[44] Vallée, R. A. L.; Tomczak, N.; Kuipers, L.; Vancso, G. J.; van Hulst, N. F. *Phys. Rev. Lett*. **2003**, *91*, 038301.

[45] Hall, D. B.; Underhill, P.; Torkelson, J. M. *Polym. Eng. Sci.* **1998**, *38*, 2039.

[46] Lobo, R. F. M.; Pereira-da-Silva, M. A.; Raposo, M.; Faria, R. M.; Oliveira, O. N., Jr. *Nanotechnology*, **1999**, *10*, 389.

[47] Ton-That, C.; Shard, A. G.; Bradley, R. H. *Langmuir* **2000**, 1*6,* 2281.

[48] Vallée, R. A. L.; Tomczak, N.; Gersen, H.; van Dijk, E. M. H. P.; García Parajó, M. F.; Vancso, G. J.; van Hulst, N. F. *Chem. Phys. Lett.* **2001**, *348*, 161.

[49] de Gennes, P. G. *Rev. Mod. Phys.* **1985,** *57*, 827.

[50] Muller-Buschbaum, P.; Vanhoorne, P.; Scheumann, V.; Stamm, M. *Europhys. Lett.* **1997**, *40*, 655.

[51] Muller-Buschbaum, P.; Gutmann, J. S.; Cubitt, R.; Stamm, M. *Colloid Polym. Sci.* **1999**, *277*, 1193.

[52] Muller-Buschbaum, P.; Gutmann, J. S.; Stamm, M. *Phys. Chem. Chem. Phys*. **1999**, *1*, 3857.

[53] Tolan, M.; Seeck, O. H.; Schlomka, J.-P.; Press, W.; Wang, J.; Sinha, S. K.; Li, Z.; Rafailovich, M. H.; Sokolov, J. *Phys. Rev. Lett.* **1998**, *81*, 2731.

[54] Redon, C.; Brochard-Wyart, F.; Rondolez, F. *Phys. Rev. Lett.* **1991**, *66*, 715,

[55] Tidswell, I. M.; Rabedeau, T. A.; Pershan, P. S.; Kasowsky., S. D. *Phys. Rev. Lett.* **1991**, *66*, 2108.

[56] Wang, C.; Krausch, G.; Geoghegan, M. *Langmuir* **2001**, *17*, 6269.

[57] Stange, T. G.; Mathew, R.; Evans, D. F. *Langmuir* **1992**, *8*, 920,

[58] Reiter, G. *Phys. Rev. Lett.* **1992**, *68*, 75.

[59] Reiter, G. *Europhys. Lett.* **1993**, *23*, 579.

[60] Silberberg, A. J. *Colloid Interface Sci.* **1982**, *90*, 86.

[61] Silberberg, A. J. *Colloid Interface Sci.* **1988**, *125*, 14.

[62] Sauer, B. B.; Walsh, D. J. *Macromolecules* **1994**, *27*, 432.

[63] Mattson, J.; Forrest, J. A.; Borjesson, L. *Phys. Rev. E* **2000**, *62*, 5187.

[64] Keddie, J. L.; Jones, R. A. L.; Cory, R. A. *Faraday Discuss.* **1995**, *98*, 219.

[65] Sharp, J. S.; Forrest, J. A. *Phys. Rev. Lett.* **2003**, *91*, 235701.

[66] Baschnagel, J.;.Binder, K. *Macromolecules* **1995**, *28*, 6808.

[67] van Zanten, J. H.; Wallace, W. E.; Wu, W. *Phys. Rev. E* **1996,** *53*, R2053.

[68] Mansfield, K. F.; Theodorou, D. N. *Macromolecules* **1991**, *24*, 6283.

[69] Kumar, S. K.; Vacatello, M.; Yoon, D. Y. *J. Chem. Phys.* **1988,** *89*, 5206.

[70] Mayes, A. M. *Macromolecules* **1994**, *27*, 3114.

[71] Zhao, W.; Zhao, X.; Rafailovich, M. H.; Sokolov, J.; Composto, R. J.; Smith, S. D.; Satkowski, M.; Russell, T. P.; Dozier, W. D.; Mansfield, T. *Macromolecules* **1993**, *26*, 561.

[72] Affrossman, S.; Hartshorne, M.; Jerome, R.; Pethrick, R. A.; Petitjean, S.; Rei Villar, M. *Macromolecules* **1993**, *26*, 6251.

[73] de Gennes, P. G. *Eur. Phys. J. E* **2000**, *2*, 201.

Chapter 8

Single light emitters in electrospun nanofibers

Fluorescent 1,1',3,3,3',3'-haxamethylindodicarbocyanine ($DiIC_1(5)$) molecules and CdSe/ZnS core-shell semiconductor nanoparticles have been embedded into poly(ethylene oxide) (PEO) and poly(methyl methacrylate) (PMMA) electrospun fibers at various concentrations, down to the single molecule level. The fibers have been characterized by using scanning confocal and wide-field fluorescence microscopies. The mean fluorescence lifetime of single $DiIC_1(5)$ molecules embedded in PMMA fibers appeared independent on the fiber diameter, yet when the diameter of the fibers was below 500 nm, a significant broadening of the fluorescence lifetime distributions was found. Possible explanations for the broadening are discussed.

Polymer fibers with a bead-on-a-string morphology have been prepared and investigated. $DiIC_1(5)$ molecules in PEO beads are observed mainly at the bead edges, probably due to the exclusion of the chromophores from the PEO crystalline phase during crystallization following the spinning process. Polarized emission of $DiIC_1(5)$ molecules from PEO beads suggests that the emitters acquire a well-defined orientation within the beads. Fluorescence lifetime studies showed that $DiIC_1(5)$ molecules in PEO beads decay faster when located at the bead edges compared to the straight parts of the fibers. In contrast, the decay rate of $DiIC_1(5)$ at the edges of a PMMA bead is found to be slower when compared to the bead center. Influence of the fiber geometry on the fluorescence emission of embedded molecules and its potential application in radiative decay engineering are discussed.

8.1 Introduction

Electrospinning of polymer solutions (and melts) is a versatile technique used to fabricate polymer fibers with diameter ranging from tens of nanometers to several micrometers [1-9]. Electrospinning of various amorphous or semi-crystalline polymers [10], polymer blends [11,12] or block copolymers [13] have been reported. Recent advances in electrospinning allowed one to perform controlled co-spinning of coaxial nanofibers made of two different materials [14,15]. Due to low-cost instrumentation combined with inherent high surface to volume ratios of the structures obtained, electrospun fibers find applications in drug delivery [16-18], membranes [19], electronics [11,20], chemical sensors [21-23], photovoltaics [25], composite materials [9,26-28], and medicine [29,30].

Preparation of micro- and nanoscale materials, made of polymers, for photonic applications is an ever-growing field of research [31-33]. Simultaneously, there is a strong interest in studying the behavior of light in wavelength-scale structures. It was shown in Chapter 6, that relatively simple thin film geometry already modifies substantially the behavior of light emitters embedded in the films. In principle, one can engineer polymer structures, where surface to volume ratios are much higher than in thin films and where the confinement of light occur in more than just one dimension. Electrospinning offers the possibility to obtain fibers with diameters ranging from $\lambda/60$ to 10λ, λ being the wavelength of light. An additional level of complexity can be introduced into the fibers by a careful control of the spinning conditions. One can obtain new fiber morphologies such as the bead-on-a-string morphology [34], where a number of dielectric spheres with diameters in the micrometer range, placed in regular distances, are connected to each other by a thin polymer dielectric fiber. Although optical properties of dielectric thin films, dielectric spheres or shells are being studied extensively, the photonic properties of dielectric cylinders remain relatively unexplored.

Even though the range of applications of electrospun fibers is steadily growing, still little is known about the fiber structure and mechanical or thermal properties [2,35-39]. For example, for photonic applications, it is important to know the effects the electrospinning has on the resulting polymer chain anisotropy. Such artificially induced anisotropies might change the properties and structure of the crystalline phase of the polymer (for a semicrystalline polymer), which subsequently will influence the optical properties of the embedded emitters. Simultaneously mechanical properties e.g. the Young modulus will also be affected and limit the number of possible end-product applications. Additionally to the changes induced in structure, the presence of large surface to volume ratios of nanoscale fibers will influence changes in thermal properties similarly to those found for thin polymer films (see Chapter 7) [40].

To carefully investigate the properties of electrospun fibers one needs to prepare defect free samples with narrow distributions of the fiber diameter. This, however, still remains a challenge for the electrospinning technique.

Single-molecule detection (SMD) and spectroscopy methods (for review see references [41-45]) offer the unique possibility to investigate matter at the nanoscale with the simultaneous ability to resolve the ensemble averages [46-49]. Therefore one can avoid the polydispersity problem and study the samples at the single fiber level. Additionally, multiparameter microscopy (e.g. combination of molecular orientation, spectral properties and fluorescence lifetime) allows one to decipher complex systems and to acquire information about the role of many parameters simultaneously [50].

Single molecule level studies presented in this chapter are the first steps towards probing the structure and dynamics of polymer fibers with simultaneous investigations of the resulting fiber optical properties. First, we show how electrospinning is used to prepare luminescent micro- and nanofibers. Fluorescent molecules and luminescent semiconductor nanoparticles (quantum dots) are embedded into polymer fibers with diameters ranging from 50 nm to several microns and investigated at the single molecule level. Later, we show that the fiber diameter influences the single molecule fluorescence lifetime distributions of the embedded chromophores. Finally, we obtain the bead-on-a-string morphology of the fibers and show that single molecule investigation can simultaneously give information on both the structure and optical properties of the polymer beads. Throughout the chapter we discuss the potential of electrospun fibers in radiative decay engineering and photonics applications.

8.2 Experimental section

8.2.1 Materials and sample preparation

As a substrate in electrospinning circularly shaped glass cover slides (used in microscopy) were employed. These slides (Φ = 20 mm, Fisher Scientific) were cleaned using a Piranha solution (mixture of 1:4 of 30% H_2O_2 and concentrated H_2SO_4), rinsed with Milli-Q water and ethanol, and finally dried in a stream of nitrogen gas. Samples of luminescent polymer fibers were prepared by electrospinning polymer solutions containing 1,1',3,3,3',3'-haxamethylindodicarbocyanine ($DiIC_1(5)$) molecules (Molecular Probes, D-307) or CdSe/ZnS core-shell semiconductor nanoparticles (source and characteristics of the nanoparticles can be found in [51,52]) directly onto glass cover slides. The polymers used were poly(methyl methacrylate) (PMMA, amorphous) and poly(ethylene oxide) (PEO. semicrystalline).

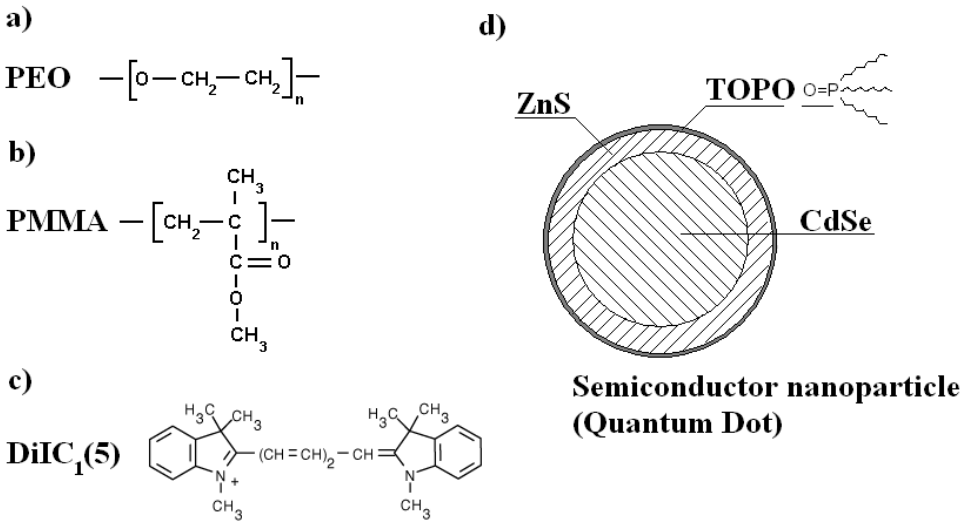

Figure 1. Chemical structures of polymers: poly(ethylene oxide) (a) poly(methyl methacrylate) (b) and probes: $DiIC_1(5)$ (c) and CdSe/ZnS quantum dot (d) used in this chapter. The quantum dot was shown schematically as spherical, although in reality quantum dots are crystalline, facetted and more irregular.

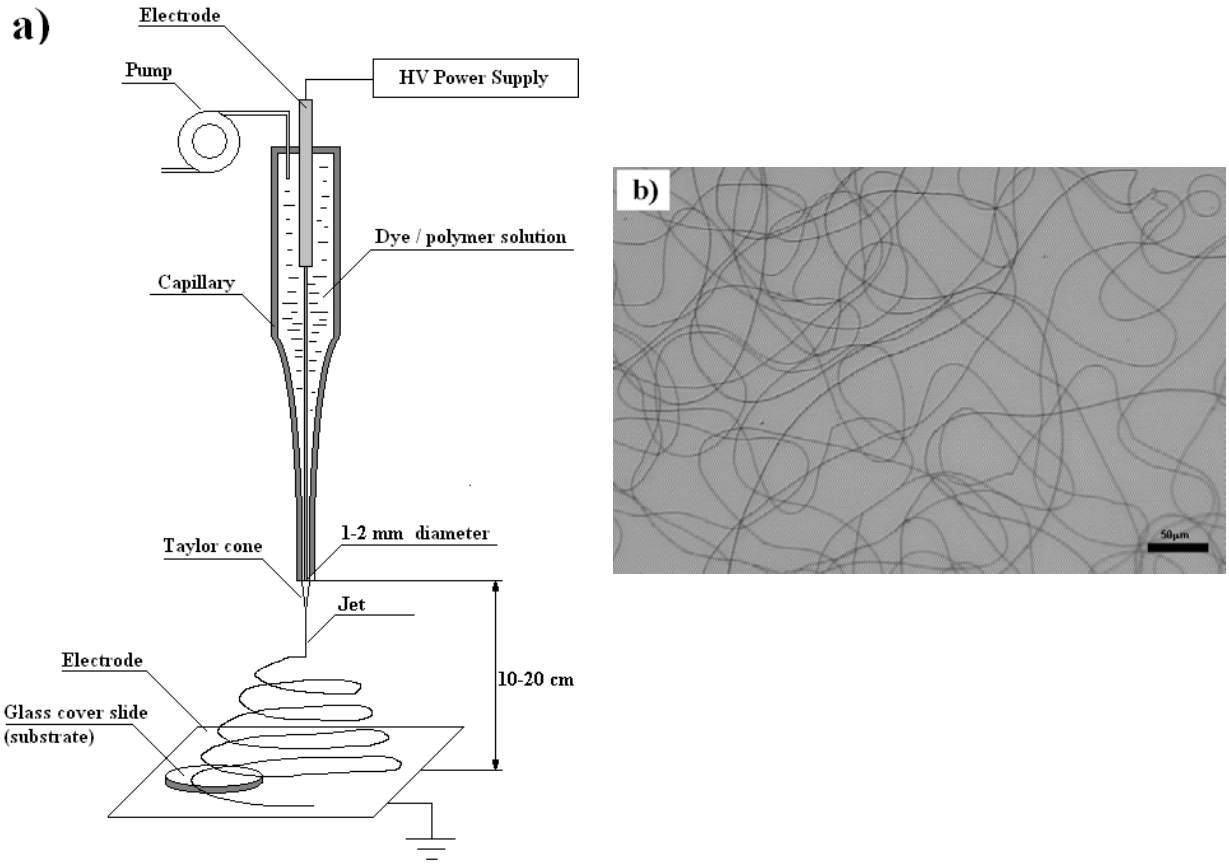

Figure 2. a) Scheme of the electrospinning setup. b) Optical micrograph of electrospun PEO fibers deposited on a glass cover slide. The fibers have a diameter of approximately 2-3 μm. The scale bar is 50 μm.

The electrospinning device (see Figure 2a) consists of a capillary that includes a wire electrode, a grounded counter electrode placed at a well-defined distance from the capillary and a high voltage source. Constant pressure inside the capillary is obtained by a pump. The potential between the electrodes is adjusted with a high-voltage power supply. More details about the electrospinning method and the electrospinning device used in this study can be found elsewhere [5][9]. For efficient collection, the cover slides were placed on the lower electrode, off-axis with respect to the capillary. The amount of the fibers deposited on the cover slides was controlled by the spinning time. The total amount of the fibers on the slides was kept low to ensure that the fibers are laying flat onto the substrate. The diameter and morphology of the obtained fibers was tuned by the concentration of the polymer in the spun solutions, by the applied voltage between the electrodes, and by the distance between the electrodes.

8.2.2 Atomic Force Microscopy

A NanoScope IIIa (Veeco, Digital Instruments, Santa Barbara, USA) Atomic Force Microscope (AFM) was used to determine the height of the electrospun fibers. The AFM was operated in the tapping mode using a cantilever with a nominal spring constant of 40-60 N/m. The images were plane-fitted before analysis and the diameter was calculated from the height of flat-laying fiber assuming a cylindrical cross-section.

8.2.3 Scanning Confocal Microscopy

A picosecond-pulsed dye lasers (635 nm, PicoQuant, 800-B, 100mW. 476 nm, PicoQuant, 800-B, 80 MHz repetition rate) or a CW Ar^+/Kr^+ ion laser (Spectra Physics, Beamlok 2060) at a wavelength of 514 nm were used for excitation and time-resolved experiments. The excitation light was made circularly polarized by a ¼λ plate and focused onto the sample to a diffraction-limited spot using a high NA oil objective (Olympus, NA=1.4, 100x). To separate the fluorescence emission from the excitation, suitable dichroic mirrors, emission, and excitation filters, were used. Fluorescence photons were collected by the same objective and split into two paths. The first path went to two avalanche photodetectors (SPCM-AQ-14, EG&G Electro Optics) placed after a polarization beam splitter (splitting into two orthogonal components). The fluorescence photons in the second path were directed to a prism and dispersed on a cooled CCD camera. A custom-built piezo-scan table with an active x-y feedback loop mounted on a commercial optical microscope (Zeiss Axiovert inverted microscope) was used. The sample was scanned through the focus of the excitation spot at a pixel frequency of 1kHz, producing two-dimensional (256x256 pixels) fluorescence intensity images (including two independent polarization channels, when required). For time resolved

experiments the detected fluorescence signal was fed into a time-correlated single photon counting card. The fluorescence spectra were obtained by integrating the arriving photons over the period of 1s. Custom LabView software was used to control the scanning process, for data acquisition and to synchronize the CCD camera with the TCSPC card. The experiments were performed in air under ambient conditions (22+/- 2 degrees). Bright field images were obtained by placing an intense light source directly above the sample and using an additional CCD camera placed onto one of the ports of the confocal microscope. The data acquisition was performed with the help of a commercial software (Hauppauge WinTV2000).

8.2.4 Wide-Field Microscope

Light from a CW HeNe laser at a wavelength of 632 nm was used for excitation. A circularly polarized laser beam passed through a beam expander and was focused onto the back aperture of a high NA objective (Zeiss, NA= 1.4, oil immersion). The fluorescence photons emitted from the illuminated area were collected by the same objective and after passing through emission filters were split into two orthogonal polarization channels using a Wollaston prism (Linos 037808) and subsequently imaged with a 500 mm lens (Linos 063827) onto an intensified charged coupled device (CCD camera, Pentamax Gen IV). The data acquisition rate was set to 100ms/frame. The images from the camera were processed by custom LabView software. Simultaneous intensity and polarization information was obtained from each pixel on the acquired frames. More information about the experimental setup can be found in Chapter 4.

8.2.5 Bright field imaging

Bright field images were obtained using an Olympus BX 60 light microscope, or by placing an intense light source above the samples and collecting the transmitted light using a CCD camera placed on one of the ports of the confocal microscope or using the CCD camera in the wide-field setup.

8.3 Results and discussion

8.3.1 Electrospun luminescent fibers

In electrospinning, when a potential is applied between two electrodes, the liquid droplet suspended at the end of the capillary thins and forms the so-called "Taylor cone" [8]. By increasing the potential further, the surface tension of the liquid is being overcome and the liquid is ejected towards the counter electrode. By placing an additional substrate in the way of the ejected fibers they can be collected for use and further analysis (Figure 2b). The diameter of the resulting fibers depends on a number of parameters; the most important parameters are solution viscosity, surface tension, applied voltage and the distance between the electrodes [5]. We have incorporated $DiIC_1(5)$ chromophores into fibers made of PEO (semicrystalline) and PMMA (amorphous) by mixing the components prior to spinning. Figure 3a shows a 10x10 μm^2 fluorescence intensity scan of luminescent $DiIC_1(5)$/PEO fibers. The spinning time was used to control the amount of the deposited fibers, down to the level, where the fibers where laying flat on the substrate and did not cross each other on the length scale of several micrometers. Luminescent fibers with diameters ranging from 50 nm to 2μm (as measured with Atomic Force Microscope; not shown here) were prepared. Figure 3a also shows that the fluorescent molecules are rather uniformly and homogeneously distributed within and along the fibers. Fluorescence spectra taken from individual fibers confirm that the optical signal comes from the $DiIC_1(5)$ molecules (Figure 3b). A small red shift of the emission of about 10 nm when compared to a bulk solution is observed and attributed to the different dielectric properties (solvent versus polymer) of the surroundings. We will investigate in more details the effects that a dielectric cylindrical structure has on the excited state lifetime of the chromophores later in this chapter. The most important point here is to show that the electrospinning technique offers a unique possibility to prepare fibrous dielectric structures which can incorporate additional functionality such as light sources.

Semiconductor nanoparticles - quantum dots (QD) – are another class of light sources [51,52], which can be use to obtain luminescent nanofibers. Investigation of optical properties of semiconductor nanoparticles at both the ensemble and single-molecule levels is a very active field of research at present. Quantum dots are particularly interesting as light emitters because of their size tunable optical properties, narrow emission lines and low photobleaching rates that make them an attractive choice as luminescent chromophores for optoelectronics [53], laser applications [54], biological encoding or as probes for biotechnological applications [55-58].

We have embedded CdSe/ZnS core-shell semiconductor nanoparticles (Figure 1d) into electrospun fibers made of PEO and PMMA. There were only two reports to date about embedding nanoparticles [25,59] into electrospun fibers and we are the first to report embedding of QDs into such structures. Embedding nanoparticles into the fibers was done the same way as for organic chromophores. Hybrid polymer/quantum dot luminescent fibers were prepared by mixing the nanoparticles with the polymer solution prior to ectrospinning. Figure 4a shows a PEO/QD composite fiber with a high concentration (10^{-5} M) of the quantum dots. The QDs are uniformly and homogeneously distributed over the length and width of the fiber. Fluctuations in the QD emission intensity visible on the scan are due to frequent blinking of the quantum dots [60,61]. By decreasing the QD concentration in the initial spinning solution (10^{-9} M) we decreased the amount of the nanoparticles in the fibers to the level, such that single nanoparticles were separated in the fibers (Figure 4b). In Figure 4b the dashed lines represent the fiber boundaries as estimated from the bright field images (1.2 μm fiber).

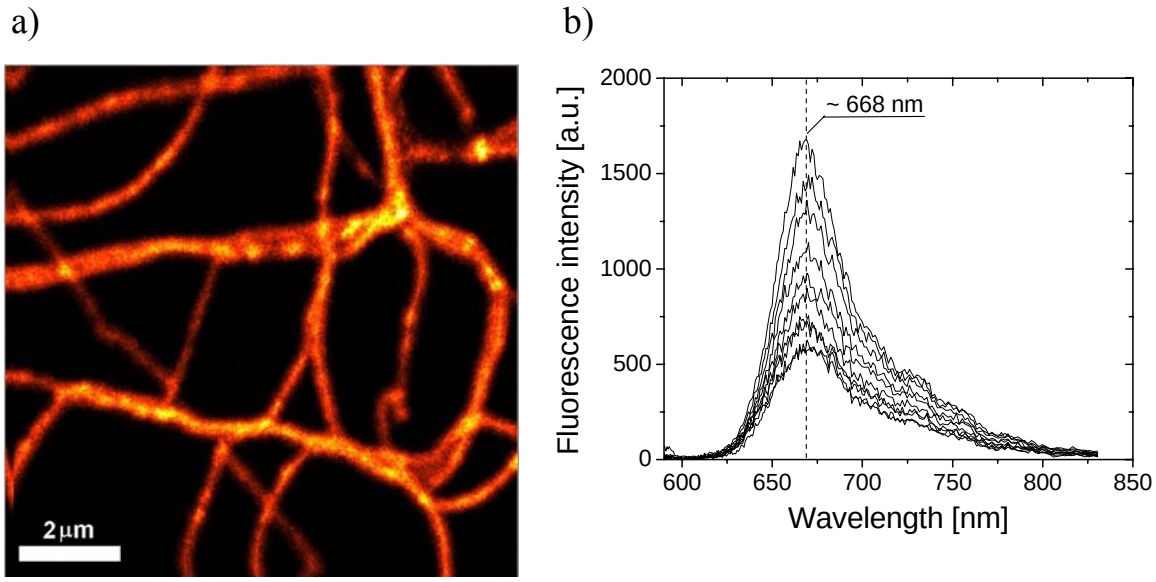

Figure 3. a) 10x10 μm^2 scanning confocal microscope fluorescence intensity scan of $DiIC_1(5)$ molecules (10^{-3} M) embedded in PEO fibers. The molecules are uniformly distributed within and along the fibers. The variations in the intensity are mainly caused by the presence of the fibers at different heights with respect to the focal plane. b) Fluorescence spectra of $DiIC_1(5)$ taken from individual fibers. The emission peak at ~668 nm is redshifted by 10 nm with respect to the bulk solution spectrum.

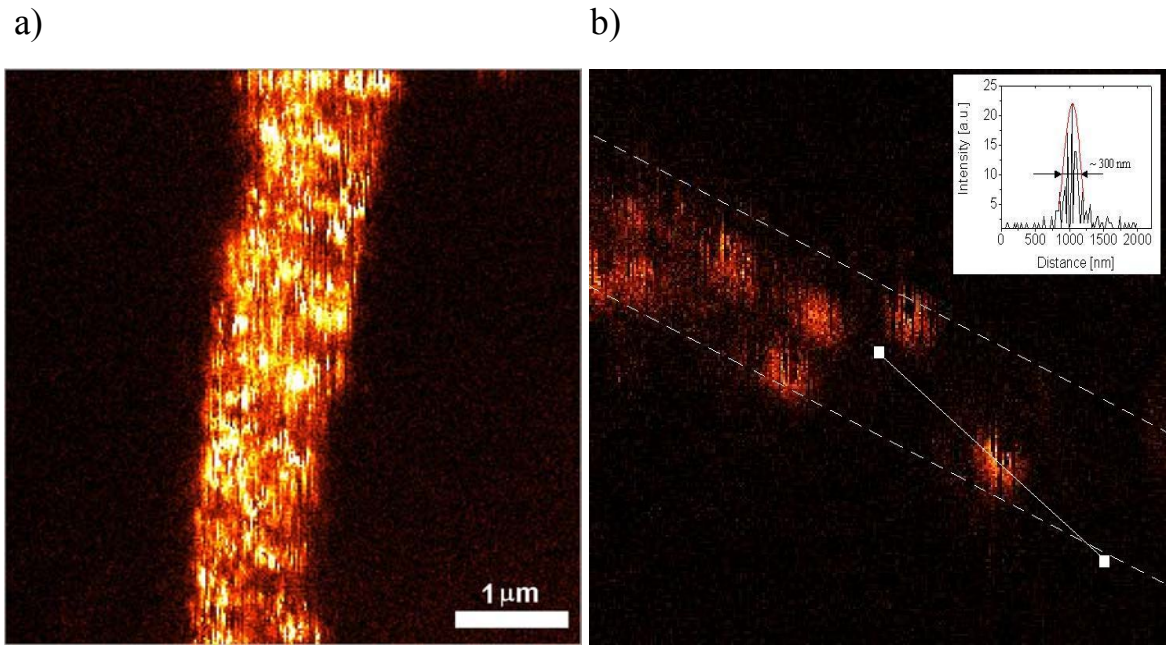

Figure 4. a) 5x5 µm^2 fluorescence intensity scan of CdSe/ZnS quantum dots embedded in an electrospun PEO fiber. The fiber diameter is ~ 1 µm. Intensity changes along the fast scanning direction (vertical) caused by changes in the emission rate of the QDs are visible. b) 5x5 µm^2 fluorescence intensity scan of QDs embedded in an electrospun 1.2 µm PMMA fiber. The dashed white lines correspond to the fiber boundaries estimated from a bright field image of the same fiber at the same location. Inset: intensity cross-section (indicated on the scan with a white line) through a single spot. Frequent excursions to the background level (blinking) on the millisecond timescale are clearly visible on the fluorescence scan indicating that the spots are single quantum dots. The full width at half maximum of the QD emission envelope (inset) is smaller than 300 nm. From the image the QD concentration in the fibers is estimated to be 10^{-9} M.

The full-width at half-maximum of the intensity cross-section through an isolated fluorescence spot (inset of Figure 4b) was equal to ~300 nm, slightly larger than expected for a diffraction limited spot of ~ 220 nm when imaged with a 1.4 NA objective. The reason for the broadening can be the size of the focus of the excitation light during imaging.

In Figure 5a we show intensity and simultaneously acquired spectral time-traces obtained by dispersing the emitted photons over a cooled CCD camera after passing through a prism. The excitation wavelength was 514 nm, and the integration time used was 1s. The emission peaks are located around 600 nm at the same wavelength as obtained from a bulk solution of QD in chloroform (Figure 5b). Compared with the solution spectrum the full width at half maximum (between arrows) of the emission peak for a single QD is equal to 22 nm and is 78 % of that found in a chloroform solution. The narrower emission spectrum of single QDs within the fibers is probably due to the size polydispersity of the QDs causing the solution spectrum to look broader [62]. The finding that no wavelength shift is observed for the emission spectrum maximum of a QD as compared to the spectrum in solution, underline the different way the

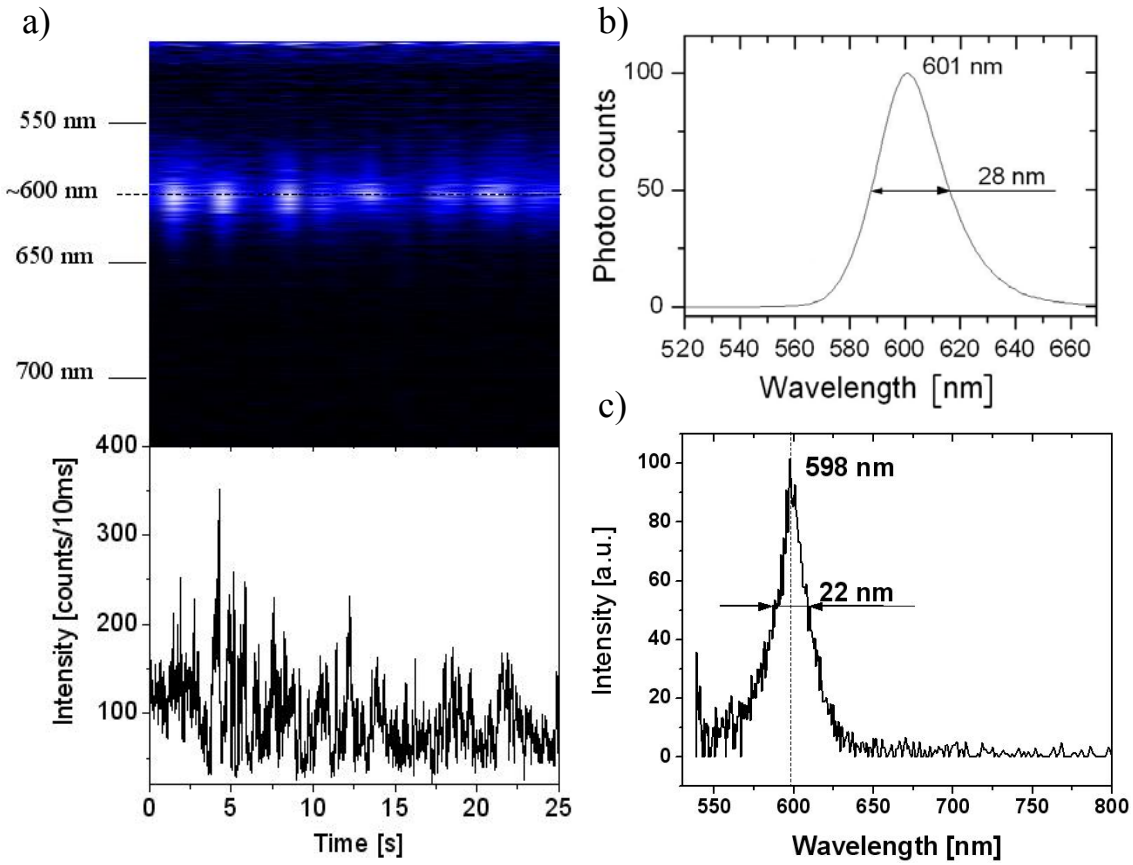

Figure 5. a) Spectral and intensity time-traces of a single QD embedded in a 1.3 μm PEO electrospun fiber. Intensity changes on the time scale of seconds are clearly visible. b) Luminescence spectrum of a bulk QD solution in chloroform. c) One of the fluorescence emission spectra taken from the time-trace presented in a). The excitation wavelength was 514 nm. The full width at half maximum (between arrows) of the emission remains narrow after embedding the nanoparticles into the fibers and is equal to 22nm. No substantial shifts of the maximum emission wavelength are present.

organic chromophores and QDs are sensitive to the changes in the properties of their environments. Organic fluorescent molecules are primarily affected by the chemistry and structure of the surroundings [63-65]. The structure of the QDs together with a "shielding" effect of the ligands (TOPO) (Figure 1d) present at the QD surface makes them rather immune to the chemistry of the environment and only sensitive to the more global dielectric properties. It was suggested that the QDs emission properties are highly sensitive to the QD surface chemistry and to the chemistry at the ligand/ZnS interface [66,67]. On the other hand, it was also shown that for CdSe quantum dots the spontaneous emission rate dependence on the dielectric constant follows the microscopic model [68], thus the decay rate is mainly influenced by the interaction of the large excitonic electric dipole with the dipoles of the surrounding dielectric [69]. Quantum dots are therefore a good candidate for the use as molecular probes whenever one wishes that the chemistry and structure of the material does

not influence the probes simultaneously. It would be of interest to investigate, in the future, whether QDs can be used as probes of e.g. the degree of crystallinity in the surrounding polymer matrix.

As demonstrated here, the technology to introduce single light emitters into nanoscale dielectric fibers is readily available. The versatility of the electrospinning process allows one to obtain fibers were both the polymer and the light emitter can be varied, therefore allowing for number of interesting applications e.g. as sensor devices or in photovoltaics.

The electrospun polymer fibers with embedded light emitters can find application also in photonics. For example, fibers described in this Chapter can be applied as single-mode waveguides [70]. For fibers, a lower limit for the diameter (D), for which the structure will function as a waveguide exists [71]:

$$D > \frac{2.4\lambda}{(n_1^2 - n_0^2)^{0.5}\pi}, \qquad (1)$$

where, λ is the wavelength of light, n_1 and n_0 are the refractive indices of the fiber and the surrounding medium respectively. For emission around λ=600nm (as in the case of quantum dots in this Chapter) the calculated value of D is equal to 470 nm (n_0=1 (air) and n_1=1.48 (for PMMA)). In principle, electrospinning is able to deliver fibers with diameters from 10 nm to several microns, therefore crossing the guiding/nonguiding length scale for a combination of different light sources and polymer materials. Spinning polymeric materials with higher dielectric constants would allow to decrease the critical fiber diameter. When thinking about a hypothetical device, smaller fiber diameters would allow the density of the structures per unit area to be higher. Internal, stable light sources naturally overcome light coupling problems. For a number of applications QDs would be advantageous over organic chromophores due to their stability or tunability. Additionally, photon generation can be achieved through electron injection into QDs. Electrospun polymer fibers are thus a promising candidate for advanced photonic technologies.

8.3.2 Fluorescence lifetime of single $DiIC_1(5)$ embedded in electrospun PMMA fibers

Having developed a method to obtain polymer fibers with embedded chromophores we move towards more detailed investigations of the optical properties of the obtained structures. One of the applications of the electrospun fiber is in radiative decay engineering, where the emission rates of light emitters are controlled through a carefully structured environment.

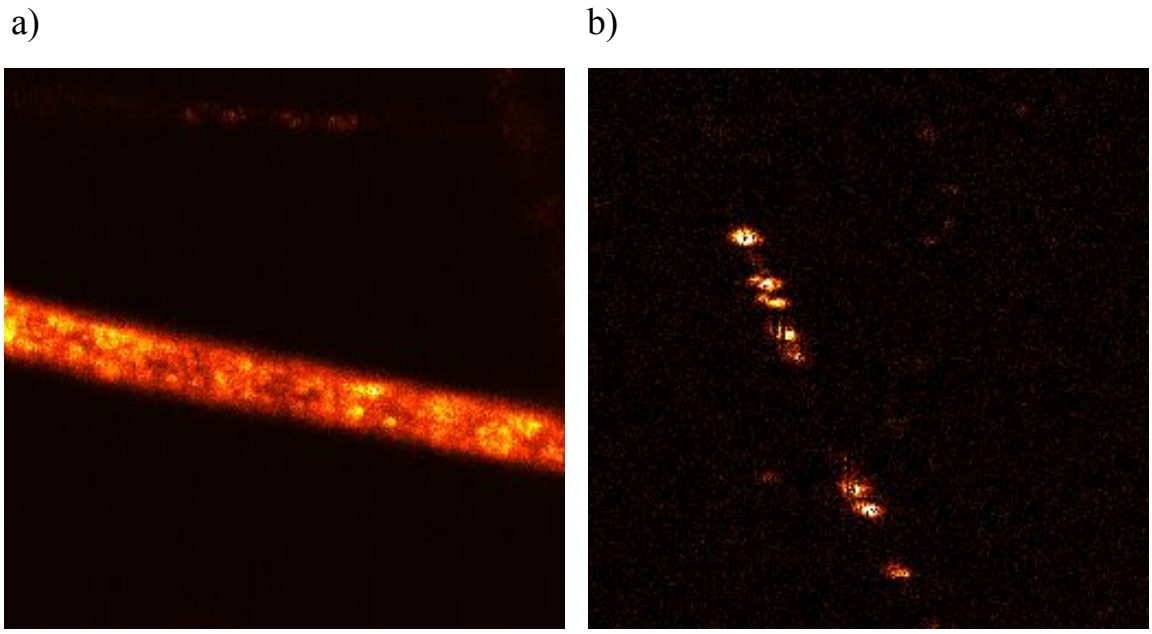

Figure 6. 10 x 10μm^2 fluorescence intensity scans of $DiIC_1(5)$ molecules embedded in PMMA fibers at 10^{-3} M (a) and 10^{-11} M (b) concentrations. Blinking and one-step photobleaching of the molecules visible in (b) confirm single molecule behavior.

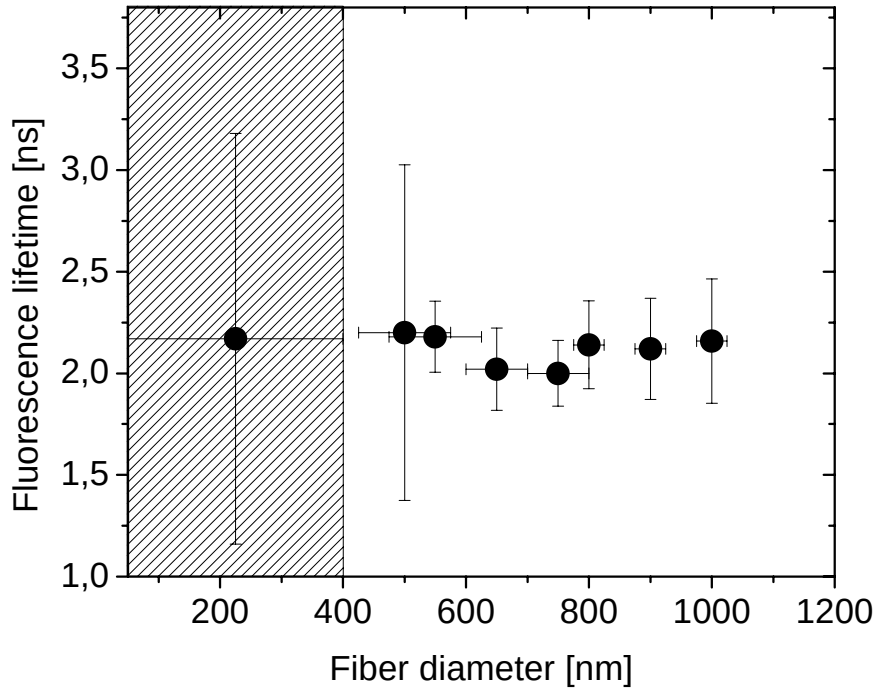

Figure 7. Fluorescence lifetime of $DiIC_1(5)$ molecules embedded in electrospun PMMA fibers as a function of fiber diameter. The vertical bars represent the widths of single molecule τ_F distributions. The shaded area indicates the region, where the data was grouped for all fiber diameters below ~400 nm.

In Chapter 6 we have shown that already a relatively simple geometry of thin films can substantially change the fluorescence lifetime of single chromophores. Here, we report on the investigation of the fluorescence lifetime of single molecules as a function of the fiber diameter. $DiIC_1(5)$ molecules were successfully incorporated into fibers made of amorphous PMMA (Figure 6a). By decreasing the concentration of the chromophores in the initial spinning solution, observations at single molecule levels were achieved (10^{-11} M) (Figure 6b). Frequent blinking of the fluorescence signal and one-step photobleaching are confirmations of single molecule behavior [72-74]. Such single, spatially separated molecules were used in further investigations. By parking the molecules at the focus of the excitation, and by using time-correlated single-photon counting, the fluorescence lifetime of single $DiIC_1(5)$ molecules was obtained [48]. A histogram of fluorescence lifetime was build for subsequent analysis from at least 50 single molecule data for every fiber diameter.

The mean values of the obtained fluorescence lifetime distributions are plotted in Figure 7. The fiber diameter was estimated from bright-field images. For calibration, we have used fluorescent polymer lines prepared by soft-lithography, which allowed comparing directly the length scales in fluorescence and bright-field images. The horizontal error bars in Figure 7 represent the error in estimation of the fiber diameter and are estimated by comparing fibers of known diameter to the ones seen on the bright-field images. Unfortunately, we were not able to determine accurately in-situ the size of the fibers in the bright field images when the diameter of the fibers was lower than ~400 nm. We have grouped all fluorescent lifetime results for such fibers into one data point and placed it at 225 nm with horizontal error bars spanning from 50 to 400 nm (indicated in Figure 7 with dashed lines). The vertical bars for data points in Figure 4 represent the widths of the fluorescence lifetime distributions obtained by fitting a Lorentzian function to the data. For fibers with diameters above 500 nm the mean fluorescence lifetime of the embedded $DiIC_1(5)$ molecules is almost independent on the fiber diameter and its value is centered around 2.0 -2.2 ns. The widths of the distributions (as indicated by the bars) are narrow and comparable to the experimental lifetime error. Although the *mean* τ_F of $DiIC_1(5)$ in fibers with diameter smaller than 500 nm in diameter is comparable to the rest of the data points, a significant broadening of the τ_F distributions is observed for low fiber diameters. To appreciate the broadening, we have plotted in Figure 8 the values of τ_F of molecules in a fiber with 900 nm diameter and that of molecules in fibers with a diameter below 400 nm. The broadening is slightly asymmetric towards higher values and fluorescence lifetimes as high as 4.5 ns were observed.

In the section below we discuss the possible reasons that can explain the broadening of the single molecule fluorescence lifetime histograms. In principle several effects could contribute including: influence of the radiative properties by the presence of close-by interfaces, fiber structure (fiber morphology), and finally a mixture of both of these effects combined with

induced chromophore orientation by the spinning process. It is known that the presence of dielectric interfaces influences the radiative transition frequencies and decay rates [75-78]. Longer fluorescence lifetimes were found for ensembles or single molecules closer to the dielectric/air interface and with transition dipole moments oriented perpendicular to the interfaces [47-49]. Comparing to single molecule studies in thin films, in the case of fibers substantially higher amount of molecules (within the distributions) can be present with their dipole moments perpendicular to the interfaces. Also, for a cylindrical geometry, the molecules are on average closer to the interfaces for thinner fibers. Therefore, one can relate the broadening towards higher fluorescence lifetimes to the electromagnetic boundary condition (EBC) effects described in more details in Chapter 6. It should be mentioned that the relatively simple EBC arguments cannot explain the broadening towards lower fluorescence lifetimes and also other effects apparently play a role e.g. quenching processes will cause broadening towards lower lifetime values. We are not aware of any theoretical studies of the radiative properties of light emitters placed in cylindrical dielectrics with diameters presented in this study and to our knowledge we are the first to report single molecule experimental results. The main advantage of using single molecule technique is that it avoids ensemble averaging. In case of the investigations of fluorescence lifetime in electrospun fibers shown in this Chapter the averaging would be performed twofold. The first averaging is done over a distribution of fiber diameters and possible effects associated with fiber diameter would not be resolved. Additionally, the results would obviously not show up the broadening of the distributions.

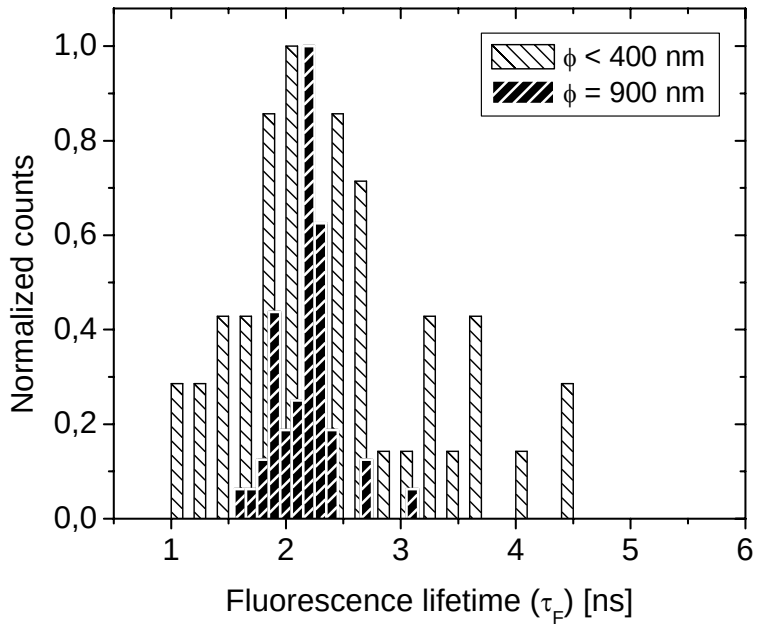

Figure 8. Distributions of fluorescence lifetime for individual $DiIC_1(5)$ molecules embedded in electrospun PMMA fibers. The distribution is significantly broader for fibers with diameter below 400nm.

The second averaging is done over all chromophore locations and orientations within the fibers. Having said this, we realize the need for two main improvements to our experiments. Firstly, a reliable in-situ method (e.g. Atomic Force Microscopy) to determine the diameters of the fibers is needed. Secondly, it would be advantageous to determine the location and 3D orientation of the molecules in the fibers with the highest possible precision. Near-field optical microscopy can in principle be used to determine the size of the fibers and accurately obtain the position and orientation of the molecules, however reliable determination of fluorescence lifetimes still remains a challenge.

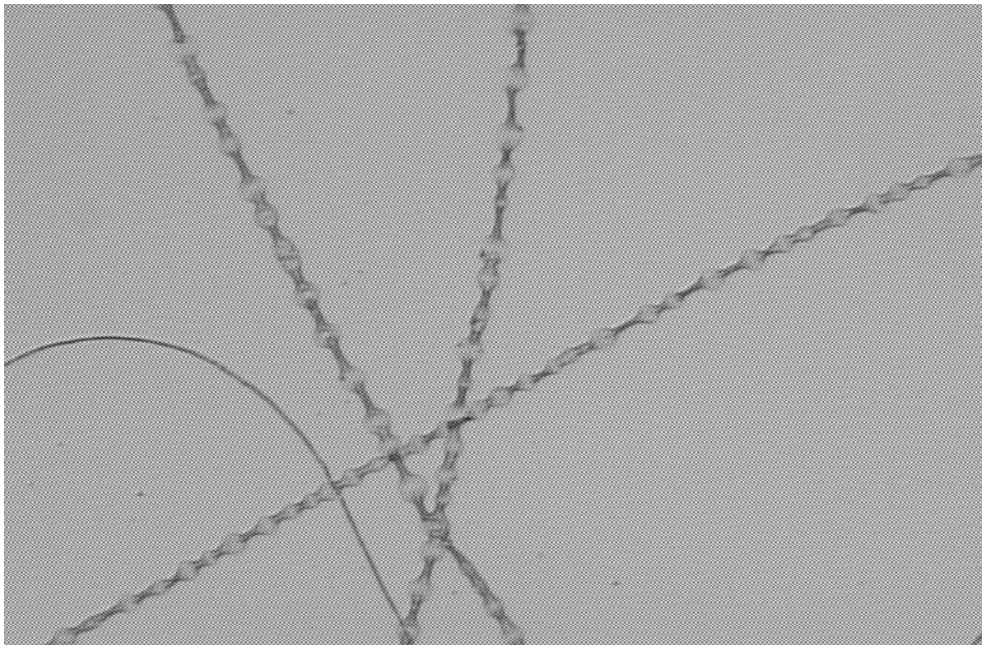

Figure 9. Optical micrograph of electrospun PEO fibers exhibiting a bead-on-a-string morphology. The beads are formed because of fluid instabilities occurring in the liquid jet exiting a capillary.

8.3.3 Light emitters in polymer beads

Complex dielectric structures allow one to control the photonic properties of the embedded chromophores. The electrospinning method not only allows one to obtain fibers with a broad range of diameters and made of many different polymeric materials, but also, for specific experimental conditions, one can obtain other structures like the bead-on-a-string morphology (Figure 9). The formation of droplets for electrically driven low molecular weight liquids is due to the capillary breakup by surface tension [34]. In the case of polymers, the filaments between the droplets instead of breaking are stabilized and a bead structure is formed. The size and shape of the beads, and the distance between the beads depends mainly on the polymer concentration (viscosity), solvent used (surface tension) and applied voltage

[34,79,80]. Figure 10 shows a fluorescence intensity scan of $DiIC_1(5)$ molecules embedded in beads formed along a PEO fiber. The color scale represents the polarization of the incoming fluorescence (See chapter 4). Remarkably, the scanning confocal images show that the dyes are not uniformly distributed within the beads but are concentrated around the bead edges. Two possibilities exist to explain this behavior. The first is that the beads are hollow, no material is present within, and a shell-like structure is being formed. The second possibility is that the dyes were excluded from the semi-crystalline phase of the PEO during the crystallization process, which takes place in the central regions of the beads. For comparison fibers were made of an amorphous polymer – PMMA (Figure 11). When embedding $DiIC_1(5)$ in beads of PMMA, the shell-like structure could not be visualized giving support for the second mechanism. When we compared the concentration of the chromophores in the beads and in the fiber sections between them, we observed that for PMMA the concentration of the chromophores within the beads is the same as in the straight parts of the fibers. For PEO, however, the concentration of $DiIC_1(5)$ in the beads is approximately two orders of magnitude smaller than in the straight fibers, when assuming that the PEO beads are homogeneously filled. This suggests a shell-like structure, since the concentration of the chromophores per unit volume in the spinning solution is uniform.

a) b)

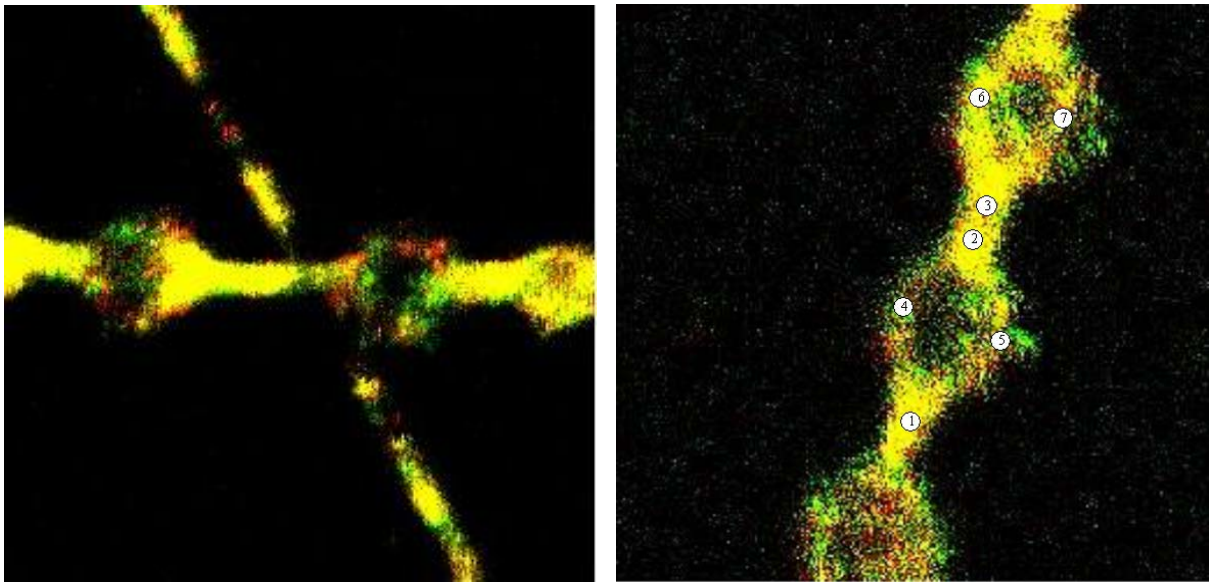

Figure 10. 10x10 μm^2 fluorescence intensity scans of PEO fibers. The $DiIC_1(5)$ molecules are mostly segregated near the bead edges. The color scale indicates the orientation of the emission dipole moment of the molecules. One-color spots visible at the bead edges indicate that the spots are single molecules.

a) b)

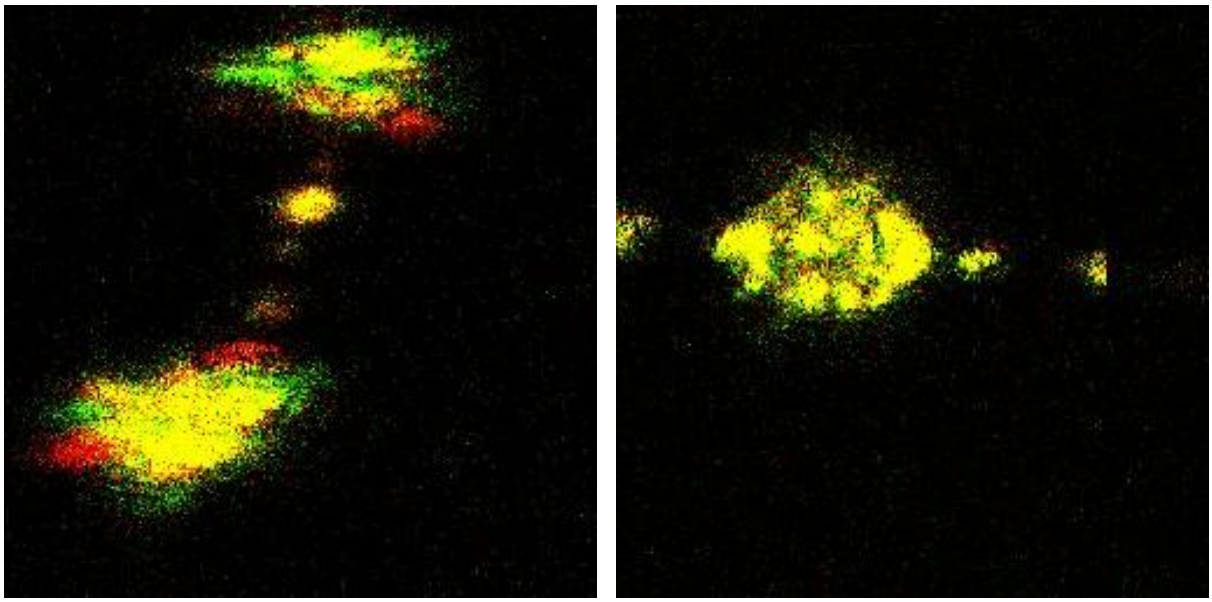

Figure 11. 5x5 μm^2 fluorescence intensity scans of $DiIC_1(5)$ molecules embedded in PMMA beads. The color-scale represents the polarization of the incoming fluorescence. The molecules are distributed uniformly within the beads volume.

In order to verify whether the beads formed along the fibers are hollow or filled with material we have also performed an additional check by imaging the fibers using wide field fluorescence imaging. In contrast to confocal microscopy, in wide-field microscopy all molecules are being excited at the same time (Figure 12a). Figures 12b and 12c show the fluorescence emitted by $DiIC_1(5)$ molecules embedded in PEO and PMMA fibers, respectively. PMMA beads are present on the right hand side of Figure 12c and a larger bead is shown in Figure 12d. The images look essentially similar to these obtained with SCM. Clearly, the PMMA beads are filled with molecules uniformly over their entire volume. An additional feature on the images of PEO beads is a small fluorescence spot almost exactly in middle of each bead (Figures 12 e-h). This might be due to the focusing effect of such large, micrometer-size, dielectric beads as described earlier in the literature e.g. by Barnes et al. [81]. Beads made of PMMA should also display such focusing effects, however due to the presence of molecules distributed all over the PMMA bead, such emission spots would be overshadowed by the overall emission intensity and could not be clearly identified. Indeed, when bleaching the majority of the chromophores in the bead the center spots come forward. Wide-field imaging confirmed that depending on the material used one could obtain different polymer beads with different structure. It is important to investigate further the relationship between the polymer properties and the final bead structure. This can help to understand the electrospinning process in more details.

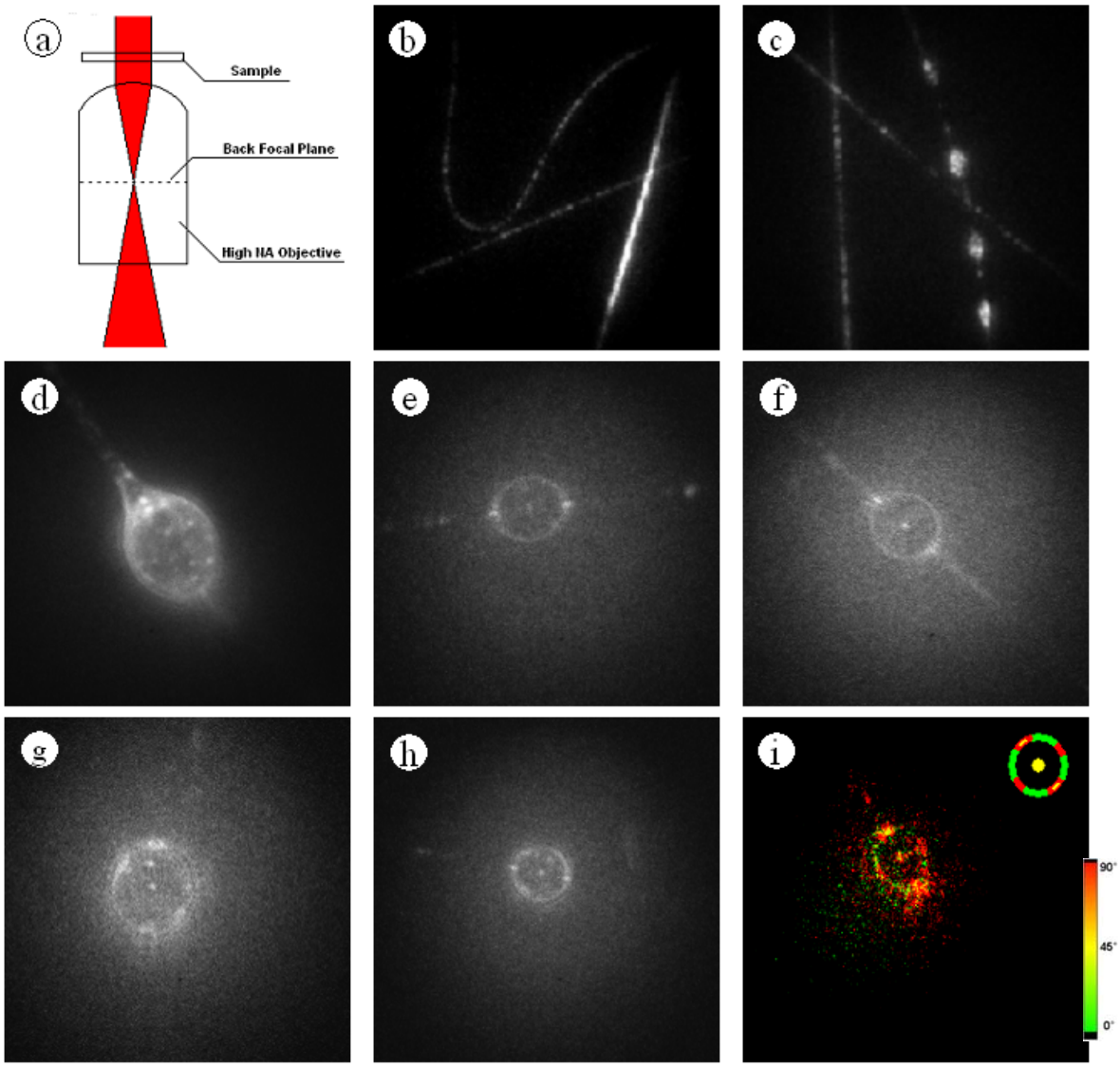

Figure 12. (a) Scheme of the wide-field illumination. An area of 380 μm^2 (22 μm in diameter) is being illuminated simultaneously. Part (b) and part c) shows fluorescence from $DiIC_1(5)$ molecules embedded in PEO and PMMA electrospun fibers, respectively. c) PMMA beads formed on PMMA fibers filled entirely with $DiIC_1(5)$ molecules are visible on the right hand side of the image. A shell-like emission pattern around the bead and a wave-like pattern extending outside the bead are visible for all PMMA and PEO beads (d-h). In contrast to PMMA, there is no significant fluorescence signal coming from within the PEO beads (e-i). Additionally, a peculiar, almost diffraction limited spot is clearly visible in the center of each PEO bead (e-i). Such emission pattern can be caused by a focusing effect of a spherical bead [81]. The wave-like pattern around PEO beads is even more pronounced than in PMMA beads (g-h). The collected fluorescence for PEO beads has a well-defined polarization even though a large amount of $DiIC_1(5)$ molecules is embedded within the structure (i). The false color scale indicates the fluorescence polarization in two orthogonal channels. In the upper-right part of (i) an extracted polarization pattern is presented.

Besides the fact that the beads formed along an electrospun fiber are hollow or filled, depending on the material used to spin, wide-field experiments revealed additionally that the dye molecules might have a preferred orientation at the bead edges with respect to the interface. We have used circularly polarized excitation light and employed a Wollaston prism, which splits the emission path into two orthogonal polarization channels. After overlaying the two channels, a color scale was applied to display the polarization state of the incoming fluorescence. Remarkably, our initial results indicate that the emission from different parts of the bead is strongly polarized (inset of Figure 12i shows the extracted pattern). More careful investigations of the distribution of orientations of the embedded chromophores could help to solve, in the future, some questions related to internal structure of the electrospun fibers at the molecular level.

8.3.4 Fluorescence lifetime of dyes in PMMA and PEO beads

The size (microns) and shape (approximated as spherical) of the beads obtained in this work suggest that our structures could have interesting optical properties, namely they can exhibit resonance effects, similar to those found in dielectric microspheres [82,83] or suspended micrometer liquid droplets [81,84]. We have measured fluorescence lifetimes of $DiIC_1(5)$ molecules at different positions in PEO fibers and compared them to the fluorescence lifetime found for $DiIC_1(5)$ embedded in a thick PEO film. While the fluorescence lifetime of $DiIC_1(5)$ in the straight parts of the fibers (points 1,2,3 in figure 10 b) was essentially the same as in thick PEO sample (~2.3 ns), the lifetime of molecules embedded at the bead edges (points 4,5,6,7) was shorter by almost 25% (~1.7 ns). Remarkably, the fluorescence lifetime of $DiIC_1(5)$ molecules in PMMA beads displayed an opposite behavior. The fluorescence decay rates of $DiIC_1(5)$ at the bead center and in the straight parts of the fiber were equal to a bulk value (~2.2 ns). At the edges of the beads, however, $DiIC_1(5)$ molecules were decaying from their excited state almost twice as slower, and the excited state lifetime approached an average of 4.2 ns. One of the possible explanations is that filled PMMA beads prevent quenching processes to occur and the fluorescence lifetime is dominated by the presence of interfaces, and its influence on the excited state lifetime of a perpendicularly oriented chromophore. In case of PEO the chromophores at the surface sites are more sensitive to quenching and therefore the fluorescence lifetime is on average lower. Another possible explanation of such remarkably opposite trend is that in case of PEO cavity effects will dominate. However, to answer the question whether the reported behavior of the fluorescence lifetime is due to specific optical properties of the beads or is due to the structure and organization of the chromophore surroundings will require a more thorough analysis combined with spectral measurements.

8.4 Conclusions

Luminescent micro- and nanofibers were prepared by electrospinning. Fluorescent molecules and luminescent CdSe/ZnS core-shell semiconductor nanoparticles were embedded into polymer fibers with diameters ranging from 50 nm to several micrometers. The single molecule approach used in this Chapter to investigate luminescent nanofibers has served two purposes. Firstly, the chromophores were used to report on the structure of the electrospun fibers. Bead-on-a-string morphology of PMMA and PEO fibers was obtained. The chromophores in PEO beads were located mainly at the bead edges. In contrasts to PEO, the chromophores in PMMA beads where evenly distributed within the beads volume. Secondly, the chromophores reported how the cylindrical geometry of a dielectric influences the radiative properties of the embedded light emitters. The fluorescence lifetime of single $DiIC_1(5)$ molecules embedded in PMMA fibers was independent on the fiber diameter. However, significant broadening of the single-molecule fluorescence lifetime distributions was observed for fibers with diameter below 500 nm. Possible explanation of the observed broadening was the modification of the radiative decay rates through the effect of the electromagnetic boundaries and quenching effects at the fiber surface. The feasibility and relative ease of preparation of the structures presented in this Chapter may lead to fabrication of advanced optical components for photonics at low-cost.

8.5 References

[1] Formhals, A. U.S. Patent 2,116,942, 1938.

[2] Srinivasan, G.; Reneker, D. H. *Polym. Int.* **1995**, *36*, 195.

[3] Doshi, J.; Reneker, D. H. *J. Electrostatics* **1995**, *35*, 151.

[4] Reneker, D. H.; Chun, I. *Nanotechnology* **1996**, *7*, 216.

[5] Jaeger, R.; Bergshoef, M. M.; Batlle, C. M. I.; Schonherr, H.; Vancso, G. J. *Macromol. Symp.* **1998**, *127*, 141.

[6] Shin, Y. M.; Hohman, M. M.; Brenner, M. P.; Rutledge, G. C. *Appl. Phys. Lett.* **2001**, *78*, 1149.

[7] Huang, Z. M.; Zhang, Y. Z.; Kotaki, M.; Ramakrishna, S. *Compos. Sci. Technol.* **2003**, *63*, 2223.

[8] Jayaraman, K.; Kotaki, M.; Zhang, Y. Z.; Mo, X. M.; Ramakrishna, S. *J. Nanosci. Nanotech.* **2004**, *4*, 52.

[9] Bergshoef, M. M.; Vancso, G. J. *Adv. Mater.* **1999**, *11*, 1362.

[10] Jaeger, R.; Schönherr, H.; Vancso, G. J. *Macromolecules* **1996**, *29*, 7634.

[11] Norris, I. D.; Shaker, M. M.; Ko, F. K.; MacDiarmid, A. G. *Synth. Met.* **2000**, *2*, 109.

[12] Bognitzki, M.; Frese, T.; Steinhart, M.; Greiner, A.; Wendorff, J. H.; Schaper, A.; Hellwig, M. *Polym. Eng. Sci.* **2001**, *41*, 982.

[13] Fong, H.; Reneker, D. H. *J. Polym. Sci., Part B: Polym. Phys.* **1999**, *37*, 3488.

[14] Sun, Z. C.; Zussman, E.; Yarin, A. L.; Wendorff, J. H.; Greiner, A. *Adv. Mat.* **2003**, *15*, 1929.

[15] Loscertales, I. G.; Barrero, A.; Marquez, M.; Spretz, R.; Velarde-Ortiz, R.; Larsen, G. *J. Am. Chem. Soc.* **2004**, *126*, 5376.

[16] Kenawy, E. R.; Bowlin, G. L.; Mansfield, K.; Layman, J.; Simpson, D. G.; Sanders, E. H.; Wnek, G. E. *J. Controlled Release* **2002**, *81*, 57.

[17] Verreck, G.; Chun, I.; Peeters, J.; Rosenblatt, J.; Brewster, M. E. **2003**, *20*, 810.

[18] Jing, Z.; Xu, X. Y.; Chen, X. S.; Liang, Q. Z.; Bian, X. C.; Yang, L. X.; Jing, X. B. **2003**, *92*, 227.

[19] Gibson, P.; Schreuder-Gibson, H.; Rivin, D. *Colloids Surf., A* **2001**, *187*, 469.

[20] Pinto, N. J.; Johnson, A. T.; MacDiarmid, A. G.; Mueller, C. H.; Theofylaktos, N.; Robinson, D. C.; Miranda, F. A. *Appl. Phys. Lett.* **2003**, *83*, 4244.

[21] Wang, X. Y.; Drew, C.; Lee, S. H.; Senecal, K. J.; Kumar, J.; Samuelson, L. A. *J. Macromol. Sci.* **2002**, *A39*, 1251.

[22] Wang, X. Y.; Lee, S. H.; Ku, B. C.; Samuelson, L. A.; Kumar, J. *J. Macromol. Sci.* **2002**, *A39*,1241.

[23] Wang, X. Y.; Drew, C.; Lee, S. H.; Senecal, K. J.; Kumar, J.; Samuelson, L. A. *Nano Lett.* **2002**, *2*, 1273.

[24] Liu, H. Q.; Kameoka, J.; Czaplewski, D. A.; Craighead, H. G. *Nano Lett.* **2004**, *4*, 671.

[25] Drew, C.; Wang, X. Y.; Senecal, K.; Schreuder-Gibson, H.; He, J. N.; Kumar, J.; Samuelson, L. A. **2002**, *A39*, 1085.

[26] Kim, J. S.; Reneker, D. H. **1999**, *20*, 124.

[27] Fong, H.; Liu, W. D.; Wang, C. S.; Vaia, R. A. *Polymer* **2002**, *43*, 775.

[28] Sen, R.; Zhao, B.; Perea, D.; Itkis, M. E.; Hu, H.; Love, J.; Bekyarova, E.; Haddon, R.C. *Nano Lett.* **2004**, *4*, 459.

[29] Matthews, J. A.; Wnek, G. E.; Simpson, D. G.; Bowlin, G. L. **2002**, *3*, 232.

[30] Li, W. J.; Laurencin, C. T.; Caterson, E. J.; Tuan, R. S.; Ko, F. K. *J. Biomed. Mat. Res.* **2002**, *60*, 613.

[31] Shen, Y.; Prasad, P. N. *Appl. Phys. B* **2002**, *74*, 641.

[32] Prasad, P. N. *Curr. Opin. Solid State Mater. Res.* **2004**, *8*, 11.

[33] Prasad, P. N. *Nanophotonics*; Wiley-Interscience: New York, 2004.

[34] Lee, K. H.; Kim, H. Y.; Bang, H. J.; Jung, Y. H.; Lee, S. G. *Polymer* **2003**, *44*, 4029.

[35] Kim, J. S.; Lee, D. S. *Polym. J.* **2000**, *32*, 616.

[36] Zussman, E.; Rittel, D.; Yarin, A. L. *Appl. Phys. Lett.* **2003**, *82*, 3958.

[37] Stephens, J. S.; Frisk, S.; Megelski, S.; Rabolt, J. F.; chase, D. B. *Appl. Spectrosc.* **2001**, *55*, 1287.

[38] Kahol, P. K.; Pinto, N. J. *Solid State Commun.* **2002**, *124*, 195.

[39] Dersch, R.; Liu, T. Q.; Schaper, A. K.; Greiner, A.; Wendorff, J. H. J. *Polym. Sci., Part A: Polym. Chem.* **2003**, *41*, 545.

[40] Tomczak, N.; Vallée, R. A. L.; van Dijk, E. M. H. P.; Kuipers, L.; van Hulst, N. F.; Vancso, G. J. *J. Am. Chem. Soc.* **2004***, 126*, 4748.

[41] Moerner, W.E. *Acc. Chem. Res.* **1996**, *29*, 563.

[42] Xie, X. S. *Acc. Chem. Res.* **1996**, *29*, 598.

[43] Xie, X. S.; Trautman, J. K. *Annu. Rev. Phys. Chem.* **1998**, *49*, 441.

[44] Ambrose, W. P.; Goodwin, P. M.; Jett, J. H.; Van Orden, A.; Werner, J. H.; Keller, R. A. *Chem. Rev.* **1999**, *99*, 2929.

[45] Kulzer, F.; Orrit, M. *Annu. Rev. Phys. Chem.* **2004**, *55*, 585.

[46] Moerner, W. E.; Dickson, R. M.; Norris, D. J. *Mater. Sci. Eng.* **1997**, *B48*, 169.

[47] Macklin, J. J.; Trautman, J. K.; Harris, T. D.; Brus, L. E. *Science* **1996**, *272*, 255.

[48] Vallée, R. A. L.; Tomczak, N.; Gersen, H.; van Dijk, E. M. H. P.; García-Parajó, M. F.; Vancso, G. J.; van Hulst, N. F. *Chem. Phys. Lett.* **2001**, *348*, 161.

[49] Kreiter, M.; Prummer, M.; Hecht, B.; Wild, U. P. *J. Chem. Phys.* **2002**, *117*, 9430.

[50] Prummer, M.; Sick, B.; Renn, A.; Wild, U. P. *Anal. Chem.* **2004**, *76*, 1633.

[51] Dabbousi, B. O.; Rodriguez-Viejo, J.; Mikulec, F. V.; Heine, J. R.; Mattoussi, H.; Ober, R.; Jensen, K. F.; Bawendi, M. G. *J. Phys. Chem. B* **1997**, *101*, 9463

[52] Qu, L.; Peng, X. *J. Am. Chem. Soc.* **2002**, *124*, 2049.

[53] Colvin, V. L.; Schlamp, M. C.; Alivisatos, A. P. *Nature* **1994**, *370*, 354.

[54] Klimov, V. I.; Mikhailovsky, A. A.; Xu, S.; Malko, A.; Hollingsworth, J. A.; Leatherdale, C. A.; Eisler, H. J.; Bawendi, M. G. *Science* **2000**, *290*, 314.

[55] Weiss, S. *Science* **1999**, *283*, 1676.

[56] Chan, W. C. W.; Maxwell, D. J.; Gao, X. H.; Bailey, R. E.; Han, M. Y.; Nie, S. M. *Curr. Opin. Biotech.* **2002**, *13*, 40.

[57] Han, M. Y.; Gao, X. H.; Su, J. Z.; Nie, S. *Nat. Biotech.* **2001**, *19*, 631.

[58] Dubertret, B.; Skourides, P.; Norris, D. J.; Noireaux, V.; Brivanlou, A. H.; Liblacher, A. *Science* **2002**, *298*, 1759.

[59] Yang, Q. B.; Li, D. M.; Hong, Y. L.; Li, Z. Y.; Wang, C.; Qiu, S. L.; Wei, Y. *Synth. Met.* **2003**, *137*, 973.

[60] Nirmal, M.; Dabbousi, B. O.; Bawendi, M. G.; Macklin, J. J.; Trautman, J. K.; Harris, T. D.; Brus, L. E. *Nature* **1996**, *383*, 802.

[61] Efros, A. L.; Rosen, M. *Phys. Rev. Lett.* **1997**, *78*, 1110.

[62] Empedocles, S. A.; Neuhauser, R.; Shimizu, K.; Bawendi, M. G. *Adv. Mat.* **1999**, *11*, 1243.

[63] Liver, N.; Nitzan, A.; Amirav, A.; Jortner, J. *J. Phys. Chem.* **1988**, *88*, 3516.

[64] Kador, L.; Jahn, S.; Haarer, D.; Silbey, R. *Phys. Rev. B* **1990**, *41*, 12215.

[65] Moerner, W. E. *Science* **1994**, *265*, 46.

[66] Nazzal, A. Y.; Wang, X.; Qu, L.; Yu, W.; Wang, Y.; Peng, X.; Xiao, M. *J. Phys. Chem.* **2004**, *108*, 5507.

[67] Hohng, S.; Ha, T. *J. Am. Chem. Soc.* **2004**, *126*, 1324.

[68] Crenshaw, M. E.; Bowden, C. M. *Phys. Rev. Lett.* **2000**, *85*, 1851.

[69] Wuister, S. F.; de Mello Donega, C.; Meijerink, A. *J. Chem. Phys.* **2004**, *121*, 4310.

[70] Balzer, F.; Bordo, V. G.; Simonsen, A. C.; Rubahn, H.-G. *Phys. Rev.* **2003**, *B 67*, 115408.

[71] Duan, X.; Huang, Y.; Agarwal, R.; Lieber, Ch. M. *Nature* **2003**, *421*, 241.

[72] Orrit, M.; Bernard, J. *Phys. Rev. Lett.* **1990**, *65*, 2716.

[73] Ha, T.; Enderle, T.; Chemla, D. S.; Selvin, P. R.; Weiss, S. *Chem. Phys. Lett.* **1997**, *271*, 1.

[74] Veerman, J. A.; García-Parajó, M. F.; Kuipers, L.; van Hulst, N. F. *Phys. Rev. Lett.* **1999**, *83*, 2155.

[75] Drexhage, K. H. *Bull. Am. Phys. Soc.* **1969**, *14*, 873.

[76] Kuhn, H. *J. Chem. Phys.* **1970**, *53*, 101.

[77] Chance, R. R.; Prock, A.; Silbey, R. *J. Chem. Phys.* **1974**, *60*, 2744.

[78] Lukosz, W.; Kunz, R. E. *Opt. Commun.* **1977**, *20*, 195.

[79] Fong, H.; Chun, I.; Reneker, D. H. *Polymer* **1999**, *40*, 4585.

[80] Hsu, C.; Shivkumar, S. *J. Mat. Sci.* **2004**, *39*, 3003.

[81] Barnes, M. D.; Kung, C-Y.; Whitten, W. B.; Ramsey, J. M.; Arnold, S; Holler, S. *Phys. Rev. Lett.* **1996**, *76*, 3931.

[82] Schiro, P. G.; Kwok, A. S. *Optics Express* **2004**, *12*, 2857.

[83] Woggon, U.; Wannemacher, R.; Artemyev, M. V.; Moller, B.; Lethomas, N.; Anikeyev, V.; Schops, O. *Appl. Phys. B* **2003**, *77*, 469.

[84] Barnes, M. D.; Whitten, W. B.; Arnold, S.; Ramsey, J. M. *J. Chem. Phys.* **1992**, *97*, 7842.

Chapter 9

Outlook

9.1 Introduction

We have shown throughout the Chapters of this Thesis that single-molecule based experimental methods give an unprecedented insight into the structure and dynamics of polymers. Moreover, we have shown that dielectric structures with dimension smaller than the wavelength of light affect the radiative properties of the single molecule probes. The advantage of single molecule methods, as underlined many times, lays in the nonaveraging over a distribution of properties in combination with the simultaneous ability to look at the local, segmental scale polymer processes. Such approach gives direct evidence that the averaged, bulk, macroscopic properties are a manifestation of a broad distribution of microscopic, short scale, segmental relaxation processes. The results obtained in the course of this thesis work, are relevant for a broad spectrum of scientific activities ranging from fundamental and theoretical physics, biology (e.g. protein conformation studies through the monitoring of fluorescence lifetime fluctuations), to current technological applications (e.g. solar cells, biomimicry) and possible future technologies based on light as a means of information transmission and processing.

In this Chapter, we would like to present in a number of points what we think should be the extension of the studies presented here. We also would like to point out that polymer probing with single molecules is a method still in its infancy and that an enormous potential is still waiting to be harvested. We hope that our studies will stimulate further research of microscopic structure and dynamics in different polymer systems.

9.2 Outlook

1. It should be kept in mind that each of the methods presented in this Thesis deserves an in-depth follow-up. Having developed a broad platform for single molecule probing of polymers we realize the need for focused and systematic studies. It is desirable to extend the presented investigations with experiments, where the probe size, chemistry, shape and physicochemical parameters are variables rather than constants.

This would allow one to obtain a more detailed picture of molecular-level processes inside a polymer matrix. Varying temperature would allow one to obtain the information on the activation energies involved in various processes. Performing temperature dependent studies would also resolve the degree of coupling between the probe behavior and relaxation processes in the polymer matrix. Going one step further, covalently linking the probes to the polymer chains would allow one to monitor the polymer chain dynamics directly. Besides amorphous glasses, nanometer-scale probing of more complex polymer structures like polymer networks, block copolymers, blends or semicrystalline polymers should be the next step in investigations using methods presented in this Thesis.

2. Single molecule based investigations give the possibility to confront the assumptions of microscopic theories of polymer dynamics directly to experimental observations. As mentioned across different Chapters, application of bulk definitions, bulk-derived theories or equations is not always appropriate if not hopeless and misleading. Resolving the dynamics and structure on the nanometer scale gives new insights into microscopic theories of molecular diffusion. Looking at full distributions rather than at the ensemble averaged picture will additionally shed light onto the segmental scale relaxation near to the glass transition temperature. Additional processes like the hopping mechanism for diffusion should be included in the theoretical development of spatially heterogeneous dynamics.

3. In Chapter 4 we have shown that one can look at long-range molecular diffusion processes (far above the glass transition) or at rotational molecular motion (close to T_g) by using single light emitters. It would be of great significance for the understanding of the polymer microscopic relaxation processes near to the glass transition temperature to study both parameters simultaneously and as a function of temperature. Such single molecule based investigations will shed light on the reported rotational-translational paradox for diffusion close to the glass transition.

4. The sensitivity and responsiveness of the probes to the changes in their environment (i.e. Chapter 5) motivates also the development of a new class of fluorescent probes for use in single molecule imaging [1]. We propose to explore the possibility of semiconductor nanoparticles (quantum dots) as probes. Quantum dots offer several advantages with respect to usually used organic chromophores, namely stability, emission wavelength tunability, and narrow optical lines; properties, which organic chromophores are lacking [2]. Most importantly QDs offer a well-defined chemistry at the probe/polymer interface, which is independent on the probe size. Investigations where probe size is a variable are important in studies of e.g. diffusion processes in

polymers. Additionally, QDs can be used as alternative light sources in radiative decay engineering.

5. Investigation of polymers confined into nanometer scale structures is currently an active field of research. We would extend the experiments presented in Chapter 7 to study polymer films with thickness in the nanometer range. Also we would employ the methods presented in Chapter 4 to study the diffusion processes in self-assembled multilayer films. Such structures are very promising candidates in e.g. various types of nanofluidic applications. In view of the results obtained in Chapter 7 it is also desirable to have a more detailed picture of polymer dynamics in polymer fibers and spheres with the diameters in the range from tens to hundreds of nanometers.

6. In radiative decay engineering (RDE) the nanostructured environment serves as a means to control the optical properties of light emitters. Combination of RDE studies with single molecule methods allows one to obtain a detailed picture of all parameters influencing the resulting optical properties. The ultimate goal of such studies would be to engineer nanometer scale polymer structures with chromophores placed at well-defined positions and with well-defined orientations with respect to the interfaces. It is also known that polymer-based structures are limited in their use in RDE due to their dielectric properties. A challenging task will be to combine polymers with metals to produce composite structures for improved control over the optical properties of the embedded chromophores. For example, gold nanoshells present around a fluorescent core can strongly enhance the radiative decay rate of the whole composite nanoparticle [3].

7. Finally we would also introduce additional methods, which could be useful in polymer probing. A technique, which was not used in this thesis, was single molecule fluorescence resonance energy transfer (FRET) [4]. This technique would allow one to experimentally verify, for example, the theoretical estimations of the degree of fluctuations in the end-to-end distance of a polymer or a biomolecular chain and its collapse above the theta temperature [5,6]. Additionally, one can covalently link multiple amounts of probes to the polymer chain to perform two- and three-color FRET [7] in solution or in the melts at different experimental conditions.

9.3 References

[1] Willets, K. A.; Callis, P. R.; Moerner, W. E. *J. Chem. Phys. B* **2004**, *108*, 10465.

[2] Schutz, G. J.; Gruber, H. J.; Schindler, H.; Schmidt, T. *J. Lumin.* **1997**, *72-74*, 18.

[3] Baer, R.; Neuhauser, D.; Weiss, S. *Nano Lett.* **2003**, *4*, 85.

[4] Ha, T.; Enderle, T.; Ogletree, D. F.; Chemla, D. S.; Selvin, P. R.; Weiss, S. *Proc. Natl. Acad. Sci. U.S.A.* **1996**, *93*, 6264.

[5] Bodunov, E. N.; Berberan-Santos, M. N.; Martinho, J. M. G. *J. Lumin.* **2002**, *96*, 269.

[6] Gopich, I. V.; Szabo, A. *J. Phys. Chem. B* **2003**, *107*, 5058.

[7] Hohng, S.; Joo, C.; Ha T. *Biophys. J.* **2004**, *87*, 1328.

Summary

This thesis presents developments in the field of nanoscale probing of polymers. New experimental methods based on single molecule fluorescence detection were developed and applied to polymer studies. Localization of, and communication with individual fluorescent molecules embedded in a glassy polymer or immersed in a polymer melt have been realized by using various, optical techniques e.g. Scanning Confocal Microscopy and Wide-Field Microscopy. Location of single molecules as well as their orientation, emission spectra or fluorescence lifetime have been followed in time. This allowed us to perform dynamical studies in the time domain. Since full distributions of single molecule behavior (e.g. rotational diffusion constants, fluorescence lifetimes) were obtained, systems with heterogeneous dynamics could be clearly identified and sub-ensembles, which could be characterized with different dynamic properties, were separated and investigated. Besides polymer probing studies, it was also shown how relatively simple structures can be prepared and used to engineer the emission properties of single molecules. In particular, the fluorescence emission of single molecules in thin polymer films and in electrospun polymer fibers was shown to depend on the size of the structures. The following paragraphs give a more detailed summary of the results.

Chapter 2 and Chapter 3 were introductory chapters. Introduction to topics in polymer physics is presented in Chapter 2. A special accent was put on the reviewing of the current status in the investigations of the dynamic properties of polymers at interfaces and in different degree of confinement. In Chapter 3 single molecule fluorescence methods were introduced and their application in polymer studies was reviewed. The need for the development of new experimental techniques to investigate polymers on the nanoscale was underlined. Techniques based on optical single molecule detection were shown to be the most promising candidates to resolve the controversies present in the polymer field concerning segmental scale dynamics or heterogeneous dynamics near the glass transition.

Wide-field microscopy was employed to investigate polymer dynamics across the glass transition and the results of these investigations were presented in Chapter 4. Far above the glass transition temperature translational diffusion of single molecules was observed and translational diffusion constant were extracted. At temperatures close to the glass transition, using light polarization detection scheme, the orientational diffusion of many different single probes was followed simultaneously. The molecules were shown to be immobile, to hop between different sites within the matrix, or to diffuse freely on different time-scales. Such

observations gave a significant insight into the heterogeneous dynamics present in a polymer host above and near the glass transition temperature. It was also found that the nonexponential character of the single molecule diffusion processes near the glass transition was a result of the changes in the probe behavior in time. Below the glass transition temperature the changes of the photophysical properties of single emitters in response to the changes in the environment were monitored and gave a valuable insight into the structural heterogeneity present in a glassy polymer matrix.

In Chapter 5 density fluctuations in a glassy polymer matrix were detected through the monitoring of single molecule fluorescence lifetime fluctuations. Using this newly developed method, direct information on the local, nanoscale host dynamics was obtained. From the experimental data, using the Simha – Somcynsky thermodynamic equation of state, we were able to obtain the number of polymer segments (N_S) taking part in the elementary rearrangement processes around the probe. For two different polymers, polystyrene and poly(isobutyl methacrylate) N_S was a function of temperature and it decreased with increasing temperature. Interestingly, it was found that N_S has similar temperature dependence for different polymers when normalized with respect to the glass transition temperature of the polymer used. A unique combination of small probed volumes and nonensemble measurements allowed us to directly visualize the spatially heterogeneous dynamics present within a polymer matrix below the glass transition temperature. Such a result is otherwise difficult, if not impossible, to achieve using other experimental techniques.

In planar, stratified media (e.g. glass/polymer/air) consisting of optically different materials the fluorescence emission of single molecules can be strongly modified due to the near-by presence of electromagnetic boundaries. The radiative decay rate in these cases should be dependent on the size of the layers, the distance of the molecule to the interfaces and to the orientation of the molecule emission dipole moment with respect to the interfaces. Before starting to investigate segmental scale dynamics in polymer structures with dimensions comparable to the wavelength of light it is important to perform a check whether the optical characteristics of the chromophoric probes are not influenced by the electromagnetic boundary conditions. In Chapter 6 we showed that the fluorescence lifetime of single molecules embedded in thin polymer films changes depending on the thickness of the films and increases when the film thickness decreases. Calculations of fluorescence lifetime of light emitters embedded within layered structures have shown that the presence of the interfaces is the main actor in the modifications of the fluorescence lifetime. Although important to realize, such “global” effects were found to not significantly affect the method presented in Chapter 5 if the chromophores are not reorienting within the polymer matrix or translating with respect to the interfaces. As shown in Chapter 4 and Chapter 5 this was not the case for molecules in a polymer like polystyrene at room temperature

In Chapter 7 we used the single molecule lifetime fluctuation technique to study the influence of the film thickness on local polymer dynamics on the nanometer length scale at temperatures far below the glass transition temperature. We found modified segmental scale dynamics when the polymer was confined into films with thickness below 60-70 nm corresponding to 6 times the radius of gyration of the polymer used. This behavior was attributed to the effect of the polymer free surface with enhanced dynamics. The effects of the interfaces propagated deep into the polymer sample over distances larger than the radius of gyration.

Investigations of hybrid polymer/light emitter nanofibers made of glassy or semicrystalline materials (PMMA, PEO) prepared by electrospinning was presented in Chapter 8. Organic molecules, as well as semiconductor nanocrystals (quantum dots), have been incorporated into the structures at different concentrations down to the single molecule level. The electrospinning technique has been proven to be a good and reliable method to prepare quasi one-dimensional luminescent structures on length scales ranging from tens of nanometers to several microns. The fluorescence lifetime distributions of single molecules embedded in PMMA fibers were shown to become broader for fibers with diameters below 500 nm. This was attributed to the effect of the interfaces on the excited state lifetime of the chromophores. Bead-on-a-string morphology of electrospun polymer fibers was obtained. The structure of the beads was found to be dependent on the polymer used to spin. In particular, when a semicrystalline polymer was used for electrospinning, the fluorescent molecules were excluded from the bead interior probably due to the growing polymer crystals. Additionally, there was evidence that the molecules adopt a specific orientation at the bead edges. The beads displayed also interesting photonic properties, which could be used in future applications based on advanced polymer structures.

In Chapter 9 a brief outlook into the possible future research directions was presented. The necessity of an in-depth follow-up of the methods presented throughout the thesis was underlined. We are confident that the research presented in this thesis will prove to be powerful in the investigations of various polymers systems or complex polymer structure e.g. block copolymers or polymer networks.

Samenvatting

Dit proefschrift beschrijft een onderzoek naar de microscopische eigenschappen van polymeren op de nanometerschaal. Hiertoe zijn nieuwe experimentele methodes, gebaseerd op detectie van fluorescentie van individuele moleculen, ontwikkeld specifiek voor toegepassing in dit polymeeronderzoek. Individuele fluorescerende moleculen worden ingebed in het te onderzoeken polymeer (glasfase of smeltfase) en vervolgens gelokaliseerd door gebruik te maken van verschillende microscopische technieken, zoals wide-field en scanning confocal microscopy. De locatie en oriëntatie van de afzonderlijke moleculen, hun emissiespectra en fluorescentielevensduur worden in de tijd gemeten. Hierdoor is het mogelijk om de polymeerdynamica in de tijd te volgen. Dit levert verdelingen van individueel moleculaire parameters, zoals rotatie diffusie constanten en fluorescentielevensduur op. Hierdoor is het mogelijk om zowel systemen met heterogene dynamica te identificeren als om sub-ensembles, d.w.z. deelverzamelingen met verschillende dynamische eigenschappen, te isoleren en te onderzoeken. Naast het onderzoek aan de polymeerdynamica laten we ook zien hoe met relatief eenvoudige polymeerstructuren de emissieeigenschappen van de moleculen zelf kunnen worden beïnvloed. Het fluorescentiesignaal en de fluorescentielevensduur van individuele moleculen in dunne polymere lagen en in polymere vezels, verkregen door middel van electrospinning, is direct gerelateerd aan de afmetingen van de structuren. Hieronder wordt de inhoud van dit proefschrift per hoofdtstuk in meer detail samengevat.

Hoofdstukken 2 en 3 zijn inleidende hoofdstukken. Een inleiding in polymeerfysische aspecten wordt gepresenteerd in Hoofdstuk 2. Hierbij is de nadruk gelegd op recente ontwikkelingen in het onderzoek naar dynamische eigenschappen van polymeren, zowel aan grensvlakken als in structuren met verdere restricties. In Hoofdstuk 3 worden methodes voor de detectie van individuele molecuulfluorescentie geïntroduceerd en hun toepassing in polymeeronderzoek besproken. Tevens wordt ingegaan op de noodzaak tot ontwikkeling van nieuwe experimentele technieken om specifiek polymeren op de nanoschaal te onderzoeken. Technieken gebaseerd op optische waarneming van enkele moleculen zijn duidelijk zeer geschikt voor het opnemen en oplossen van heersende controverses in het polymeeronderzoek, zoals segmentele schaaldynamica en heterogene dynamica nabij de glasovergang.

Wide-field microscopy is toegepast om de dynamica in polymeren rond de glasovergang te onderzoeken, waarvan de resultaten in Hoofdstuk 4 worden gepresenteerd. Ver boven de

glasovergang is temperatuur-afhankelijke translationele diffusie van individuele moleculen waargenomen en zijn de translatie diffusieconstanten bepaald. Bij temperaturen dicht bij de glasovergang is de oriëntationele (rotationele) diffusie van een groot aantal afzonderlijke probes gelijktijdig gevolgd door gebruik te maken van de polarisatierichting van de uitgezonden fluorescentie. De metingen laten zien dat de moleculen niet beweeglijk zijn, verspringen tussen verschillende beschikbare posities in de polymeermatrix of vrij diffunderen over verschillende tijdschalen. Deze waarnemingen geven een belangrijk inzicht in de mate van heterogene dynamica van de moleculen aanwezig in een polymere gastmatrix, zowel boven als in de nabijheid van de glasovergangstemperatuur. De diffusieprocessen van afzonderlijke moleculen in de omgeving van de glasovergang vertonen veelal een niet-exponentiëel karakter, een directe indicatie voor tijdsafhankelijke veranderingen in het gedrag van de moleculaire probe. Ook onder de glasovergangstemperatuur zijn de veranderingen in de fotofysische eigenschappen van individuele fluoroforen gevolgd, zoals deze veroorzaakt worden door de heterogeniteit in de structuur van een glasachtige polymere matrix.

Hoofdstuk 5 behandelt de dichtheidsfluctuaties in een glasachtige polymere matrix door het volgen van fluctuaties in de fluorescentielevensduur van afzonderlijke moleculen. Deze methode is in dit project nieuw ontwikkeld en geeft directe informatie over de lokale dynamica in de polymeermatrix op nanoschaal. Uitgaande van de experimentele data zijn we in staat geweest het aantal polymere segmenten (N_S) te bepalen, dat bijdraagt aan de elementaire herordeningsprocessen rond het gekozen “probe” molecuul, waarbij gebruik is gemaakt van de Simha-Somcynsky thermodynamische toestandsvergelijking. Voor twee verschillende polymeren, polystyreen en poly(isobutyl methacrylaat), neemt N_S direct af met een toename in de temperatuur. Opmerkelijk genoeg blijkt N_S een vergelijkbare temperatuursafhankelijkheid te vertonen voor verschillende polymeren, indien genormaliseerd wordt naar de glasovergangstemperatuur van het betreffende polymeer. De unieke combinatie van het kleine “probe” volume en de niet-ensemble metingen stelt ons voor het eerst in staat om de ruimtelijke heterogene dynamica aanwezig in een polymere matrix onder de glasovergangstemperatuur in beeld te brengen. Een dergelijk detail is moeilijk, zo niet onmogelijk te verkrijgen met alternatieve bestaande experimentele technieken.

In vlakke, gelaagde media met verschillende optische eigenschappen (bijvoorbeeld glas/polymeer/lucht), kan de fluorescentieemissie van afzonderlijke moleculen door de aanwezigheid van nabije grensvlakken sterk gemodificeerd worden. De mate van spontane emissie (fluorescentie) wordt in zulke gevallen afhankelijk van de dikte van de lagen, de afstand van de moleculen tot de grensvlakken en de oriëntatie van het dipoolmoment van de fluorescentieemissie t.o.v. de grensvlakken. Bij het bestuderen van segmentele schaal

dynamica in polymere structuren met dimensies in de orde van grootte van de golflengte van licht, is het van belang eerst te bepalen in welke mate de optische eigenschappen van de chromoforen worden beïnvloed door de elektromagnetische randcondities aan het grensvlak. In Hoofdstuk 6 laten we zien dat de fluorescentielevensduur van individuele moleculen ingebed in een dunne polymeerlaag verandert en toeneemt met afnemende dikte van de polymere laag. Berekeningen van de fluorescentielevensduur van fluoroforen ingebed in gelaagde structuren bevestigen dat de aanwezigheid van grensvlakken een dominante rol speelt in de modificatie van de fluorescentielevensduur. Het is dus belangrijk om rekening te houden met laagdikte en molecuulorientatie. Toch blijken deze globale effecten de levensduurexperimenten zoals beschreven in Hoofdstuk 5 niet significant te beïnvloeden, zolang we relatieve levensduurfluctuaties meten en de chromoforen zich niet herschikken in de polymere matrix of verplaatsen ten opzichte van de grensvlakken. Dit is het geval voor glasfase polymeren zoals polystyreen bij kamertemperatuur, in Hoofdstukken 4 en 5.

In Hoofdstuk 7 gebruiken we de techniek van fluorescentie levensduurfluctuaties van enkele moleculen om op de nanometerschaal de invloed van de laagdikte op lokale polymeerdynamica te bestuderen, bij temperaturen die ver onder de glasovergangstemperatuur liggen. De segmentele schaal dynamica verandert voor polymeerlagen met een dikte onder de 60-70 nm, wat overeenkomt met 6 keer de gyratiestraal van het gebruikte polymeer. Dit gedrag wordt toegewezen aan het effect van een vergrote dynamica door het vrije polymeergrensvlak. Het grensvlakeffect werkt duidelijk diep door in het polymeer over afstanden groter dan de gyratiestraal.

Onderzoek naar hybride nanovezels van interne lichtbronnen in een polymeer, bestaande uit glasachtige of semi-kristallijne materialen (PMMA, PEO), verkregen door middel van electrospinnen, wordt gepresenteerd in Hoofdstuk 8. Zowel organische fluoroforen als halfgeleidende nanokristallen (quantum dots) zijn verwerkt in de structuren, met verschillende concentraties tot aan het niveau van individuele moleculen. De techniek van electrospinnen heeft zich bewezen als een goede en betrouwbare methode om quasi ééndimensionale, luminescerende structuren te fabriceren met dimensies die variëren van tientallen nanometers tot enkele micrometers. Distributies van fluorescentielevensduren van individuele moleculen ingebed in PMMA vezels met verschillende diameter zijn gemeten. De verdeling blijkt verbreed voor vezels met diameters onder 500 nm. Dit wordt wederom toegeschreven aan de invloed van de grensvlakken op de levenduur van de aangeslagen toestand. Onder bepaalde electrospincondities wordt een kralenketting-structuur (beads-on-string) van polymeervezels verkregen. Deze ‘beads’ zijn in detail bekeken d.m.v. lokale molecuul fluorescentiedetectie. De structuur van de beads is sterk afhankelijk van het type polymeer. Specifiek in het geval van het electrospinnen van een semikristallijn polymeer worden de fluorescerende moleculen uitgesloten van de beads, waarschijnlijk als gevolg van

het groeien van polymere kristallen. Tevens zijn er aanwijzingen dat de moleculen op de oppervlakken van de beads een specifieke oriëntatie aannemen. De beads vertonen verder interessante optische eigenschappen die gebruikt zouden kunnen worden in toekomstige toepassingen gebaseerd op geavanceerde polymere structuren.

Hoofdstuk 9 geeft een korte vooruitblik op mogelijke toekomstige onderzoeksrichtingen. Het belang van een gedetailleerd vervolgonderzoek op basis van de methodes gepresenteerd in dit proefschrift wordt toegelicht met het oog op verschillende polymeersystemen en complexe polymeerstructuren, zoals bijvoorbeeld blok copolymeren en polymere netwerken.

Acknowledgements

First of all I would like to thank Prof. Julius Vancso and Prof. Niek van Hulst for giving me the opportunity to work in their research groups at the University of Twente. Julius, Niek, working with you on this truly cooperative project was a pleasure and I thank you both for the freedom I got during my four years of research.

Special thanks to Dr. Renaud Vallée, my daily supervisor during the first two years of my stay in Twente. Renaud, thank you very much for what I have learned from you, for your patience and good spirit. I thank you also for accepting to be a member of my defense committee.

The work described in this thesis was an effort of many people. I would like to thank all the people who contributed in any way to this thesis during the four years of research. In particular, I cordially acknowledge the following persons: Dr. Maria García-Parajó, Prof. Kobus Kuipers, Dr. Erik van Dijk, Dr. Jordi Hernando, Jeroen Korterik and Frans Segerink for their constant help with the experimental setups, data analysis software, article readings and for all the scientific and non-scientific discussions we had together during coffee breaks. Without you all my life in OT would be much harder during my PhD research. Hugo van Bergen, Jeroen Smit and Gert-Jan Bakker are acknowledged for their involvement in the development of the wide-field setup (Chapter 4). Also many thanks to Antonella Cristiano and Qi Chen for their contributions to Chapter 4. Dr. Henkjan Gersen is acknowledged for kindly providing me the software for fluorescence lifetime calculations (Chapter 6). Lanti Yang and Shuying Gu are acknowledged for their work with the electrospinning setup and for providing polymer fiber samples (Chapter 8). Quantum dots used in Chapter 8 were kindly provided by Dr. Mingyong Han (IMRE, NUS Singapore). Mark Hempenius and Clemens Padberg are acknowledged for their constant support in the labs and for assistance during the experiments and synthesis. Mark, thank you for carefully reading this thesis and for all the corrections you made.

Special thanks to Geneviève Rietveld, Cindy Lammertink, and Nancy Trip for their enormous help with all type of paperwork, for their patience and continuous support. Life would be much harder without all your help during the last four years.

A lot of the research ideas were developed during many fruitful discussions in our "air-conditioned" office at CT. Many thanks to Igor Korczagin, Alex Shovsky, In Yee Phang and Sandra Garcia-Garabal for all the coffee breaks and stimulating discussions.

During my stay in Twente I met many wonderful colleagues, most of them have already left UT. It is not possible to mention all of them here, and I apologize if I forgot somebody: Jason, Marcin, Szczepan, Holger, Henrik, Giorgio, Menno, Léon, Leon, Maria, Beata, Douwe-Wiebe, Barbara, Attila, Monique, Ewa, Herman, Bärbel, Marjolein, Robert, Jasper, Gabriel, Ali, Eliane, Eric, Wouter, Willem-Jan, Elske, Dorota, Edgar, Wouter, Bas, Shan, Jing, Joris, Yuije, Chuanliang, Nina, Marina, Steffi, Ewelina, Ivan, Ramon, and many, many others.

Special thanks to Monique Roerdink and Ewa Tocha for accepting to be my paranimfs.

Jagoda and Patrycja, you are the source of constant inspiration, strength, hope and good spirit. Ewa, thank you for your constant and unconditional support. Without you these four years in Enschede would have never been the same. Kochana Ewo, Ty najlepiej wiesz ile jest Twojej pracy i ofiarności w tym doktoracie. Dziękuje Tobie za te cztery lata spędzone razem w Enschede. Kocham Cię bardzo, całe życie jest jeszcze przed nami.

I would like to thank my wonderful parents Elwira and Leonard Tomczak for their constant support and for giving me the freedom to choose whatever I would like to do in my life. Kochani rodzice, dziękuje wam bardzo za ciągłe wsparcie jakie otrzymuję przez całe moje życie. Dzięki wam moglem osiągnąć to o czym marzyłem.

I wish all the best for all of you,

Nikodem